

## ***Journal of Science & Technology***

### **About the Journal**

*Pertanika* is an international peer-reviewed journal devoted to the publication of original papers, and it serves as a forum for practical approaches to improving quality in issues pertaining to tropical agriculture and its related fields. *Pertanika* began publication in 1978 as the Journal of Tropical Agricultural Science. In 1992, a decision was made to streamline *Pertanika* into three journals to meet the need for specialised journals in areas of study aligned with the interdisciplinary strengths of the university. The revamped Journal of Science & Technology (JST) aims to develop as a pioneer journal focusing on research in science and engineering, and its related fields. Other *Pertanika* series include Journal of Tropical Agricultural Science (JTAS); and Journal of Social Sciences and Humanities (JSSH).

JST is published in **English** and it is open to authors around the world regardless of the nationality. It is currently published two times a year, i.e. in **January** and **July**.

### **Goal of *Pertanika***

Our goal is to bring the highest quality research to the widest possible audience.

### **Quality**

We aim for excellence, sustained by a responsible and professional approach to journal publishing. Submissions are guaranteed to receive a decision within 12 weeks. The elapsed time from submission to publication for the articles averages 5-6 months.

### **Indexing of *Pertanika***

*Pertanika* is now over 33 years old; this accumulated knowledge has resulted in *Pertanika* journals being indexed in SCOPUS (Elsevier), EBSCO, DOAJ, AGRICOLA, and CABI etc. JST is indexed in SCOPUS, EBSCO and DOAJ.

### **Future Vision**

We are continuously improving access to our journal archives, content, and research services. We have the drive to realise exciting new horizons that will benefit not only the academic community, but society itself.

We also have views on the future of our journals. The emergence of the online medium as the predominant vehicle for the ‘consumption’ and distribution of much academic research will be the ultimate instrument in the dissemination of research news to our scientists and readers.

### **Aims and Scope**

*Pertanika* Journal of Science and Technology aims to provide a forum for high quality research related to science and engineering research. Areas relevant to the scope of the journal include: *bioinformatics, bioscience, biotechnology and biomolecular sciences, chemistry, computer science, ecology, engineering, engineering design, environmental control and management, mathematics and statistics, medicine and health sciences, nanotechnology, physics, safety and emergency management*, and related fields of study.

### **Editorial Statement**

*Pertanika* is the official journal of Universiti Putra Malaysia. The abbreviation for *Pertanika* Journal of Science & Technology is *Pertanika J. Sci. Technol.*

## **Editorial Board**

2011-2013

Editor-in-Chief

**Mohd. Ali HASSAN**, Malaysia

*Bioprocess engineering, Environmental biotechnology*

Executive Editor

**Nayan D.S. KANWAL**, Malaysia

*Environmental issues- landscape plant modelling applications*

## **Editorial Board Members**

**Abdul Halim Shaari** (Professor Dr), *Superconductivity and Magnetism*, Universiti Putra Malaysia, Malaysia.

**Adem KILICMAN** (Professor Dr), *Mathematical Sciences*, Universiti Putra Malaysia, Malaysia.

**Ahmad Makmom Abdullah** (Associate Professor Dr), *Ecophysiology and Air Pollution Modelling*, Universiti Putra Malaysia, Malaysia.

**Ali A. MOOSAVI-MOVAHEDI** (Professor Dr), *Biophysical Chemistry*, University of Tehran, Tehran.

**Amu THERWATH** (Professor Dr), *Oncology, Molecular Biology*, Université Paris, France.

**Angelina CHIN** (Professor Dr), *Mathematics, Group Theory and Generalisations, Ring Theory*, University of Malaya, Malaysia.

**Biswa Mohan BISWAL** (Associate Professor Dr), *Medical, Clinical Oncology, Radiotherapy*, Universiti Sains Malaysia, Malaysia.

**Christopher G. JESUDASON** (Professor Dr), *Mathematical Chemistry, Molecular Dynamics Simulations, Thermodynamics and General Physical Theory*, University of Malaya, Malaysia.

**Kaniraj R. SHENBAGA** (Professor Dr), *Geotechnical Engineering*, Universiti Malaysia Sarawak, Malaysia.

**Kanury RAO** (Professor Dr.), *Senior Scientist & Head, Immunology Group, International Center for Genetic Engineering and Biotechnology, Immunology, Infectious Disease Biology and Systems Biology*, International Centre for Genetic Engineering & Biotechnology, New Delhi, INDIA.

**Karen Ann CROUSE** (Professor Dr), *Chemistry, Material Chemistry, Metal Complexes – Synthesis, Reactivity, Bioactivity*, Universiti Putra Malaysia, Malaysia.

**Ki-Hyung KIM** (Professor Dr), *Computer and Wireless Sensor Networks*, AJOU University, Korea.

**Megat Mohamad Hamdan MEGAT AHMAD** (Professor Dr), *Mechanical and Manufacturing Engineering*, Universiti Pertahanan Nasional Malaysia, Malaysia.

**Mirnalini KANDIAH** (Associate Professor Dr), *Public Health Nutrition, Nutritional Epidemiology*, Universiti Putra Malaysia, Malaysia.

**Mohamed Othman** (Professor Dr), *Communication Technology and Network, Scientific Computing*, Universiti Putra Malaysia, Malaysia.

**Mohd Adzir Mahdi** (Professor Dr), *Physics, Optical Communications*, Universiti Putra Malaysia, Malaysia.

**Mohd Sapuan Salit** (Professor Dr), *Concurrent Engineering and Composite Materials*, Universiti Putra Malaysia, Malaysia.

**Prakash C. SINHA** (Professor Dr), *Physical Oceanography, Mathematical Modelling, Fluid Mechanics, Numerical Techniques*, Universiti Malaysia Terengganu, Malaysia.

**Rajinder SINGH** (Dr), *Biotechnology, Biomolecular Science, Molecular Markers/ Genetic Mapping*, Malaysian Palm Oil Board, Kajang, Malaysia.

**Renuganth VARATHARAJOO** (Associate Professor Dr), *Engineering, Space System*, Universiti Putra Malaysia, Malaysia.

**Sabira KHATUN** (Professor Dr), *Engineering, Computer Systems and Software Engineering, Applied Mathematics*, University Malaysia Pahang, Malaysia.

**Shiv Dutt GUPTA** (Dr), *Director, IIHMR, Health Management, public health, Epidemiology, Chronic and Non-communicable Diseases*, Indian Institute of Health Management Research, India.

**Shoba RANGANATHAN** (Professor Dr), *UNESCO Chair of Biodiversity Informatics Bioinformatics and Computational Biology, Biodiversity Informatics, Protein Structure, DNA sequence*, Macquarie University, Australia.

**Suan-Choo CHEAH** (Dr), *Biotechnology, Plant Molecular Biology*, Asiatic Centre for Genome Technology (ACGT), Kuala Lumpur, Malaysia.

**Waqar ASRAR** (Professor Dr), *Engineering, Computational Fluid Dynamics, Experimental Aerodynamics*, International Islamic University, Malaysia.

**Wing-Keong NG** (Professor Dr), *Aquaculture, Aquatic Animal Nutrition, Aquafeed Technology*, Universiti Sains Malaysia, Malaysia.

**Yudi SAMYUDIA** (Professor Dr Ir), *Chemical Engineering, Advanced Process Engineering*, Curtin University of Technology, Malaysia.

## **International Advisory Board**

**Adarsh SANDHU** (Professor Dr), *Editorial Consultant for Nature Nanotechnology and contributing writer for Nature Photonics, Physics, Magnetoresistive Semiconducting Magnetic Field Sensors, Nano-Bio-Magnetism, Magnetic Particle Colloids, Point of Care Diagnostics, Medical Physics, Scanning Hall Probe Microscopy, Synthesis and Application of Graphene, Electronics-Inspired Interdisciplinary Research Institute (EIIRIS), Toyohashi University of Technology, Japan.*

**Graham MEGSON** (Professor Dr), *Computer Science, The University of Westminster, U.K.*

**Kuan-Chong TING** (Professor Dr), *Agricultural and Biological Engineering, University of Illinois at Urbana-Champaign, USA.*

**Malin PREMARATNE** (Professor Dr), *Advanced Computing and Simulation, Monash University, Australia.*

**Mohammed Ismail ELNAGGAR** (Professor Dr), *Electrical Engineering, Ohio State University, USA.*

**Peter G. ALDERSON** (Associate Professor Dr), *Bioscience, The University of Nottingham Malaysia Campus.*

**Peter J. HEGGS** (Professor Emeritus Dr), *Chemical Engineering, University of Leeds, U.K.*

**Ravi PRAKASH** (Professor Dr), *Vice Chancellor, JUIT, Mechanical Engineering, Machine Design, Biomedical and Materials Science, Jaypee University of Information Technology, India.*

**Said S.E.H. ELNASHAIE** (Professor Dr), *Environmental and Sustainable Engineering, Penn. State University at Harrisburg, USA.*

**Suhash Chandra DUTTA ROY** (Professor Emeritus Dr), *Electrical Engineering, Indian Institute of Technology (IIT) Delhi, New Delhi, India.*

**Yi LI** (Professor Dr), *Chemistry; Photochemical Studies, Organic Compounds, Chemical Engineering, Chinese Academy of Sciences, Beijing.*

## **Pertanika Editorial Office**

Office of the Deputy Vice Chancellor (R&I),  
1st Floor, IDEA Tower II, UPM-MTDC Technology Centre  
Universiti Putra Malaysia, 43400 Serdang, Selangor, Malaysia  
Tel: +603 8947 1622  
E-mail: [ndeeps@admin.upm.edu.my](mailto:ndeeps@admin.upm.edu.my)

## **Publisher**

The UPM Press  
Universiti Putra Malaysia  
43400 UPM, Serdang, Selangor, Malaysia  
Tel: +603 8946 8855, 8946 8854 • Fax: +603 8941 6172  
[penerbit@putra.upm.edu.my](mailto:penerbit@putra.upm.edu.my)  
URL: <http://penerbit.upm.edu.my>

---

The publisher of Pertanika will not be responsible for the statements made by the authors in any articles published in the journal. Under no circumstances will the publisher of this publication be liable for any loss or damage caused by your reliance on the advice, opinion or information obtained either explicitly or implied through the contents of this publication.

All rights of reproduction are reserved in respect of all papers, articles, illustrations, etc., published in Pertanika. Pertanika provides free access to the full text of research articles for anyone, web-wide. It does not charge either its authors or author-institution for refereeing/ publishing outgoing articles or user-institution for accessing incoming articles.

No material published in Pertanika may be reproduced or stored on microfilm or in electronic, optical or magnetic form without the written authorization of the Publisher.

**Copyright © 2012 Universiti Putra Malaysia Press. All Rights Reserved.**

**Pertanika Journal of Science & Technology**  
**Vol. 20 (1) Jan 2012**

**Contents**

**Review Articles**

- Factors Affecting the Cold Flow Behaviour of Biodiesel and Methods for Improvement – A Review 1  
*Odeigah Edith*
- A Review on Robot Motion Planning Approaches 15  
*S. H. Tang, W. Khaksar, N. B. Ismail and M. K. A. Ariffin*

**Regular Articles**

- Effect of Glycerol Feed in Methanol Induction Phase for Hepatitis B Surface Antigen Expression in *Pichia pastoris* Strain KM71 31  
*A. R. Morvarid, N. A. Zeenathul, Y. J. Tam, H. Zuridah, M. L. Mohd-azmi and B. O. Azizon*
- Relative Power Performance of *t*-test and Bootstrap Procedure for Two-Sample 43  
*Nor Aishah Ahad, Suhaida Abdullah, Lai Choo Heng and Nazihah Mohd. Ali*
- New Semi-blind Channel Estimation in MIMO based on Second Order Statistics 53  
*Dinh-Thuan Do*
- Performance Evaluation of A Mobile Road Traffic Infraction Registration System through Benchmark 63  
*Arasteh-Rad, H., Khairulmizam Samsudin, Abdul Rahman Ramli and Mohammad Ali Tavallaie*
- Effect of Rare Earth Elements Substitution in La site for LaMnO<sub>3</sub> Manganites 81  
*Wong Jen Kuen, Lim Kean Pah, Abdul Halim Shaari, Chen Soo Kien, Ng Siau Wei and Albert Gan Han Ming*
- Exact Parallel Plurality Voting Algorithm for Totally Ordered Object Space Fault-Tolerant Systems 89  
*Abbas Karimi, Faraneh Zarafshan, Adznan Jantan, Abdul Rahman Ramli, M. Iqbal b. Saripan and S. A. R. Al-Haddad*
- An Audit of Type 2 Diabetes Care in a Malaysian Public Community Polyclinic 97  
*Chew, B. H., Palikat, J. M., Nur Syamimi, A., Nor Azillah, A., See, J. K., Hafiz, A. R., Siti Nazira, A., Aienum, Y., Muhamad Zaid, M., Palaniappan, K. and Tan, Y. Y.*

**Selected Articles from the World Engineering Congress 2010: Advanced Processes and Materials**

**Guest Editor:** Siti Mazlina Mustapa Kamal

**Guest Editorial Board:** Suraya Abdul Rashid, Farah Saleena Taip and Rosnita A. Talib

- Residence Time Distribution of Tapioca Starch-Poly(lactic acid)-Cloisite 10A 103  
Nanocomposite Foams in an Extruder  
*Lee, S. Y.*

- Ex-Situ Experimental Set-Up for Pink Guava Juice Fouling Deposit Study 109  
*Ong C. A., Abdul Aziz, N., Taip, F. S. and Ibrahim M. N.*

- Effect of Solid Solution Treatment on Semisolid Microstructure of Zn-22Al Alloy 121  
*M. A. M. Arif, M. Z. Omar and N. Muhamad*

- Effect of Epoxidized Natural Rubber on Mechanical Properties of Epoxy 129  
Reinforced Kenaf Fibre Composites  
*Abu Bakar, M. A., Ahmad, S. and Kuntjoro, W.*

**Selected Articles from the World Engineering Congress 2010: Natural Resources and Green Technology**

**Guest Editor:** Hasfalina Che Man

**Guest Editorial Board:** Rozita Omar, Salmiaton Ali, Samsuzana Abdul Aziz, Shafreeza Sobri, Badronnisa Yusuf, Aida Isma Mohd Idris, Hazmin Mansor and Khairunniza Bejo

- Catalytic Gasification of Empty Fruit Bunch for Enhanced Production of Hydrogen 139  
Rich Fuel Gas  
*Mohammed M. A. A., Salmiaton A., Wan Azlina W. A. K. G.,  
Mohamad Amran M. S., Omar R., Taufiq-Yap Y. H. and Fakhru'l-Razi A.*

- Earthquake and Tsunami Research in USM: The Role of Disaster Research Nexus 151  
*Hock Lye Koh, Su Yean Teh, Taksiah A. Majid, Tze Liang Lau and  
Fauziah Ahmad*

- Synthesis of *Jatropha curcas*-based Methyl Ester and Ethyl Ester as 165  
Biodiesel Feedstocks  
*Azhari Muhammad Syam, Robiah Yunus, Tinia Idaty Mohd. Ghazi and  
Thomas Choong Shean Yaw*

- New Vane-Type Wind Turbine of High Efficiency 175  
*R. Usubamatov, A. Y. Qasim and Z. M. Zain*

- Fabrication of Cellulose Acetate Film From Oil Palm Empty Fruit Bunch 189  
(OP-EFB) and Cytotoxicity Evaluation  
*Dasmawati Mohamad, Wan Suzaini Wan Hamzah, Wan Rosli Wan Daud,  
Zainul Ahmad Rajion, Wan Zaripah Wan Bakar and Mazlan Ibrahim*

# **Editorial<sup>1</sup>**

## **The inside story behind materials engineering**



Materials engineering is a fascinating branch of engineering and has glorious past to its credit as well as a bright future ahead. Historical eras have been named after various materials which were being used in that era. Stone age, bronze age, iron age, plastics age and composites age are to name a few. Presently we are in the era of smart materials.

The comforts of life would not have been possible but for the researches and development of new materials. Light materials made it possible to have satellites without which there would not be any of the modern communication and transportation services. Newer electronic materials have made faster and smaller

computers possible. Fighters, bombers, rockets, missiles etc. are all possible because of the development of newer and lighter materials. We still do need even more lighter materials to go for hypersonic planes from supersonic planes.

Materials have made tremendous inroads in biomedical applications too. A number of bio-metals, biopolymers and bio-ceramics are being used for making various prostheses. Hip prosthesis, knee prosthesis, elbow prosthesis, ankle prosthesis, wrist prosthesis etc. are being commonly used employing all these engineering materials. They are also being used for implant applications such as dental implants, orthopaedic implants and implants for bridging large osteoperiosteal gaps. Biomaterials are also being used for making fracture fixation plates, intra-medullary nails and interlocking screws besides being used for ophthalmic applications, cardiovascular applications, as suture materials, for drug delivery systems and tissue connectivity etc.

Materials research area is also very interesting indeed and one seeks answers to certain basic questions. For example, we all know that due to fatigue, materials fail at much lower loads than they should and the question arises as to why fatigue should occur at all. After thoroughly investigating the phenomenon, one realizes that due to push-pull loading or flexural loading, stresses change from tensile to compressive and back to tensile. Hence if during tensile loading, plastic deformation takes place near micro-defects due to stress concentration, the deformation is permanent elongation and this permanent elongation cannot be undone during compressive cycle where the loading cycle tries to permanently compress the body. Due to this mismatch, fatigue crack nucleates and starts

propagating in subsequent cycles. Similarly, when you tear a paper or break a twig, you hear some sound. Where does this sound come from? Sound is a form of energy and it cannot be produced. We can only change one form of energy to the other form. Hence some energy form must be getting converted into sound energy. On thorough investigation, one finds that every material has stored elastic energy within the volume of material which get released on plastic deformation, phase transformation or fracture. There are several such questions and which would always be investigated by materials scientists to keep the material research going and resulting in development of newer materials and newer technologies. The future of materials engineering is very bright indeed.

### **PROFESSOR RAVI PRAKASH, Ph D**

Vice Chancellor  
Jaypee University of Information Technology Waknaghat  
District Solan, 173234  
Himachal Pradesh  
India

[ravi.prakash@juit.ac.in](mailto:ravi.prakash@juit.ac.in)

May 27, 2011

Ravi Prakash is currently the Vice Chancellor of Jaypee University of Information Technology (JUIT) Waknaghat in India. Professor Prakash obtained his Bachelor's degree in Mechanical Engineering in 1971 from Institute of technology, Banaras Hindu University; Master's degree in Engineering Design in 1973 from University of Salford, U.K. and Doctoral degree in Materials in 1975 from Cranfield University, U.K. He did post doctoral research in the area of Materials at University of Bath, U.K. (1979-1980) and was Visiting Professor at Hartshill Medical institute, Stoke-on-Trent, U.K. (1986-1987). Professor Prakash was Scientific Attaché at the Indian Embassy, Washington, D.C., USA (1992-1995). He has been in teaching profession for a long time. First at Institute of Technology, Banaras Hindu University for 20 years, then at Birla Institute of Technology and Science, Pilani for 15 years and now at JUIT Waknaghat. He has supervised eight doctoral theses and a large number of M. Phil/MS/M.Tech dissertations. He is Fellow of a number of professional societies and has published more than 100 research papers in prominent peer-reviewed journals. Professor Prakash sits on the International Advisory Board of Pertanika Journal of Science & Technology.

---

#### **<sup>1</sup>DISCLAIMER**

The views expressed in this article are those of the author and do not necessarily represent the views of, and should not be attributed to, the *Pertanika* Journal or the *Pertanika* Editorial Board.

*Review Article*

## **Factors Affecting the Cold Flow Behaviour of Biodiesel and Methods for Improvement – A Review**

**Odeigah Edith**

*Department of Biological and Agricultural Engineering,  
Universiti Putra Malaysia,  
43400 Serdang, Selangor, Malaysia  
E-mail: edith\_odeigah@yahoo.com*

### **ABSTRACT**

Biodiesel is an attractive renewable energy source, which is suitable as a substitute to the non-renewable petroleum diesel. However, it is plagued by its relatively bad cold flow behaviour. In this review, the factors affecting the cold flow of biodiesel, vis-à-vis the contradicting requirement of good cold flow and good ignition properties, are discussed. Fuel filter plugging, and crystallization of biodiesel are considered, together with the cold flow properties such as Pour Point (PP), Cloud Point (CP), Cold Filter Plugging Point (CFPP) and Low Temperature Filterability Test (LTFT). In addition, various methods used to improve the cold flow of biodiesel are also presented, with a special emphasis laid on the effects of these methods in reducing the Cloud Point. Strategies to improve cold flow, and yet maintaining the good ignition quality of biodiesel, are also proposed. As far as the cold flow of biodiesel is concerned, desirable attributes of its esters are short, unsaturated and branched carbon chains. However, these desirable attributes present opposing properties in terms of ignition quality and oxidation stability. This is because esters with short, unsaturated and branched carbon chains possess very good cold flow but poor ignition quality and oxidation stability. The target is therefore to produce biodiesel with good cold flow, sufficient ignition quality, and good oxidation stability. This target proves to be quite difficult and is a major problem in biodiesel research. New frontiers in this research might be the design of the new cold flow improvers that is similar to those used in the petroleum diesel but is tailored for biodiesel. Genetic modifications of the existing feedstock are also desirable but the food uses of this particular feedstock should always be taken into consideration.

**Keywords:** Biodiesel, cold flow properties, pour point, cloud point, cold filter plugging point and low temperature filterability test

### **ABBREVIATIONS**

PP	: Pour Point
Cp	: Cloud Point
CFPP	: Cold Filter Plugging Point
LTFT	: Low Temperature Filterability Test
CI	: Compression Ignition Engine

---

Received: 22 June 2010

Accepted: 8 Feb 2011

WAI	:	Wax Appearance Index
DSC	:	Digital Scanning Calorimetry
ASTM	:	American Standard Testing Methods
TCO	:	Crystallization Onset Temperature
CFI	:	Cold Flow Improvers
EVA	:	Ethylene-co-Vinyl Acetate
WASA	:	Wax Anti Settling Agents
ULSD	:	Ultra Low Sulfur Diesel
MME	:	Madhuca Indica Biodiesel
E20	:	20% Ethanol blend with biodiesel

## INTRODUCTION

Biodiesel consists of complex mixtures of esters obtained by the trans-esterification of triglycerides (fatty acids) from agricultural fats and oils with lower alcohol. Methanol is mostly employed for the trans-esterification because of its low cost; hence, methyl esters are mostly produced (de Oliveira *et al.*, 2009; Joelianingsih *et al.*, 2008; Ma & Hanna, 1999; Wang, 2007; Xu & Hanna, 2009). There are various types of biodiesel fuels, depending on the feedstock oil. In particular, biodiesel exhibits fuel properties that are similar to those of petroleum diesel and as such, it can be used in an unmodified diesel engine.

At 40°C, biodiesel exhibits viscosities ranging from 3.88mm<sup>2</sup>/s to 5.3mm<sup>2</sup>/s (Benjumea *et al.*, 2009; de Oliveira *et al.*, 2009; Sharma *et al.*, 2008). This is much lower than that of the feedstock oil and close to that of petroleum diesel #2, which ranges from 1.9mm<sup>2</sup>/s to 4.1mm<sup>2</sup>/s, and is also an advantage over their feedstock oils (Demirbas, 2005). Biodiesel has densities between 0.860g/cm<sup>3</sup> and 0.897g/cm<sup>3</sup> at 15°C which is higher than that of petroleum diesel (Bhale *et al.*, 2009). This high density can be said to make up for their lower volumetric energy content. On the basis of ignition quality, biodiesel is said to be better than the petroleum diesel. The ignition quality of a diesel fuel is a measure of the relative ease by which the fuel will ignite in an internal combustion compression ignition engine. The ignition quality of diesel fuels is measured by their cetane number, i.e. a high cetane number indicates a good ignition quality and vice versa. Biodiesel exhibits higher cetane numbers than petroleum diesel and hence burns smoother in a diesel engine than petroleum diesel. This high cetane number is as a result of the presence of greater quantities of straight hydrocarbon chains in the esters than in petroleum diesel. More so, biodiesel has higher flash and fire points than the petroleum diesel. The flash point of a fuel is the lowest temperature at which the fuel can form an ignitable mixture with air and the fire point of the fuel is the lowest temperature at which the fuel will continue to burn even after the source of ignition has been removed. The fire point is usually slightly higher than the flash point. A higher flash and fire point indicates that biodiesel is less flammable than petroleum diesel; hence, biodiesel is safer to handle. In fact, biodiesel has better lubricant than the petroleum diesel, and this indicates that an engine running on biodiesel will last longer and less prone to wear out.

However, biodiesel exhibits worse oxidation stability than petroleum diesel and will deteriorate under prolonged storage due to oxidation in the presence of air. Furthermore, biodiesel exhibits worse cold flow behaviour as compared to its fossil cousin. This bad cold flow behaviour is otherwise known as the low temperature flow property which is a major property of biodiesel that hampers

its usage as a neat fuel (B100), especially in temperate regions. Knothe *et al.* (2005) discusses at length the properties of biodiesel. The cold flow behaviour of biodiesel is determined by two major factors, namely:

1. The fatty acid composition of its constituent esters and
2. The presence of minor components such as monoglycerides and steryl glycosides.

This paper discusses at length the relation between the cold flow behaviour of biodiesel fuels and the fatty acid composition of its constituent esters. The effect of the minor components on the cold flow of biodiesel has been discussed in detail by Dunn (2009).

### **COMPRESSION IGNITION (C.I) ENGINE AND FUEL FILTER PLUGGING**

In cold weather, diesel fuels tend to crystallize and become gel-like. The temperature at which fuel filter plugging occurs varies from fuel to fuel depending on the composition of the fuel. However, this temperature is higher for biodiesel than petroleum diesel, for example: palm oil biodiesel will start to crystallize at about 16°C and will form a gel at about 12°C. This makes biodiesel not favourable in cold weather.

The fuel injection pump and the fuel injectors of the compression ignition (CI) engine are precision equipment with very close tolerances. It is thus very important that clean fuel gets into the system because impurities may block the fuel injector and also cause wear within the engine. Engine wear reduces output torque and increases brake's specific fuel consumption of the engine. Meanwhile, large particles cause fuel filter plugging and reduce fuel supply to the injector and the combustion chamber, resulting in a loss of power and probable engine shut down. A plugged engine will have intermittent starting problem or may not start at all.

### **THE BASIC CONCEPT OF CRYSTALLIZATION AND GEL FORMATION**

Gelling involves crystallization of the molecules of a liquid forming a continuous network of crystals within the bulk of the liquid. For crystallization to occur, the molecules of the liquid must generate sufficient thermodynamic force by strong intermolecular interaction. This thermodynamic force is generated when the temperature of the liquid is reduced to below its melting point.

Crystallization occurs in two major and interrelated steps known as nucleation and crystal growth. Nucleation is the first stage of crystallization and it occurs when the molecules of the liquid come together to form solid embryos called crystal lattices or crystallites. Crystal growth is subsequent to nucleation. It involves the growth of the crystal lattices formed. Meanwhile, the lattices grow by the nucleation of the layers of new lattices on the existing ones to form large crystals. This growth continues until a continuous network of crystals is formed (Gunstone *et al.*, 2007).

In a homogenous mixture of many components with different melting points, crystallization is governed by the solubility of the components in the mixture. The low melting point components act as the solvent, while the high melting point components act as the solute (Marangoni & Narine, 2002). At any temperature below the melting point of the solute, crystallization will only occur if the solute is supersaturated in the solvent at that temperature. A solute is said to be supersaturated in a solvent when the solvent has dissolved more of the solute than it can hold at that particular temperature. Thus, super-saturation depends on:

1. The temperature of the solution
2. The concentration of the solute in the solution

In general, solubility decreases and super-saturation increases with the decrease in the temperature. In addition, super-saturation increases with the increase in the concentration of the solute in the solution. Thus, as temperature reduces and the concentration of the solute increases, the rate of crystallization will increase as well.

## FACTORS AFFECTING THE COLD FLOW BEHAVIOUR OF BIODIESEL

The cold flow properties of biodiesel like every other of its fuel properties are influenced by the composition of its esters. Trans-esterification of triglycerides is a chemical process that does not involve any change in the inherent properties of the fatty acids present in the triglyceride, thus the composition of fatty acids in feedstock oils plays a vital role in determining the properties of the biodiesel.

Three types of fatty acids can be found in any oil or fat (Xu & Hanna, 2009), these are:

1. Saturated fatty acids
2. Mono-unsaturated fatty acids
3. Poly-unsaturated fatty acid

Biodiesel from various feedstock oils exhibit closely related properties; however, these properties vary with the varying compositions of the types of fatty acids that are present in the feedstock oil. Saturated fatty acids have no double bonds in their carbon chain; some examples of these are palmitic acid and stearic acid with 16 and 18 carbon atoms, respectively. Mono-unsaturated fatty acids have only one double bond in their carbon chain, such as palmitoleic acid and oleic acid which are also with 16 and 18 carbon atoms, respectively. Meanwhile, poly-unsaturated fatty acids have either two or three double bonds in their carbon chain, such as linoleic acid and linolenic acid each with 18 carbon atoms and two and three double bonds, respectively. Various studies on these fatty acids and the resulting esters show that saturated fatty acids result in esters with higher cetane number, lower NO<sub>x</sub> emissions, higher oxidation stability and higher lubricity, whereas unsaturated fatty acids result in esters with better cold flow. Singh *et al.* (2009) reported a comprehensive fatty acid composition of various vegetable oils that had been used as biodiesel feedstock.

Meanwhile, saturated fatty acids, due to their high degree of saturation, have higher melting points and temperatures of crystallization and in cold temperature they will crystallize before the mono-unsaturated and poly-unsaturated fatty acids. The melting points of the commonly encountered fatty acids and their corresponding methyl esters are given in Table 1. Due to the high temperature of crystallization exhibited by the saturated fatty acids, biodiesel with high composition of saturated fatty acid esters exhibits worse cold flow and has higher cloud points indicating the crystallization of the esters of these saturated fatty acids.

Studies on the Differential Scanning Calorimetry (DSC) of palm oil biodiesel indicated that two crystallization peaks were observed, with the first peak corresponding to the crystallization of methyl palmitate and methyl stearate at the onset of crystallization and the second peak corresponding to the crystallization of methyl oleate (Foon *et al.*, 2006; Narváez *et al.*, 2008). Dunn (1999) reported a DSC cooling thermogram for soybean methyl esters, which showed split peaks between -30°C to 10°C, indicating a fusion event during the melting process as expected for the mixtures of saturated and unsaturated fatty esters. The high peak is due to the saturated fatty esters and the low peak is due to the unsaturated fatty esters. This explains the really poor cold flow exhibited by palm oil biodiesel which has a high composition of esters of palmitic and stearic acids (Dunn, 1999; Ramos *et al.*, 2009) and the relatively good cold flow exhibited by soybean biodiesel which is richer in esters of oleic acid (Wang, 2007). Imahara *et al.* (2006) reported that saturated acid esters have a

very significant effect on the cold flow of biodiesel; in particular, biodiesel with higher percentages of saturated fatty esters has higher cloud points.

TABLE 1  
The melting points of fatty acids and their corresponding methyl esters

Fatty acid	Melting point (°C)	Methyl ester	Melting point (°C)
Lauric acid (C12:0)	44	Methyl laurate (C12:0)	5
Myristic acid (C14:0)	54	Methyl myristate (C14:0)	18.5
Palmitic acid (C16:0)	63	Methyl palmitate (C16:0)	30.5
Stearic acid (C18:0)	70	Methyl stearate (C18:0)	39.1
Oleic acid(C18:1)	16	Methyl oleate (C18:1)	-20
Linoleic acid (C18:2)	-5	Methyl linoleate (C18:2)	-35
Linolenic acid (C18:3)	-11	Methyl linolenate (C18:3)	-52

N.B: The first number before the colon in the parenthesis stands for the number of carbon atoms, while the second number stands for the number of double bonds in the molecule.

Adapted from Foon *et al.* (2006) & Gunstone (1996).

Long carbon chain fatty acids also have a negative effect on the cold flow of biodiesel. Long carbon chain fatty acids have a higher temperature of crystallization as compared to the shorter carbon chain fatty acids and a high composition of esters of these fatty acids will worsen the cold flow of the biodiesel. Ramos *et al.* (2009) explained that the poor cold flow exhibited by peanut oil biodiesel is due to the presence of lingoceric and behenic acids, which have 22 and 24 carbon atoms without any double bond.

The presence of branches in the carbon chain of fatty acids gives the fatty acid a structure, which requires an increase in the thermodynamic force required for crystallization, and thus, decreasing the temperature of crystallization of the fatty acid. This in turn has a positive impact on the cold flow of the resultant biodiesel. In fact, the increase in the branching of resultant fatty acids by trans-esterification with branched chain alcohols has been employed as a means of improving the cold flow of biodiesel (Wang, 2007).

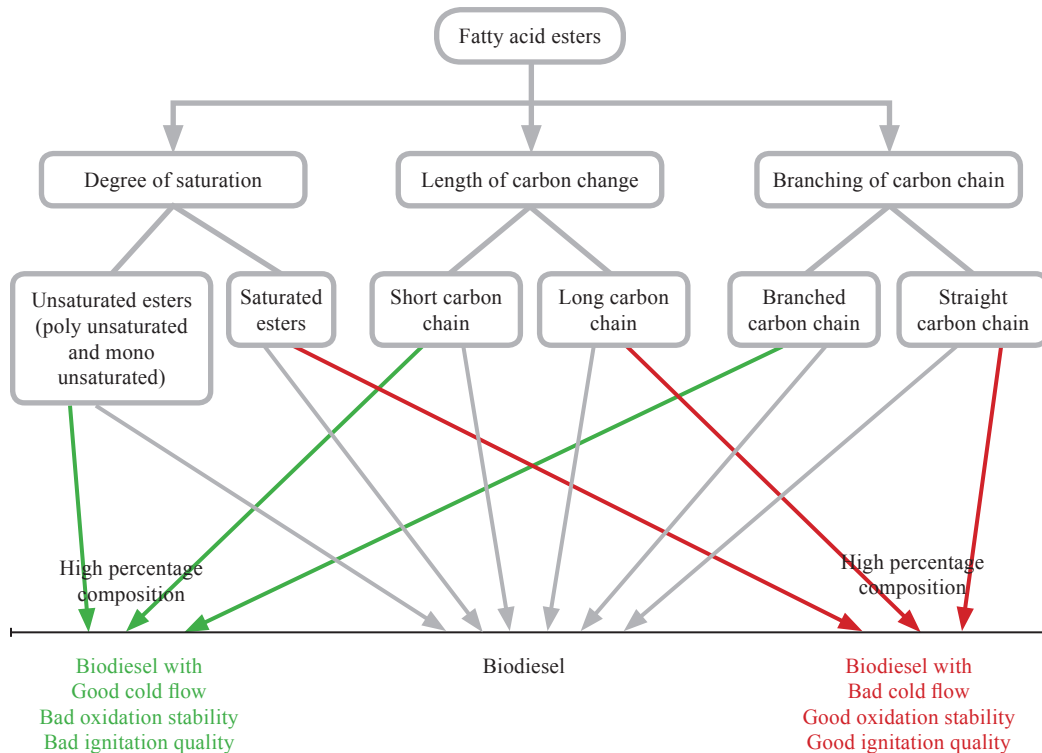
Meanwhile, the presence of carry-overs from the trans-esterification process has also been reported to increase the cloud point of the biodiesel, and thus, having a negative effect on the cold flow of the biodiesel (Fernando *et al.*, 2007; Ma & Hanna, 1999b). These carry-overs are triglycerides, diglycerides and monglycerides. *Fig. 1* summarizes the effects of fatty esters on the cold flow of biodiesels. As indicated earlier on, the biodiesel with high percentage composition of unsaturated, branched and short chain fatty esters exhibits improved cold flow properties.

## CHARACTERIZATION OF THE COLD FLOW OF BIODIESEL

Four parameters are usually used to characterize the cold flow of biodiesel, namely;

1. Pour point (PP)
2. Cloud point (CP)
3. Cold filter plugging point (CFPP), and
4. Low temperature filterability test (LTFT)

Meanwhile, pour points (PP) and cloud points (CP) have been widely used to estimate the behaviour of diesel fuels in cold weather, but these parameters cannot accurately predict the performance of the diesel fuels in the fuel system of compression ignition engines. According to



Green arrows indicates a higher composition of short, unsaturated and branched fatty acids ester which produces biodiesel with good cold flow but poor oxidation stability and poor ignition quality; the red arrows indicate a higher composition of the long, saturated and straight fatty esters which produce biodiesel with poor cold flow but good oxidation stability and good ignition quality. In between is a balanced in the attributes of the fatty esters.

*Fig. 1: The effects of fatty esters compositions on the cold flow properties of biodiesel*

the ASTM standard, the pour point (PP) is the “lowest temperature at which movement of the oil is observed”, whereas the cloud point (CP) is the highest temperature at which crystals formed within the oil become visible (in form of cloudiness). However, the pour point (PP) approach is too optimistic because diesel fuels will exhibit fuel filter plugging problems at temperatures higher than their pour point. Moreover, since fuel filter plugging does not necessarily occur at the cloud point of the diesel fuel, the cloud point is really not sufficient to estimate the cold flow of biodiesel. However, the cloud point is a good parameter for quality control in the operation of diesel engines in low temperatures and the pour point is a good indicator of the behaviour of diesel fuels in wide storage and pipeline distribution (Gerpen *et al.*, 2004).

The Cold Filter Plugging Point (CFPP) and the Low Temperature Filterability Test (LTFT) can better predict the operation of diesel fuels within the fuel system of compression ignition engines; these parameters estimate the filterability of diesel fuels in the fuel filter system at low temperatures. The LTFT reports the lowest temperature at which 180mL of a sample can pass through the filter in 60 seconds or less, while the CFPP reports the lowest temperature at which 20mL of sample can pass through the filter in 60 seconds or less. Although both the tests are identical, the LTFT is a better approach because it takes into account the rigorous conditions within the engine. In more

specific, even though the LTFT involves a larger quantity of the sample, smaller filter wire mesh size and slower cooling rates, the CFPP is more user-friendly. LTFT is more accepted in North America but both are equally accepted in other parts of the world. The ASTM standard test methods for obtaining the four said parameters are given in Table 2.

CFPP and LTFT are proportional to CP; LTFT has been reported to have a 1:1 correlation with CP, while CFPP values are a bit lower than the LTFT values, i.e. about  $3.3^{\circ}\text{C} \pm 2.1^{\circ}\text{C}$  below LTFT (Dunn *et al.*, 1996). Thus, a reduction in CP is translated into a significant reduction in CFPP and LTFT, and when working on improving the cold flow of biodiesel, a reduction in CP is more effective than a reduction in PP. Other parameters that are also indicative of the cold flow behaviours of biodiesel include the wax appearance index (WAI) and freezing point. The differential scanning calorimetry has been proved to be an effective, accurate, fast and easy method of obtaining the cloud points and pour points of biodiesel (Dunn, 1999; Foon *et al.*, 2006; Narváez *et al.*, 2008). The DSC crystallization onset temperature ( $T_{\text{co}}$ ) is reported as the cloud point and the melting point temperature is reported as the pour point.

TABLE 2  
Standard test methods

Parameters	Standard test methods
Cloud point	ASTM D-2500
Pour point	ASTM D-97
Cold filter plugging point	ASTM D-6371
Low temperature filterability test	ASTM D-4539

Adapted from ASTM (2003)

### IMPROVING THE COLD FLOW OF BIODIESEL

Improving the cold flow of biodiesel has been proven to be quite a heavy task because in most cases, it has had adverse effects on other fuel properties of the biodiesel, especially ignition quality and oxidation stability. This is because the saturated esters, which give rise to bad cold flow of biodiesel, have very good ignition qualities and oxidation stability, and thus, removing the saturated esters will result in biodiesel having lower ignition quality and oxidation stability. Furthermore, the economic viability of the process is an important parameter as biodiesel is already more expensive than the petroleum diesel and any method which will result in a very high increase in the production cost of biodiesel may not be economically feasible. The following methods have been employed to improve the cold flow of biodiesel:

1. Blending with petroleum diesel
2. Trans-esterification with branched chain alcohol
3. Winterization
4. Use of chemical additives
5. Modification of fatty acid profiles of biodiesel

#### *Blending with Petroleum Diesel*

In the present times, blending biodiesel with petroleum diesel is the most widely employed method for the application of biodiesel, and the European committee for standardization has a limit of a maximum of 5% (by volume) of biodiesel blended in petroleum diesel (Schnopf, 2006). A number

of work, which has been done on blending biodiesel with petroleum diesel, show that when blended with petroleum diesel in small quantities, the cold flow of the biodiesel is improved significantly. At low blend levels, petroleum diesel fuel, being miscible with biodiesels, dominates the effect of the high melting point of saturated esters.

However with increasing levels of biodiesel in the blend the cold flow of the resulting blend is worsen. It has been reported that to achieve the best result, a 20% by volume, biodiesel in diesel fuel #2 and 35% by volume, biodiesel in diesel fuel #1 is required (Dunn & Bagby, 1995). Diesel fuel #1 can accommodate a higher volume of biodiesel because it exhibits a better cold flow than diesel fuel #2 [National Research Council (U.S.). 1982]. Choo *et al.* (2006) were able to produce a patent on a palm-oil based biodiesel formulation with enhanced cold flow properties comprising a blend with not more than 40 percent volume of biodiesel in petroleum diesel blended with a cold flow improver.

#### *Trans-esterification with Branched Chain Alcohol*

Trans-esterification of fatty acids with branched chain alcohols, as opposed to the commonly used methanol, was proposed by Lee *et al.* (1995) to improve the cold flow of biodiesel. These branched chain alcohols increase the branching in the fatty ester structure and thereby reduce the temperature of crystallization and its cloud point. Lee *et al.* (1995) reported that isopropyl soyate had a  $T_{co}$  5.5°C less than that of propyl soyate, but that the use of highly branched alcohols resulted in lower yields and incomplete trans-esterification reaction. Wu *et al.* (1998) reported that isopropyl tallowate had a cloud point of 9°C, which was lower than that of methyl tallowate whose value was 15°C; similarly, isopropyl tallowate was reported to be more viscous than methyl tallowate, and this was probably due its higher molecular weight.

Kleinova *et al.* (2007) studied the effect of the branching on the CFPP of sunflower oil and castor oil biodiesel and reported that the increase in the branching of the fatty ester did not significantly reduce the CFPP in comparison to methyl ester. Moreover, the branched chain alcohols are more expensive than methanol and utilizing them will translate into an increased production cost. To mitigate this high production cost, as a result of trans-esterification with branched chain alcohols, Dunn (2009) studied the effects of blending the more expensive propyl and butyl esters with the cheaper methyl and ethyl esters on the cold flow of the resulting biodiesel. The study reported a 65% by volume requirement of isopropyl soyate in an admixture with methyl soyate to reduce the CP of methyl soyate by 5.1°C to -3.7°C. This, however, still has an adverse effect on the production cost of biodiesel. Yori *et al.* (2006) sought to increase the branching in the methyl ester structure without incurring any extra cost associated with the use of branched alcohol by isomerizing the methyl esters in the liquid phase over solid catalysts. Thus, to achieve the best result, the biodiesel was first fractionated into a saturated ester fraction and an unsaturated ester fraction, after which the unsaturated esters were isomerized at 150°C over  $\text{SO}_4\text{-ZrO}_2$  catalyst and the saturated esters were isomerized at 200°C over H-Mordenite catalyst. However, the authors concluded that this method might not be favourable because the decrease in the cloud point was accompanied by a relative decrease in cetane number and viscosity.

#### *Winterization*

Winterization is a process which was employed in old times to improve the quality of oils and fats, especially salad oils, so that they do not become cloudy at low temperatures. It is a physical process which involves fractionating the oil to remove its high melting components. Extending this approach to biodiesel has been found to significantly reduce the cloud points and pour points of

the biodiesel (Fernando *et al.*, 2007). Biodiesel is cooled to a temperature between its cloud point and pour point and any crystals formed are fractionated; this process is repeated until the crystals are no longer formed when the sample is held at that temperature for more than three hours. The crystals formed are usually crystals of the high melting point saturated fatty esters and the resultant biodiesel has a lower percentage composition of saturated fatty acids.

A study on winterization of soybean biodiesel by Dunn *et al.* (1996) shows that the cloud point of soybean biodiesel can be reduced to -16°C by winterization. The percentage composition of methyl palmitate was reduced by a factor of three and thereby translating to an increased composition of oleate and linoleate. However, five to six steps were required, and the yield was low (about 25%) and there was a 20% loss of starting materials. From the study, it was suggested that in order to increase the yield and reduce the loss of starting materials, a pre-treatment of the biodiesel with cold flow is needed to improve additives before the winterization process and more advanced fractionating techniques for the removal of the crystals after the winterization process could be used.

Fractionation of the crystals formed during winterization with a solvent has been employed in a bid to increase the yield from the winterization process. This particular method is very effective but it increases the production cost (Knothe *et al.*, 2005). Common solvents employed are hexane, isopropanol, and ethanol. Fractionation with hexane as a solvent presented a relatively interesting result as compared to the other solvents. There was appreciable decrease in the cloud point; however, the decrease in the percentage composition of saturated esters was relatively small. This decrease in the cloud point might have been due to the small quantities of hexane in the biodiesel, which were carried over from the fractionation process.

The reduction of the saturated fatty esters by winterization has been reported to have an adverse effect on the cetane number of the biodiesel because these saturated fatty esters have better ignition qualities and higher cetane numbers than the unsaturated fatty esters. Moreover, the various steps required to achieve a significant reduction in cloud point and the low yield translate into a higher production cost which impedes the widespread use of this particular method.

### *The Use of Chemical Additives*

The use of cold flow improvers (CFI) is the conventional method employed to improve the cold flow of petroleum diesel. This method seems to be the most economically and technically favoured means of improving the cold flow of biodiesel. Cold flow improvers improve cold flow either by reducing the pour point (PP) of the diesel fuel or by reducing its cold filter plugging point (CFPP). Conventional additives used for petroleum diesel fuel are mainly polymeric materials like polyacrylate, polymethacrylate of poly(ethylene-co-vinyl acetate) (EVA). These additives have chemical structures consisting of a hydrocarbon chain that is able to co-crystallize with the hydrocarbon chain of the fuel and thereby affecting the growth and nucleation of the wax crystals (Yu-hui & Ben-xian, 2006). The modes of action of these additives are very similar. The CFPP reducing additives, which are otherwise called “CFPP depressants”, act during nucleation by altering the structure of the crystals formed from an orthorhombic shape to a needle-like shape so that fuel filters are not blocked, and then, they inhibit the growth of the crystals formed to make sure that they remain in a fine suspension rather than gelling up. Furthermore, they are usually used with wax anti settling agents (WASA). The “PP depressants”, however, do not alter the shape of the crystals formed; instead, they collect on the surface of the crystals formed to hinder their growth and prevent gel network formation (Soni *et al.*, 2008).

Dunn *et al.* (1996) studied 12 commercial CFI additives for diesel fuels on soybean biodiesel and reported that the additives effectively reduced the PP of neat soybean biodiesel by 3°C to 6°C; thereby, suggesting that the mechanism of nucleation and crystal growth in biodiesel is similar to

that in petroleum diesel. However, these additives did not have any significant effect on the CP of both the neat biodiesel and its blend with petroleum diesel; this could be due to the fact that these additives started to take effect after the onset of crystal nucleation. In addition, these additives were also observed to be more effective at lower biodiesel blend ratios. Four additives on soybean biodiesel blends with petroleum diesel#1 were also not effective in reducing the cloud point of the fuel although they had a significant effect on the pour point (Chiu *et al.*, 2004).

Studies carried out an investigation on the effect of ozonized vegetable oils and found no significant CP depression for soybean, sunflower, and rapeseed; however, the cloud point of the palm oil biodiesel was reduced by about 5°C to about 12°C, which is still on the high side (Soriano *et al.*, 2006). The ozonized oil was prepared by passing a mixture of ozone and oxygen into the vegetable oil. Ozonized oil is a more effective pour point depressant when it is prepared from the same vegetable oil as the biodiesels. This is because there is a better interaction between ozonized oil and biodiesel from the same feedstock. It was also noted that the addition of ozonized oil greatly increased the flash point of the biodiesels.

Estolides and ethylhexyl esters of castor oil and lesquerella oil were also studied for their effects on the cold flow of biodiesel and its blend with ultra low sulphur diesel fuels (ULSD) (Moser *et al.*, 2008). From the study, it was observed that these additives did not have any significant effect on the CP and PP of soybean biodiesel, but all four were able to reduce the pour point of palm oil biodiesel by about 3°C. In particular, the estolides and ethylhexyl esters of castor oil and lesquerella oil were attractive to the authors because of their very good cold flow characteristics, oxidation stabilities and lubricities. Serdari *et al.* (1999) used diacid esters and Knothe *et al.* (2000) Synthesized diols of diacids; however, no significant reductions of CP and PP were reported in both studies.

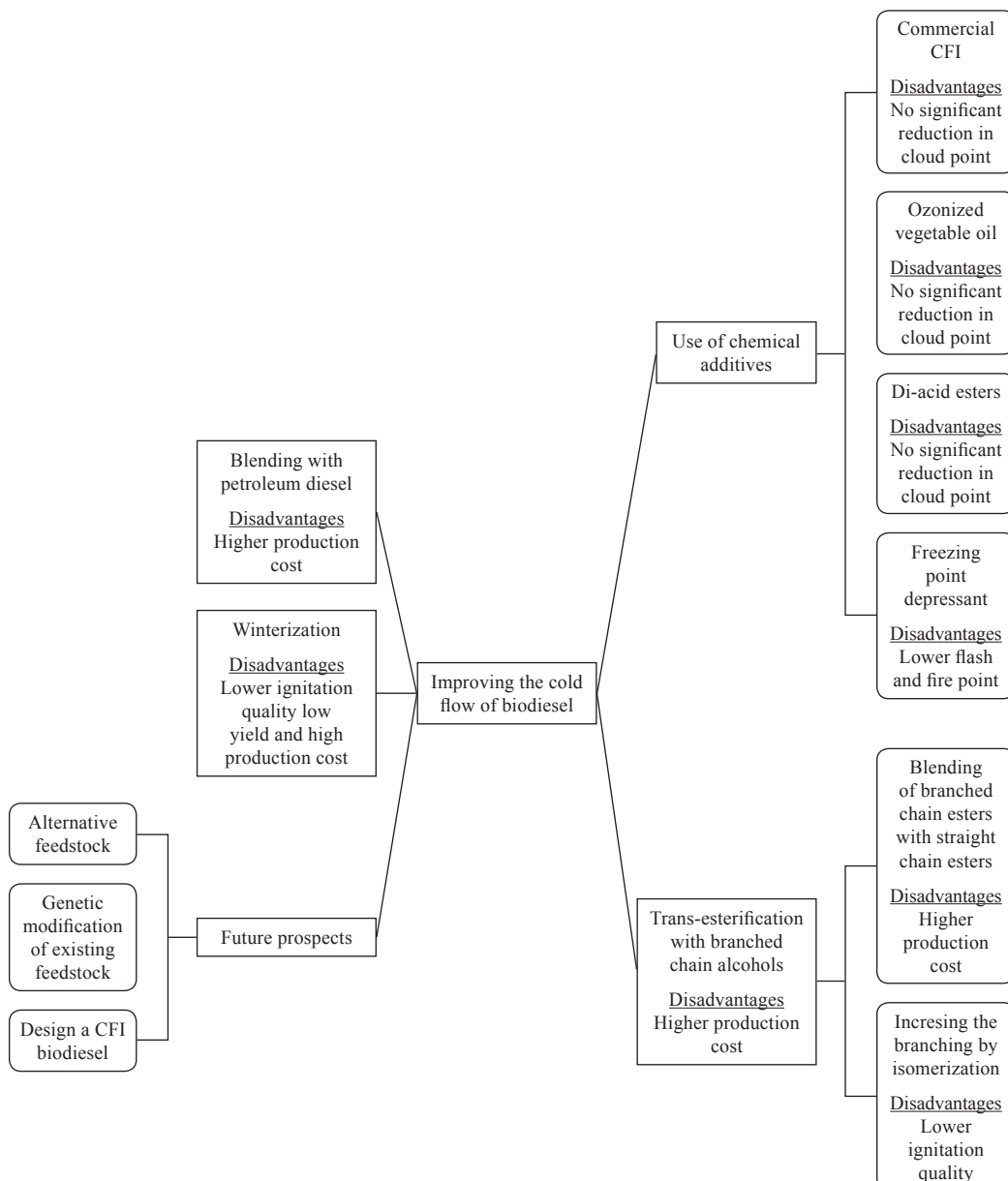
Bhale *et al.* (2009) studied the effect of ethanol, Lubrizol 7671 and kerosene on the cold flow properties of neat madhuca indica biodiesel (MME); Lubrizol 7671 is a pour point depressant developed by an American company named Lubrizol. From this study, it was observed that the cloud point was reduced by 10°C with 20% ethanol and 13°C with 20% kerosene, but there was no effect on the cloud point when blended with Lubrizol. Meanwhile, ethanol and kerosene reduced the flash and fire point of MME, and hence, higher blends should be discouraged. The ethanol-blended biodiesel also showed low NO<sub>x</sub> emissions and was in fact the lowest for the E20 blend.

#### *Modification of the Fatty Acid Profiles of Biodiesel*

More recently, Knothe (2009) proposed that modification of the fatty ester composition of biodiesel could improve its fuel properties, especially its cold flow properties. This modification could be by either genetic modification of the feedstock or the use of alternative feedstock. The production of biodiesels rich in short chain monounsaturated fatty acids, especially methyl oleate by genetic modifications of agricultural fats and oils, is highly desired (Krishna *et al.*, 2007). However, these genetic modifications should take into account the fact that these fats and oils are utilized not only for fuel production but also for food purposes and thus, a balance should be reached between the two purposes. Polyunsaturated fatty acids are healthier and more desirable for food purposes, and hence, the oil should contain both the monounsaturated and poly unsaturated fatty acids. Among other, a combination of 71% oleic acid and 21% lenoleic acid was suggested. For alternative feedstock, oleaginous algae and non-lipid sources like carbohydrates were suggested.

Further research into designing new chemical additives that would be effective with biodiesel should also be encouraged. Meanwhile, conventional cold flow improvers (CFI) for petroleum diesel are co-polymeric substances that have a paraffin backbone similar to the paraffin components of the diesel fuel with polar moieties attached to the backbone to give comb-like structures; the paraffin backbone provides for an interaction between the diesel and the additive, while the polar

moieties actively alter the shape of crystals that are formed during the nucleation process. The idea behind these CFIs can be a basis of the design of a similar compound which would work well with biodiesel. In addition, renewable chemical substances that can be blended with biodiesel to act as freezing point depressants for the esters in biodiesel may also be sought. *Fig. 2* shows a summary of the various methods employed to improve the cold flow of biodiesel and their disadvantages.



This is a summary of all the methods that have been employed to improve the cold flow of biodiesel.

*Fig. 2: The methods employed to improve the cold flow of biodiesel and their disadvantages*

## CONCLUSION

Biodiesel is a renewable alternative to petroleum diesel fuel; however, biodiesel crystallizes to form gel in cold weather, which causes fuel filter plugging in the compression ignition engine. Saturated, long and straight carbon chain esters have high melting points and when their composition in the biodiesel is high, crystallization tends to occur at a higher temperature. Reducing the composition of these saturated, long and straight carbon chain esters in the biodiesel will result in a better cold flow but will also cause a decrease in the ignition quality of the fuel of which the saturated fatty esters are responsible for. It is imperative that any improvement to the cold flow of the fuel does not sacrifice its good ignition quality. Towards this end, a desirable strategy would be to address the long and straight carbon chain issues and improve or retain the saturated carbon chain - the target being to significantly reduce the cloud point.

Blending with petroleum diesel reduces the impact of the high melting point and is a good immediate strategy, but it limits the amount of biodiesel in the blend. Meanwhile, winterization removes the saturated esters and reduces the ignition quality of the fuel. Trans-esterification with branched chain alcohol increases branched carbon chain and hence improves cold flow; however, it also increases the production cost of the fuel. So far, employing the existing chemical additives has only been able to reduce the pour point, not the cloud point. Further exploration into a more cost effective method of increasing the branching and the design of a new cold flow improver tailored for biodiesel is therefore desirable. Genetic modification of the existing feedstock should be parallel with the accompanying legalities of handling and processing of the products in order to avoid contamination of food stuff.

## REFERENCES

- ASTM Committee D-2 on Petroleum Products and Lubricants. (2003). *Analytical Chemistry*, 24(12), 2010-2013.
- Benjumea, P., Agudelo, J., & Agudelo, A. (2009). Effect of altitude and palm oil biodiesel fuelling on the performance and combustion characteristics of a HSDI diesel engine. *Fuel*, 88(4), 725–731.
- Bhale, P. V., Deshpande, N. V., & Thombre, S. B. (2009). Improving the low temperature flow properties of biodiesel fuel. *Renewable Energy*, 34(3), 6.
- Chiu, C. W., Schumacher, L. G., & Suppes, G. J. (2004). Impact of cold flow improvers on soybean biodiesel blend. *Biomass and Bioenergy*, 27(5), 485–491.
- Choo, Y. M., Ma, A. N., Basiron, Y., Yung, C. L., & Cheng, S. F. (2006). United States patent No. 20060288637.
- de Oliveira, J. S., Leite, P. M., de Souza, L. B., Mello, V. M., Silva, E. C., & Rubim, J. C. (2009). Characteristics and composition of *Jatropha gossypiifolia* and *Jatropha curcas* L. oils and application for biodiesel production. *Biomass and Bioenergy*, 33(3), 449–453.
- Demirbas, A. (2005). Biodiesel production from vegetable oils via catalytic and non-catalytic supercritical methanol transesterification methods. *Progress in Energy and Combustion Science*, 31(5–6), 466–487.
- Dunn, R. O. (2009a). Effects of minor components on cold flow properties and performance of biodiesel. *Progress in Energy and Combustion Science*, 35(6), 481–489.
- Dunn, R. O. (2009b). Cold-flow properties of soybean oil fatty acid monoalkyl ester admixtures†. *Energy & Fuels*, 23(8), 4082–4091.
- Dunn, R. (1999). Thermal analysis of alternative diesel fuels from vegetable oils. *Journal of the American Oil Chemists' Society*, 76(1), 109–115.

Factors Affecting the Cold Flow Behaviour of Biodiesel and Methods for Improvement – A Review

- Dunn, R., Shockley, M., & Bagby, M. (1996). Improving the low-temperature properties of alternative diesel fuels: Vegetable oil-derived methyl esters. *Journal of the American Oil Chemists' Society*, 73(12), 1719–1728.
- Dunn, R., & Bagby, M. (1995). Low-temperature properties of triglyceride-based diesel fuels: Transesterified methyl esters and petroleum middle distillate/ester blends. *Journal of the American Oil Chemists' Society*, 72(8), 895–904.
- Fernando, S., Karra, P., Hernandez, R., & Jha, S. K. (2007). Effect of incompletely converted soybean oil on biodiesel quality. *Energy*, 32(5), 844–851.
- Foon, C. S., Liang, Y. C., Dian, N. L. H. M., May, C. Y., Hock, C. C., & Ngan, M. A. (2006). Crystallisation and melting behaviour of methyl esters of palm oil. *American Journal of Applied Sciences*, 5(3), 1859–1863.
- Gunstone, F. D. (Ed.). (1996). *Fatty Acid and Lipid Chemistry*. Weinheim: Blackie Academic & Professional.
- Gunstone, F. D., Harwood, J. L., & Dijkstra, A. J. (Ed.). (2007). *The lipid handbook* (3<sup>rd</sup> ed.). New York: Tailor & Francis.
- Imahara, H., Minami, E., & Saka, S. (2006). Thermodynamic study on cloud point of biodiesel with its fatty acids composition. *Fuel*.
- Joelianingsih, Maeda, H., Hagiwara, S., Nabetani, H., Sagara, Y., & Soerawidjaya, T. H. (2008). Biodiesel fuels from palm oil via the non-catalytic transesterification in a bubble column reactor at atmospheric pressure: A kinetic study. *Renewable Energy*, 33(7), 1629–1636.
- Kleinová, A., Paligová, J., Vrbová, M., Mikulec, J., & Cvengros, J. (2007). Cold Flow Properties of Fatty Esters. *Process Safety and Environmental Protection*, 85(5), 390–395.
- Knothe, G. (2009). Improving biodiesel fuel properties by modifying fatty ester composition. *Energy and Environmental Science*, 2(7), 759–766.
- Knothe, G., Dunn, R., Shockley, M., & Bagby, M. (2000). Synthesis and characterization of some long-chain diesters with branched or bulky moieties. *Journal of the American Oil Chemists' Society*, 77(8), 865–871.
- Knothe, G., Van Gerpen, J., & Krahl, J. (Ed.). (2005). *The Biodiesel Handbook*. AOCS Press.
- Krishna, C. R., Thomassen, K., Brown, C., Butcher, T. A., Anjom, M., & Mahajan, D. (2007). Cold flow behaviour of biodiesels derived from biomass sources. *Industrial & Engineering Chemistry Research*, 46(26), 8846–8851.
- Lee, I., Johnson, L., & Hammond, E. (1995). Use of branched-chain esters to reduce the crystallization temperature of biodiesel. *Journal of the American Oil Chemists' Society*, 72(10), 1155–1160.
- Ma, F., & Hanna, M. A. (1999). Biodiesel production: A review. *Bioresource Technology*, 70(1), 1–15.
- Marangoni, A. G., & Narine, S. S. (Ed.). (2002). *Physical properties of lipids*. New York: Marcel Dekker, Inc.
- Moser, B. R., Cermak, S. C., & Isbell, T. A. (2008). Evaluation of castor and lesquerella oil derivatives as additives in biodiesel and ultralow sulfur diesel fuels. *Energy and Fuels*, 22, 1349–1352.
- Narváez, P. C., Rincón, S. M., Castañeda, L. Z., & Sánchez, F. J. (2008). Determination of some physical and transport properties of palm oil and of its methyl esters. *Latin American Applied Research*, 38, 1–6.
- Ramos, M. J., Fernández, C. M., Casas, A., Rodríguez, L., & Pérez, Á. (2009). Influence of fatty acid composition of raw materials on biodiesel properties. *Bioresource Technology*, 100(1), 261–268.
- Schnopf, R. (2006). *European union Biofuels policy and Agriculture: An Overview*.
- Serdari, A., Lois, E., & Stournas, S. (1999). Impact of esters of mono- and dicarboxylic acids on diesel fuel quality. *Industrial & Engineering Chemistry Research*, 38(9), 3543–3548.

- Sharma, Y. C., Singh, B. & Upadhyay, S. N. (2008). Advancements in development and characterization of biodiesel: A review. *Fuel*, 87(12), 2355–2373.
- Singh, S. P. & Singh, D. (2009). Biodiesel production through the use of different sources and characterization of oils and their esters as the substitute of diesel; A review. *Renewable and Sustainable Energy reviews*. In Press, Corrected Proof.
- Soni, H. P., Kiranbala, & Bharambe, D. P. (2008). Performance-Based Designing of Wax Crystal Growth Inhibitors. *Energy & Fuels*, 22(6), 3930-3938.
- Soriano, N. U., Migo, V. P. & Matsumura, M. (2006). Ozonized vegetable oil as pour point depressant for neat biodiesel. *Fuel*, 85(1), 25–31.
- Van Gerpen, J., Shanks, B., Pruszko, R., Clements, D., & Knothe, G. (2004). *Biodiesel Analytical Methods*. Colorado: National Renewable Energy Laboratory.
- Wang, P. S. (2007). *Isopropyl esters as solution to biodiesel challenges*. Unpublished Dissertation. University of Idaho: Idaho.
- Wu, W. H., Foglia, T., Marmer, W., Dunn, R., Goering, C., & Briggs, T. (1998). Low-temperature property and engine performance evaluation of ethyl and isopropyl esters of tallow and grease. *Journal of the American Oil Chemists' Society*, 75(9), 1173-1178.
- Xu, Y. X. & Hanna, M. A. (2009). Synthesis and characterisation of hazelnut oil-based biodiesel. *Industrial Crops and Products*, 29, 473-479.
- Yori, J. C., D'Amato, M. A., Grau, J. M., Pieck, C. L., & Vera, C. R. (2006). Depression of the Cloud Point of Biodiesel by Reaction over Solid Acids. *Energy & Fuels*, 20(6), 2721-2726.
- Yu-hui, G. & Ben-xian, S. (2006). QSAR Research of the Activity of Span Surfactants as Wax Antisettling Additives for Diesel. *Energy & Fuels*, 20(4), 1579-1583.

*Review Article*

## A Review on Robot Motion Planning Approaches

**S. H. Tang, W. Khaksar\*, N. B. Ismail and M. K. A. Ariffin**

*Department of Mechanical and Manufacturing Engineering,*

*Faculty of Engineering, University Putra Malaysia,*

*43400 Serdang, Selangor, Malaysia*

\*E-mail: [wkhie@yahoo.com](mailto:wkhie@yahoo.com)

### ABSTRACT

The ability of a robot to plan its own motion seems pivotal to its autonomy, and that is why the motion planning has become part and parcel of modern intelligent robotics. In this paper, about 100 research are reviewed and briefly described to identify and classify the amount of the existing work for each motion planning approach. Meanwhile, around 200 research were used to determine the percentage of the application of each approach. The paper includes comparative tables and charts showing the application frequency of each approach in the last 30 years. Finally, some open areas and challenging topics are presented based on the reviewed papers.

**Keywords:** Autonomy, intelligent robotics, robot motion planning

### INTRODUCTION

A fundamental need in robotics is to have the algorithms that convert high level specifications of tasks from human into low-level descriptions movements. The terms motion planning and trajectory planning are often used for these kinds of problems. A classic version of motion planning problem, which is sometimes referred to as the piano mover's problem, is defined as follows:

Let  $\beta$  be a robot system having  $k$  degree of freedom and free to move within two or three dimensional domain  $v$  which is bounded by various obstacles whose geometry is known to the system. The motion planning problem for  $\beta$  is, given the initial and desired final placements of the system  $\beta$ , to determine whether a continuous motion from the initial placement to the final one exists during which  $\beta$  avoids collision with the known obstacles, and if so, to plan such a motion (Halperin, 1994).

In this pure formulation of the problem, the only interest is on the geometric aspects of the motion and ignores many issues, such as acceleration, speed, uncertainty or incompleteness in the geometric data, control strategies for executing the motion, etc.

The basic issues and steps in any motion planning formulation are: Computation of Configuration, Object Representation, Approaches to Motion planning, Search Methods, and Local Optimization of motion (Hwang & Narendra, 1992).

From this early piano mover's problem, motion planning has evolved to address a huge number of variations on the problem, allowing applications in areas such as animation of digital characters, surgical planning, automatic verification of factory layouts, mapping of unexplored environments, navigation of changing environments, assembly sequencing, and drug design. New applications

---

Received: 6 July 2010

Accepted: 29 January 2011

\*Corresponding Author

bring new considerations that must be addressed in the design of motion planning algorithms. In this review, after surveying about 200 papers in the field, the amount of existing works were collected and classified for future analysis.

In the following sections, each group of approaches are firstly introduced, and this is followed by an analysis of the amount of usages of each approach through different time sections. Finally, based on the reviewed researches in the field of motion planning, the open areas and future challenges in this field are discussed.

## MATERIAL AND METHODS

A considerable amount of research is available in the field of robot motion planning approaches. The discipline was launched in mid 60's, but it was not until the work of Lozano and Wesley (1979) on spatial planning that motion planning drew most researchers' attention. The current developed methods are variations of a few general approaches, such as Bug Algorithms, Roadmap, Cell Decomposition, Potential Fields, Sampling-based motion planning, Kalman filtering, Heuristic Approaches and, Mathematical programming. These methods are not necessarily mutually exclusive, and their combination is often used in developing a motion planner (Masehin & Amin Naseri, 2004; Dongbin & Jianqiang, 2006). After surveying a total of 198 papers in the field (from 1980 to 2010), the amount of existing works for each approach was identified and classified. In total, ninety seven papers were used to briefly describe each approach. The following sections introduce each of these approaches and mention the most important works of each one.

### *Bug Algorithm*

Even a simple planner can present interesting and difficult issues. The Bug1 and Bug2 algorithms (Lumelsky & Stepanov, 1987) are among the earliest and simplest sensor-based planners with provable guarantees. These algorithms assume the robot is a point operating in the plane with a contact sensor or a zero range sensor to detect obstacles. When the robot has a finite range (non-zero range) sensor, the Tangent Bug algorithm (Kamon *et al.*, 1996) is a Bug derivative that can then use that sensor information to find shorter paths to the goal. The Bug and Bug-like algorithms are straightforward to implement. Moreover, a simple analysis shows that their success is guaranteed, when possible. These algorithms require two behaviours; namely, Motion to the Goal and Boundary Following. It has been proven that the path length in Bug 1 and Bug 2 has the following condition:

$$L_{\text{Bug1}} \leq d(q_{\text{start}}, q_{\text{goal}}) + 1.5 \sum_{i=1}^n p_i$$

$$L_{\text{Bug2}} \leq d(q_{\text{start}}, q_{\text{goal}}) + 0.5 \sum_{i=1}^n n_i p_i$$

Where,  $d(q_{\text{start}}, q_{\text{goal}})$  is the Euclidian distance between the start and goal,  $p_i$  is the perimeter of the  $i_{\text{th}}$  obstacle,  $n$  is the number of obstacles, and  $n_i$  is the number of the intersection between M-line and the  $i_{\text{th}}$  obstacle.

A Performance Comparison of Bug Navigation Algorithms is provided in James and Bräunl (2007).

### *Potential Fields*

The Potential Fields concept shown in *Fig. 1* (Choset *et al.*, 2005) was first introduced by Oussama Khatib (1986). A potential function is a differentiable real-valued function  $U : \mathbb{R}^m \rightarrow \mathbb{R}$ . The value

of a potential function can be viewed as energy and hence, the gradient of the potential is force. The gradient is a vector which points in the direction that locally maximally increases  $U$ .

$$\nabla U(q) = DU(q)^T = \left[ \frac{\partial U}{(\partial q_1)(q)}, \dots, \frac{\partial U}{(\partial q_m)(q)} \right]^T$$

A robot in the potential field method is treated as a point that is represented in the configuration space as a particle under the influence of an artificial potential field  $U$  whose local variations reflect the structure of the free space.

The potential function can be defined over free space as the sum of an Attractive potential pulling the robot towards the goal configuration and a Repulsive potential pushing the robot away from the obstacles (Latombe, 1991).

$$U(q) = U_{att}(q) + U_{rep}(q)$$

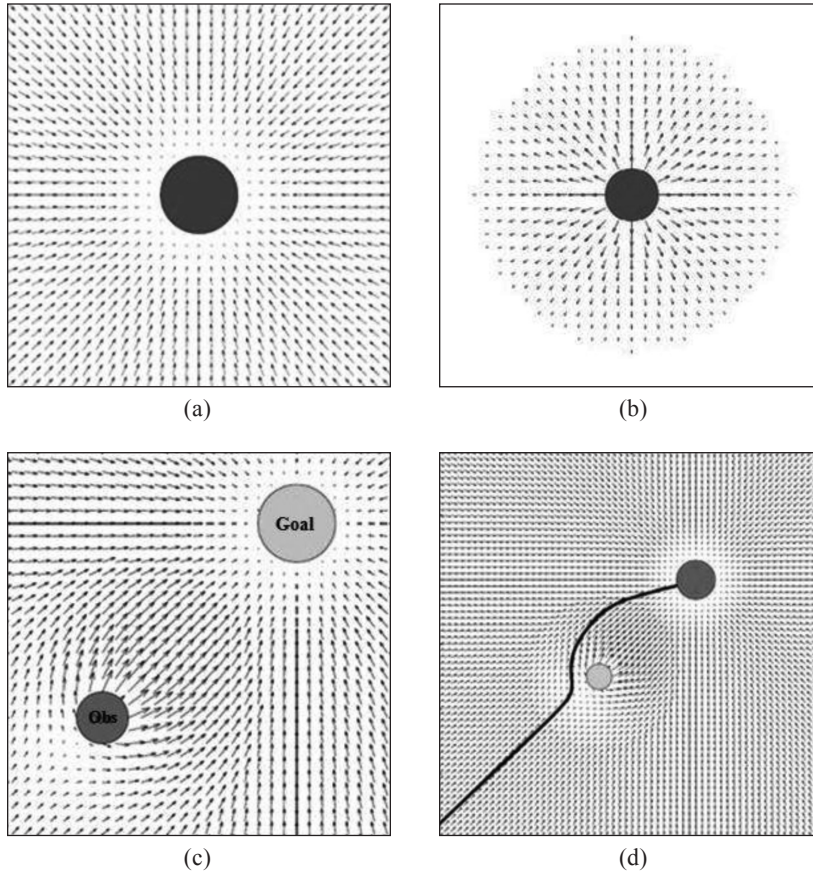


*Fig. 1: Potential Fields, (a) Attractive Potential field near the goal, (b) Repulsive potential field near the obstacles, (c) Interaction between attractive and repulsive potential fields, and (d) the final path.*

The attractive ( $U_{att}(q)$ ) and repulsive ( $U_{rep}(q)$ ) potential functions can be formulized as follows:

$$U_{att}(q) = \frac{1}{2} \zeta d^2(q, q_{goal})$$

$$(U_{rep}(q)) = \begin{cases} \frac{1}{2} \eta \left( \frac{1}{D(q)} - \frac{1}{Q^*} \right)^2, & D(q) \leq Q^* \\ 0, & D(q) \geq Q^* \end{cases}$$

Where  $\zeta$  is a parameter used to scale the effect of the attractive potential, the  $Q^* \in R$  factor allows the robot to ignore obstacles sufficiently far away from it and  $\eta$  can be viewed as a gain on the repulsive gradient.

Due to its low computational costs, the potential Fields method remains as a major path planning approach, especially when a high degree of freedom is involved (Hwang & Narendra, 1992).

### *Roadmaps*

In the roadmap approach, the free Configuration space ( $C_{free}$ ), i.e. the set of feasible motions, is retracted, reduced to, or mapped onto a network of one-dimensional lines. This particular approach is also called the retraction, skeleton, or highway approach. The search for a solution is limited to the network, and motion planning becomes a graph-searching problem. In this approach, motion planning is done in three steps; first, the robot is moved from its starting configuration to a point on the roadmap, using a canonical method; second, the robot is moved from goal configuration to a point on the roadmap likewise; and third, the two points on the roadmap are connected using lines in the roadmap. The roadmap must represent all topologically distinct feasible paths in C-space (Hwang & Narendra, 1992). Otherwise, the motion planning algorithm is not complete. The well-known roadmaps are Visibility graph (Asano *et al.*, 1985), Voronoi diagram (Osamu, 1989), Silhouette (Canny, 1988), Cell Decomposition (Keil & Sack, 1985), and the Subgoal Network (Faverjon & Toumassoud, 1987) (Fig. 2).

### *Sampling-Based Motion Planning*

The Probabilistic Roadmap planner (PRM) (Kavraki *et al.*, 1996) demonstrated the tremendous potential of the sampling-based methods. PRM fully exploits the fact that it is cheap to check whether or not a single robot configuration is in  $Q_{free}$ . PRM creates a roadmap in  $Q_{free}$ . It uses rather coarse sampling to obtain the nodes of the roadmap and very fine sampling to obtain the roadmap edges, which are the free paths between node configurations. After the roadmap has been generated, planning queries can be answered by connecting the user-defined initial and goal configurations to the roadmap and using the roadmap to solve the path-planning problem at hand. Initially, node sampling in PRM was done using a uniform random distribution. This planner is called basic PRM. It was observed that random sampling worked very well for a wide variety of problems (Owermars & Svestka, 1995) and ensured the probabilistic completeness of the planner (Kavraki *et al.*, 1998). However, it was also observed by Kavraki (1995) that random sampling is only a baseline sampling for PRM and many other sampling schemes are useful and also bound to be efficient for many planning problems as the analysis of the planner revealed. Today, these sampling schemes range from importance sampling in areas that during the course of calculations are found difficult to explore, to deterministic sampling such as quasirandom sampling and sampling on a grid.

PRM was conceived as a multiple-query planner. When PRM is used to answer a single query, some modifications are made: the initial and goal configurations are added to the roadmap nodes

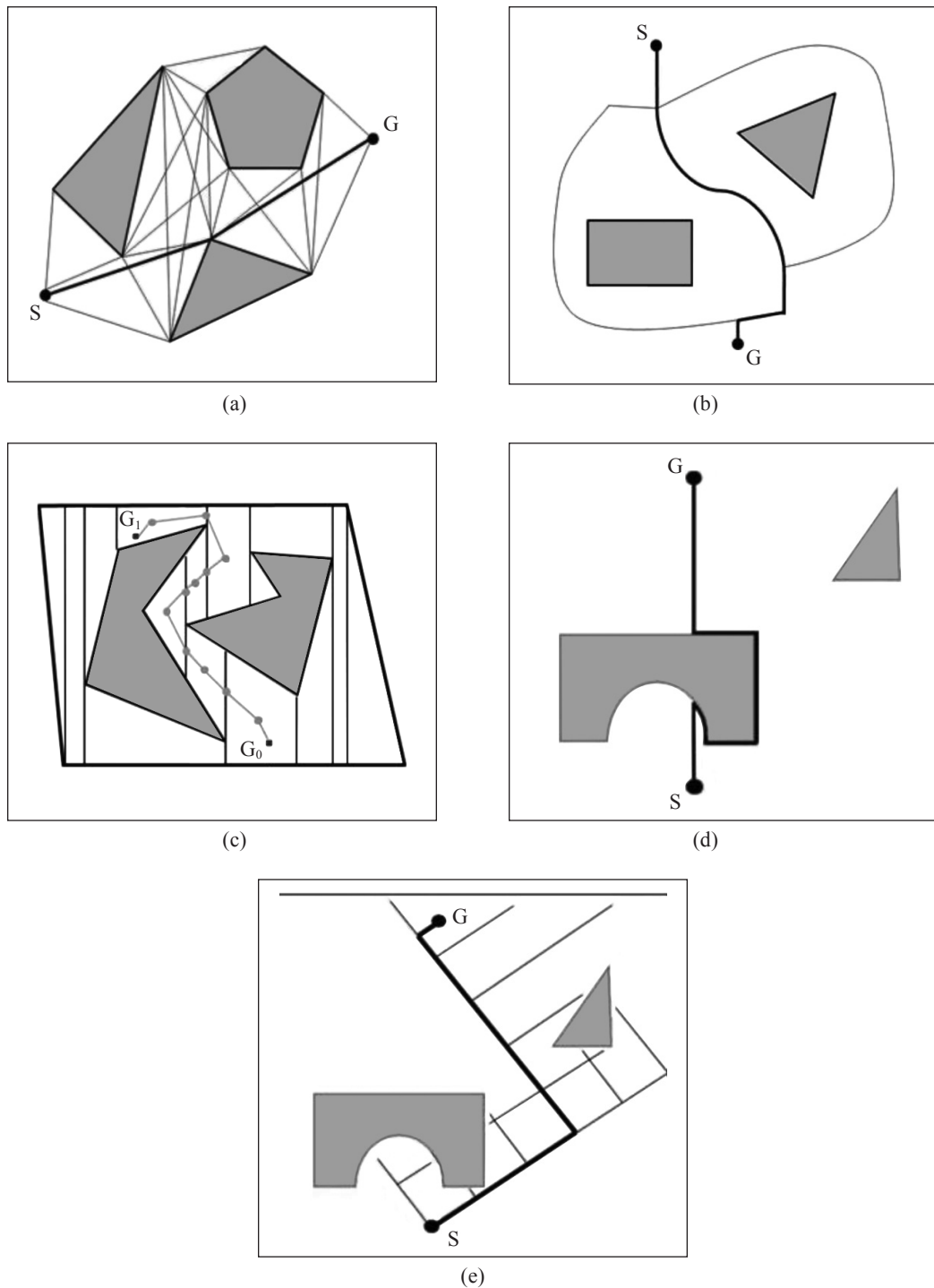


Fig. 2: Roadmaps; (a) Visibility graph, (b) Voronoi diagram, (c) Cell decomposition, (d) Silhouette, (e) Subgoal networks

and the construction of the roadmap is done incrementally and stopped when the query at hand can be answered. However, PRM may not be the fastest planner to be used for single queries. There are some other sampling-based planners that are particularly effective for single-query planning, including the Expansive-Spaces Tree planner (EST) (Hsu, 2000) and the Rapidly-exploring Random Tree planner (RRT) (Kuffner & LaValle, 2000). These planners exhibit excellent experimental performance.

A combination of the above methods is also possible and desirable in many cases. The Sampling-Based Roadmap of Trees (SRT) planner (Bekris *et al.*, 2003) constructs a PRM-style roadmap of single-query-planner trees. It has been observed that for very difficult path planning problems, single-query planners need to construct large trees in order to find a solution. In some cases, the cost of constructing a large tree may be higher than the cost of constructing a roadmap of with SRT. This illustrates the distinction between the multiple-query and single-query planning, and its importance.

Despite their simplicity, which is exemplified in the basic PRM planner, the sampling-based planners are capable of dealing with robots with many degrees of freedom and with many different constraints. Among other, the sampling-based planners can take into account kinematic and dynamic constraints (Hsu *et al.*, 2002), closed-loop kinematics (Han & Amato 2001), stability constraints (Kuffner *et al.*, 2001), reconfigurable robots (Fitch *et al.*, 2003), energy constraints (Lamiraux & Kavaraki 2001), contact constraints (Ji & Xiao, 2001), visibility constraints (Danner & Kavaraki 2000) and others. Clearly, some planners are better at dealing with specific types of constraints than the others. For example, EST and RRT planners are particularly useful for problems that involve kinematic and dynamic constraints.

Meanwhile, PRM, EST, RRT, SRT, and their variants have changed the way path planning is performed for high-dimensional robots. They have also paved the way for the development of planners for problems beyond basic path planning (Choset *et al.*, 2005).

### *Kalman Filtering*

Heretofore, the planner has been assumed to have the access to either an exact geometric description of its environment or a suite of sensors (e.g. sonar) that provide perfect information about the environment. In this part, cases for which the robot's knowledge of the world derives from measurements provided by imperfect, noisy sensors are first to be considered. The Kalman filter is one of the most useful estimation tools available today. In other words, the Kalman filtering provides a recursive method of estimating the state of a dynamical system in the presence of noise (Maybeck, 1990). A key feature of the Kalman filter is that it simultaneously maintains the estimates of both the state vector and the estimate error covariance matrix ( $P$ ) which are equivalent to saying that the output of a Kalman filter is a Gaussian probability density function ( $PDF$ ) with the mean and covariance  $P$ . In the context of localization, the Kalman filter output is then a distribution of likely robot positions instead of a single position estimate. As such, the Kalman filter is a specific example of a more general technique known as the probabilistic estimation techniques (Choset *et al.*, 2005).

### *Mathematical Programming*

The mathematical programming approach represents the requirement of obstacle avoidance with a set of inequalities on the configuration parameters. Motion planning is then formulated as a mathematical optimization problem that finds a curve between the start and goal configurations minimizing a certain scalar quantity. Since such an optimization is non-linear and has many inequality constraints, a numerical method is used to find the optimal solution. Reiswijk *et al.* (1992)

implemented a method of planning geometrical trajectories for two cooperating robots in an assembly cell. A trajectory of robot joints in joint-interpolated space is partitioned into separate convex or concave sub-paths by Sinha and Ho (1992). In this way, they abstract the trajectory in such a way that it becomes smoother for piecewise trajectories, and the information amount required to describe a path reduces drastically. Delaplace *et al.* (1992) implemented vision-sensor-based information to a real world tricycle robot. A closed-loop control system is used to maintain the distance of the robot and a straight or curved trajectory. Papanikolopoulos and Khoshla (1992) suggested a method to solve the robotic visual tracking problem by combining linear quadratic Gaussian control technique with the optical flow technique of vision-based motion tracking. Meanwhile, Sinha and Benmounah (1992) computed a safe path from the start to goal points by applying the trigonometric calculations of angles, along with the steering wheel of the robot which must be orientated. Reiswijk *et al.* (1992) proposed a new approach to optimize pre-calculated trajectories in joint space. They focused on a simultaneous integration of time-optimal curve, and thus benefited from a parallel execution which reduced computational time. An initial path which possibly has collision with obstacles is iteratively improved by performing a dynamic programming search in a sub-manifold of the C-space containing the current path in (Barraquand & Ferbach, 1993). Gifford and Murphy (1996) applied dynamic programming by triangulating the workspace and finding the shortest paths through vertex-nodes. Habibi *et al.* (2007) presented a novel algorithm for path planning of point robots in 2D known environment using binary integer programming.

### *Heuristic Approaches*

The aforementioned conventional approaches suffer from many drawbacks, such as high time complexity in high dimensions, and trapped in local minima, which make them inefficient in practice. On the other hand, it is proven that the path planning problem is NP-complete (Canny, 1988). Therefore, probabilistic algorithms have been developed, including Probabilistic Roadmaps and Rapidly-exploring Random Trees, with high-speed implementation as their major advantages. Other related approaches in motion planning are Level set and Linguistic Geometry. To fix the local minima problem, many heuristic and Meta-heuristic algorithms are used in motion planning, such as the combination of the Simulated Annealing technique and Potential Fields. Other related approaches include Neural Network (Zhu & Yang, 2006), Genetic Algorithms (Quingfu *et al.*, 2007), Simulated Annealing (Manousakis *et al.*, 2005), Ant Colony Optimization (Mohamad *et al.*, 2006), Particle Swarm Optimization (Saska *et al.*, 2006), Stigmergy (Cazangi *et al.*, 2006), Wavelet Theory (Pai & Reissel, 1998), Tabu Search (Masehian & Amin Naseri, 2004) and Fuzzy Logic (Lee & Wu, 2003). Heuristic algorithms do not guarantee to find a solution, but if they do, are likely to do so much faster than deterministic methods.

## **RESULTS AND DISCUSSIONS**

A total of ninety seven papers were surveyed in this research, covering a sufficient depth of works in the robot motion planning field for the time span of 1980 to 2010. One hundred and ninety eight papers were considered so as to provide different comparisons among these approaches. At the same time, the researchers also tried to bring together major applications of conventional and heuristic techniques in the literature and to come to conclusions about the nature and the course of research in motion planning discipline. The motion planning algorithms were started by some simple methods, and after a while, some more complex methods were also developed. After that, the heuristic methods were developed to increase the effectiveness and efficiency of the solutions. As illustrated in *Fig. 3* (considering a total of 198 papers), the application of the heuristic methods

was increased due to their success in coping with the problems of combinatorial explosion and local minima. As shown in *Fig. 3*, the 80<sup>th</sup> decade was the climax period for the conventional methods and, the appearance period for the heuristic methods. Meanwhile, the 90<sup>th</sup> decade was the descent time for the conventional approaches and improvement of the heuristic ones. The last 10 years (2001-2010) were the climax period for the heuristic methods, and the appearance period for the compound and meta-heuristic methods. Some studies which are in this field include those by Masehian and Amin Naseri (2004) and Dongbin and Jianqiang (2006). It seems that in the near future, the application of the heuristic approaches will decline, whereas the application of the compound and meta-heuristic methods will improve in order to achieve some better solutions in shorter time and lesser cost, but with more effectiveness and efficiency.

Tables 1-3 and *Fig. 4-5* represent the percentage of each approach and compare these approaches together. In total, about 25% of the papers are related to conventional approaches and 75% to heuristic approaches. The severe different between the portions of the conventional and heuristic methods indicates the rate of interest to the heuristic methods, according to their ability to decrease the time and error.

Table 1 (considering a total of 198 papers) shows the portions of the surveyed major methods in detail. As given in Table 1, it is indicated that research were mostly done in the fields of fuzzy logic, neural networks and genetic algorithms, whereas fewer studies were conducted in the areas of visibility graph and cell decomposition.

Table 2 and *Fig. 4* (considering a total of 50 papers in the field of Conventional approaches) provide a more detailed analysis on the conventional approaches and their relative application in robot motion planning. As presented in this table, about 32% of the research was done in the field of mathematical programming.

Table 3 and *Fig. 5* (considering a total of 148 papers in the field of heuristic approaches) show a more detailed analysis on the heuristic approaches and their relative application in robot motion

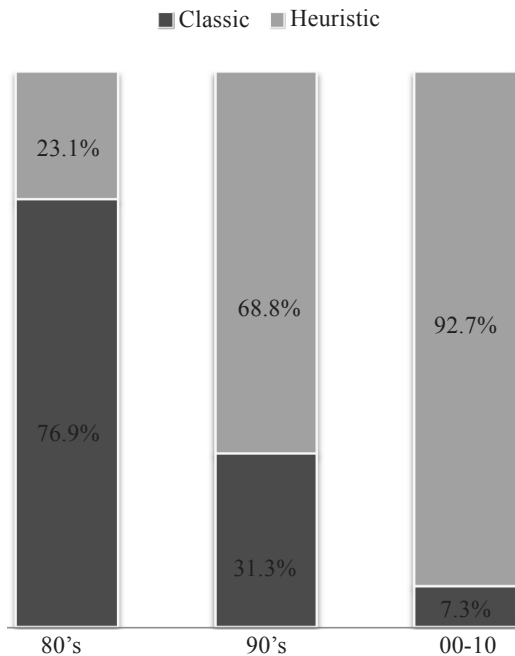


*Fig. 3: A Comparison of the conventional and heuristic algorithms*

A Review on Robot Motion Planning Approaches

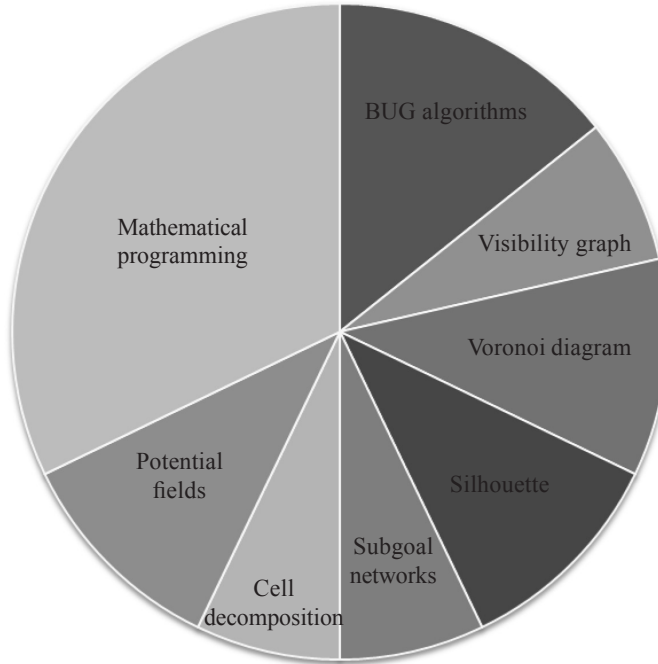
TABLE 1  
A Comparison of major motion planning approaches

Approach	10 year periods (from 1980 up to now)			Total
	80's (%)	90's (%)	00-10 (%)	
BUG algorithms	18.18	2.13	2.50	3.92
Visibility graph	9.09	2.13	0.00	1.96
Voronoi diagram	18.18	0.00	2.50	2.94
Silhouette	18.18	2.13	0.00	2.94
Subgoal networks	9.09	2.13	0.00	1.96
Cell decomposition	9.09	2.13	0.00	1.96
Potential fields	9.09	4.26	0.00	2.94
Mathematical programming	0.00	17.02	2.50	8.82
Neural networks	9.09	14.89	12.50	12.75
Genetic algorithm	9.09	12.77	15.00	12.75
Simulated annealing	0.00	6.38	5.00	4.90
Ant colony optimization	0.00	6.38	12.50	7.84
Particle swarm optimization	0.00	4.26	12.50	5.88
Stigmergy	0.00	2.13	5.00	2.94
Wavelets	0.00	4.26	2.50	2.94
Tabu	0.00	4.26	2.50	3.92
Fuzzy	9.09	14.89	27.50	18.63

TABLE 2  
Conventional approaches in motion planning

Approach	80's (%)	90's (%)	00-10 (%)	Total (%)
BUG algorithms	20	0.7	33	14.3
Visibility graph	10	0.7	0	7.1
Voronoi diagram	10	0	33	10.7
Silhouette	10	0.7	0	10.7
Subgoal networks	10	0.7	0	7.1
Cell decomposition	10	0.7	0	7.1
Potential fields	10	1.4	0	10.7
Mathematical programming	0	95.1	33	32.1
Total	100	100	100	100

planning. It is important to note that the Fuzzy logic is the most researched approach in the field. The complexities of the modern systems emphasize the type of imprecision rather than randomness. Even in a fully automated system, the critical parametric changes have to be made by a human expert, who usually expresses his control and diagnostic strategies linguistically as a set of heuristic decision rules. Fuzzy logic, as a mathematical tool to handle uncertainties, has been used to model the systems that are hard to define precisely. As a methodology, the fuzzy set theory incorporates imprecision and subjectivity into the model formulation and solution process. Therefore, the fuzzy logic has the most portions among the heuristic methods for robot motion planning.



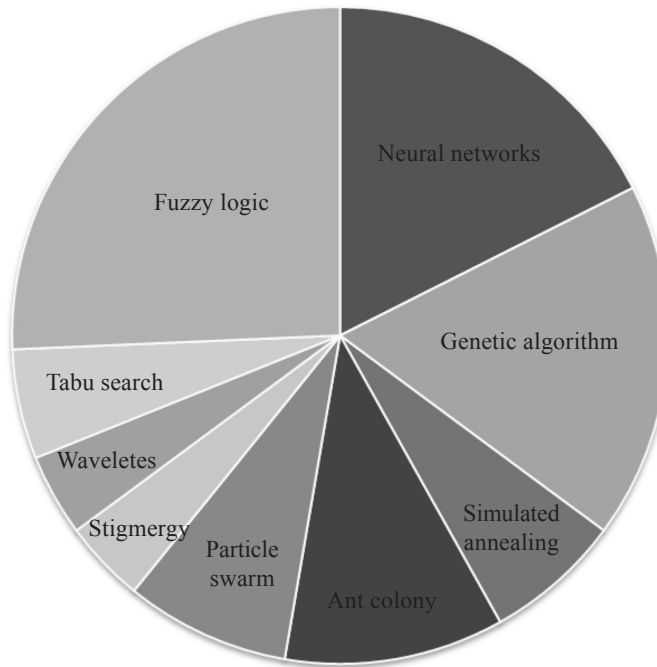
*Fig. 4: The portion of each conventional approach*

TABLE 3  
Heuristic approaches in motion planning.

Approach	80's (%)	90's (%)	00-10 (%)	Total (%)
Neural networks	33.3	21.2	13.2	17.6
Genetic algorithm	33.3	18.2	15.8	17.6
Simulated annealing	0.0	9.1	5.3	6.8
Ant colony optimization	0.0	9.1	13.2	10.8
Particle swarm optimization	0.0	6.1	13.2	9.5
Stigmergy	0.0	3.0	5.3	4.1
Wavelets	0.0	6.1	2.6	4.1
Tabu search	0.0	6.1	2.6	4.1
Fuzzy logic	33.3	21.2	28.9	25.7
Total	100	100	100	100

### CURRENT ISSUES AND CHALLENGES IN THE FIELD OF MOTION PLANNING

According to the papers that were reviewed in this paper and the comparisons made between the different approaches in the field of robot motion planning, it is clear that some algorithms are more useful, and thus, there are better opportunities to do some research about them. As shown in Tables 1-3, these approaches are fuzzy logic, neural networks, genetic algorithm and mathematical programming. On the other hand, it seems that each approach, especially the conventional ones,



*Fig. 5: The portion of each heuristic approach*

suffer from many drawbacks. In order to improve the efficiency of these approaches, one of the best ways is to combine some of them together.

The overall paradigm of the most practical motion planners has seven main elements (Ahirkenciekh & Seireg, 1994), namely, Discretization of configuration space, Collision detection, Search Mechanism, Uncertainty, Completeness, Time and Local minima. There are some areas in motion planning which seem to have come to an end. For example, Potential-fields-Based approaches are well understood and that one should not simply report yet another minor variant of it, unless, of course, it has some significant contribution as is the case with harmonic potentials (Gupta & Del Pobil, 1998).

After analyzing the existing researches in the field of motion planning, the following new intellectual challenges, new applications, and emerging issues for motion planning are proposed:

- A crucial open issue: How does motion planning interact with perception and control modules? How can we merge the geometric model-based approaches with the reactive sensor-based approaches?
- Dealing with a partially unknown environment calls for the use of input from the real world. Online sensor-based motion planning should integrate vision and motion planning. This raises another important issue, i.e., How do we combine sensing with motion planning in an incremental way? This issue has recently received some attention.
- The new emerging field of micro-scale robots will present fertile ground and novel issues for motion planning research. At such microscopic scales, thermodynamical laws will need to be taken into account.

- New applications should be explored to keep this field alive. The motion planning-type algorithms have a great application potential in virtual prototyping, mechanical design and ergonomics. CAD tools are becoming increasingly inexpensive and common. There are possible applications of the motion planning-type algorithms in consumer technology, including computer animation and virtual reality.
- The advent of the so-called service robotics applications poses new major challenges. Since planning is a prediction of the future, dealing with incompleteness, error in information robustness in uncertainty will become key issues in practical motion planning.
- Since motion planning is just a part of the humans interaction system with the world, an open future direction is how to integrate motion planning approaches with the other related problems, such as grasp planning, manipulation, and fine motion planning.

Each of the existing approaches for the motion planning has its own advantages and drawbacks. This is because each algorithm is for a specific goal and considers the priority among different performance criteria. There are several measures for the performance of an algorithm, such as time for path traversal, velocity of manipulator links or joint, energy, actuator forces and proximity of obstacles. A mathematical comparison between the time complexity and path length of some of the main algorithms is provided in Table 4.

TABLE 4  
A mathematical comparison

Approach	Advantage	Disadvantage
Potential fields	Real-Time	Not complete
Cell decomposition	Complete, Sound	Heavy computation, time
Visibility graph	Complete and yields minimum length paths	Heavy computation, generates semi-free paths to the obstacles, time
Voronoi diagram	Complete and generates roadmap with maximum distance	Possibly inefficient paths, time
Heuristic approaches	Less time, parallel search	Not complete, not sound
Exact cell decomposition	Complete	Heavy computation, time
Approximate cell decomposition	Sound and useful when only a coarse representation of workspace is available	Not complete
Bug 1	Complete	Long paths, time
Bug 2	Complete	Long paths, time

## CONCLUSION

In this paper, after analyzing about 150 papers in the field of robot motion planning approaches, the amount of the existing works for each approach has been identified and classified. This paper divides the motion planning algorithms into two major groups, namely, the Conventional Approaches and Heuristic Approaches. The conventional approaches are BUG Algorithms, Roadmap, Cell Decomposition, Potential Fields, and, Mathematical programming, whereas the heuristic approaches include the Neural Network, Genetic Algorithms, Particle Swarm Optimization,

## A Review on Robot Motion Planning Approaches

Ant Colony, Stigmergy, Wavelet Theory, Fuzzy Logic and Tabu Search. After a brief introduction of each approach, the important works in each field were presented. A complete discussion of the portion of each approach in the field of robot motion planning is also presented, including different comparative figures and charts.

## REFERENCES

- Ahrikencheikh, C., & Seireg, A. (1994). *Optimized Motion Planning: Theory and Implementation*. Wiley-Interscience Publication.
- Asano, T., Asano, T., Guibas, L., Hershberger, J., & Imai, H. (1985, 21-23 Oct. 1985). *Visibility-polygon search and euclidean shortest paths*. Paper presented at the Foundations of Computer Science, 1985., 26th Annual Symposium on.
- Barraquand, J., & Ferbach, P. (1993). *Path Planning Through Variational Dynamic Programming*. Paris Research Laboratory, Research Report #33.
- Bekris, K. E., Chen, B., Ladd, A., Plaku, E., & Kavraki, L. E. (2003). Multiple query motion planning using single query primitives. *IEEE/RSJ International Conference on Intelligent Robots and Systems*, 656–661.
- Canny, J. F. (1988). *The Complexity of Robot Motion Planning*. Cambridge, Massachusetts: MIT Press.
- Cazangi, R. R., Von Zuben, F. J., & Figueiredo, M. F. (2006). *Evolutionary Stigmergy in Multipurpose Navigation Systems*. Paper presented at the Evolutionary Computation, 2006. CEC 2006. IEEE Congress on.
- Choset, H., Lynch, K. M., Hutchinson, S., Kantor, G., Burgard, W., Kavraki, L. E., & Thrun, S. (2005). *Principles of Robot Motion: Theory, Algorithms, and Implementation*, Cambridge, Massachusetts, MIT Press.
- Danner, T., & Kavraki, L. E. (2000). *Randomized planning for short inspection paths*. Paper presented at the Robotics and Automation, 2000. Proceedings. ICRA '00. IEEE International Conference on.
- Delaplace S., Blazevic P., Fontaine J. G., Pons N., & Rabit J. (1992). Trajectory Tracking for Mobile Robot. In *Robotic Systems Tzafestas S. G.* (Eds.). Netherlands: Kluwer Academic Publishers, 313-320.
- Dongbin, Z., & Jianqiang, Y. (2006). Robot Planning with Artificial Potential Field Guided Ant Colony Optimization Algorithm. *ICNC 2006, Part II, LNCS 4222*, Springer-Verlag Berlin Heidelberg, 222 – 231.
- Faverjon, B., & Tournassoud, P. (1987). A local approach for path planning of manipulators with a high number of degrees of freedom. In *Proceeding of IEEE International Conference on Robotics and Automation*, 1152-1159.
- Fitch, R., Butler, Z., & Rus, D. (2003). Reconfiguration planning for heterogeneous self-reconfiguring robots. In *IEEE/RSJ International Conference on Intelligent Robots and Systems*.
- Gifford, K., & Murphy, R. (1996). Incorporating Terrain Uncertainties in Autonomous Vehicle Path Planning. In *Proceeding of IEEE/RSJ International Conference on Intelligent Robots and Systems*, Osaka Japan (p. 1134-1140).
- Gupta, K., & Del Pobil, A. P. (1998). *Practical Motion Planning in Robotics*. John Wiley & Sons.
- Habibi, G., Masehian, E., & Beheshti, M. T. H. (2007, 5-8 Nov. 2007). *Binary Integer Programming Model of Point Robot Path Planning*. Paper presented at the Industrial Electronics Society, 2007. IECON 2007. 33rd Annual Conference of the IEEE.
- Halperin, D. (1994). Robot Motion Planning and the single cell problem in arrangements. *Journal of Intelligent and Robotics Systems*, 11(1994), 45-65.

- Han, L., & Amato, N. M. (2001). A kinematics-based probabilistic roadmap for closed chain systems. In B. R. Donald, K. Lynch, and D. Rus (eds.). *New Directions in Algorithmic and Computational Robotics*, 233–246, AK Peters.
- Hsu, D. (2000). *Randomized Single-Query Motion Planning In Expansive Spaces*. PhD Thesis, Department of Computer Science, Stanford University.
- Hsu, D., Kindel, R., Latombe, J. C., & Rock, S. (2002). Randomized kinodynamic motion planning with moving obstacles. *International Journal of Robotics Research*, 21(3), 233–255.
- Hwang Yong K., & Ahuja Narendra. (1992). Gross Motion Planning- A Survey. *ACM Computing Surveys*, 24(3), 219-291.
- James, N.G., & Bräunl, T. (2007). Performance Comparison of Bug Navigation Algorithms, *Journal of Intelligent and Robotic Systems*, 50, 73-84.
- Ji, X., & Xiao, J. (2001). Planning motion compliant to complex contact states. *International Journal of Robotics Research*, 20(6), 446–465.
- Kamon, R. E., & Rimon, E. (1996) .A new range-sensor based globally convergent navigation for mobile robots. In *IEEE Int'l. Conf. on Robotics and Automation*, Minneapolis, MN.
- Kavraki, L. E. (1995). *Random Networks in Configuration Space for Fast Path Planning*. PhD thesis, Stanford University.
- Kavraki, L. E., Latombe, J. C., Motwani, R., & Raghavan, P. (1998). Randomized query processing in robot path planning. *Journal of Computer and System Sciences*, 57(1), 50–60.
- Kavraki, L. E., Švestka, P., Latombe, J. C., & Overmars M. H. (1996). Probabilistic roadmaps for path planning in high-dimensional configuration spaces. *IEEE Transactions on Robotics and Automation*, 12(4), 566–580.
- Keil J. M., & Sack J R. (1985). Minimum decomposition of polygonal objects, Computational Geomeometry, 197-216.
- Khatib, O. (1986). Real-Time Obstacle Avoidance for Manipulators and Mobile Robots, *International Journal of Robotics Research*, 5 (1), 90-99.
- Kuffner, J. J., & LaValle, S M. (2000). RRT-connect: An efficient approach to single-query path planning. In *IEEE International Conference on Robotics and Automation* (p. 995–1001).
- Kuffner, J., Nishiwaki, K., Kagami, S., Inaba, M., & Inoue, H. (2001). *Motion planning for humanoid robots under obstacle and dynamic balance constraints*. Paper presented at the Robotics and Automation, 2001. Proceedings 2001 ICRA. IEEE International Conference on.
- Lamiraux, F., & Kavraki, L. E. (2001). Planning paths for elastic objects under manipulation constraints. *International Journal of Robotics Research*, 20(3), 188–208.
- Latombe, J. C. (1991). *Robot Motion Planning*. London: Kluwer Academic Publishers.
- Lozano-Perez, T., & Wessley, M. A. (1979). An algorithm for planning collision-free paths among polyhedral obstacles. *Communications of the ACM*, 22(10), 560-570.
- Lumelsky, V., & Stepanov, A. (1987). Path planning strategies for point mobile automaton moving amidst unknown obstacles of arbitrary shape. *Algorithmica*, 2, 403–430.
- Manousakis, K., McAuley, T., Morera, R., & Baras, J. (2005, 13-16 June 2005). *Using multi-objective domain optimization for routing in hierarchical networks*. Paper presented at the Wireless Networks, Communications and Mobile Computing, 2005 International Conference on.

## A Review on Robot Motion Planning Approaches

- Masehian, E., & Amin Naseri, M. R. (2004). A Tabu Search based Approach for Online Motion Planning. *Journal of Robotic Systems*, 21(6), 275-300.
- Masehian, E., & Amin Naseri, M. R. (2004). A voronoi diagram-visibility graph-potential fields compound algorithm for robot motion. *Journal of Robotic Systems*, 21(6), 275-300.
- Maybeck, P. (1990). The Kalman filter: An introduction to concepts. In *Autonomous Robot Vehicles*. Springer verlag.
- Mohamad, M. M., Taylor, N. K., & Dunnigan, M. W. (2006, Sept. 2006). *Articulated Robot Motion Planning Using Ant Colony Optimisation*. Paper presented at the Intelligent Systems, 2006 3rd International IEEE Conference on.
- Osamu, T., & Schilling, R. J. (1989). Motion Planning in a Plane Using Generalized Voronoi Diagram. *IEEE Transactions on Robotics and Automation*, 5(2), 143-150.
- Oussama, K. (1986). Real-Time Obstacle Avoidance for Manipulators and Mobile Robots. *The International Journal of Robotics Research*, 5(1), 90-98.
- Overmars, M., & Švestka, P. (1995), A probabilistic learning approach to motion planning. In K. Goldberg, D. Halperin, J. C. Latombe, and R. Wilson (eds.). *Algorithmic Foundations of Robotics (WAFR)*, 19–37, A. K. Peters, Ltd.
- Pai, D. K., & Reissell, L. M. (1998). Multiresolution rough terrain motion planning. *IEEE Transaction on Robotic and Automation*, 14(1), 19- 33.
- Papanikolopoulos, N. P., & Khoshla, P. K. (1992). Real-Time LQG Robotic Visual Tracking Robotic Systems. In S.G. Tzafestas (Ed.), (Vol. 10, p. 305-312). Netherlands: Kluwer Academic Publishers.
- Qingfu, Z., Jianyong, S., Gaoxi, X., & Tsang, E. (2007). Evolutionary Algorithms Refining a Heuristic: A Hybrid Method for Shared-Path Protections in WDM Networks Under SRLG Constraints. *Systems, Man, and Cybernetics, Part B: Cybernetics, IEEE Transactions on*, 37(1), 51-61.
- Reiswijk, T. A., Schalkwijk, P., & Honderd, G. (1992). Planning and Optimization of Geometrical Trajectories inside Collision-Free Subspace with the Aid of High Order Hermite Splines. In S.G. Tzafestas (Ed.). *Robotic Systems: Advanced Techniques and Applications* (p. 225-233). Netherlands: Kluwer Academic Publishers.
- Reiswijk, T. A., Sirks, M., Honderd, G., & Jongkind, W. (1992). A Fast and Efficient Algorithm for the Computation of Path Constrained Time-Optimal Motions. In S. G. Tzafestas (Ed.) *Robotic Systems* (p. 235-243). Netherlands: Kluwer Academic Publishers.
- Saska, M., Macas, M., Preucil, L., & Lhotska, L. (2006, 20-22 Sept. 2006). *Robot Path Planning using Particle Swarm Optimization of Ferguson Splines*. Paper presented at the Emerging Technologies and Factory Automation, 2006. ETFA '06. IEEE Conference on.
- Sinha, P. K., & Benmounah, A. (1992). Mobile Robot Trajectory Planning. In S.G. Tzafestas (Ed.), *Robotic Systems* (p 279-286). Netherlands: Kluwer Academic Publishers.
- Sinha, P. K., & Ho, P-L. (1992). Three-Dimension Abstraction of Convex Space Path Planning. In S.G. Tzafestas (Ed.), *Robotic Systems* (p. 245-252). Netherlands: Kluwer Academic Publishers.
- Tsong-Li, L., & Chia-Ju W. (2003). Fuzzy Motion Planning of Mobile Robots in Unknown Environments. *Journal of Intelligent and Robotic Systems*, 37, 177–191.
- Zhu, A., & Yang, S. X. (2006). A Neural Network Approach to Dynamic Task Assignment of Multirobots. *IEEE Transaction on Neural Networks*, 17(5), 1278-1287.



## Effect of Glycerol Feed in Methanol Induction Phase for Hepatitis B Surface Antigen Expression in *Pichia pastoris* Strain KM71

A. R. Morvarid<sup>1</sup>, N. A. Zeenathul<sup>1\*</sup>, Y. J. Tam<sup>1</sup>, H. Zuridah<sup>2</sup>,  
M. L. Mohd-azmi<sup>1</sup> and B. O. Azizon<sup>2</sup>

<sup>1</sup>LIVES, Institute of Bioscience, Universiti Putra Malaysia,  
43400 Serdang, Selangor, Malaysia

<sup>2</sup>Jabatan Patologi, Hospital Tuanku,  
70400 Seremban, Negeri Sembilan, Malaysia.

\*E-mail: zeenathul@putra.upm.edu.my

### ABSTRACT

This study describes expression of HBs Ag in methylotrophic yeast, *Pichia Pastoris* under alcohol oxidase promoter. A single copy number of HBs Ag gene was transformed into *pichia* strain of KM 71, a Mut<sup>a</sup> type, by using pAO815 *pichia* expression vector. The recombinant was cultivated in a shake flask either using methanol or a mixed feed of glycerol -methanol for induction. The HBs Ag gene integrity was justified using direct PCR method. The expressed products in the soluble cell extracts were analyzed by Western blot, SDS page, Bradford assay and ELISA tests. The recombinant HBs Ag was expressed successfully in *Pichia pastoris* strain KM71 at a high level of HBs Ag protein expression. Thus, an addition of glycerol in the ratio of glycerol per methanol 1/1 (g g<sup>-1</sup>) consistently produced 2-fold increment in both biomass accumulation and HBs Ag productivity.

**Key words:** Biomass, Hepatitis B, KM71 strain, pAO815 expression vector, *Pichia pastoris*, Surface Ag

### INTRODUCTION

Hepatitis B virus (HBV) is without any doubt one of the most common human viruses. Two billions of the six billions people alive today show evidence of past or current infection with HBV. Meanwhile, about 350 million people are chronically infected with hepatitis B virus (HBV) worldwide. Two-thirds of these patients develop liver cirrhosis resulting in portal hypertension, liver failure and hepatocellular carcinoma (Schumann *et al.*, 2007). Chronic infection may lead to cirrhotic liver failure, while infected people have a 100-fold increased risk of developing hepatocellular carcinoma (Chisari, 2000). Nevertheless, infection with HBV has become a vaccine-preventable disease.

One of the most remarkable features of HBV is its production of surface-antigen particles (termed as HBs Ag) that are stabilized by disulfide bonds and contain carbohydrates and phospholipids (Dane *et al.*, 1970; Robinson *et al.*, 1974; Tiollais *et al.*, 1985). By the early 1980s, advances in genetic engineering and biotechnologies allowed the first HB vaccine to be obtained through formulation of HBs Ag produced in the recombinant strains of the yeast *Saccharomyces cerevisiae* (Elliot *et al.*, 1994). In line with *S. cerevisiae* based approach, the technology for the large-scale obtainment of HBs Ag was developed based on the expression of the HBs Ag gene under control of the *Pichia pastoris* alcohol oxidase I (*AOXI*) enzyme gene promoter (Eugenio *et al.*, 2000).

\*Corresponding Author

The methylotrophic yeast *P. pastoris* has been developed into a commercially important host for the production of heterologous proteins (Cereghino & Cregg, 2000; Lin Cereghina *et al.*, 2001). The expression level was high in this eukaryotic *pichia* system, and most of the proteins are soluble (Shao *et al.*, 2003). It is important to note that *pichia* is capable of growing at very high cell densities in a simple mineral medium. In fact, it does not have the endotoxin problem associated with bacteria or the viral contamination problem of proteins produced in animal cell culture.

Furthermore, *P. pastoris* can utilize methanol as a carbon source in the absence of glucose. High-level expression and efficient assembly of HBs Ag has been reported in *P. pastoris* by integrating a single copy of the HBs Ag gene under control of the AOX1 promoter (Cregg *et al.*, 1987). In addition, multiple copy integration of recombinant HBs Ag genes in Pichia has also been demonstrated to increase the expression of a desired protein in the *Pichia* strain of GS115 (Vassileva *et al.*, 2001). The aim of this study was to develop the genetically engineered *Pichia pastoris* system in Pichia KM71 strain system for the production of HBs Ag. The production would focus on the influence of glycerol feed during methanol induction phase.

## MATERIALS AND METHODS

### *Strain and Vector*

The *pichia* strain of KM 71, a histidine requiring auxotroph and the intracellular expression vector, pA0815 (Invitrogen, USA) were used in this study. The vector contained one unique restriction site of EcoR 1. A linearization of this vector with *Sal* I enzyme will generate His<sup>+</sup> Mut<sup>s</sup> in KM 71.

### *Nucleotide Sequence of HBs Ag (681bp)*

```
ATGGAGAACATCACATCAGGATTCTAGGACCCCTGCTCGTGTACAGGCAGGG  
TTTTCTTGTGACAAGAACCTCACAATACCGCAGAGTCTAGACTCGTGGTGG  
ACTTCTCTCAATTCTAGGGGGATCTCCCGTGTCTGGCAAATTTCGC  
AGTCCCCAACCTCCAATCACTCACCAACCTCCTGCCTCCAATTGCTCTGG  
TTATCGCTGGATGTGTCTGCGGCGTTTATCATATTCCCTTCATCCTGCTGC  
TATGCCTCATCTTATTGGTTCTGGATTATCAAGGTATGTTGCCCGTT  
GTCCTCTAATTCCAGGATCAACAAACAAACAGTACGGGACCATGCAAAACC  
TGCACGACTCCTGCTCAAGGCAACTCTATGTTCCCTCATGTTGCTGTAC  
AAAACCTACGGATGGAATTGCACCTGTATTCCCATCCATCGTCTGGGC  
TTTCGCAAAATACCTATGGAGTGGCCTCAGTCCGTTCTGGCTCAG  
TTTACTAGTGCCTTGTCAGTGGTTCTGGGCTTCCCCACTGTTGG  
CTTCAGCTATATGGATGATGTGGTATTGGGGGCCAAGTCTGTACAGCATCG  
TGAGTCCCTTATACCGCTGTTACCAATTCTTTGTCTGGTATAACATTAA
```

### *Cloning into Pichia Expression Vector*

The HBs Ag of 681bp was initially amplified by PCR, from plasmid pEco63 (ATCC 31518; American Type Culture Collection, Rockville, Md.), which contains a full length of HBs Ag gene. The coding sequence of HBs Ag was amplified with the primers, designated as FHBs Ag (forward primer), 5'-G **GAA** **TTC** AAG CTT **ATG** GAG AAC ATC ACA TCA GG-3' (Invitrogen, California, USA) and RHBs Ag (reverse primer), 5'G **GAA** **TTC** AAG CTT **TTA** AAT GTA TAC CCA GAG AC-3' (Invitrogen, California, USA) (the *Eco*R1 recognition sites are underlined; the initiation codon in the forward primer and the reverse complement of the termination codon in the reverse primer are in boldface letters). PCR was carried out with 1 to 2  $\mu$ l of the plasmid DNA in a mixture of 10x

## Effect of Glycerol Feed in Methanol Induction Phase for Hepatitis B Surface Antigen Expression

PCR buffer, 2.5 mM MgCl<sub>2</sub>, 0.25 mM dNTP, 50 pmol (each) sense and antisense primer, as well as 1 U of KOD HiFi DNA polymerase (Novagen, Germany) in a final volume of 50 µl. Amplification was performed for 30 cycles with denaturation at 94°C for 1 min, annealing at 60°C for 30 sec, extension at 72°C for 1 min and finally at 72°C for 7 min. The PCR product was analyzed using 1% agarose gel electrophoresis and visualized by ethidium bromide staining.

Meanwhile, the amplified PCR product of 707 base pairs fragment of HBs Ag was gel purified using GeneClean (QBIogene, California, USA). The pA0815 vector and the purified PCR product were double digested with *EcoRI* restriction enzyme at 37°C for 16 h. The vector was then treated with Antarctic phosphatase (New England Biolabs INC., Ipswich, UK) for ½ h at 37°C, and this was followed by inactivation at 65°C for 5 min. Both the digested PCR product and the linearized vector were purified using phenol, followed by chloroform-isoamyl alcohol (24:1) and finally precipitated by adding 0.1 volume of 3 M sodium acetate (pH 5.4) and 2.5 volume of 95% ethanol. It was then incubated at -20°C for 15 min and centrifuged at a high speed using micro centrifuge at 4°C for 15 min (22R, Hettich, Tuttlingen, Germany). The supernatant was discarded and the pellet was washed with 70% ethanol. The PCR product, together with the linearized vector, was then ligated at 14°C overnight. A total volume of 100 ng ligated DNA was chemically transformed into Top 10F' competent cell by heat shock at 42°C for 1 min, and followed by incubation at 37°C with agitation for 1 h. This was then spread onto ampicillin LB agar plates and incubated at 37°C overnight. About 20 colonies were selected on the next day and sub-cultured into ampicillin LB broth. The recombinant plasmids were extracted by using a conventional plasmid extraction method.

The recombinant plasmids were verified by PCR for the correct direction of the gene inserted, using FHBs Ag as forward primer, with RAOX1 (5'-GCA AAT GGC ATT CTG ACA TCC-3') as reverse primer, and/or FAOX1 (5'-GAC TGG TTC CAA TTG ACA AGC-3') as a forward primer with RHBs Ag reverse primer. The selected positive clones were sub-cultured (see Figure 1) and purified using Concert High Purity plasmid purification system (Marligen 'Bioscience, USA).

### In Vitro Multimerization

The size of the vector, containing one copy gene insert, was 8417 bp in length. It was then digested with enzyme *Bgl* I and *Bam*H I for 16 h at 37 °C. The digested product was analyzed using 1% agarose electrophoresis. The band size of 1980 bp (containing one copy gene cassette) was excised from the gel, and this was followed by gel purification using GeneClean (QBIogene, California, USA). This particular vector was also digested with *Bgl* I and *Bam*H I at 37 °C for 16 h and dephosphorylated for ½ h at 37 °C. Then, the DNA was extracted using phenol as described above. After that, the one copy gene cassette and the linearized vector were ligated at 14 °C overnight. The ligated DNA was chemically transformed into Top 10F' competent cell as mentioned in the discussion above. On the following day, about 20 colonies were selected and sub-cultured into the ampicillin LB broth. The recombinant plasmids were extracted using the conventional plasmid extraction method and also verified by PCR using the primer as mentioned above and double enzyme digestion by *Bgl* I and *Bam*H I to determine the correct direction of the gene insert. The selected positive cloned was sub-cultured and purified using Concert High Purity plasmid purification system for the subsequent transformation step in *Pichia*.

### Transformation into *Pichia*

The selected plasmid without gene insert pA0 (as negative control), and plasmid with one copy gene insert (pA1) were sub-cultured and purified. The total amount of 10 µg DNA was digested with *Sal* I enzyme at 37 °C for 16 h, followed by dephosphorylation. The linearized DNA was phenol

extracted as mentioned above. A total of 5 $\mu$ g of linearized DNA was prepared to be transformed into KM 71 *pichia* competent cell. The DNA was mixed with 40 $\mu$ l of *pichia* competent cell for 3 min. It was then transferred into a 2 mm electroporation cuvette, incubated for 5 min on ice and pulsed once at 1800 volt (EC 100 Electroporator, Krackeler Scientific, Inc., Albany, New York, USA). After the electroporation, 1 ml of ice-cold sorbitol was immediately added, and incubated for 1h and 30 min without shaking. Later, it was spread onto RDB (1M Sorbitol, 2% dextrose, 1.34% YNB, 4 x 10<sup>-5</sup>% biotin, 0.005% amino acids & 20g/L agar) plates and incubated at 30°C. The recombinant *pichia* colonies were analyzed for HBs Ag gene through direct colony PCR using the primers of FAOX1 and RAOX1.

#### *PCR Screening of Pichia Transformants*

The KM 71 *pichia* colonies were analyzed for the presence of the HBs Ag gene insert through direct colony PCR using the primers of FAOX1 and RAOX1. Briefly, a pinpoint sized part of a single colony was picked from a master plate and suspended in 10 $\mu$ l distilled water. Later, 5 $\mu$ l zymolase (1mg/ml of 60 000 unit zymolase) was added into it, mixed and incubated at 30°C for 10 min. The mixture was immediately frozen at -80°C for 10 min. After the lysis step, 1  $\mu$ l of the mixture was template used for the PCR using the hot start method. The PCR reactions were 5  $\mu$ l of 10x PCR buffer, 2.5  $\mu$ l of 50mM MgCl<sub>2</sub>, 2.5  $\mu$ l of 10mM dNTP and 50pmol primer each. The reaction mixture was allowed to go for 95°C for 5 min and this was followed by adding the 2 U of *Taq* polymerase (New England Biolabs ING., Ipswich, UK). The positive clones were then sub-cultured onto MD (1.34% YNB, 4x10<sup>-5</sup>% biotin, 2% dextrose) agar plates.

#### *HBs Ag Production in Shaking Flask*

A single colony from the MD agar was inoculated into 100ml of BMGY media (1% yeast extract, 2% peptone, 100mM potassium phosphate, pH 6.0, 1.34% YNB, 4x 10<sup>-5</sup> % biotin, 1% glycerol) in a 500 ml baffled flask, and cultured at 30°C in a shaking incubator (300 rpm) until culture reached OD<sub>600</sub>=2 (20h). The cells were then harvested by centrifugation at 1500x g for 5 min at room temperature. The supernatant was discarded and the cell pellet was resuspended in a 100 ml BMGY medium (the same as BMGY, except that the glycerol was replaced with 0.5% methanol) in a 500 ml baffled flask. During the induction phase, 100% methanol and 1g glycerol/g were added into the culture on a daily basis and to a final concentration of 1% so as to maintain the induction for the methanol fed culture. At each time before induction, samples of the cell culture were collected to determine the OD and dry cell weight until Day 13. In addition, the cell samples were also collected daily up to Day 13, while the culture was harvested by centrifugation at 5000g for 20 min at 4 °C. The cell pellet was recovered and stored at -80°C until it ready for assay.

#### *Optical Density*

The OD was determined at 600 nm using a biophotometer (Eppendorf, Hamburg, Germany). The samples were diluted by PBS in an appropriate dilution.

#### *Dry Cell Weight*

A total volume of 2 ml (in duplicate) of the *pichia* culture was pelleted in a pre-weighed eppendorf microcentrifuge tubes by low centrifugation 5000x g, 10min, washed twice with PBS and centrifuged at 5000x g for 5 minutes. The pellet was dried at 80°C with a drier (Memmert, Braunschweig, Germany) and weighed after 1 day.

#### *Preparation of the Cell Extract*

A total volume of 1 ml of the *pichia* culture was pelleted by low centrifugation (5000x g, 10 min) and washed twice with PBS to remove the medium. The washed cells were resuspended in a 200 $\mu$ l lysis buffer (10mM sodium phosphate buffer, pH 7.2; 5mM EDTA, 0.5M NaCl, 0.1% (v/v) Triton X-100, 1mM PMSF), together with an equal volume of acid wash glass bead. The cell was lysed by 10 times vortexing using VX100 (Vortex Mixer, Labnet, NJ, USA) per min at the maximum speed and each was followed by chilling on ice for 1 min. Next, it was centrifuged at the maximum speed (12000 x g for 20 min) to collect the supernatant for Bradford, SDS page, Western blot and ELISA assays.

#### *Bradford Assay*

The dye reagent was diluted in 1-part dye reagent and 4-part double distilled water. Three to five dilutions of protein standard were prepared (from 2 mg/ml to approximately 10 mg/ml). Meanwhile, 10  $\mu$ l aliquot standard and sample solution were added to separate microtiter wells. Then, a volume of 200  $\mu$ l diluted dye reagent was added to each well. The microtiter plate was incubated for at least 5 min and the results were determined by reading at a wavelength of 590 nm using the ELISA reader (Tecan, Sunrise, Melbourne, Australia).

#### *SDS PAGE Analysis*

Sodium dodecyl sulphate polyacrylamide gel (SDS-PAGE) was prepared according to Sambrook and Maniatis (1989) to determine the molecular weight of the expressed protein. The resolving gel, containing 12% acrylamide, 0.1% SDS and 0.375M Tris HCL (pH 8.8), was prepared. In addition, ammonium persulphate was also added, and this was followed by adding TEMED before it was allowed to solidify. The stacking gel, containing 4.75% acrylamide, 0.1% SDS and 0.125M Tris-HCL (pH6.8), was also prepared. The prepared cell lysate was mixed with a loading buffer (8% SDS; 50%  $\beta$ -ME; 1 M DTT, pH 6.8) and denatured by boiling for 10 min. The lysate was later loaded into the gel. After the electrophoresis of about 2 hrs, the gel was stained with Coomassie blue. After destaining, the bands were visualized using the gel documentation system (Alpha Innotech Corp., California, USA).

#### *Western Blot Analysis*

To analyse the expression of HBsAg, cell lysates were appropriately diluted with 1x SDS sample disruption buffer. After denaturation, the samples were loaded onto SDS gel and proteins were separated by gel electrophoresis. After the electrophoresis, the proteins were transferred to PVDF membrane (Immobilon-PSQ, Millipore corp., Billerica, MA, USA). The non-specific binding sites were blocked using a blocking buffer (BSA 1%). The antigen-bound antibodies on the membrane were detected using HBs Ag primary monoclonal antibody and goat anti-mouse secondary antibody IgG HRP (Bio-Rad, California, USA). Finally, the signals were developed using the Western blotting ABTS substrate and the bands were visualized.

#### *Dot Blot Analysis*

The PVDF membrane (Immobilon-PSQ, Millipore Corp., Billerica, MA, USA) was wetted with methanol for 15 sec and rinsed with ultrapure water. After that, the membrane was placed in PBS for 5 min. About 5  $\mu$ l of the sample was spotted onto the membrane and air dried. The dried membrane was rewetted with methanol for 5 min. Next, the membrane was placed into a blocking solution

(PBS; 1% BSA; 0.05% Tween 20). The mouse monoclonal antibody against HBs Ag (Biodesign, Phoenix, Arizona, USA) was diluted in 1000 folds and was added onto the membrane for 2 h. Then, the membrane was washed with PBS. The goat anti-mouse secondary antibody IgG HRP (Bio-Rad, California, USA) was diluted about 5000 folds, added onto the membrane and incubated for 1 hr. Later, the membrane was washed with PBS. Then, the DAB substrate was added onto the membrane and incubated for 10 min. The reaction was finally stopped with distilled water.

#### *Enzyme Linked Immunosorbent Assay (ELISA)*

The concentration of the protein HBs Ag in the soluble cell extracts was determined using the SURASE B-96 ELISA kit (General Biologicals Co., Taiwan). The kit was modified and re-optimized so that it could be used for a quantitative of HbsAg from the *pichia* cell extract. In particular, the *pichia* of pA0 was used as a negative control (vector without gene insert). Meanwhile, pure HBs Ag was used as a standard and to construct a standard curve using a serial dilution of commercial HBs Ag (Chemicon, Temecula, CA, USA) (0- 10 ng). The cell extracts of pA1 were diluted in 500 folds with a lysis buffer. As described by the manufacturer, 50 µl of the samples were then added into the wells and 50 µl guinea pig antibody (anti HBs) IgG HRP conjugated was also added and incubated for 1 hr. After that, it was washed three times. The TMB solution was added into the wells and incubated for 30 min. The reaction was stopped with 2 N H<sub>2</sub>SO<sub>4</sub> (Fisher Scientific, Loughborough, UK) and read at a wavelength of 450/650 nm using the ELISA reader (Tecan, Sunrise, Melbourne, Australia).

## RESULTS

The single copy number of HBs Ag gene was successfully cloned into the *pichia* expression vector pA0815 and designated as pA1. The PCR and DNA sequencing analysis of the pA1 indicated a correct orientation of HBs Ag gene insertion (see Fig. 1). Meanwhile, the DNA sequencing results revealed 100% matching to the 681bp of HBs Ag encoding 226 amino acids. The recombinant vector pA1 digestion, with *Bgl*II and *Bam*H1 restriction enzymes, produced three fragments of 4.2 kb, 2.3 kb and 2 kb. The HBs Ag gene resided in the 2 kb fragment.

The Coomasie blue stained SDS page gel demonstrated 23kDa band of HBs Ag from the *pichia* cell lysate (Fig. 2). In addition, Pichia HBs Ag particles have dimers of disulfide-bonded polypeptides with a molecular mass of about 23kDa. The dimer and oligomer showed 46 kDa and 89 kDa bands (see Fig. 2). The monomer (23KD), dimer (49KD) and oligomer (89KD) bands in the Western blotting (Figure 3), as well as the positive result obtained in the dot blot (see Fig. 4), have been confirmed to produce HBs Ag protein from the cell lysate. Furthermore, ELISA was also used to quantify the HBs Ag expression from the *pichia* recombinants. The technique was optimized using a standard curve from 0-10 ng/ml prepared using commercial HBs Ag so as to enable the determination of HBs Ag production level in pA1 *pichia* recombinant HBs Ag (see Fig. 5).

Prior to cultivation in the shake flask, the KM71 Mut<sup>s</sup> was initially cultured in the MD agar to isolate the recombinants. The cultures grown in the BMGY media were replaced at day-3 with fresh BMMY containing either glycerol /methanol at 0/1 ratio (g g<sup>-1</sup>) or a mixed feed of glycerol/ methanol at 1/1 ratio (g g<sup>-1</sup>) for expression induction. The samples were collected until day-13 of cultivation. The results obtained from ELISA revealed that the production of HBs Ag expression started at day-1 of the induction until day-10. Meanwhile, the bio-mass DCW achieved at day-10 (day 6 of induction) was 9.4 g/l in glycerol /methanol at 0/1 ratio (g g<sup>-1</sup>) and 21 g/l for glycerol / methanol at 1/1 ratio (g g<sup>-1</sup>) fed culture, respectively. The maximum production level of HBs Ag was achieved on day-10 but this gradually and subsequently declined for both the induction cultures (Fig. 5).

Effect of Glycerol Feed in Methanol Induction Phase for Hepatitis B Surface Antigen Expression

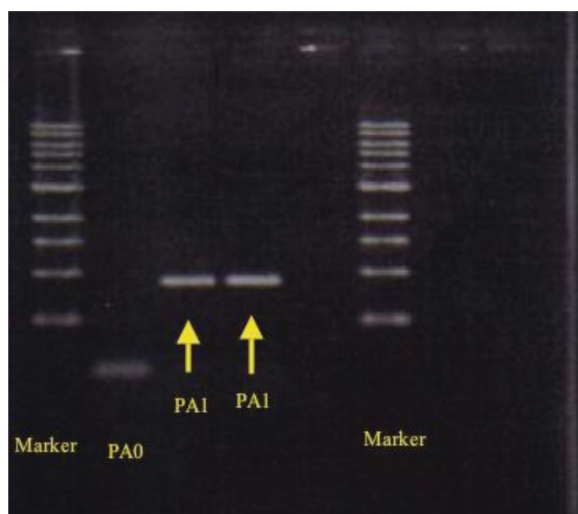
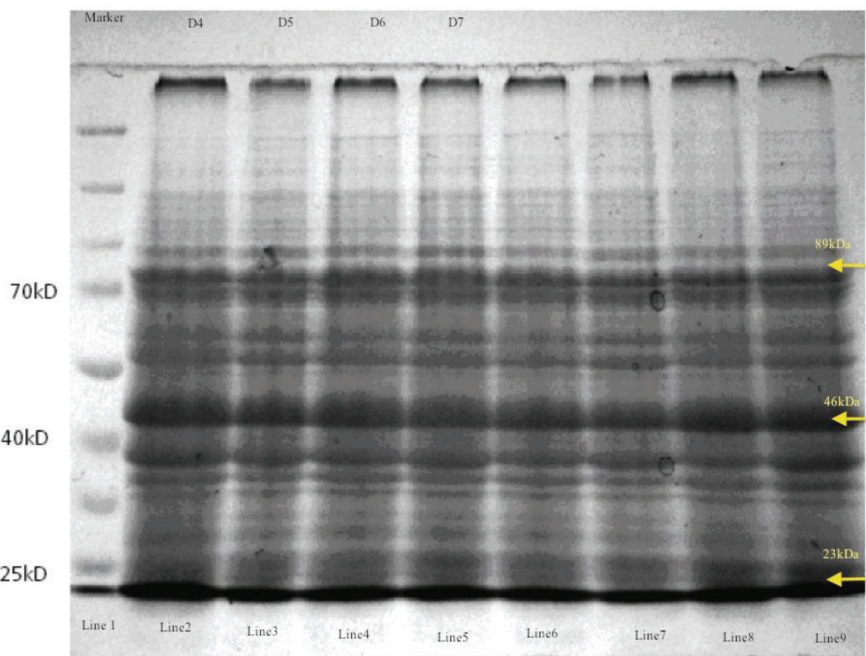


Fig. 1: A PCR analysis of the *Pichia KM 71* recombinant. Lane 1: 1 kb DNA Marker. Lane 2: *pA0* negative control recombinant *KM 71*(7700 kb). Lanes 3 and 4: Arrows indicate *pA1*, recombinant *KM 71* that contained one copy of gene insert (8417 kb). Line 5: Empty. Lane 6: 1 kb DNA Marker



\*D: Days

Fig. 2: The production of recombinant HBs Ag protein in *KM71* strains (*pA1*) was analyzed by SDS page. The data showed that HBs Ag produced on Days 4 to 7 of the cultivation. Lane 1: protein marker. Lanes 2 to 5: *KM71 pA1* culture in BMGY from Days 4 to 7. Lines 5 to 9 are repeated. They are fed with 0.5% methanol daily. The monomers protein size is about 23kD. The bands (Arrows) corresponding to dimer (46 kDa) and oligomer (89 kDa) are present as well as monomer (23 kDa)

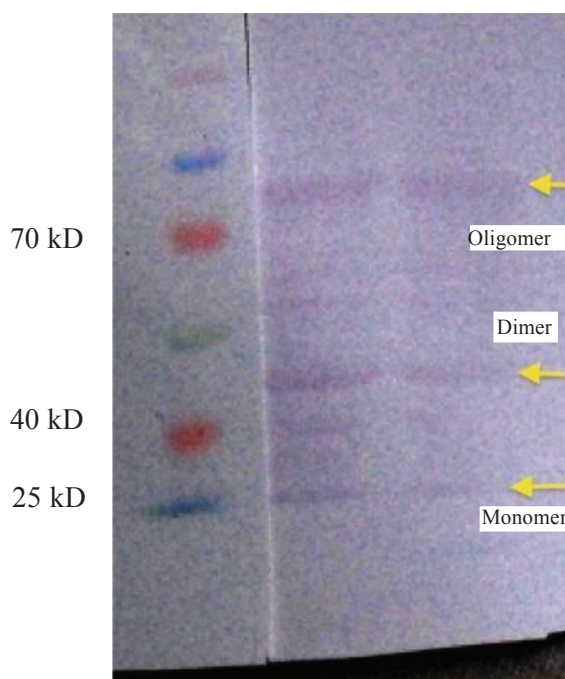


Fig. 3: The Western blotting analysis of the recombinant HBs Ag protein in the KM71 strain with anti HBs. The monomers, dimers and oligomers bands were confirmed by the Western blot with anti-HBs mAb



Fig. 4: The dot blot analysis of the recombinant KM 71 showed a positive signal. The left arrow showed the positive result confirming that the HBs Ag protein was expressed in Pichia

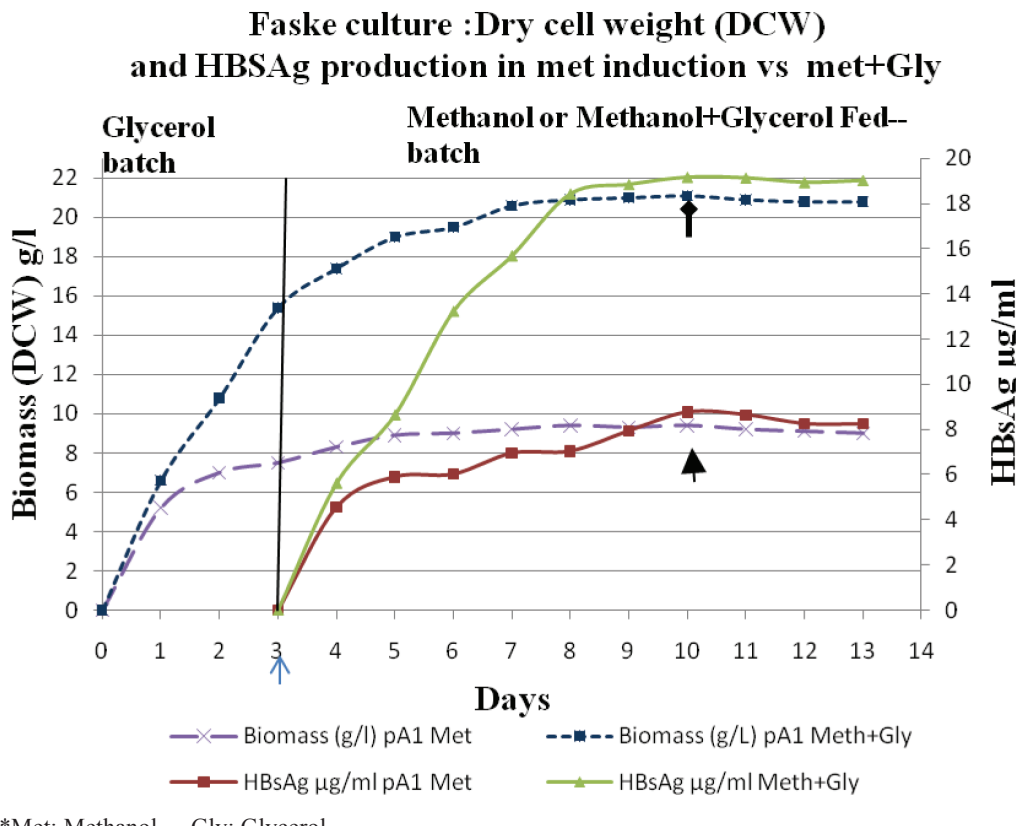


Fig. 5: The recombinant KM71 strain pA1 in shake flask culture. The induction phase was started at ↑ Day 3 (Blue arrow). The biomass achieved 9.4 g/l (indicated by the thick arrow) in the glycerol /methanol at 0/1 ratio (g g<sup>-1</sup>) and 21 g/l (indicated by thin arrow) for glycerol/ methanol at 1/1 ratio (g g<sup>-1</sup>) fed cultures at Day 10. The expression of HBs Ag started at Day 4 and it achieved the highest level at Day 10 (day 7 of induction) in pA1 (see arrows)

## DISCUSSION

All *Pichia* expression strains are derivatives of NRRL-Y 11430 (Northern Regional Research Laboratories, Peoria, IL); these examples included GS115, KM 71, MC100-3, SMD 1168, SMD 1165 and SMD 1163. Most of them have mutation in the histidinol dehydrogenase gene (*HIS4*) upon transformation (Cregg *et al.*, 1985). Therefore, they need complex media with histidine supplementation. It is crucial to note that there are three types of host strains available. These vary according to their ability to utilize methanol which resulted from deletion in one or both *AOX* genes. The strains with deleted *AOX* genes are sometimes better producers of a foreign protein in corporation as compared to wild-type strains (Cregg *et al.*, 1987; Chirulova *et al.*, 1997; Tschopp *et al.*, 1987). Moreover, these strains also require much less methanol to induce expression, which can be useful in large fermentor cultures. However, the most commonly used expression host is GS115, which is a wild type with regard to the *AOX1* and *AOX2* genes, and it grows on methanol at the wild-type rate (Mut<sup>+</sup>). Meanwhile, in KM 71 *pichia* strain, the chromosomal *AOX1* gene is largely deleted and replaced with *S. cerevisiae* *ARG4* gene (Cregg & Madden, 1987). Therefore, it

must rely on the much weaker *AOX2* gene for *AOX* and grow on the methanol at a slow rate (*Mut<sup>S</sup>*). It has been suggested that a fast growing *Mut<sup>+</sup>* strain was not as efficient as *Mut<sup>S</sup>* in producing HBs Ag particles (Ottone *et al.*, 2007). The activity of the *AOX1* promoter in the methanol grown cells is significantly higher than the glucose grown cells with GAP promoter (Sears *et al.*, 1998).

*Pichia pastoris* uses glycerol as carbon source during the initial cultivation and then utilizes methanol as a carbon source in the methanol fed-batch phase by converting it into formaldehyde. However, formaldehyde accumulation can inhibit cell growth. In the initial step of fermentation in the shake flask, the cells are initially grown on the media with glycerol (BMGY). In the second phase, the medium with glycerol (BMGY) would be replaced with the medium containing 0.5% of methanol (BMMY). In the final phase (induction phase), either the ratio of glycerol /methanol at 0/1 ratio (g g<sup>-1</sup>) or glycerol /methanol at 1/1 ratio (g g<sup>-1</sup>) was added into the culture. In a standard fermentation of *Mut<sup>S</sup>* strain, the methanol fed rate should not exceed 0.3% (Invitrogen, 2000). Hence, the *AOX* promoter was induced to produce protein in both the fed-batch cultures.

Some previous studies have shown that a mixture of glycerol/methanol can be continuously added into *pichia* culture in various ratios (Ottone *et al.*, 2007). The finding indicated a significant improvement in the cell culture viability and cell density upon induction with glycerol/methanol at 1/1 ratio (Table 1). A 2.3 fold biomass increment was produced as compared to the methanol induced cells in the shake flask method. In particular, the biomass in the shake flask reached 9.4 g/l and this was 21 g/l in the dry cell weight in methanol and in the mixed glycerol per methanol 1/1 (g g<sup>-1</sup>) inductions, respectively (Table 1). Using a similar approach, Ottone *et al.* (2007) achieved 1.2 fold higher biomass accumulations in a bioreactor system. There are two types of biomass determination, namely dry cell weight (DCW) and wet cell weight (OD<sub>600</sub> measurement). However, the dry cell weight (2.3 fold) measurement is more accurate than OD<sub>600</sub> (1.8 fold) because during yeast budding, not all new cells get separated from the parent cell after division and they may stick together even until the next division. Thus, OD<sub>600</sub> measurement does not measure the exact amount of cell density (Invitrogen, 2000).

In this study, a direct correlation of biomass increment with HBs Ag production (2.2 fold increment) was achieved as the transformant had a single copy number of integrant (pA1). Nonetheless, many fold increment of HBs Ag can be obtained with a multicopy integrant and

TABLE 1

A comparison of the expression of HBs Ag in the *Mut<sup>S</sup>* strain (KM71) in a shake flask. Glycerol/ methanol mixed feed during the induction phase. A 2.3-fold biomass increment was produced when glycerol was added with methanol in the induction phase. Consequently, total protein and HBs Ag product were increased by increasing the biomass

Parameters	PA1 (single copy)	
	Glycerol/methanol 0/1 (g g <sup>-1</sup> )	Glycerol/methanol 1/1 (g g <sup>-1</sup> )
Dry cell weight (DCW g/l)	9.4	21
Wet cell weight (WCW g/l)	40	73
Final OD <sub>600</sub>	46.5	86
HBs Ag (mg/l)	8.719.1	19.1
Specific yield mg HBs g <sup>-1</sup> DCW	0.92	0.91
Specific yield mg HBs g <sup>-1</sup> WCW	0.21	0.25
Total protein	6.2	13.51

\*DCW: Dry Cell Weight

WCW: Wet Cell Weight

## Effect of Glycerol Feed in Methanol Induction Phase for Hepatitis B Surface Antigen Expression

bioreactor application (Ottone *et al.*, 2007). The finding derived at in the current study could be considered as significantly high in terms of the total HBs Ag expression level using a single copy integrant as compared to that of the previous study (Vassileva *et al.*, 2001). In more specific, the results obtained in the present study demonstrated a 40.6 folds higher HBs Ag production (3.48 mg/100 OD cells) in the shake flask system using a single copy HBs Ag gene.

## CONCLUSION

The HBs Ag has been successfully expressed in the *Pichia* strain KM71 recombinant. Consequently, a higher expression level of HBs Ag could be enhanced in the *Pichia* KM 71 strain by mixing feed methanol/glycerol at the 1/1 ratio (g g<sup>-1</sup>) for induction.

## REFERENCES

- Brierley, R. A., Davis, G. R., & Holtz, G. C. (1994). Production of insulin-like growth factor-1 in methylotrophic yeast cells. *United States Patent 5*, 324, 639.
- Cerechino, J. L., & Cregg, J. M. (2002). Heteroloquous protein expression in the methylotrophic yeast *Pichia pastoris*. *FEMS Microbiology Reviews*, 24, 45-66.
- Chirulova, V., Cregg, J. M., & Meagher, M. M. (1997). Recombinant protein production in an alcohol oxidase-defective strain of *Pichia pastoris* in fed batch fermentations. *Enzyme Microbiology Technology*, 21, 277-283.
- Chisari, F. V. Rous-Whipple Award Lecture. (2000). Viruses, immunity, and cancer: lessons from hepatitis B. *American Journal of Pathology*, 156, 1118-1132.
- Cregg, J. M., Vedvick, T. S., & Raschke, W. C. (1993). Recent advances in the expression of foreign genes in *Pichia pastoris*. *Bio/Technology*, 11, 905-910.
- Cregg, J. M., Madden, K. R., Barringer, K. J., Thill, G. P., & Stillman, C. A. (1989). Functional characterization of the two alcohol oxidase genes from the yeast *Pichia pastoris*. *Molecular Cell Biology*, 9, 1316-1323.
- Cregg, J. M., Tschopp, J. F., Stillman, C., Siegel, R., Akong, M., Craig, W. S., Buckholz, R. G., Madden, K. R., Kellaris, P. A., Davis, G. R., Smiley, B. L., Cruze, J., Torrengrossa, R., Velicelebi, G., & Thill, G. P. (1987). High-level expression and efficient assembly of hepatitis B surface antigen in the methylotrophic yeast *Pichia pastoris*. *Biotechnology*, 5, 479-485.
- Cregg, J. M., & Madden, K. R. (1987). Development of yeast transformation systems and construction of methanol-utilization-defective mutants of *Pichia pastoris* gene disruption. In G.G. Stewart, I. Russell, R.D. Klein, and R. R. Hiebsch (eds.). *Biological Research on Yeasts, Vol. II*, 1-18
- Cregg, J. M., Barringer, K. J., Hessler, A. Y., & Madden, K. R. (1985). *Pichia pastoris* as a host system for transformations. *Molecular Cell Biology*, 5, 3376-3385.
- Dane, D. S., Cameron, C. H., & Briggs, M. (1970). Virus-like particles in serum of patients with Australia antigen associated hepatitis. *Lancet II*, 695-698.
- De Hoop, M. J., Cregg, J., Keizer, G. I., Sjollema, K., Veenhuis, M., & Ab, G. (1991). Overexpression of alcohol oxidase in *Pichia Pastoris*. *FEBS Letters*, 291, 299.
- Elliot, A. Y., Morges, W., & Olson, M. G. (1994). Experience in manufacturing, testing and licensing a hepatitis B vaccine produced by recombinant technology. In A. S. Lubinniecki, & S. A. Vargo. (eds). *Regulatory Practives for Biopharmaceutical Production*, 256-269
- Eugenio, H., Eduarado, M., David, D., Raul, D., Daniel, G., & Luis, H. (2000). Large scale production of recombinant hepatitis B surface antigen from *Pichia pastoris*. *Biotechnolog*, 77, 157-167.

- Fortuin, M. J., Chotard, A. D., Jack, N. P., Maine, M., Mendy, A. J., Hall, H. M. I., George, M. O., & Whittle, H. C. (1993). Efficacy of hepatitis B vaccine in the Gambian expanded programme on immunization. *Lancet*, 341, 1129-1131.
- Lin Cereghino, G. P., Sunga A. J., Line Cereghino, J., & Clegg, J. M. (2001). Expression of foreign genes in the yeast *Pichia pastoris*. *Genet. Eng.*, 23, 157-169.
- O'Keefe, D.O., & Paiva, A.M., (1995). Assay for recombinant hepatitis B surface antigen using reversed-phase high-performance liquid chromatography. *Anal. Biochem.*, 230, 48-54.
- Robinson, W. S., Clayton, D. A., & Greenman, R. L. (1974). DNA of a human hepatitis B virus candidate. *Virology*, 14, 384-391.
- Shao, J., Hayashi, T., & Wang, P. G. (2003). Enhanced production of alpha-galactosyl epitopes by metabolically engineered *Pichia pastoris*. *Appl Environ Microbiol*, 69(9), 5238-5242.
- Sambrook, J., Fritsch, E. F., & Manyanis, T. (1989). *Molecular cloning: a laboratory manual* (2<sup>nd</sup> ed). , Cold Spring Harbor, N.Y.: Cold Spring Harbor Laboratory Press.
- Schmann, A., Fiedler, M., Dahmen, U., Grossewilde, D., Roggendorf, M., & Lindeman, M. (2007). Cellular and Humoral Immune Response to a Third Generation Hepatitis B Vaccine. *Protein Expression and Purification*, 56, 177-188.
- Shao, J., Takahisa, H., & Peng, G. W. (2003). Enhanced production of galactosyl epitopes by metabolically engineered *pichia pastoris*. *Applied and Environmental Microbiology*, 69 (9), 5238-5242.
- Ottone,S., Nguyen, X., Bazin, J., Berard, C., Jimenez, S., & Letourneur, O. (2007). Expression of hepatitis B surface antigen major subtypes in *Pichia Pastoris* and purification for *in vitro* diagnosis. *Protein Expression and Purification*, 56, 177-188.
- Thill, G. P., Davis, G. R., Stillman, C., Holtz, G., Brierley, R., Engel, M., Buckholtz, R., Kinny, J., Provow, S., Vedvick, T., & SIEGEL, R.S. (1990). Positive and negative effect of multy copy integrated expression vectors on protein expression in *Pichia pastoris*. In Proceeding of 6<sup>th</sup> International Symposium on genetic of microorganisms. Societe Francaise de microbiologies, Paris, 2: 477-490.
- Vassileva, A., Chugh, D. A., Swaminathan, S., & Khanna, N. (2001). Effect of copy number on the expression levels of Hepatitis B surface antigen in the methylotrophic yeast *Pichia pastoris*. *Protein Expression and Purification*, 21(1), 71-81.

## Relative Power Performance of *t*-test and Bootstrap Procedure for Two-Sample

Nor Aishah Ahad<sup>1\*</sup>, Suhaida Abdullah<sup>1</sup>, Lai Choo Heng<sup>2</sup> and Nazihah Mohd. Ali<sup>3</sup>

<sup>1</sup>*UUM College of Arts and Sciences, Universiti Utara Malaysia,  
06010 Sintok, Kedah*

<sup>2</sup>*School of Distance Education, Universiti Sains Malaysia,  
11800, Pulau Pinang*

<sup>3</sup>*Jabatan Matematik, Fakulti Sains, Universiti Putra Malaysia,  
43400 Serdang, Selangor, Malaysia*

\*E-mail: aishah@uum.edu.my

### ABSTRACT

The classical procedures of comparing two groups, such as *t*-test are, usually restricted with the assumptions of normality and equal variances. When these assumptions are violated, the rates of the Type I errors of the independent samples *t*-test are affected, particularly when the sample sizes are small. In this situation, the bootstrap procedure has an advantage over the parametric *t*-test. In this study, the performances of the bootstrap procedure and the independent sample *t*-test were investigated. The investigation focused on the power of both the test procedures to compare the two groups under different design specifications for normal and chi-square distributions. The results showed that the bootstrap procedure has a slight edge over the conventional *t*-test in term of the rate of achieving the benchmark level for both the distributions. In fact, the bootstrap procedure consistently outperformed the conventional *t*-test across all the combinations of the test conditions.

**Key words:** Bootstrap, power, *t*-test

### INTRODUCTION

The classical procedures of comparing two groups such as *t*-test are usually restricted by the assumptions of normality and equal variances. Moreover, in the real world, these assumptions are not always fulfilled. Over the years, many procedures arose to handle the violation of these assumptions. Note that nonparametric procedures are viable alternatives that can be used when the distribution is not normal. Meanwhile, robust hypothesis testing procedures, such as James (1951), Welch (1951) and also Alexander and Govern (1994), are some examples of the procedures that have been developed to handle the problem of unequal variances.

With the increase of computational power, the statistical technique has also improved consistently. Computational intensive techniques have benefited from these and made a come back in terms of their usage. Bootstrapping is one of the recently revived techniques used for making certain kinds of statistical inferences. The essence of bootstrapping is the idea that, in the absence of any other knowledge about a population, the distribution of values found in a random sample of size  $n$  from the population is the best guide to the distribution in the population (Manly, 1997). In situation where classical test assumptions are not met, the bootstrap procedure offers a viable

---

\*Corresponding Author

alternative as it uses computational power to perform intricate calculation. More importantly, the bootstrap procedure does not rely on a theoretical sampling distribution (such as central limits theorem that requires large samples) as in the classical tests. Othman, Keselman, Padmanabhan, Wilcox and Fradette (2003) listed out a practical advantage of using the bootstrap procedure. They noted that certain variations of the bootstrap procedure do not require the knowledge of the sampling distribution of the test statistic, and thereby, not requiring explicit expressions for standard errors of estimators. This condition makes hypothesis testing quite flexible.

Meanwhile, Krishnamoorthy, Lu and Mathew (2007) made a comparison between the bootstrap procedure and the general  $F$  test, Welch test and James test. The researchers suggested using the bootstrap method for the reason that it is the only procedure that performs satisfactorily, regardless of the sample sizes, values of the error variances, and the number of means being compared under unequal variances.

In the same vein, Higgins (2005) adopted and simplified the process of bootstrapping. The bootstrap method relies on Monte Carlo random number generators to generate bootstrap samples. In addition to carrying out hypothesis testing with the test statistic of unknown sampling distribution, the bootstrap procedure is also capable of assessing the performance of statistical test in terms of Type I error and power. Therefore, this facilitates the design of the new test procedure without resorting to proving them analytically first. Moreover, the bootstrap procedure is also capable of conducting sensitivity analyses on the performance of known parametric, nonparametric or Monte Carlo based methods under usual and extreme operating conditions. Hence, these sensitivity analyses are also comparative analyses if the analyses are performed on both the new and known procedures.

This study was conducted to evaluate the performance of the bootstrap method as compared to the classical pooled variance  $t$ -test in terms of their statistical power for the two groups. These tests were evaluated at various combinations of test conditions (namely, sample sizes, variances ratios and underlying distributions).

## DESIGN OF THE STUDY

For comparison purposes, this study considered unbalanced groups with the sample sizes of 5 and 15 and as well as investigated the performance of the procedures under normal and chi-square distributions. The total sample size was set to be equivalent to 20 so as to maintain the small sample size (for each sample size and both) because the effect of non-normality would when dealing with small sample size (i.e. less than 30). In this study, the ratio of the group sample size (1:3) was to reflect the unbalanced design. Other researchers also had their own preference, such as Lix and Keselman (1998) whereby they used a group sample size ratio of 1:2. In order to examine the effect of distributional shapes on power value, this study used data from normal distribution as well as from skewed distribution. Chi-square with three degrees of freedom has skewness of 1.63 and kurtosis 4.00 was chosen to simulate a positively skewed distribution with a minimum at zero (Soong, 1981).

Meanwhile, the variance ratios used were 1:1 and 1:9. For heterogeneous variances, the ratio 1:9 was chosen as it reflects extreme variance heterogeneity. Hess, Olejnik and Huberty (2001), in their study, considered any variance ratio larger than 1:8 as extreme variance heterogeneity. Accordingly, this study sought to investigate how well both the tests performed under more extreme condition. These unequal variances were paired with unbalanced sample sizes positively and negatively. Positive pairing was done when the group with the smallest sample size was paired with the smallest variance while the group with the largest sample size was paired with the largest variance. For the negative pairing, the group with the largest sample size was paired with the smallest variance and the group with the smallest sample size was paired with the largest variance.

## METHODS

This study was based on the simulated data generated by subroutine RANDGEN from SAS (1999). The nominal level of significance was set at  $\alpha=0.05$ . For each condition examined, 1000 data sets were generated and for the bootstrap procedure, 1000 more bootstrap samples were generated for each of the data set. In the real world studies, the usual recommended bootstrap replicate is 100 and this was done with the trade-off between computational cost and accuracy. Meanwhile, Pattengale, Alipour, Bininda-Emonds, Moret and Stamatakis (2010) recommended bootstrap replicates of 100 to 500 range for the real world data where a practitioners would no longer have to enter a guess nor worry about the quality of estimates. Most conservative criteria may for several thousand replicates which only reduce the effects of random sampling errors. Wilcox (2005) stated that the choice of the number of bootstrap replicates has to be sufficiently large so that if the seed in the random number generator is altered, the same conclusions would essentially still be obtained. Chernick (2008) urged practitioners to choose the number of bootstrap replications that make the sampling variance sufficiently small so as to ensure that the bootstrap approximation is close to the actual bootstrap estimate. He further suggested at least 1000 bootstrap replications in the case of confidence interval estimation and hypothesis testing problem.

The power of a test is the probability that a test will yield statistically significant results or reject the false null hypothesis. It can be denoted as  $1 - \beta$ . As reported by Yin and Othman (2009), the power of a test depends on three factors, namely, significance criterion ( $\alpha$ ), sample size ( $n$ ) and effect size (EF).  $\alpha$ , which is also known as Type I error, is positively related to power. The power values increase as the standard for determining significance increases. The sample size,  $n$ , is also positively related to power. The larger the sample size, the higher the power value. The effect size, EF, is the magnitude of the effect under alternate hypothesis. The power values increase when the effect size increases.

For the two groups, the effect size index is the effect size that is to be detected. Thus, the effect size index ( $d$ ) is defined as:

$$d = \frac{|\mu_1 - \mu_2|}{\sigma}$$

Where,

$d$  = effect size index

$\mu_1 - \mu_2$  = population means

$\sigma$  = the standard deviation of either population (if they are equal)/the smallest standard deviation (if they are unequal).

According to Cohen (1988), the effect size is considered as small when  $d = 0.2$ , medium when  $d = 0.5$ , and large when  $d = 0.8$ . The effect size index is used to choose the values of population means for the true alternative hypothesis. Assuming that  $\mu_1 > \mu_2$  and  $\mu_2 = 0$ , we can have a range of values to represent  $\mu_1$ . In order to cover all the conditions, the value of the shift parameter can systematically varied from 0.5 to 7.5 with the increments of 0.5. Table 1 represents the possible choices for  $\mu_1$  and  $\mu_2$  for all the conditions and methods. Murphy and Myors (1998) noted that the power of a test is usually judged to be adequate if the value is 0.8 and above. Fig. 1 outlines the steps to determine the power value for both the *t*-test and bootstrap procedure.

## RESULTS AND DISCUSSION

The entries in Table 2 and Table 3 are power rates for the *t*-test and bootstrap procedure, respectively, on both the test distributions. Similarly, Tables 4 and 5 show the power values of both the procedures

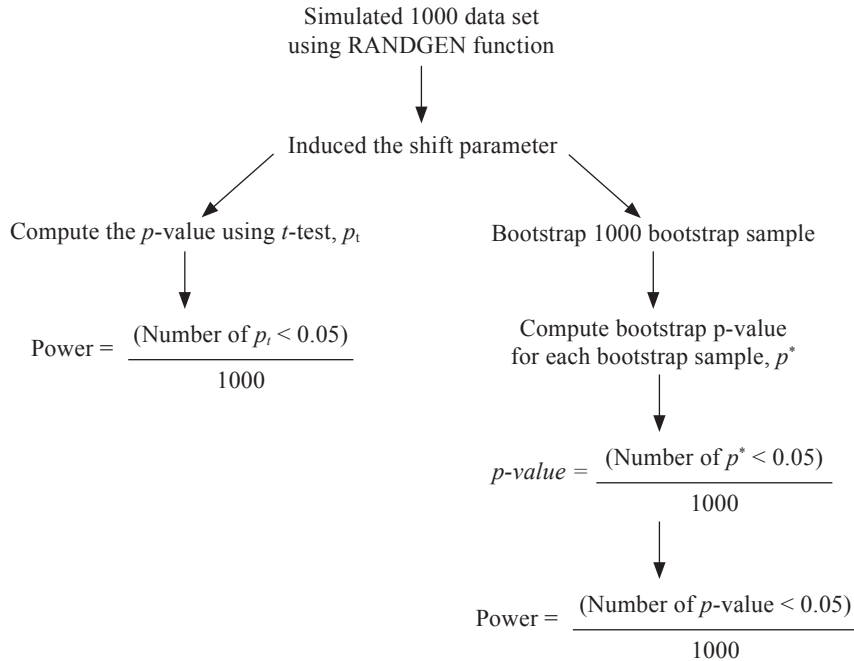


*Fig. 1: A diagrammatic outline to determine the power values for the t-test and the bootstrap procedure*

TABLE 1  
Possible choices of shift parameter for all conditions and methods

Group sample sizes	Group variances	Effect size	Range for shift parameter
{5, 15}	{1, 1}	$\frac{\mu_1 - \mu_2}{0.547}$	0.5, 1, 1.5, ...
{5, 15}	{1, 9}	$\frac{\mu_1 - \mu_2}{1.449}$	1.5, 3, 4.5, ...
{5, 15}	{9, 1}	$\frac{\mu_1 - \mu_2}{0.949}$	1, 2, 3, ...
Bootstrap	difference	$\mu_1 - \mu_2$	1, 2, 3, ...

for the normal and chi-square distributions. On the other hand, *Fig. 2* and *Fig. 3* displayed the power curves of the *t*-test and bootstrap procedure. The results and discussion for the *t*-test method and bootstrap procedure are separately presented.

#### *The t-test Method*

Table 2 shows the power rates of the pooled variance *t*-test under normal and chi-square distributions. The bolded entries are power rates that are above the benchmark power rate of 0.80. For a clear viewing, *Fig. 2* displays the power curves of the pooled variance *t*-test under normal and chi-square distributions with all the variance ratios that have been considered.

As shown in Table 2 and *Fig. 2*, the homogeneous variances produced higher power rates under normal distribution than the heterogeneous variances, whereas in terms of pairing, the negative pairing produced higher power rates than positive pairing. The power rates of the pooled variance *t*-test behave similarly under the chi-square distribution, where the highest power rates are in homogeneous variances while in terms of pairing, the negative pairing is higher than positive. Nonetheless, the performance of the *t*-test does not vary between the two distributions. The power rate reaches the benchmark point of 0.8 at almost the same level. However, the chi-square distribution achieved the benchmark rate at a lower shift parameter when the variances are negatively paired.

### *The Bootstrap Procedure*

Table 3 and *Fig. 3* show the power values and power curves for the bootstrap procedure, respectively. The bolded entries in Table 3 are power rates that exceed the benchmark power rate of 0.80. The bootstrap procedure produces similar trends as that of the pooled variance *t*-test. Under normal distribution, the high power rate was achieved the fastest in the presence of variance homogeneity, while the slowest was when the pairing of variance and sample size was positive.

For the chi-square distribution, once again just like in the pooled variance *t*-test, the results of power rates were found as not incredibly different with that of the normal distribution where groups with homogeneous variances attained the high power the fastest. While in terms of pairing, the negative pairing reached the highest power earlier than the positive pairing.

When the two distributions were compared under normal distribution with homogeneous variances and positive pairing, the results showed that the bootstrap procedure reached the power of 0.80 much faster as compared to the chi-square distribution. However, for the groups with the negative pairing, the performance of the bootstrap procedure under the chi-square distribution was shown to be better as compared to the normal distribution because at shift parameter = 2.5, the power is 0.81 whereas the power for normal distribution is just 0.765.

### *Comparative Study*

For the comparative study, an attempt was done to determine which of the two procedures would be the fastest in term of achieving the benchmark power. The detail of the comparative study is shown in Table 4 for the normal distribution and Table 5 for the chi-square distribution.

By comparison, the bootstrap procedure has a slight edge over the conventional *t*-test in term of the rate of achieving the benchmark level with the normal distribution. The entries for the bootstrap procedures across various variance ratios exceeded the benchmark level relatively faster as compared to the *t*-test. Similarly, with the chi-square distribution, the bootstrap procedure is capable of achieving a faster rate. Conclusively, the bootstrap procedure consistently outperformed the conventional *t*-test across all the combinations of the test conditions.

## CONCLUSIONS

The bootstrap procedure has a slight edge over the conventional *t*-test in terms of the rate of achieving the benchmark level for both the normal and chi-square distributions. In particular, the bootstrap procedure consistently outperformed the conventional *t*-test across all the combinations of the test conditions.

Evidently, both the tests are capable of achieving the benchmark level at a faster rate in the situation of homogeneity of variances across distributions. Similarly, they are sensitive to effect size

### Power curves for t-test method

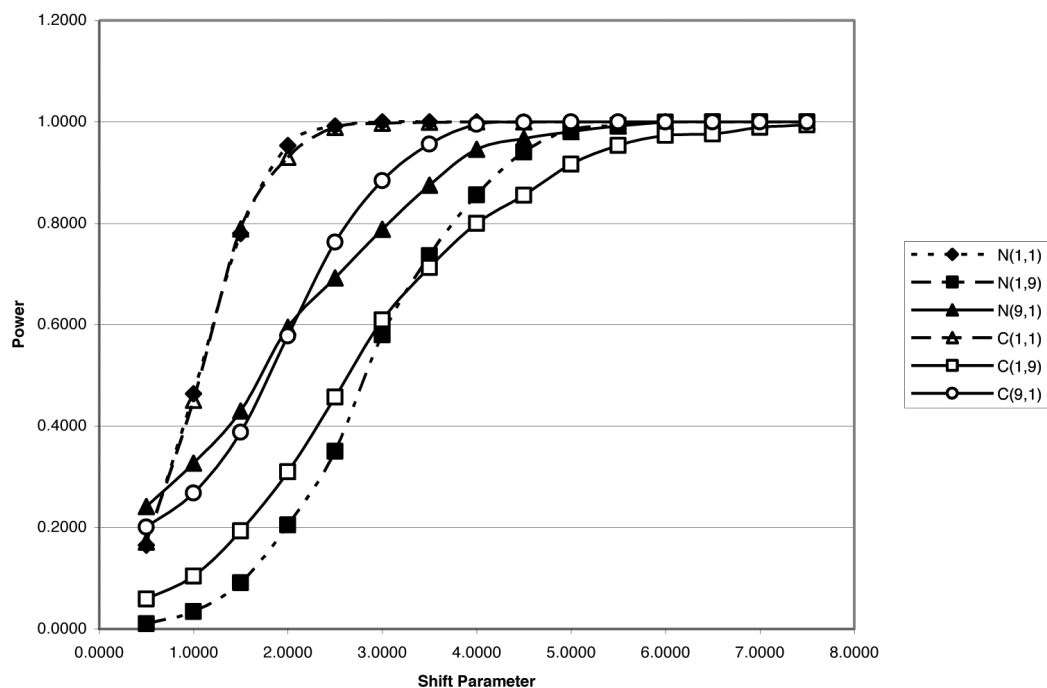


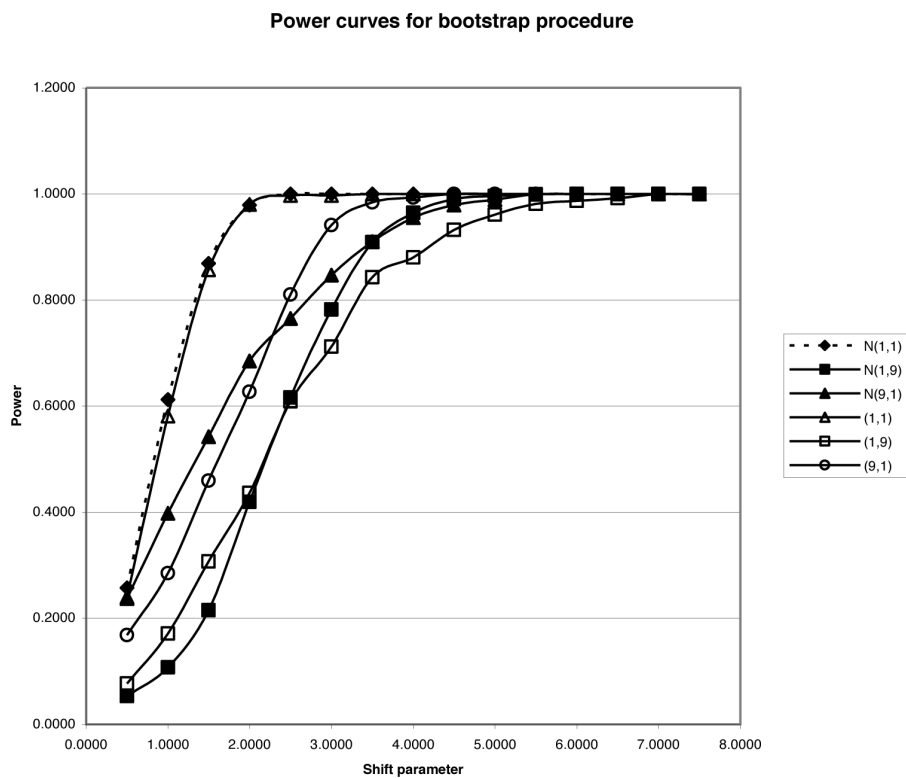
Fig. 2: Power curves for the pooled variance t-test

TABLE 2  
Power values for the two sample t-test with pooled variances

Shift parameter	Normal			Chi-square (3)		
	Var (1,1)	Var (1,9)	Var (9,1)	Var (1,1)	Var (1,9)	Var (9,1)
0.5	0.165	0.010	0.241	0.171	0.059	0.201
1.0	0.464	0.034	0.327	0.451	0.104	0.268
1.5	0.780	0.091	0.430	0.789	0.193	0.388
2.0	<b>0.953</b>	0.205	0.595	<b>0.930</b>	0.310	0.578
2.5	<b>0.992</b>	0.350	0.692	<b>0.989</b>	0.457	0.763
3.0	<b>1.000</b>	0.580	0.788	<b>0.997</b>	0.609	<b>0.884</b>
3.5	<b>1.000</b>	0.736	<b>0.875</b>	<b>0.999</b>	0.713	<b>0.956</b>
4.0	<b>1.000</b>	<b>0.856</b>	<b>0.946</b>	<b>1.000</b>	<b>0.800</b>	<b>0.995</b>
4.5	<b>1.000</b>	<b>0.940</b>	<b>0.967</b>	<b>1.000</b>	<b>0.855</b>	<b>0.999</b>
5.0	<b>1.000</b>	<b>0.984</b>	<b>0.981</b>	<b>1.000</b>	<b>0.916</b>	<b>1.000</b>
5.5	<b>1.000</b>	<b>0.993</b>	<b>0.992</b>	<b>1.000</b>	<b>0.953</b>	<b>1.000</b>
6.0	<b>1.000</b>	<b>0.999</b>	<b>0.999</b>	<b>1.000</b>	<b>0.973</b>	<b>1.000</b>
6.5	<b>1.000</b>	<b>1.000</b>	<b>1.000</b>	<b>1.000</b>	<b>0.976</b>	<b>1.000</b>
7.0	<b>1.000</b>	<b>1.000</b>	<b>1.000</b>	<b>1.000</b>	<b>0.989</b>	<b>1.000</b>
7.5	<b>1.000</b>	<b>1.000</b>	<b>1.000</b>	<b>1.000</b>	<b>0.994</b>	<b>1.000</b>

Note: Values indicated in bold show power rate  $\geq 0.80$ .

Relative Power Performance of t-test and Bootstrap Procedure for Two-Sample



*Fig. 3: Power curves for the bootstrap procedure*

TABLE 3  
Power values for the bootstrap procedure

Shift parameter	Normal			Chi-square (3)		
	Var (1,1)	Var (1,9)	Var (9,1)	Var (1,1)	Var (1,9)	Var (9,1)
0.5	0.257	0.053	0.237	0.240	0.077	0.168
1.0	0.612	0.107	0.398	0.581	0.171	0.285
1.5	<b>0.869</b>	0.215	0.542	<b>0.857</b>	0.307	0.459
2.0	<b>0.979</b>	0.419	0.685	<b>0.980</b>	0.436	0.627
2.5	<b>1.000</b>	0.616	0.765	<b>0.997</b>	0.609	<b>0.810</b>
3.0	<b>1.000</b>	0.782	<b>0.847</b>	<b>0.997</b>	0.712	<b>0.941</b>
3.5	<b>1.000</b>	<b>0.909</b>	<b>0.910</b>	<b>1.000</b>	<b>0.843</b>	<b>0.984</b>
4.0	<b>1.000</b>	<b>0.964</b>	<b>0.955</b>	<b>1.000</b>	<b>0.880</b>	<b>0.993</b>
4.5	<b>1.000</b>	<b>0.990</b>	<b>0.979</b>	<b>1.000</b>	<b>0.932</b>	<b>1.000</b>
5.0	<b>1.000</b>	<b>0.996</b>	<b>0.989</b>	<b>1.000</b>	<b>0.961</b>	<b>1.000</b>
5.5	<b>1.000</b>	<b>0.999</b>	<b>0.999</b>	<b>1.000</b>	<b>0.981</b>	<b>1.000</b>
6.0	<b>1.000</b>	<b>1.000</b>	<b>1.000</b>	<b>1.000</b>	<b>0.987</b>	<b>1.000</b>
6.5	<b>1.000</b>	<b>1.000</b>	<b>1.000</b>	<b>1.000</b>	<b>0.992</b>	<b>1.000</b>
7.0	<b>1.000</b>	<b>1.000</b>	<b>1.000</b>	<b>1.000</b>	<b>0.999</b>	<b>1.000</b>
7.5	<b>1.000</b>	<b>1.000</b>	<b>1.000</b>	<b>1.000</b>	<b>0.999</b>	<b>1.000</b>

*Note:* Values indicated in bold show power rate  $\geq 0.80$ .

TABLE 4  
Power values for the normal distribution

Shift parameter	Var (1,1)		Var (1,9)		Var (9,1)	
	t-test	Bootstrap	t-test	Bootstrap	t-test	Bootstrap
0.5	0.165	0.257	0.010	0.053	0.241	0.237
1.0	0.464	0.612	0.034	0.107	0.327	0.398
1.5	0.780	<b>0.869</b>	0.091	0.215	0.430	0.542
2.0	<b>0.953</b>	<b>0.979</b>	0.205	0.419	0.595	0.685
2.5	<b>0.992</b>	<b>1.000</b>	0.350	0.616	0.692	0.765
3.0	<b>1.000</b>	<b>1.000</b>	0.580	0.782	0.788	<b>0.847</b>
3.5	<b>1.000</b>	<b>1.000</b>	0.736	<b>0.909</b>	<b>0.875</b>	<b>0.910</b>
4.0	<b>1.000</b>	<b>1.000</b>	<b>0.856</b>	<b>0.964</b>	<b>0.946</b>	<b>0.955</b>
4.5	<b>1.000</b>	<b>1.000</b>	<b>0.940</b>	<b>0.990</b>	<b>0.967</b>	<b>0.979</b>
5.0	<b>1.000</b>	<b>1.000</b>	<b>0.984</b>	<b>0.996</b>	<b>0.981</b>	<b>0.989</b>
5.5	<b>1.000</b>	<b>1.000</b>	<b>0.993</b>	<b>0.999</b>	<b>0.992</b>	<b>0.999</b>
6.0	<b>1.000</b>	<b>1.000</b>	<b>0.999</b>	<b>1.000</b>	<b>0.999</b>	<b>1.000</b>
6.5	<b>1.000</b>	<b>1.000</b>	<b>1.000</b>	<b>1.000</b>	<b>1.000</b>	<b>1.000</b>
7.0	<b>1.000</b>	<b>1.000</b>	<b>1.000</b>	<b>1.000</b>	<b>1.000</b>	<b>1.000</b>
7.5	<b>1.000</b>	<b>1.000</b>	<b>1.000</b>	<b>1.000</b>	<b>1.000</b>	<b>1.000</b>

Note: Values indicated in bold show power rate  $\geq 0.80$ .

TABLE 5  
Power Values for the Chi-Square Distribution

Shift parameter	Var (1,1)		Var (1,9)		Var (9,1)	
	t-test	Bootstrap	t-test	Bootstrap	t-test	Bootstrap
0.5	0.171	0.240	0.059	0.077	0.201	0.168
1.0	0.451	0.581	0.104	0.171	0.268	0.285
1.5	0.789	<b>0.857</b>	0.193	0.307	0.388	0.459
2.0	<b>0.930</b>	<b>0.980</b>	0.310	0.436	0.578	0.627
2.5	<b>0.989</b>	<b>0.997</b>	0.457	0.609	0.763	<b>0.810</b>
3.0	<b>0.997</b>	<b>0.997</b>	0.609	0.712	<b>0.884</b>	<b>0.941</b>
3.5	<b>0.999</b>	<b>1.000</b>	0.713	<b>0.843</b>	<b>0.956</b>	<b>0.984</b>
4.0	<b>1.000</b>	<b>1.000</b>	<b>0.800</b>	<b>0.880</b>	<b>0.995</b>	<b>0.993</b>
4.5	<b>1.000</b>	<b>1.000</b>	<b>0.855</b>	<b>0.932</b>	<b>0.999</b>	<b>1.000</b>
5.0	<b>1.000</b>	<b>1.000</b>	<b>0.916</b>	<b>0.961</b>	<b>1.000</b>	<b>1.000</b>
5.5	<b>1.000</b>	<b>1.000</b>	<b>0.953</b>	<b>0.981</b>	<b>1.000</b>	<b>1.000</b>
6.0	<b>1.000</b>	<b>1.000</b>	<b>0.973</b>	<b>0.987</b>	<b>1.000</b>	<b>1.000</b>
6.5	<b>1.000</b>	<b>1.000</b>	<b>0.976</b>	<b>0.992</b>	<b>1.000</b>	<b>1.000</b>
7.0	<b>1.000</b>	<b>1.000</b>	<b>0.989</b>	<b>0.999</b>	<b>1.000</b>	<b>1.000</b>
7.5	<b>1.000</b>	<b>1.000</b>	<b>0.994</b>	<b>0.999</b>	<b>1.000</b>	<b>1.000</b>

Note: Values indicated in bold show power rate  $\geq 0.80$ .

in this situation. Conversely, both the tests produced lower rate when large variance was associated with the larger sample, signifying a low sensitivity to effect size. Despite the slight difference in the rate, both the *t*-test and bootstrap procedures produced a consistent power performance across the two distributions. For each test, the rates of achieving the benchmark level were found to be similar for both the normal and chi-square distributions, but the bootstrap procedure achieved it at a faster rate.

## REFERENCES

- Alexander, R. A., & Govern, D. M. (1994). A new and simpler approximation for ANOVA under variance heterogeneity. *Journal of Educational Statistics*, 19, 91-101.
- Chernick, M. R. (2008). *Bootstrap methods. A guide for practitioners and researchers* (2<sup>nd</sup> ed). New York: John Wiley & Sons.
- Cohen, J. (1988). *Statistical power analysis for the behavioral sciences*. New York: Academic Press.
- Hess, B., Olejnik, S., & Huberty, C. J. (2001). The efficacy of two improvement-over-chance effect sizes for two-group univariate comparisons under variance heterogeneity and nonnormality. *Educational and Psychological Measurement*, 61, 909-936.
- Higgins, G. E. (2005). Statistical significance testing: The bootstrapping method and an application to self-control theory. *The Southwest Journal of Criminal Justice*, 2(1), 54-75.
- James, G. S. (1951). The comparison of several groups of observations when the ratios of the population variances are unknown. *Biometrika*, 38, 324-329.
- Krishnamoorthy, K., Lu, F., & Mathew, T. (2007). A parametric bootstrap approach for ANOVA with unequal variances: Fixed and random models. *Computational Statistics & Data analysis*, 51, 5731-5742.
- Lix, L. M., & Keselman, H. J. (1998). To trim or not to trim: Tests of location equality under heteroscedasticity and nonnormality. *Educational and Psychological Measurement*, 58(3), 409-429.
- Manly, B. F. J. (1997). *Randomization, bootstrap and Monte Carlo methods in biology* (2<sup>nd</sup> ed). London: Chapman & Hall.
- Murphy, K. R., & Myors, B. (1998). *Statistical power analysis: A simple and general model for traditional and modern hypothesis tests*. Mahwah, NJ: Lawrence Erlbaum.
- Othman, A. R., Keselman, H. J., Padmanabhan, A. R., Wilcox, R. R., & Fradette, K. (2003). An improved robust Welch-James test statistic. In the proceeding of the Regional Conference on Integrating Technology in the Mathematical Sciences, 2003. Universiti Sains Malaysia, Pulau Pinang, Malaysia.
- Pattengale, N. D., Alipour, M., Bininda-Emonds, O. R., Moret, B. M., & Stamatakis, A. (2010). How many bootstrap replicates are necessary? *Journal of Computational Biology*, 17(3), 337-354.
- SAS Institute Inc. (1999). *SAS/IML User's Guide version 8*. Cary, NC: SAS Institute Inc.
- Soong, T. T. (1981). *Probabilistic modeling and analysis in science and engineering*. New York: John Wiley & Sons.
- Welch, B. L. (1951). On the comparison of several mean values: An alternative approach. *Biometrika*, 38, 330-336.
- Wilcox, R. R. (2005). *Introduction to robust estimation and hypothesis testing* (2<sup>nd</sup> ed). New York: Academic Press.
- Yin, T. S., & Othman, A. R. (2009). When does the pooled variance *t*-test fail? *African Journal of Mathematics and Computer Science Research*, 2(4), 56-62.



## New Semi-blind Channel Estimation in MIMO based on Second Order Statistics

Dinh-Thuan Do

Department of Electrical and Electronics, Ton Duc Thang University, Vietnam  
E-mail: dodinhthuan@gmail.com

### ABSTRACT

A new channel estimation approach for orthogonally coded multiple input multiple output (MIMO) system is proposed. The main idea of the technique proposed in this study involves the use of specific properties of the orthogonal space-time block codes (OSTBCs) in the estimation based on the second order statistic (SOS) to estimate the channel matrix after the application of singular value decomposition (SVD). This modified solution directly brings simple parameters in comparison with conventional estimation from the channel matrix. In this investigation, the authors made an attempt to reduce the effect of ambiguity which could be seen in most of the traditional blind algorithms. As the training-based least square (LS) was still used for a part of the channel matrix, the scheme in this study could be described as the semi-blind algorithm which has strongly attracted more researchers in the wireless field. A detailed analysis carried out in this current research work has validated the performance and computational advantages of the proposed method. Meanwhile, results from the simulation have confirmed the modified scheme and illustrated that the new semi-blind channel estimation is capable of improving the quality of the overall system.

**Keywords:** MIMO, orthogonal space-time block codes, second order statistic, semi-blind estimator

### INTRODUCTION

Space time coding (STC) techniques used in the multiple input multiple output (MIMO) wireless systems are well-known method to offer significantly improved transmission rates and immunity to the fading effects as compared to early structures (Foschini & Gans, 1998; Telatar, 1999; Gesbert, *et al.*, 2003) The class of linear space-time block code (STBC) is the major category of space-time codes and it can be further divided into sub-classes like Linear Dispersion Codes, Orthogonal STBC and quasi Orthogonal STBC. Among the different space-time code schemes, the orthogonal space-time block codes (OSTBC) offer an attractive solution because they achieve full diversity at low decoding complexity. There are two advantages involved in providing transmit diversity via orthogonal designs: (1) there is no loss in bandwidth, in the sense that the orthogonal designs provide the maximum possible transmission rate at full diversity, and (2) there is an extremely simple maximum-likelihood decoding algorithm which only uses linear combining at the receiver; hence, simplicity is resulted from the orthogonality of the columns of the orthogonal design. Actually, besides decoding algorithm, the performance of MIMO systems may critically depend on the quality of the available channel state information (CSI) at the receiver. Although training-based schemes are widely used for channel estimation in MIMO as well as older techniques, a promising recent trend is to estimate the channel using efficient blind or semi-blind techniques, particularly when it is motivated by unique singular value decomposition (SVD) formulation in the matrix computation,

---

Received: 2 April 2010

Accepted: 23 August 2010

whereby SVD is used to estimate channel matrices addressing simple matrix elements which are calculated using the conventional channel estimation algorithm. Many of the existing blind channel estimators, such as those based on the second-order statistics assume that the channel is static over many OSTBC blocks. After decomposition into two sub-matrices from the channel matrix, the blind method was used for the first sub-matrix, and the least square (LS) approach was utilized for the latter. Therefore, the proposed approach is the so-called semi-blind one.

On the other hand, significant progress has been observed in the blind maximum likelihood (ML) detection techniques which go along with this new channel estimation (Larsson, E. G., *et al.*, 2002). In this investigation, the blind algorithm was also modified into closed-form for simplicity in the matrix computations. Through this modified scheme, damage in term of ambiguity from the usual blind channel estimation could be reduced. The effects of the structure of the underlying OSTBC and the symbol constellation used for this modified scheme were also investigated in this study. In practice, it is difficult to find a perfect solution for this ambiguous problem, but the optimized value can be found through statistic experiments.

The paper is organized into several sections, as follows. In section II, the structure of OSTBC using in MIMO channel is introduced. In the next part (section III), the modified semi-blind channel estimation is developed. The numerical results are presented in section IV, whereas the conclusions are drawn in section V.

Notation: The bold uppercase letters denote matrices,  $(\cdot)^\perp$  which stands for Pseudo-inverse;  $(\cdot)^H$  stands for complex conjugate transpose,  $\otimes$  is Kronecker product,  $I_N$  is the  $N \times N$  identity matrix;  $\|\cdot\|^2$  denotes Frobenius norm;  $\text{tr}(\cdot)$  is the sum of the elements on the main diagonal of the matrix;  $\text{vec}\{\cdot\}$  is the vectorization operator stacking all columns of a matrix on top of each other.

## OVERVIEW OF ORTHOGONAL SPACE-TIME BLOCK CODE FOR MIMO

Let us first consider the block transmission scheme with the block length  $T$ , the relationship between the input and the output of the MIMO system is obtained with  $N$  transmit and  $M$  receive antennas and flat block-fading channel can be expressed as:

$$\mathbf{Y} = \mathbf{XH} + \mathbf{V} \quad (1)$$

where

$$\mathbf{Y} = \begin{bmatrix} y(1) \\ y(2) \\ \vdots \\ y(T) \end{bmatrix}, \mathbf{X} = \begin{bmatrix} x(1) \\ x(2) \\ \vdots \\ x(T) \end{bmatrix}, \mathbf{V} = \begin{bmatrix} v(1) \\ v(2) \\ \vdots \\ v(T) \end{bmatrix} \quad (2)$$

are the matrices of the received signals, transmitted signals, and noise, respectively. The slow fading channel model is applied in this research work.

Besides, prior to space-time encoding, the complex information symbols are denoted as  $s_1, s_2, \dots, s_K$  and that these symbols are assumed to have the properties of zero-mean mutually uncorrelated random variables which are randomly drawn from constellations  $U_k, k = 1, 2, \dots, K$ . Let us show the vector;

$$\mathbf{s} = [s_1 s_2 \dots s_K]^T \quad (3)$$

Also note that  $s \in S$ , where  $S = \{\mathbf{s}^{(1)}\mathbf{s}^{(2)}\dots\mathbf{s}^{(L)}\}$  is the set of all possible symbol vectors and  $L$  is the cardinality of this set. The  $T \times N$  matrix  $\mathbf{X}(s)$  is known as OSTBC, if (Tarokh *et al.*, 1995):

- All the elements of  $\mathbf{X}(s)$  are the linear functions of the  $K$  complex variables  $s_1, s_2, \dots, s_K$  and these complex conjugates;
- $\mathbf{X}(s)$  must satisfies the following:

$$\mathbf{X}^H(s)\mathbf{X}(s) = \|s\|^2 \mathbf{I}_N \quad (4)$$

Whereas the matrix  $\mathbf{X}(s)$  is defined as follows:

$$\mathbf{X}(s) = \sum_{k=1}^K (\mathbf{C}_k \operatorname{Re}\{s_k\} + \mathbf{D}_k \operatorname{Im}\{s_k\}) \quad (5)$$

Where,  $\operatorname{Re}\{s_k\}$  and  $\operatorname{Im}\{s_k\}$  denote the real and imaginary parts, respectively, and

$$\mathbf{C}_k = \mathbf{X}(e_k) \quad (6)$$

$$\mathbf{D}_k = \mathbf{X}(je_k) \quad (7)$$

with  $j = \sqrt{-1}$  and  $e_k$  are respectively  $K \times 1$  vector having one in its  $k$ th element and zeros elsewhere. Using equation (5), one can rewrite (1) as:

$$\underline{\mathbf{Y}} = A(\mathbf{H})\underline{s} + \underline{\mathbf{V}} \quad (8)$$

In this paper, one can arrange the matrix in real and imaginary orders. Therefore, one denotes the “underline” operator for any matrix  $\mathbf{G}$  which is defined as:

$$\underline{\mathbf{G}} = \begin{bmatrix} \operatorname{vec}\{\operatorname{Re}(\mathbf{G})\} \\ \operatorname{vec}\{\operatorname{Im}(\mathbf{G})\} \end{bmatrix} \quad (9)$$

In most of the literature related to wireless communications, the advantage of the orthogonal feature in the calculation of matrix was used. In more specific, the algorithm in the optimized operation was applied to the  $2MT \times 2K$  real matrix  $A(\mathbf{H})$  with the following constraint:

$$A^T(\mathbf{H})A(\mathbf{H}) = \|\mathbf{H}\|^2 \mathbf{I}_{2K} \quad (10)$$

Note that the columns of  $A(\mathbf{H})$  have the same norms and are orthogonal to each others (Gharavi-Alkhansari & Gershman, 2003).

### THE MODIFIED SEMI-BLIND CHANNEL ESTIMATION TECHNIQUE

Let consider a Rayleigh flat fading MIMO channel characterized by  $\mathbf{H}$  first. Assuming that the MIMO uses  $N$  transmit and  $M$  receive antennas, the calculation is mainly based on the SVD of  $\mathbf{H}$  matrix:

$$SVD(\mathbf{H}) = \mathbf{P}\Sigma\mathbf{Q}^H \quad (11)$$

Note that where  $\mathbf{P}$  is a unitary matrix, the matrix  $\Sigma$  is a diagonal matrix with non-negative real numbers on the diagonal, and  $\mathbf{Q}$  is also a unitary matrix. Both  $\mathbf{P}$  and  $\mathbf{Q}$  must satisfy the following properties:

$$\mathbf{P}\mathbf{P}^H = \mathbf{P}^H\mathbf{P} = \mathbf{I} \quad \text{and} \quad \mathbf{Q}^H = \mathbf{Q}^H\mathbf{Q} = \mathbf{I} \quad (12)$$

Based on the previous literature, many methods are applied for estimating the matrix  $\mathbf{Q}$ , i.e. the estimation of  $\mathbf{Q}$  based on the training pilots. From these decompositions, the whitening matrix  $\mathbf{W}$  is given by  $\mathbf{W} = \mathbf{P}\Sigma$ , which can be estimated blindly, and particularly based on the received data only. Interestingly, if  $\mathbf{P}$  matrix is orthogonal, the  $\mathbf{W}$  matrix is also orthogonal. The estimation of  $\mathbf{W}$  matrix can be done by using high order statistic, but this particular technique need larger number of transmitted data to obtain the exact estimated channel. In this investigation, the channel estimation of  $\mathbf{W}$  matrix from the second order statistic was used, as it has been proven to be more effective than the other candidates, with the assumption of  $\mathbf{Q}$  matrix known perfectly. In addition, some theoretical results have shown that the estimation of the channel matrix based on estimation  $\mathbf{W}$ ,  $\mathbf{Q}$  can perform more efficiently than estimating  $\mathbf{H}$  directly from the pilot data. This is because the orthonormal matrix  $\mathbf{W}$  was applied and this led to use lesser number of parameters than the complete channel matrix  $\mathbf{H}$ , and hence, it could be estimated with greater accuracy from the limited pilot data.

Let us introduce the  $2MN \times 1$  channel vector  $\mathbf{W}$ , as:

$$\mathbf{W} = \underline{\mathbf{W}} \quad (13)$$

When  $A(\mathbf{W})$  is linear in  $\mathbf{W}$ , there exists a unique  $4KMT \times 2MN$  matrix  $\Phi$ , such that:

$$\text{vec}\{A(\mathbf{W})\} = \Phi \mathbf{W} \quad (14)$$

The key feature in this paper is based on the orthogonal matrix calculation. From equations (10) and (13), the following was obtained:

$$A^T(\mathbf{W})A(\mathbf{W}) = \|\mathbf{W}\|^2 \mathbf{I}_{2K} \quad (15)$$

Applying the trace operator to both sides of (15), the following was retrieved:

$$\mathbf{W}^T \Phi^T \Phi \mathbf{W} = 2K \|\mathbf{W}\|^2 \quad (16)$$

As equation (16) is satisfied for any  $\mathbf{W}$ , it leads to the following expression:

$$\Phi^T \Phi = 2K \mathbf{I}_{2K} \quad (17)$$

Through expression (17), it can be seen that the columns of the  $\Phi$  are orthogonal to each other.

Before introducing the blind channel estimation, the following Lemma (Manton, 2002) is needed:

**Lemma 1:** Let  $\mathbf{B}$  be an  $m \times q$  real matrix, where  $q \leq m$ ; for any  $m \times m$  real symmetric matrix  $\mathbf{M}$ , the solution to the following optimization problem:

$$\begin{aligned} & \max_{\mathbf{B}} \text{tr}\{\mathbf{B}^T \mathbf{M} \mathbf{B}\} \\ & \text{s.t. } \mathbf{B}^T \mathbf{B} = \mathbf{I}_b \end{aligned} \quad (18)$$

is given by any matrix  $\mathbf{B}_*$  whose column space is the same as the subspace spanned by the  $b$  principal eigenvector of  $\mathbf{M}$  and, for any such  $\mathbf{B}_*$

$$\text{tr}\{\mathbf{B}_*^T \mathbf{M} \mathbf{B}_*\} = \sum_{i=1}^b v_i \quad (19)$$

where  $v_i$ ,  $i = 1, 2, \dots, b$  are the  $b$  largest eigenvalues of  $\mathbf{M}$

*Proof:* See (Manton, 2002)

Next, the following set of the parameters is available:

$$\begin{aligned} b &= 2K \\ \mathbf{B} &= A(\tilde{\mathbf{W}})/\|\tilde{\mathbf{W}}\| \\ \mathbf{M} &= E\{\underline{\mathbf{Y}}\underline{\mathbf{Y}}^T\} = A(W)E\{\underline{s}\underline{s}^T\}A^T(\mathbf{W}) + (\sigma^2/2)\mathbf{I}_{2MT} \end{aligned} \quad (20)$$

Applying the Lemma above and based on equation (18), the optimized constraint was obtained to estimate matrix  $\mathbf{W}$  as follows:

$$\max_{\tilde{\mathbf{W}}} \frac{\text{tr}\{A^T(\tilde{\mathbf{W}})\}MA(\tilde{\mathbf{W}})}{\|\tilde{\mathbf{W}}\|^2} \quad (21)$$

Next, decompose the optimized equation into some elements which are calculated easily, as follows:

$$\begin{aligned} \text{tr}\{A^T(\tilde{\mathbf{W}})\}MA(\tilde{\mathbf{W}}) &= \text{vec}\{(\tilde{\mathbf{W}})\}^T(\mathbf{I}_{2K} \otimes \mathbf{M})\text{vec}\{A(\tilde{\mathbf{W}})\} \\ &= (\tilde{\mathbf{W}})^T \Phi^T (\mathbf{I}_{2K} \otimes \mathbf{M}) \Phi \tilde{\mathbf{W}} \end{aligned} \quad (22)$$

Therefore, the optimization issue (21) will be changed, as follows:

$$\max_{\tilde{\mathbf{W}}} \frac{(\tilde{\mathbf{W}})^T \Phi^T (\mathbf{I}_{2K} \otimes \mathbf{M}) \Phi \mathbf{M} \tilde{\mathbf{W}}}{\|\tilde{\mathbf{W}}\|^2} \quad (23)$$

For simplicity purposes,  $\Phi^T(\mathbf{I}_{2K} \otimes \mathbf{M})\Phi = \mathbf{U}$ , and a new optimization expression is obtained (note that the estimation of  $\mathbf{W}$  matrix is required).

$$\max_{\tilde{\mathbf{W}}} \frac{(\tilde{\mathbf{W}})^T \mathbf{U} \tilde{\mathbf{W}}}{\|\tilde{\mathbf{W}}\|^2} \quad (24)$$

In particular, note that all the solutions to this optimization depend on the sub-spaces spanned by the  $n$  linearly independent principle eigenvectors of the  $\mathbf{U}$  matrix, with  $n$  as the multiplicity order of the largest eigenvalue of this matrix. The value of  $n$  depends on the matrix  $\Phi$ , which in turn, is dependent on the structure of the underlying OSTBC (Tarokh *et al.*, 1999). It is difficult to find the relationship between the value of  $n$  and the structure of  $\Phi$ . Through the experiments, one can also observe that in most cases tested,  $n = 1$  is always true. Ignoring the scaling ambiguity, the normalized solution to (23) can be illustrated as:

$$\hat{\tilde{\mathbf{W}}} = \Omega(\mathbf{U}) \quad (25)$$

where  $\Omega(\mathbf{U})$  stands for the normalized principle eigenvector of a matrix  $\|\Omega(\mathbf{U})\|$ , and  $\hat{\tilde{\mathbf{W}}}$  is  $\mathbf{W}$  estimated matrix. In addition, the least square estimation of the  $\mathbf{Q}$  matrix, using only the pilot data, is given by:

$$\hat{\mathbf{Q}}_{LS} = \mathbf{Y} \mathbf{X}^\perp \quad (26)$$

where  $\hat{\mathbf{Q}}_{LS}$  is the estimated matrix of  $\mathbf{Q}$ , following the least square algorithm.

Finally, combining the two estimated channel matrices (both  $\mathbf{W}$  and  $\mathbf{Q}$  matrices mentioned above), a complete estimated channel estimation known as the  $\mathbf{H}$  matrix is obtained.

## SIMULATION RESULTS

In all the simulations, the performance of the proposed approach for semi-blind channel estimation is presented. Some basic parameters which have been used in this investigation are: modulation format of QPSK, 1000 Monte Carlo trials, a Rayleigh distributed channel, indicating that each element of  $\mathbf{H}$  channel follows a complex Gaussian circular law with zero-mean and unit variance, and the transmitted symbols are i.d.d. on every antenna. Moreover, a spatially white Gaussian noise is used in these simulations. The rate of the OSTBC is defined as the ratio between the numbers of symbols the encoder takes as its input and the number of space-time coded symbols transmitted from each antenna.

The authors analysed the performance of the algorithm presented in this paper with the results from the research work of Ammar *et al.* in 2007. From *Fig. 1*, the lines in term of MSE criterion collides with each other, proving that both solutions with the same quality. Besides, the extremely high complexity in blind channel estimation is determined as the reason for slow convergence at high SNR parameter.

Based on the research work of Tarokh *et al.* in 1999, some orthogonal schemes were applied for the MIMO system with  $t$  transmit and 4 receive antennas, such as OSTBC3, OSTBC4, OSTBC5, and OSTBC6, with the number of transmit antennas as 3, 4, 5, 6 respectively. In this experiment, the rate of 1/2 is set, and the number of symbols to be transmitted is 512. In the second experiment (*Fig. 2*), it can be seen that the performance is better as fewer number of transmit antennas is used, with the assumption of a fixed number of receive antennas.

In the third experiment (*Fig. 3*), the simulation for MIMO OSTBC3 is displayed with a code rate of  $\frac{3}{4}$  for the different numbers of transmitted signal. Intuitively, the solution proposed stably remains through a large number of symbols. This illustration proves that applying the SOS-based

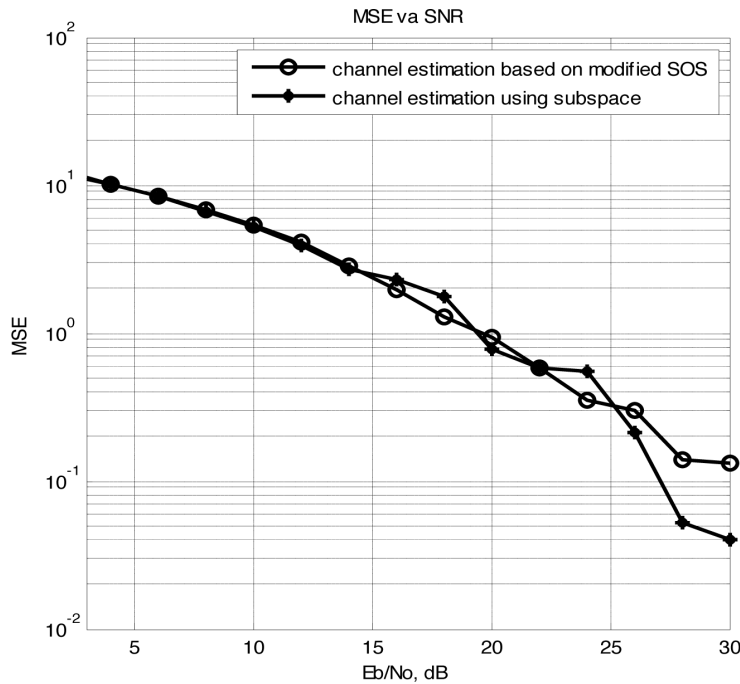


Fig. 1: The comparison between the proposed method and one using the subspace

New Semi-blind Channel Estimation in MIMO based on Second Order Statistics

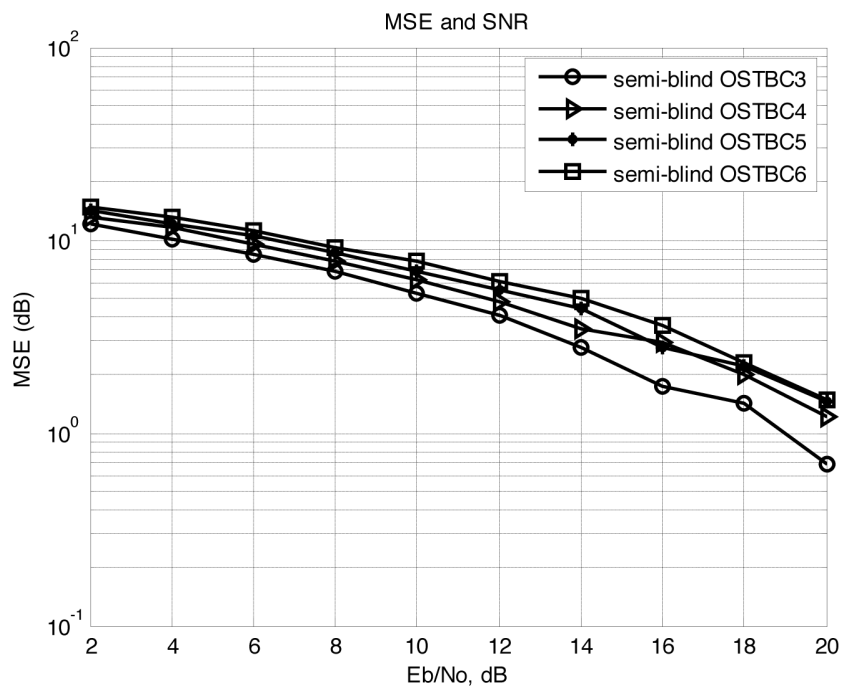


Fig. 2: The MSE performance versus SNR

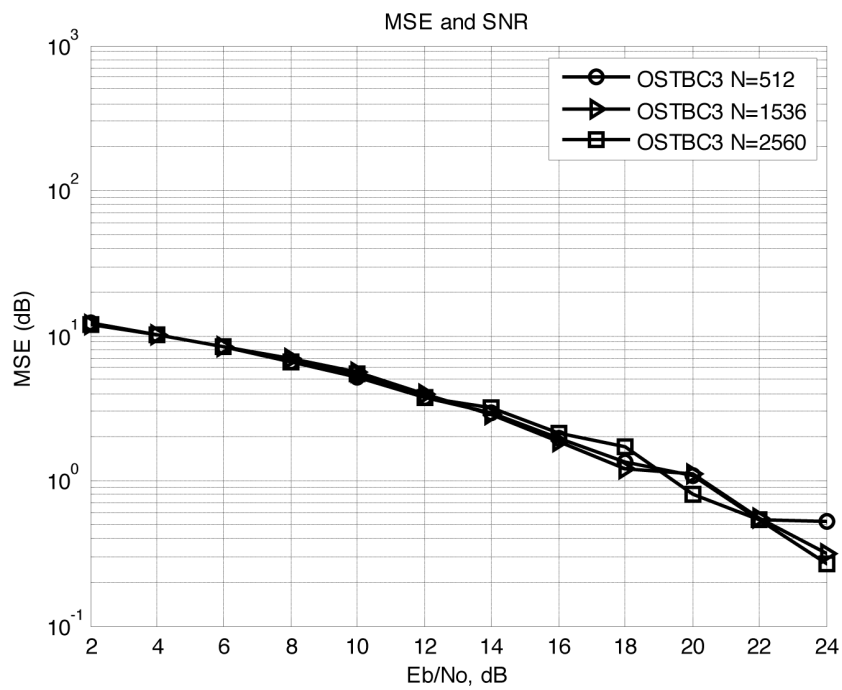


Fig. 3. The MSE performance versus SNR with different numbers of transmitted symbols (N)

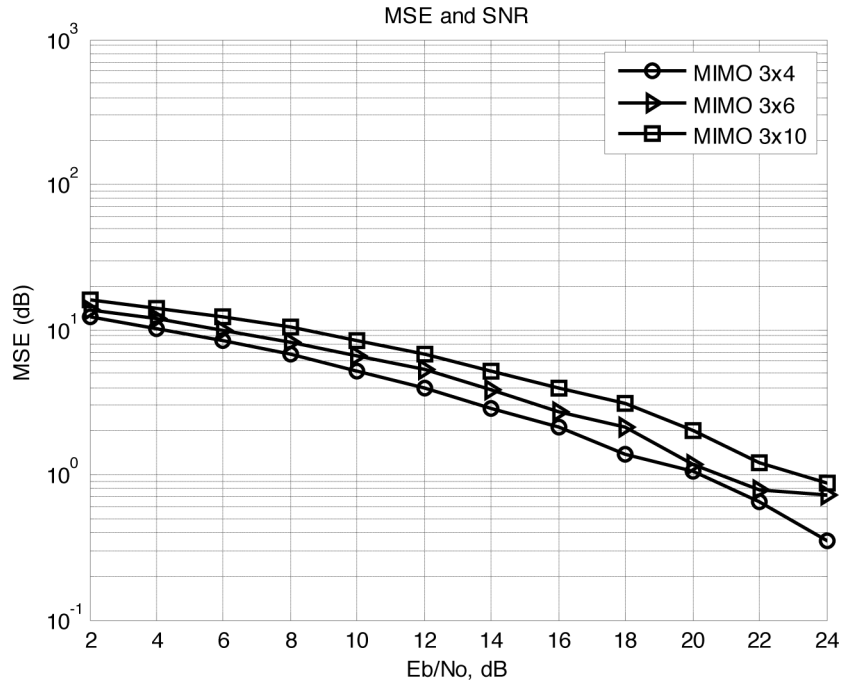


Fig. 4: The MSE performance versus SNR with different MIMO OSTBC3 systems

channel estimation for the detached matrix channel (based on the SVD calculation) leads to the optimization technique of the MIMO deployment in the reality.

In the rest of the experiments, Fig. 4 shows that the performance of MIMO OSTBC3, with 3 transmits antennas and 4, 6, 10 receive antennas, respectively. In particular, MIMO  $\frac{3}{4}$  is considered as the best performance among the three experimental approaches. It is true that balancing the number of transmits and receives antennas which help to create the improving scene. Therefore, this result also proves that the MIMO with a decreasing cost can bring a substantial capability in the wireless applications because of fewer numbers of designed antennas.

## CONCLUSION

In this study, the new semi-blind channel estimation has been presented by applying both the second order statistics and the training-based least square techniques which address the use of the properties of the orthogonal matrix columns in the transmitted signals. Through the paper, it is true that the structure of the OSTBC effect on the estimated channel is carefully calculated especially in the different MIMO systems for higher data rate. The researchers have attempted to solve the ambiguity problem in previous literature, particularly in term of blind estimation. The MSE analyses in the simulations are clear demonstrations which have provided the improvement work for channel estimators.

## REFERENCES

- Ammar, N., & Ding, Z. (2007). Blind Channel Identifiability for Generic Linear Space-Time Block Codes. *Signal Processing, IEEE Transactions on*, 55(1), 202-217.

New Semi-blind Channel Estimation in MIMO based on Second Order Statistics

- Foschini, G. J., & Gans, M. J. (1998). On Limits of Wireless Communications in a Fading Environment when Using Multiple Antennas. *Wireless Personal Communications*, 6(3), 311-335. doi: 10.1023/a:1008889222784
- Gesbert, D., Shafi, M., Da-shan, S., Smith, P. J., & Naguib, A. (2003). From theory to practice: an overview of MIMO space-time coded wireless systems. *Selected Areas in Communications, IEEE Journal on*, 21(3), 281-302.
- Gharavi-Alkhansari, M., & Gershman, A. B. (2003, 6-9 Oct. 2003). *Constellation space invariance of space-time block codes with application to optimal ML decoding*. Paper presented at the Vehicular Technology Conference, 2003. VTC 2003-Fall. 2003 IEEE 58th.
- Jagannatham, A. K., & Rao, B. D. (2006). Whitening-rotation-based semi-blind MIMO channel estimation. *Signal Processing, IEEE Transactions on*, 54(3), 861-869.
- Larsson, E. G., Stoica, P., & Li, J. (2002). On maximum-likelihood detection and decoding for space-time coding systems. *Signal Processing, IEEE Transactions on*, 50(4), 937-944.
- Manton, J. H. (2002). Optimization algorithms exploiting unitary constraints. *Signal Processing, IEEE Transactions on*, 50(3), 635-650.
- Tarokh, V., Jafarkhani, H., & Calderbank, A. R. (1999). Space-time block codes from orthogonal designs. *Information Theory, IEEE Transactions on*, 45(5), 1456-1467.
- Telatar, E. (1999). Capacity of Multi-antenna Gaussian Channels. *European Transactions on Telecommunications*, 10(6), 585-595. doi: 10.1002/ett.4460100604
- Wing-Kin, M. (2007). Blind ML Detection of Orthogonal Space-Time Block Codes: Identifiability and Code Construction. *Signal Processing, IEEE Transactions on*, 55(7), 3312-3324.
- Wing-Kin, M., Ba-Ngu, V., Davidson, T. N., & Pak-Chung, C. (2006). Blind ML detection of orthogonal space-time block codes: efficient high-performance implementations. *Signal Processing, IEEE Transactions on*, 54(2), 738-751.



## Performance Evaluation of A Mobile Road Traffic Infraction Registration System through Benchmark

**Arasteh-Rad, H.\* , Khairulmizam Samsudin, Abdul Rahman Ramli and Mohammad Ali Tavallaie**

*Department of Computer and Communication Systems Engineering,  
Universiti Putra Malaysia, 43400 Serdang, Selangor, Malaysia*

\*E-mail: *HABIB\_ARASTEH@yahoo.com*

### ABSTRACT

The rapid development of roads and the increasing number of vehicles have complicated road traffic enforcement in many countries due to limited resources of the traffic police, specifically when traffic infraction registration is done manually. The efficiency of the traffic police can be improved by a computer-based method. This study focused on mobile traffic infraction registration system benchmarking which is used to evaluate the server performance under load. The study attempts to provide a clear guideline for the performance evaluation of mobile road traffic infraction registration system, whereby the traffic police can make decision based on them to migrate from the manual-method toward computer-based method. A closed form of benchmark tool was used for the evaluation of the system performance. The tool was configured to imitate ramp scenarios, and statistics were gathered. The server was monitored at different times and works. Contributing factors include bottleneck, traffic, and response time, which are related with criteria and measurements. The system resource was also monitored for the tests.

**Keywords:** Benchmark, road traffic, infraction registration, performance evaluation

### INTRODUCTION

The telecommunication technology and information revolution are offering solutions for problems in major cities in the world; problems which include congestion, traffic control and E-commerce. The development of computer networking and the use of personal computers have made an important effect to the network applications. However, these systems have mobility limitations.

In the recent years, the advances of wireless networking, communication, and mobile technology become more popular and create new aspect of services each day. Wireless networks refer to any system of transmitters and receivers that send radio signals over the air, such as a Wi-Fi local networks, cellular networks or satellite networks (Zhu Han & K. J. Ray Liu, 2008). There are several factors and reasons that could lead to the implementation of these services. The most important factor about the wireless services is the anywhere, anytime feature that it offers (Takahashi *et al.*, 2005). Mobile systems and applications could be used to enhance the forms of existing applications (RAD Technical Rep., 2000). Nowadays, mobile equipment has large storage capacity, and a wide array of applications and connectivity options. In other words, mobile devices could create new market since they are even more accessible than PC.

The total number of mobile phone subscribers in the world was estimated to be 2.14 billion in 2005 (Mobiletracker, May 2005). The subscriber count reached 2.6 billion by the end of 2006 (PCWorld, 2006), and this would further boost to 4.5 billion in 2012 (Cellular-News, March 2008).

---

Received: 23 April 2010

Accepted: 23 August 2010

\*Corresponding Author

Around 60% of the world's population have the access to mobile network coverage than it was in 2006. This percentage was expected to increase to 90% by the year 2010 (Turettini, 2006). The rise of the mobile phone technology in developing countries is often cited as an example of the leapfrog effect. However, the cellular network was first designed for voice communication purposes (Qusay, n.d), but further developments within the network (cellular network) have made it possible to transmit data as well. For instance, the GSM technology has the data rate of 9.3 kbps and the current 3-G technology offers a data rate that goes up to 2 Mbps. Data from Informa indicated that by 2010, half of the planet's population would have the access to the Internet through a mobile device (Informa Telecoms & Media, 2008). Surprisingly, road developments have been rapidly occurring and simultaneously increasing the number of vehicles, specifically in developing countries.

For example, the growth rates of the vehicles and roads in Malaysia between 1986 and 2006 were 369% and 147%, respectively (Othman, 2010; Ahmad & Azmi, 2007), and these were 291% and 189% in Iran (Zekavat, n.d). This rapid development introduces a lot of road traffic enforcement issues which are mainly caused by the limited resources of the traffic police. Adding to the problem is that traffic infraction registration is still done manually using a pen and a notebook. Iran is among one of the countries having the highest rates of road violations in the world (Royanian, 2007). A new, convenient and efficient method for infractions registration is deemed to be urgent. In the recent years, some developed countries have initiated and funded the development of electronic ticketing systems. A combination of the E-ticket with wireless or cellular network could potentially increase the efficiency of road traffic rule enforcement. The patrol traffic officers out in the field need a powerful, yet easy-to-use, handheld solution to help them efficiently access traffic databases to collect, transmit and deal with the real-time information. For example, they need to be able to access to the driver offender information to validate the driving license and infraction traffic ticket submission anytime, anywhere. Therefore, there are a lot of officers who can access to the server and make a heavy load on it. Cronkhite states that 'information is the life blood' of police (Cronkhite, 1974). This is because an accurate and rapid flow of police information is essential for effective law enforcement. By using test tools, the server can be tested with various tests including load tests, performance tests, stress tests and ramp tests. Load tests were performed to determine the best estimate of the traffic server needs to support. Consider this as a "real world test" of the server. Performance tests are in fact used to test each part of the server or the Web application to discover how to optimize them for higher traffic. Ramp tests are a set of variations of the stress tests, in which the number of users raise during the test processes, i.e. from a single request to hundreds of requests. Stress tests constitute of the simulated "brute force" attacks that apply excessive loads to the server. For instance, Anwar *et al.* assessed the scalability and performance of a Web application based on the PHP scripts by using stress testing (Anwar & Saleem, 2002). Their experimental work focused on stress testing for two main subjects that contain bandwidth and system loads. Another example would be the work of Santra *et al.* in 2009. The researchers measured memory usage in the web enabled J2EE application under ramp test, while running multithreaded web enabled J2EE application, with and without changing user load.

In this manuscript, a computerized traffic infraction registration system was designed to replace the manual system. The new system has the capability to provide online ticket issuing to mobile officer at the scene. The server's accurate performance was evaluated under performance tests to insure traffic police to migrate from the manual-method towards computer-based method. The rest of this paper is structured as follows. The following section begins with the introduction of the problem statement and next constructs mobile road traffic infraction registration system architecture. Then, Infraction Registration Benchmark Tool (IRBT) that is familiar with the traffic infraction registration system will be elaborated. Meanwhile, experiment methodology is presented in Section 2. Section 3 presents and discusses the results. The last section concludes the present work.

### *Problems Statement*

A convenient, reliable, secure and efficient system is in dire need for tickets to be properly registered. In the new system, the patrol officers on duty should have the access to databases to collect, transmit and deal with the infraction information in real time, such as the new computer technologies allow officers to collect data at the scene, transfer the information to the police data centre, provide on-line error checks electronically, and subsequently, issue a traffic ticket in real time. Police should be satisfied with the ability of the new system to approve the migrate. Modelling, analytical system, mathematical simulation and benchmarking are ways to server's performance evaluation. Benchmark was applied in this study to assure traffic police that the new system is always reliable and stable at the expected level even under critical loads. Meanwhile, the hardware and software of server can be assessed by benchmarking under realistic workloads (SPEC, 2009). It has a responsibility for the tuning options best serve requests. Sometimes, a system is designed for a certain level of traffic; when the traffic increases beyond a certain point, response times will also increase to unacceptable time. For instance, some studies have demonstrated that when the response time takes less than 0.1 s, user feels that the system responds instantaneously. Although users are depressed with the waiting time, but they are still focused on the current transaction when the response time becomes less than 1.0 s. Whenever the waiting time gets close to 10s, the likelihood of user distraction increases, and this becomes more than 10 s, the users are most likely to be distracted from the current transaction and lose interest (Dilley, 2002; Abdelazez, 2000). Another consideration is the amount of requests that the server is expected to handle, particularly during the peak load periods. Load and time will also affect on the performance of the server. Therefore, load should be simulated on the servers before putting them online to determine how the server will perform its functions.

Is the server's bandwidth adequate? Is the server prepared for the network traffic that police have prospect? Can the server tolerate the officers' requests traffic? Where are the server's capacity boundaries? These questions can be answered after server performance evaluation has been carried out.

### *Road Traffic Infraction Registration System Infrastructure*

The mobile road traffic infractions registration system design was based on the Iranian officer's tasks to meet the requirements of traffic policing duties. The system should be able to handle officer's queries in a secure manner. In this manuscript, a request or query means an officer's request for details of offender(s) before issuing ticket or online issued ticket from the scene to the server. The mobile road traffic infraction registration system was constructed on three-tier architecture or structural design. In this system, the front-end is the mobile device, the middleware is the software server running on the desktop workstation that contains the business logic of the system and back-end is referred to the database server. *Fig. 1* shows the mobile road traffic infraction registration system structure and layout. As shown in *Fig. 1*, mobile devices are used to access the police's system. They are the front-end tier (or the clients) in the system architecture. The officer is accessing the server using the GPRS enabled mobile device, and making direct HTTP connections to the IP-based web server without going through the WAP gateway. This is due to the fact that the TCP/IP network principles and concepts over the cellular network are simulating with GPRS. The mobile device would be treated like another IP-network device (3G Americas, 2008). If an officer is communicating with the system through text messages, the police request sent goes through the SMS gateway (Labordère, 2006). The SMS gateway receives and forwards the message to the police's server. If the officer tries to connect to the system through WAP, the requests and replies go via the WAP gateway. The gateway will then convert the requests into the

format that can be understood by the IP-based network device and vice-versa (RAD, Jan 2009). The middleware and back-end contain the business logic and the database servers of the system, respectively. The server would make database accesses to retrieve or manipulate data whenever it is requested by the officers.

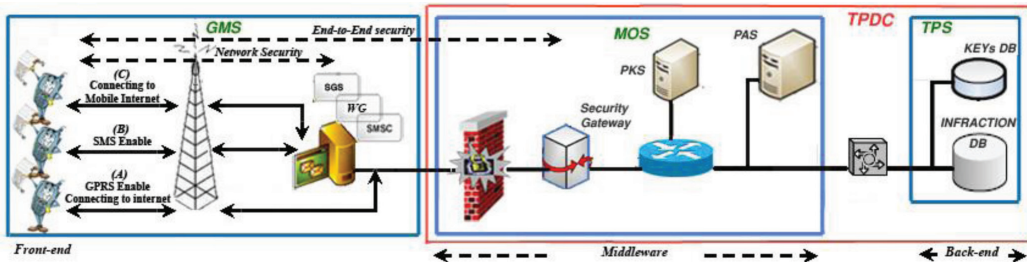


Fig. 1: The architecture of a secure traffic police mobile communication

The secure network topology is divided into three subsections, namely, the Traffic Police Subsection (TPS), the Mobile Operator Subsection (MOS) and the General Mobile Subsection (GMS) (see Fig. 1). The GMS are facilities operated by a carrier to provide public mobile telecommunication services that include wired and wireless networks. Security Gateway (SG) isolates the TPDC from GMS. The TPS and MOS are located in the TPDC. They are isolated by a VPN gateway to provide a secure real-time data exchange environment (Whale Communications Ltd., Mar 2003). The basic functionality of the TPDC is to handle officers' requests with a secure communication. It is known that mobile devices have limitations on the resources such as power and memory. In the TPDC, however, there are no resource limitations. Therefore, it was decided that most tasks would be handled by TPDC.

In this architecture, when a message (possibly a requesting message) is sent to TPDC by a user, it is first delivered from the Mobile Equipment (ME) to the GMS through the base station system (BSS). The GMS would then forward the message to the application server (PAS) through the SG. On the contrary, when a message (possibly a response message) is sent to a mobile user by the PAS, it is first delivered from the PAS to the GMS through the Security Gateway; the connection between the GMS and the SG is facilitated by a TCP/IP connection over the Internet.

## Databases

The database schema is shown in Fig. 2. The TPDC database requires using of data from other organizations' databases. For instance, citizenship identification data exist in the Personality Registration Organization (P.R.O.) database. Therefore, the TPDC database has been designed as a relational database. In this system, the main databases are *INFRACTION-DB* and *KEYs-DB*. As illustrated in Figure 2, *INFRACTION-DB* contains nine tables which include *Personal*, *PoliceMan*, *License*, *Per\_Lic*, *City*, *Infcode*, *Infraction*, *Vehicle*, *P\_I\_V*. The *Personal* table contains drivers and policeman's personal data. The *PoliceMan* table keeps officers special data such as identity number, mobile number, officer's code, officer's national number, officer's operation section and officer's ID date of expiry. Data pertaining to driving licence are kept in the *License* table and the city codes stored in the *City* table. Meanwhile, infraction code and type can be retrieved from *Infcode* table and *Infraction* table. The *Vehicle* table contains data on vehicles. The infraction data are stored in the *P\_I\_V* table and would be the most important table which is frequently used in officer's queries. Officer's transaction keys are stored in *KEYs-DB*. The internal-databases are located in TPS.

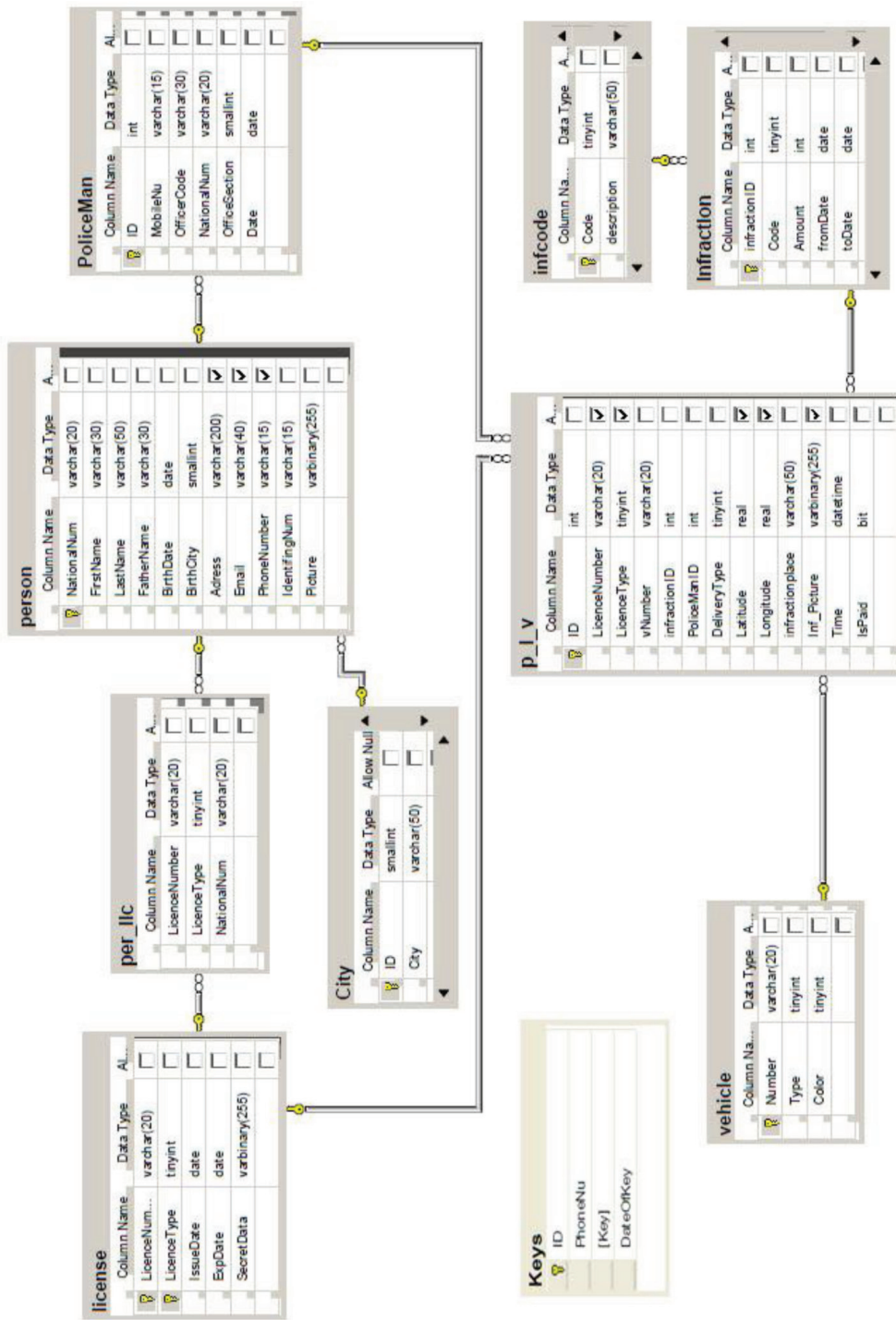


Fig. 2: Traffic police database ER diagram

### Application Server

The Security Gateway and the Police Keys Server are responsible for confirming an officer's authorization, authentication and request decryption. The application server is responsible for relaying officers' request to the database. Officer's requests (queries) can be classified in two groups, namely, officer's inquiries and traffic ticket issuing. Officer's inquiries are classified in four sub-groups, which include penalty amount history, and driving license validation, to check driving license, and vehicle confirmation.

### Security Gateway

The Security Gateway (SG), which is a gateway with security functionalities, resides in TPDC. It provides an end-to-end secure communication between the Traffic Police Data-Centre (TPDC) and its mobile officer (see Fig. 1). Security Gateway (SG) isolated MOS and GMS. It is composed of User Authentication Agent (UAA) module and Access Point (AP) module. The AP module provides the necessary interface to the police mobile clients. It communicates with the General Mobile Subsection over TCP/IP and takes the responsibility of receiving/sending messages from/to GMS. The UAA module takes the responsibility of the authentication of the mobile clients.

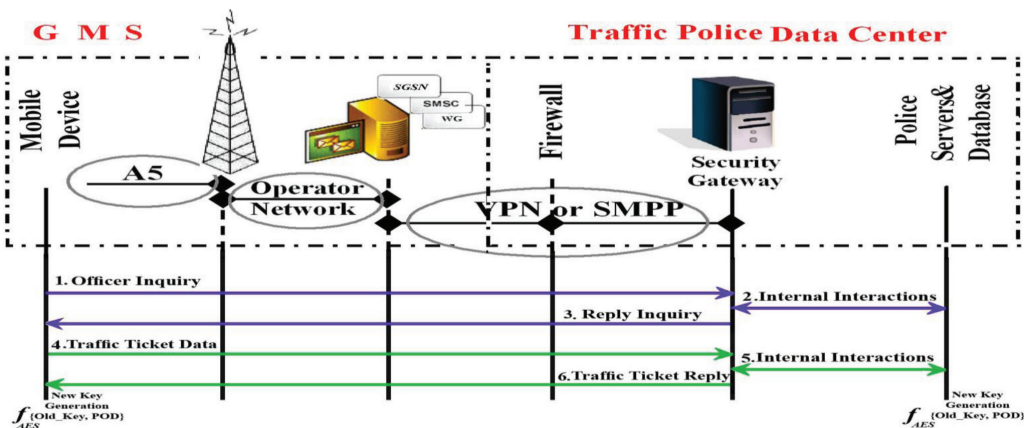


Fig. 3: Data transaction flow

### Police Keys Server

The PKS is a trusted party that validates the identities of each entity. Its main functionalities include: (1) generation of new keys, (2) cryptographic operation, and (3) maintaining a database containing valid keys, and Revocation Lists (RLs). The Police Keys Server fetches the key from the *KEYs-DB* pertaining to each request. It provides confidentiality for messages transmission.

Encryption and officer validation Symmetric encryption algorithms have been chosen to provide the necessary cryptanalytical strength and low resources consumption (Potlapally *et al.*, 2003; Gupta *et al.*, 2002; Gebotys. 2004). However, key transmissions on the network have major risk (Mobile Payment Forum, 2003). The use of key distribution techniques, such as divided key methods and submission of a key to trusted neighbour, have also been employed. In this research work, a novel protocol for security improvement has been proposed (Rad *et al.*, 2009). To reduce the risk, the novel method was introduced to enforce the changing of exclusive keys between two parties periodically. This protocol would consider that offender's driving license is an exclusive

data between the Traffic Police Data-Centre (TPDC) and the police officer. The TPDC stores the information pertaining to driving license in the database, and the police officer may obtain the driving license of the offender physically at the infraction venue. *Fig. 3* illustrates the data transaction flow for issuing ticket after an inquiry. The first key is issued to the police officer by the TPDC. The officer will use this key to encrypt the first message (i.e. offender driving license) required to verify the driving license and calculate a hash of the officer ID,

$$\text{Req\_Verify\_License} = \{\text{H}(ID_{\text{officer}}), f_{\text{AES}}(\text{Driving License})\}$$

First, the TPDC checks  $\text{H}(ID_{\text{officer}})$  and officer's mobile number, which is used as the fingerprint of the current officer's ID. If the check fails, the protocol will abort the request. Otherwise, it will fetch the key from the PKS server according to the mobile phone number and the TPDC will decrypt the transmitted data and authenticate the police officer's ID. Then, the TPDC will assign a new and temporary ID for this officer session (Daily\_session\_ID). A response will be sent to the officer to confirm the offender's driving license. This confirmation message consists of license confirmation, Daily\_session\_ID, date and time session availability. The officer will use the first key for decryption. Once the driving license has been verified, the police officer will issue the traffic ticket, encrypt traffic ticket and Daily\_session\_ID and send to TPDC. At this stage, the TPDC server and the police officer's mobile phone will generate a new key using the first key and any predetermined data from the offender information (POD):

$$\text{New\_Key} = f_{\text{AES}} \{ \text{Old\_Key}, \text{POD} \}$$

This measure provides a high level security transaction, since the key is changing periodically with each new offender. AES is the chosen symmetric algorithm even when considering the mobile resource considerations (Potlapally *et al.*, 2003).

## Mobile Client

PDAs or Web-enabled mobile devices can use mini Web browsers to access mobile Web applications via wireless Internet connection (Siau *et al.*, 2003). They are preferred for the mobile road traffic infraction registration system. Mobile Web applications are hosted on application servers and can consume Web services on the server-side. They can invoke Web services, integrate responses from these Web services, and then return the consolidated results as Web pages to mobile devices.

### *Infraction Registration Benchmark Tool (IRBT)*

The testing tools offer a wide range of functionality needed for performance testing, such as load generation and measurements. Many tools have been developed today for generating workloads on the server. For instance, some testing tools can be found from Banga and Druschel (1997), SPEC (2009), Tschalar (2001) and ServerWatch (2009). They are all based on making repeated requests as quickly as possible at a predetermined rate. For instance, TPC-W is a benchmark from the Transaction Processing Council designed to evaluate e-commerce systems (TPC, 2009). It implements an online bookstore and has three workload mixes that differ in the relative frequency of each of the transaction types. Elnikety *et al.* performed some experiments by using TPC-W and RUBiS (Elnikety *et al.*, 2007) and explored a range of the problem space by varying the size of the database. They focused on TPC-W and scale the database with a small database (0.7 GB), a medium database (1.8 GB), and a large database (2.9 GB). In addition, they varied the memory as 256 MB, 512 MB, and 1024 MB. In another experiment, they used RUBiS Benchmark. In this

attempt, the RUBiS database has a constant load of 2.2 GB. Two workloads were mixed in this experiment containing browsing mix that is read-only and a bidding mix having 15% updates. The work of Deng *et al.* can be seen as another example of the use of the performance tools based on TPC-W Benchmark, in 2004. Their work defined 14 Web interactions in the TPC-W specification. Six of those are read only, while the other 8 update the database. The researchers also defined the database in 8 tables. The test case is based on the sequence of pages to be visited, apart from the input values to be provided to pages containing forms.

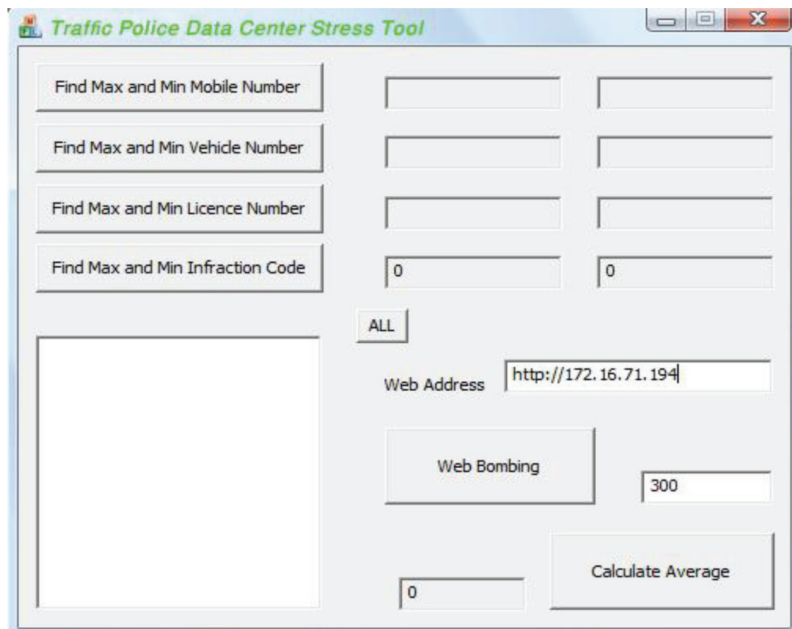


Fig. 4: A screenshot of Infraction Registration Benchmark Tool (IRBT)

However, the test tools only send a new request after the server has replied to its previous request and there is also no freedom of action to change the load-generator model. In order to obtain an in-depth information about the behaviour of the server, the authors needed to use a specific tool to emulate the behaviour of the clients. For the purpose of the experiments, a tool that is familiar with the traffic infraction registration system. A closed form benchmark tool was used for the evaluation of the system performance. Infraction Registration Benchmark Tool (IRBT) is a powerful HTTP-client/server test application that was designed to exactly determine the critical performance issues in the Traffic Police Data Centre that might prevent an optimal traffic ticket registration for officers (Arasteh-Rad *et al.*, 2009). The IRBT was designed and implemented to simulate the real-world traffic ticket generation. Fig. 4 illustrates a screenshot from the IRBT.

The tool generates independent officer's requests. Each random request includes police's phone number, vehicle number, driving license number, delivery type, infraction place and infraction code (see Fig. 5). It continuously submits requests to the server, waits for a period of time after the server has sent a reply to the request (processing time), and then submits a new request. The proposed benchmark tool can simultaneously generate from a few to several hundred requests at the same time. Each emulated traffic ticket issued is called a virtual traffic ticket, which is the key of the load-testing concept in the current study.

Request Name	Request Type	Officer Code	Police Phone Num	Delivery Type	Infraction Place	Vehicle Number	Driving License Num	Infraction Code	Date Time
--------------	--------------	--------------	------------------	---------------	------------------	----------------	---------------------	-----------------	-----------

Fig. 5: Traffic ticket format

The actual flow of control for the IRBT data generation is illustrated in Fig. 6. In the first step of the workflow, the Infraction Registration Benchmark Tool performs to estimate from the data in the INFRACTION-DB. The benchmark tool can find data fluctuating boundaries in the database related to the police's request fields. After finding the data range, the Infraction Registration Benchmark Tool randomly generates the request fields. This is followed by the total requests (traffic tickets) issued per term, the number of concurrent requests, and average request size and URL. The total request issues per term refer to the total number of requests made by the Infraction Registration Benchmark Tool during the test. ‘Concurrent requests’ in the tests also refer to the case, where two or more simultaneous requests for traffic ticket registration, which could be different, are sent to the server. This corresponds to the case where multiple officers send traffic tickets at the same time. The server URL is specified manually. The interval between the requests generation can be set optional such as manually or with a probability distribution function. Finally, when the total number of generated requests is more than the total number of requests, proceed will be finished. The number of hits and time to the last byte are important metrics for the measurement. The numbers of hits are the total number of requests made by Infraction Registration Benchmark Tool during the test run. TTLB (Time to Last Byte) is the total time, in milliseconds, that last byte of the last request is responded by the server and the client connection will be closed.

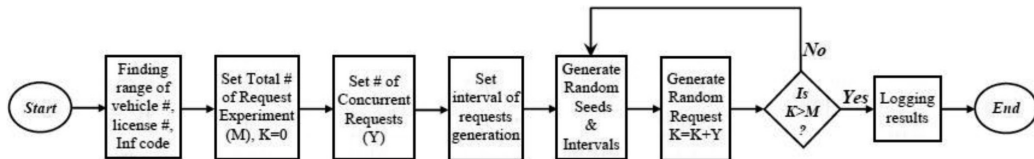


Fig. 6: Infraction Registration Benchmark Tool (IRBT) flowchart

## EXPERIMENTAL METHODOLOGY

Hardware, network and external load are basically elements that influence on the performance. These elements are given by information such as server hardware configuration, network bandwidth, database size, average size of the files served and concurrent arrival requests. The effect amounts of them depend upon the system bottlenecks. In the mobile traffic police infraction registration system, the database size and the concurrent arrival requests variations are notably important elements. For example in Iran, more than forty two million traffic tickets were issued in 2007 (Royanian, 2007). Therefore, the police database size increases every year, and the massive access to the system is also expected at the same time. Moreover, the database records should be accessible for police officer's queries. Here, the system was assumed to have enough network bandwidth.

In the following sections, the main parameters in the IRBT used in the simulation test in the benchmark, configuration parameters in the IRBT benchmark, test-bed in the proposed servers and monitoring the server performance behaviours are discussed.

### *Performance Metrics of the Experiment*

The IRBT supports various types of tests contain, load tests, stress tests, and ramp tests. The number of simultaneous requests on one URL raises during the ramp tests processes, i.e. from a single request to hundreds of requests. Ramp tests can be considered, such as a set of variations of the stress tests. Stress tests simulated excessive load to server. In this study, the focus was given on the ramp tests, while stress test, such a part of ramp test, was also highlighted.

In the experiment carried out in the current study, the system performance evaluation was based on the several factors, such as CPU load, physical memory usage, limitations of the number of users, response time and the number of users accessing to server at a given time. Any one of these factors may degrade the performance of the server. If any resource experiences a situation resembling a bottleneck, it can be a restriction for the system. For example, if CPU utilization is optimized at 100% during normal load hours, then there will be no capacity to handle a peak load.

### *Test Environment*

It is important to highlight that the same hardware was used for all the experiments. Each one contains Intel® Pentium TM Dual Core 2.40 GHz 1 MB Advanced Transfer Cache, 2048 MB DDR2 RAM, and a 320 GB Serial ATA hard drive (7200 rpm). They are connected via multiple 24 port gigabit switches and run a stock Linux Ubuntu 8.10. The TPDC was implemented based on Apache version 2.2.11 as the proposed Web-server, the PHP v.5.2.8 module to provide server side scripting for generating dynamic content and the MySQL v.5.1 database server with a default configuration. The Load-Generator was developed based on Java. Meanwhile, the database server and the application server run on a computer.

### *Test IRBT Criteria*

The IRBT with the parameters under the previously mentioned criteria was applied in the current test to help us evaluate the performance of the server under workload. The total requests issued per term, the number of concurrent requests, intervals and average request size were configuration parameters that are fixed in the tests. The system performance was evaluated by increasing the concurrent requests on six steps according to the sizes of the database. In each step, the database size increased about one thousand twenty hundred sixty (1260) Mega-bytes (i.e. approximately equivalent to ten million traffic tickets). In the experiment, the authors started with 10 concurrent requests and gradually increased the number of the concurrent requests to 180. The experiment for each concurrent step was repeated three times. The time difference between the time when a request was sent and when a successful respond was completely received specified the response time. With respect to the testbed of the current study, the average service time, average CPU load, and average physical memory usage were calculated as the sample mean of the observations.

## **DISCUSSION AND RESULTS**

The scenario ramp test was executed to determine the initial maximum load that the system resource could sustain. In the experiments, this was started with 10 concurrent requests and the number of the concurrent requests was gradually increased to 180 in six steps, according to the sizes of the database. The experiment for each concurrent step was repeated three times. The mean response time, the mean CPU utilization and the usage of RAM were measured. *Fig. 7 and 10* illustrate the relationship between the growth of the database size, service rate and service time in various concurrent arrival requests. Meanwhile, *Fig. 8 and 9* demonstrate the correspondence between the

concurrent arrival requests, service times and service rates in various database sizes. These figures explain that the concurrent requests increase the service rate for each database size, from 10 to 60. As shown in *Fig. 11*, a considerable amount of CPU utilization of the server is also increased. These figures also reveal that the service rate can considerably be reduced for each database size from 100 to 200, specifically when the database size is already large. This is due to the concurrent control cost such as context switch and logs. At this stage, CPU is utilized at 100%, and it has more no capacity for handling a peak load.

*Fig. 11* shows that CPU utilization increases almost linearly with the number of requests. This figure also reveals CPU can be the bottleneck resource, especially the peak throughput point. It jumps from 57% CPU utilization for 20 concurrent users to 100% with 90 concurrent users in the peak of database size. With more requests, the situation reverses and the CPU on the server becomes the bottleneck. *Fig. 12* shows that memory utilization also increases correspondingly. *Fig. 13* illustrates network utilization when the number of concurrent requests is set to the maximum. This particular figure also illustrates the network was used less than 2.5%.

Let consider that when the concurrent arrival is set to 20 in the peak of database size as a stress point. The results of this point can be observed as a stress test. The server could handle each request in 48.19277 milli second. Therefore, the mean service rate is approximately 20.75 per second. As shown in Figures 14 and 15, the CPU was used at around 64.14% and the usage of RAM was low, i.e. around 38.57%. *Fig. 16* depicts open and abort connection statistics in this point. Disk usage on the server is reported in *Fig. 17*. At the beginning of the experiment, when the first requests started to arrive at the server, there are a lot of disk activities and server processes. This explains the initial disk activity and the sharp rise in memory use, until the point in time at which, most of the working sets (indices and frequently used tables) are in memory. After that, there is little disk activity and the memory usage remains stable at around 39 %. Hence, it could be concluded that the resources were used moderately most of the time and could not lead to a limitation with 20 concurrent users. The service rate is also more than the arrival rate, and therefore, the average queue size is bounded and the system responds instantaneously.

## CONCLUSIONS

The performance evaluation of the mobile traffic infraction registration system is crucial, particularly due to the fact that there are a lot of traffic tickets issued in the recent years and the significance of police telecommunication. It is concluded that the most results were derived from the proposed methods and procedures through the application of the IRBT benchmark on mobile traffic infraction registration server. The results achieved are very favourable, and the current empirical study has led to the following conclusions.

It is clear that the environmental constraints can be placed on the server by benchmark tool before the application is deployed for assuring that the mobile road traffic infraction registration system is always reliable and stable at the expected level, even under critical loads.

The server is tested using the ramp test. However, the study considered that the concurrent arrival was set to 20 in a peak of the database size as a stress point. The scenario ramp test was executed to determine the initial maximum load that the system resource could sustain. The results gathered from the ramp test showed that the concurrent requests would increase the service rate for each database size from 10 to 60. It also increased a considerable amount of CPU utilization of the server. Meanwhile, the service rate could considerably be reduced for each database size from 100 to 200, especially when the database size was already large. This is due to concurrent control cost, such as context switch and logs. At this stage, CPU is utilized at 100%, and it has no more capacity for handling a peak load. Therefore, the increase in response time can lead to a

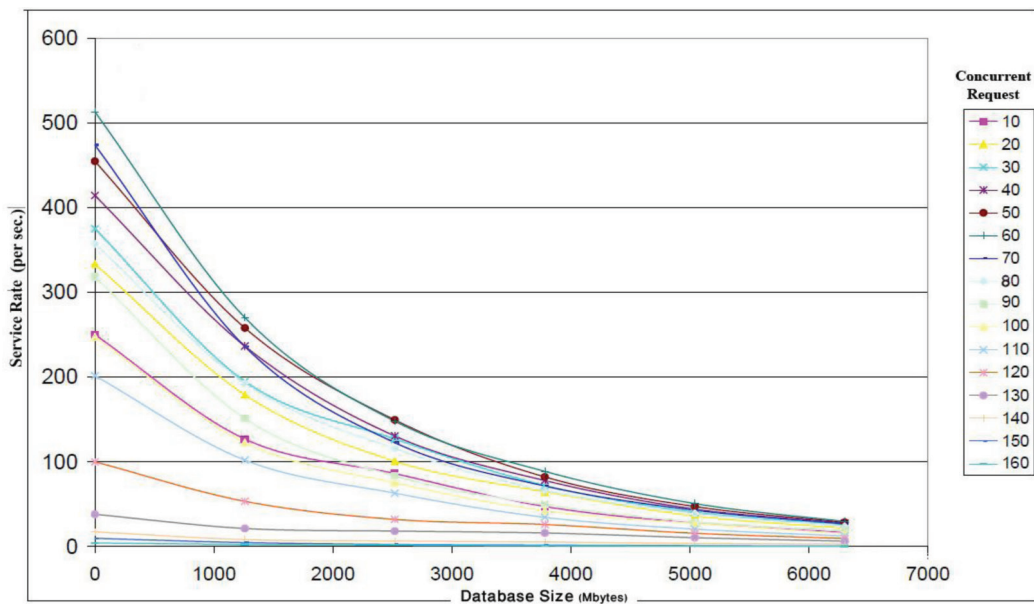


*Fig. 7: The experiment results for the correspondence between growth of database size and service rate in various concurrent requests*

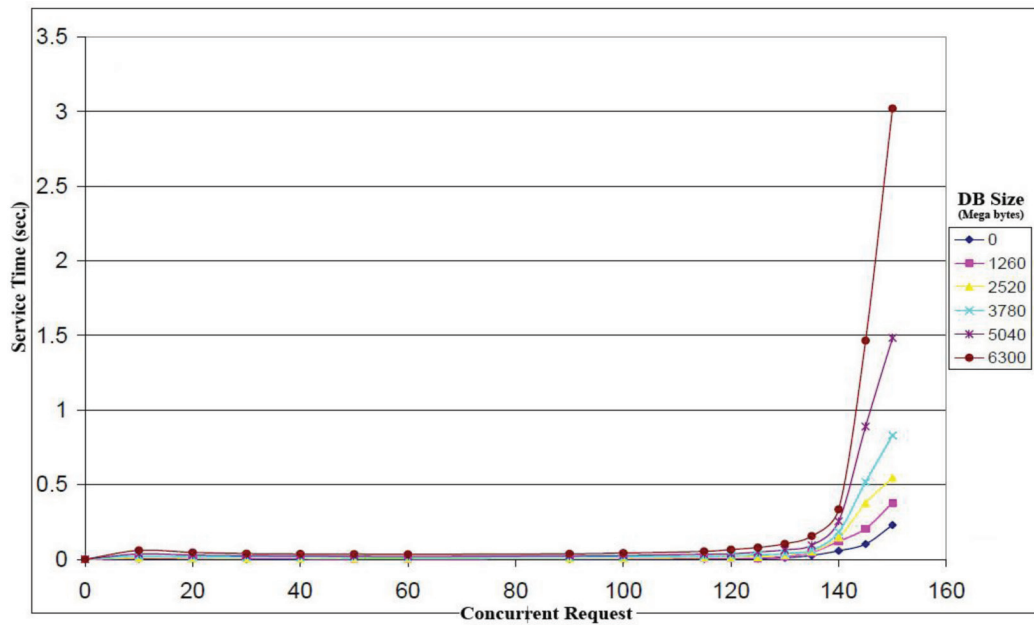


*Fig. 8: The experiment results for the correspondence between concurrent arrival requests and response time in various database sizes*

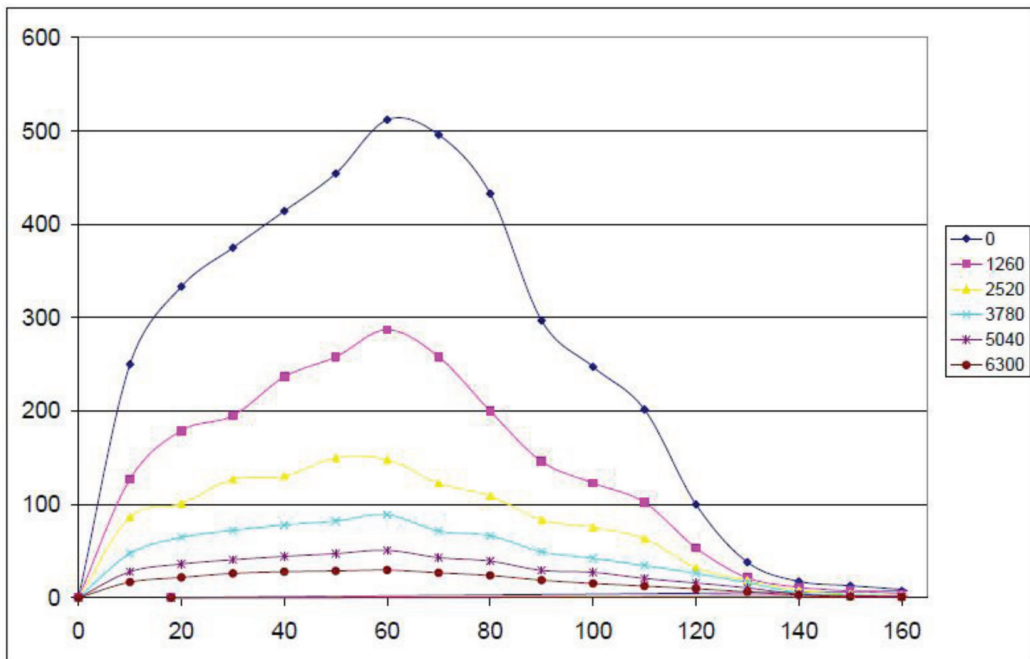


Fig. 9: The experiment results for the relationship between growth of concurrent arrival requests and service rate in various database sizes

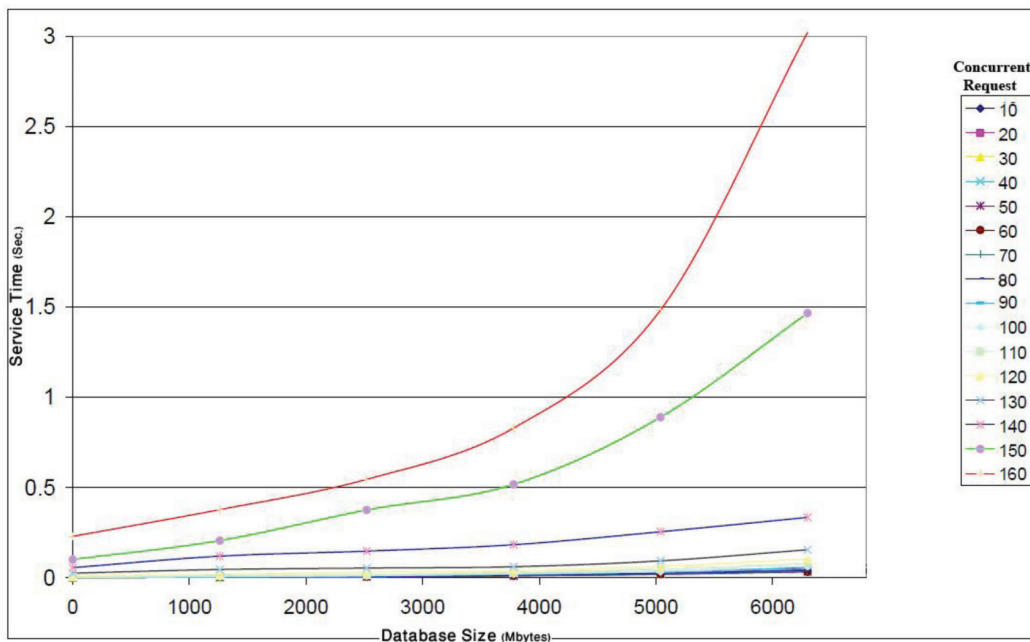


Fig. 10: The experiment results for the relationship between growth of database size and service time in various concurrent arrival requests

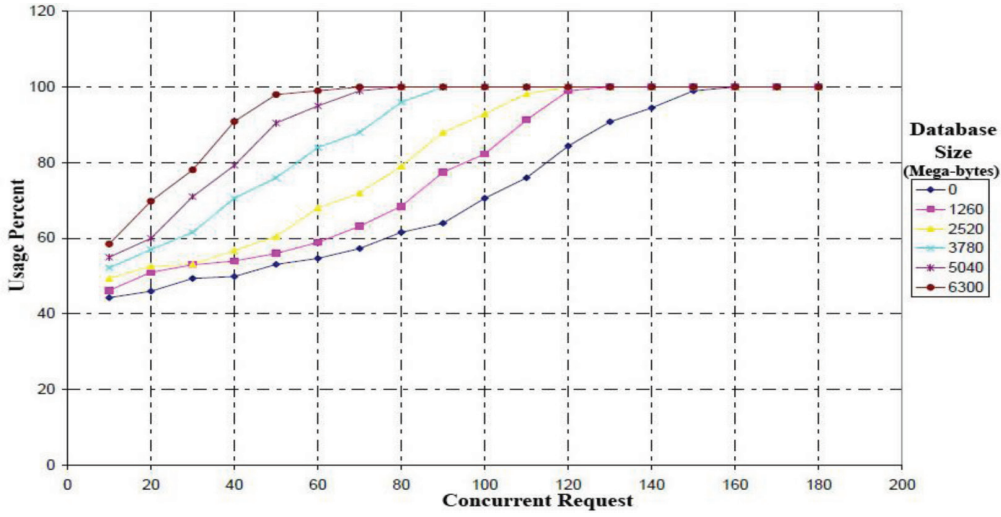


Fig. 11: CPU utilization in the ramp test

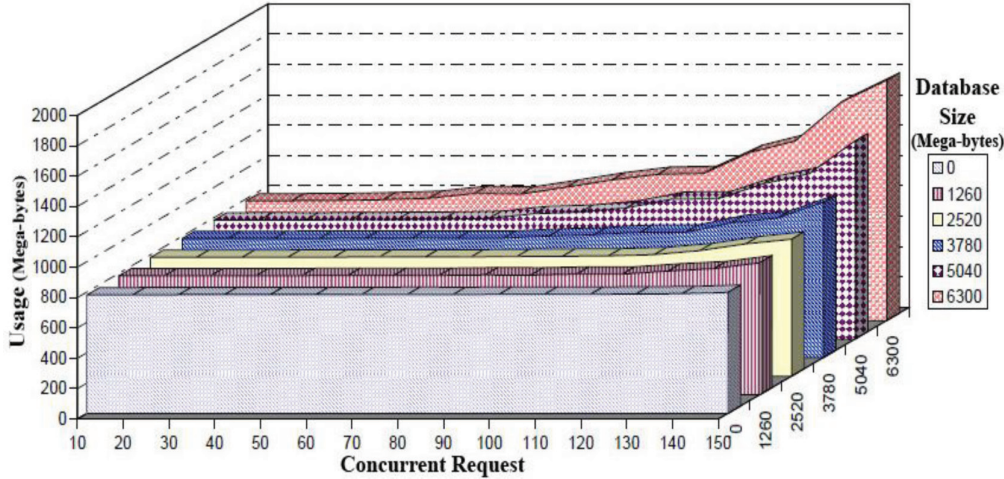


Fig. 12: Physical memory utilization in the ramp test

point where optimization of the system is unavoidable. The metrics can be further improved by upgrading hardware to professional servers. In the first step, the amount of RAM on the server could be increased if the attempt was to achieve high performance under workloads.

This manuscript has also shown CPU can be the bottleneck resource, specifically the peak throughput point. In the stress point, the server could handle each request in 48.19277 milli seconds, so the response time is 20.75 per second. The CPU was used at around 64% and the usage of RAM was low (i.e. around 38%). Therefore, it could be concluded that the resources were moderately used most of the time and the server could approximately handle triple of the maximum average arrival rate in the real time. Finally, the results provide a clear guideline for performance evaluation of mobile road traffic infraction registration system.

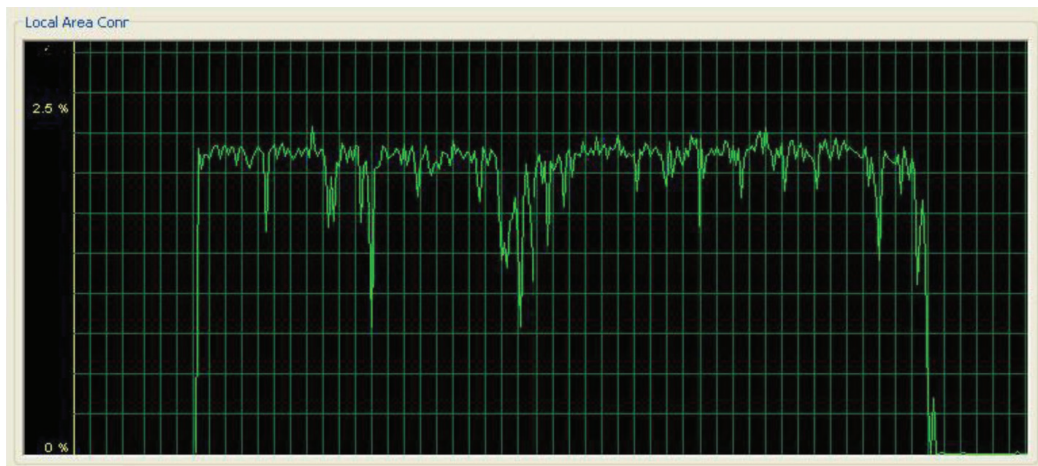


Fig. 13: Network utilization

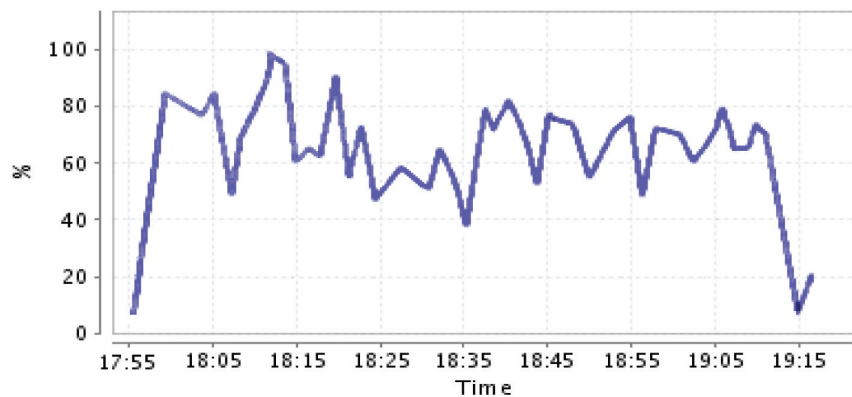


Fig. 14: CPU utilization in stress test

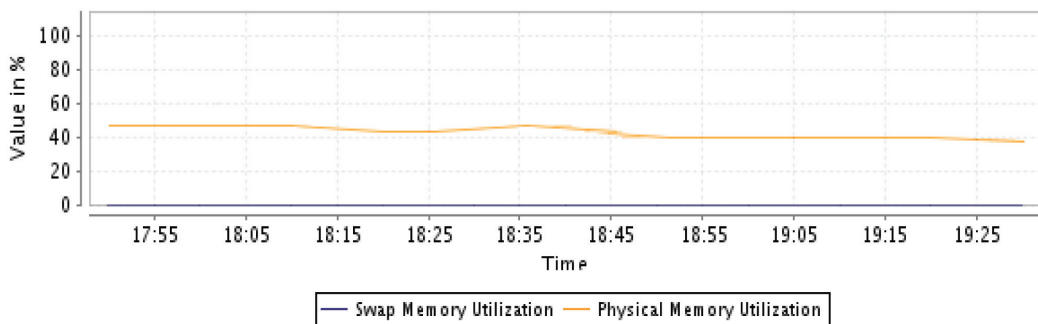


Fig. 15: Physical memory utilization in the stress test

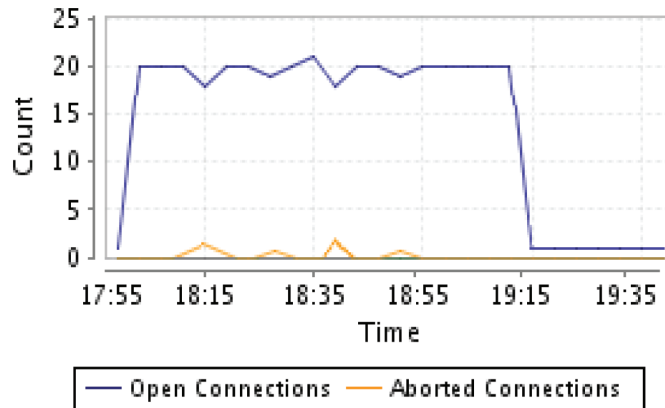


Fig. 16: Connection statistics in the stress test

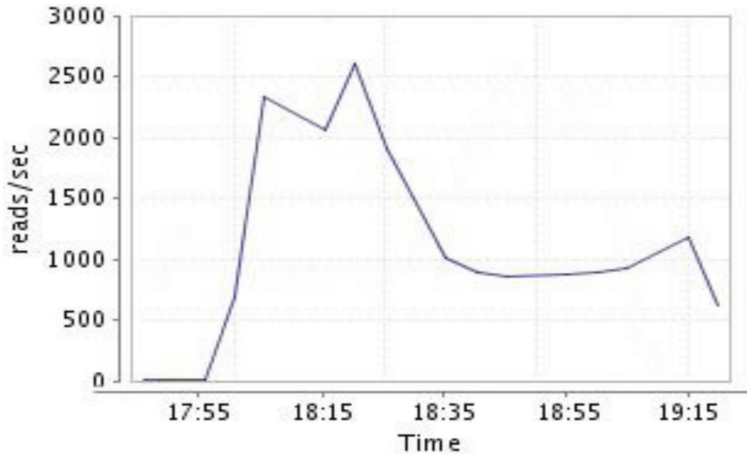


Fig. 17: Disk I/O statistics in the stress test

## FUTURE RESEARCH

The data flow over the public network and this implies that the TPDC is exposed to an unprotected environment. Therefore, a continuation of the work, or an additional research should be performed on the security evaluation of the mobile road traffic infraction registration system. Security is another major issue that it is associated with the mobile road traffic infraction registration system. The police data are almost critical or confidential. Hence, to enhance and justify the security level, a future possible research can identify the security evaluation of the mobile road traffic infraction registration system.

## REFERENCES

- 3G Americas (n.d). GPRS: General packet radio services. Retrieved on Febuary, 2008.
- Abdelazez, S. M. (2000). *Web server evaluation by using simulation model*. (Unpublished Doctoral dissertation), Egypt, 2000.

Performance Evaluation of A Mobile Road Traffic Infraction Registration System through Benchmark

- Ahmad, S. K., & Azmi, A. E. (2007). Road evolution in Malaysia: from footpaths to superhighways. Roads Branch, Public Works Department, Malaysia.
- Anwar, K. &, Saleem, A. (2004). Web Application Stress Test and Data Analysis. Retrieved from <http://www.webstar.co.uk/Stress.pdf>
- Arasteh-Rad, H., Samsudin, K., Ramlji, A. R., Tehrani, M. B., & Tavalai, M. A. (2009, April). *Securing mobile communication system for traffic infraction registration*. Paper presented at International Conference on Future Computer and Communication, Kuala Lumpur, Malaysia.
- Banga, G., & Druschel, P. (1997). *Measuring the capacity of a web server*. Paper presented at Proceedings of the USENIX Annual Technical Conference, Monterey, CA.
- Cellular-News. (2008, March). Global mobile phone subscribers to reach 4.5 billion by 2012. Retrieved from <http://www.cellular-news.com/story/29824.php>
- Cronkhite, C. L. (1974). Automation and Law Enforcement. *Charles C Thomas*.
- Deng, Y., Frankl, P., & Wang, J. (2004). Testing web database applications. *ACM SIGSOFT Software Engineering Notes*, 29, 1–10.
- Dilley, J. (n.d.). Web server workload characterization, Hewlett-Packard Laboratories, 2002. Retrieved from <http://citeseer.ist.psu.edu>
- Elnikety, S., Dropsho, S., & Zwaenepoel, W. (2007). Tashkent+: memory-aware load balancing and update filtering in replicated databases. *SIGOPS Oper. Syst. Rev.*, 41(3), 399-412.
- Gebotys, C. H. (2004, 8-10 Sept. 2004). *Low energy security optimization in embedded cryptographic systems*. Paper presented at the Hardware/Software Codesign and System Synthesis, 2004. CODES + ISSS 2004. International Conference on.
- Gupta, V., Gupta, S., Chang, S., & Stebila, D. (2002). *Performance analysis of elliptic curve cryptography for SSL*. Paper presented at the Proceedings of the 1st ACM workshop on Wireless security, Atlanta, GA, USA.
- Informa Telecoms, & Media (n.d.). World Cellular Data Metrics. Retrieved November, 2008 from <http://shop.informatm.com/marlin/30000001001/MARKT-EFFORT/marketingid/20001131760>
- Iran Daily (2007, January). Reducing Road Accidents. Retrieved from <http://irandaily.com/1385/2777/html/focus.htm>
- Labordere, A. H. (2006). *SMS and MMS Interworking in Mobile Net*. Artech House Publishers.
- Mobile Payment Forum. (2003). *White Paper: Risks and threats analysis and security best practices*.
- MobileTracker. (2005, May). The total number of mobile phone subscribers. Retrieved from <http://www.mobiletracker.net/archives/2005/05/18/mobile-subscribers-worldwide>
- Othman, M. R. (2006, November). Highway network development plan for Malaysia. *The World Road Association-PIARC*. Retrieved from <http://www.piarc.org/en/>
- PCWorld. (2006). Mobile subscribers to reach 2.6b this year. Retrieved from <http://www.pcworld.com/article/127820/mobile-subscribers-to-reach-26b-this-year.html/>
- Potlapally, N. R., Ravi, S., Raghunathan, A., & Jha, N. K. (2003, 25-27 Aug. 2003). *Analyzing the energy consumption of security protocols*. Paper presented at the Low Power Electronics and Design, 2003. ISLPED '03. Proceedings of the 2003 International Symposium on.
- Qusay, M. (n.d.). WAP for Java Developers: Develop WAP Applications with Servlets and JavaServer Pages. Retrieved June, 2007, from <http://developers.sun.com/techtopics/mobility/enterprise/articles/wap/intro/>
- RAD. (2000). Applications for WAP. Tech. Rep., 2000. Retrieved from <http://www2.rad.com/networks/2000/wap/apps.htm>.

Habibollah Arasteh Rad, Khairulmizam Samsudin, Abdul Rahman Ramli and Mohammad Ali Tavallaie

- RAD. (n.d). What is WAP?. Retrieved on January, 2009 from <http://www.pulsewan.com/data101/wap-basics.htm>.
- Rad, H. A., Samsudin, K., Ramli, A. R., & Tehrani, M. B. (2009). *The Design and Implementation of a Stress Tool for Traffic Infraction Registration System*. Paper presented at the Proceedings of the 2009 Second International Conference on Environmental and Computer Science.
- Royanian M. (2007, November 16). 45m tickets for reckless drivers. *Iran Daily*.
- Santra, A., Krishna, M., & Das, A. (2009, Sept). Measurement of memory usage in j2ee applications. *Journal of Scientific and Industrial Research*, 68, 786-788.
- ServerWatch (n.d). Server compare. Retrieved on 2009 from <http://www.serverwatch.com/stypes/compare/>
- Siau, K., Shen, Z., & Varshney, U. (2003). Communications and mobile services. *International Journal of Mobile Communications* 1, 3-14.
- Standard Performance Evaluation Corporation (n.d). SPECweb2009. Retrieved on 2009 from <http://www.spec.org/web2009/>
- Standard Performance Evaluation Corporation, SPEC (n.d). Retrieved on 2009 from <http://performance.netlib.org>
- Takahashi, H., Suganuma, T., & Shiratori, N. (2005, 20-22 July 2005). *AMUSE: an agent-based middleware for context-aware ubiquitous services*. Paper presented at the Parallel and Distributed Systems, 2005. Proceedings. 11th International Conference on.
- Transaction Processing Performance Council, TPC (n.d). TPC-Benchmark W. Retrieved on January, 2009 from <http://www.tpc.org/tpcw/default.asp>
- Tschalar, R. (2001, May). HTTPClient Version 0.3-3. Retrieved from <http://www.innovation.ch/java/HTTPClient>
- Turettini, E. (2006). Up to 90 percent of globe to have mobile coverage. Retrieved from <http://www.textually.org/textually/archives/2006/10/013841.htm>
- Whale Communications Ltd (n.d). The e-Gap remote access appliance secures SSL VPN technology for providing remote access from anywhere. Tech. Rep. Retrieved on March, 2003.
- Zekavat, S. R. (n.d). Road safety - government policy. Regional Experiences and Lessons in Financial Highway Infrastructure and Improving Road Safety, Bangkok, May 2006. Retrieved from <http://www.unescap.org/ttdw/roadsafety/StatusPapers2006/IslamicRepublicofIran-statuspaper.pdf>
- Zhu Han, & K. J. Ray Liu (2008). Resource Allocation for Wireless Networks, Basics, Techniques, and Applications. *Cambridge University Press* vol 2.

## Effect of Rare Earth Elements Substitution in La site for LaMnO<sub>3</sub> Manganites

Wong Jen Kuen\*, Lim Kean Pah, Abdul Halim Shaari, Chen Soo Kien, Ng Siau Wei and Albert Gan Han Ming

Department of Physics, Faculty of Science, Universiti Putra Malaysia,  
43400 Serdang, Selangor, Malaysia

\*E-mail: wjenkuen@hotmail.com

### ABSTRACT

With a view to understanding the effect of rare earth element (Ce, Pr, Nd, Sm and Gd) substitution for the La site in LaMnO<sub>3</sub> (LMO), the samples were prepared via solid-state reaction. Structure investigation by X-ray diffraction (XRD) showed that structure transformation from trigonal (LMO) to orthorhombic (PMO, NMO, SMO and GMO) occurred when smaller trivalent rare earth element was replaced. The MnO<sub>6</sub> octahedra were tilted and elongated or compressed, corresponding to the ionic radii of the rare earth inserted. Meanwhile, microstructure study using scanning electron microscopy (SEM) illustrated that La substitution by another rare earth element caused a reduction in grain size. This might due to the changes in enthalpy of fusion by other rare earth ions, where higher enthalpy of fusion favours formation of smaller grain size. However, CeMnO<sub>3</sub> did not form under this preparation condition. The magnetic properties studied from the hysteresis plot taken at room temperature indicated that the substitution of La with other magnetic trivalent rare earth ions strongly weakened the magnetic strength of the system.

**Keywords:** Magnetic Material, Manganite Perovskite, Rare-earth ions, Rietveld refinement, Structure Transformation

### INTRODUCTION

LnMnO<sub>3</sub> (Ln = rare earth element) has a perovskite-type structure for Ln = La to Dy. This particular compound and its solid solutions, with alkaline earth elements, have been extensively studied because of their potential applications in magnetic insulation and for Colossal Magnetoresistance (CMR) (Kobayashi *et al.*, 2008; Mahesh *et al.*, 1995). LaMnO<sub>3</sub>, which is also known as Mott Insulator (Yasuo, 2004), has A-type magnetic order, in which the spins are ferromagnetically aligned in planes while anti-ferromagnetically when aligned between the planes (Murakami *et al.*, 1998). The replacement of non-magnetic La<sup>3+</sup> with a magnetic ion would either increase or decrease the net magnetization value, M<sub>s</sub>. This value is expressed as M<sub>s</sub> = M<sub>Mn</sub> + M<sub>A</sub>, where M<sub>Mn</sub> and M<sub>A</sub> are the magnetizations of Mn and the ‘A’ site sub-lattice, respectively (Song *et al.*, 2008). Meanwhile, the crystal structure of LnMnO<sub>3</sub> consists of Mn ion surrounded by oxygen atoms forming the MnO<sub>6</sub> octahedra when different types of Ln site cations are located between them (Van Tendeloo *et al.*, 2004). From a previous study, the crystal structure of LaMnO<sub>3</sub> was found to vary from orthorhombic (*Pbnm*) to rhombohedral (*R-3c*), depending on the method of synthesis (Töpfer *et al.*, 1997) with the lattice parameters of *a* = *b* = 5.523 Å and *c* = 13.324 Å (Moreno *et al.*, 2008) as well as the oxygen stoichiometry of LnMnO<sub>3-δ</sub> (Ln= La, Pr, Nd, Sm and Y) (Atsumi *et al.*, 1997). In this work, the

Received: 11 August 2010

Accepted: 20 December 2010

\*Corresponding Author

influence of the structure changes, microstructure and room temperature magnetism induced by the substitution of different trivalent rare earth ions in the La site for  $\text{LaMnO}_3$  was studied since each trivalent rare earth ion possessed its own unique behaviour. The ionic radii of  $\text{La}^{3+}$ ,  $\text{Ce}^{3+}$ ,  $\text{Pr}^{3+}$ ,  $\text{Nd}^{3+}$ ,  $\text{Sm}^{3+}$ , and  $\text{Gd}^{3+}$  were 1.172 Å, 1.150 Å, 1.130 Å, 1.123 Å, 1.098 Å and 1.078 Å, respectively (Aspinall *et al.*, 2001).

## MATERIALS AND METHODS

Polycrystalline pellets  $\text{AMnO}_3$  ( $\text{A} = \text{La, Ce, Pr, Nd, Sm and Gd}$ ) were fabricated using a solid-state reaction method. Stoichiometric amounts of the starting powders ( $\text{La}_2\text{O}_3$ ,  $\text{CeO}_2$ ,  $\text{Pr}_6\text{O}_{11}$ ,  $\text{Nd}_2\text{O}_3$ ,  $\text{Sm}_2\text{O}_3$ ,  $\text{Gd}_2\text{O}_3$  and  $\text{MnCO}_3$ ), with the purity  $\geq 99.9\%$ , were mixed and wet-milled in acetone. The homogeneous mixture was dried at 100°C and ground before calcination (900°C for 12 hours). The samples were reground and sieved using a 38 µm sized sieve. The sieved powders were pressed into pellets and sintered at 1300°C for 24 hours. They formed  $\text{LaMnO}_3$  (LMO),  $\text{CeMnO}_3$  (CMO),  $\text{PrMnO}_3$  (PMO),  $\text{NdMnO}_3$  (NMO),  $\text{SmMnO}_3$  (SMO) and  $\text{GdMnO}_3$  (GMO). The microstructure and structure of the samples were then characterized using the scanning electron microscopy (SEM, LEO1455 VPSEM, with an OXFORD INCA ENERGY 300EDX attachment) and X-ray diffraction (XRD, Phillips PW 3040/60 Xpert Pro). The XRD data were collected using a continuous scan with the step size of 0.033° in gonio scan axis. The data were analyzed using Rietveld refinement with X'Pert HighScore Plus programme. The magnetic properties of the samples were measured at room temperature using a vibrating sample magnetometer (VSM, LakeShore Model 7407).

## RESULTS AND DISCUSSION

The SEM micrographs shown in *Fig. 1* illustrate that all the grains are well connected and in a single phase, except for the two different microstructures shown in CMO. There is a significant contrast among the grains of CMO which are separated into lighter and darker colours. This was confirmed by EDX, i.e. lighter grains contained higher amount of Ce ion while darker grains consisted of more Mn ions. The grain sizes of LMO, CMO (mixture of  $\text{CeO}_2$  and  $\text{Mn}_3\text{O}_4$ ), PMO, NMO, SMO, and GMO were found to be in the range of 7.1~9.3 µm, CMO (light grains = 1.6~5.2 µm, darker grains = 0.9~3.0 µm), 2.1~5.0 µm, 0.6~4.3 µm, 1.0~3.0 µm and 0.5~2.1 µm, respectively. It was found that the decrease in the grain size and the range of sizes were mainly due to the change in the enthalpy of fusion of different rare earth ions. As the enthalpy of fusion of  $\text{La}^{3+}$ ,  $\text{Ce}^{3+}$ ,  $\text{Pr}^{3+}$ ,  $\text{Nd}^{3+}$ ,  $\text{Sm}^{3+}$ , and  $\text{Gd}^{3+}$  were 6.2, 5.46, 6.89, 7.14, 8.62, and 10.05 kJ/mole, respectively (Barbalace, 2010), the formation of grain size decreases when the enthalpy of fusion of substituted ion increases. However, two different types of microstructure were observed in the CMO sample, and these correspond with cerium oxide and manganese oxide (confirmed via EDX). Manganese oxide is a decomposed product from manganese carbonate. Ce has the smallest value of enthalpy of fusion among the rare earth ions and due to its highly thermal stability, cerium oxide does not react with manganese oxide to form  $\text{CeMnO}_3$  (CMO).

Structure investigations were carried out using a Philips X-ray diffractometer with  $\text{CuK}\alpha$  radiation in  $2\theta$  range of 20~80°. The data for each sample were matched, refined and plotted. The matched XRD patterns of all the samples are single phase, with the exception of CMO. From the XRD database, the material obtained was the reaction with cerium oxide which gave a spectrum that matched a combination of the  $\text{CeO}_2$  and  $\text{Mn}_3\text{O}_4$  standards. This further confirmed the existence of two oxides and verified that the desired CMO was not formed using the method proposed in this work.

From the Rietveld refinement analysis with the ICSD (Inorganic Crystal Structure Database) crystallographic database, the unit cell parameters and other fitting parameters are summarized in

Effect of Rare Earth Elements Substitution in La site for  $\text{LaMnO}_3$  Manganites

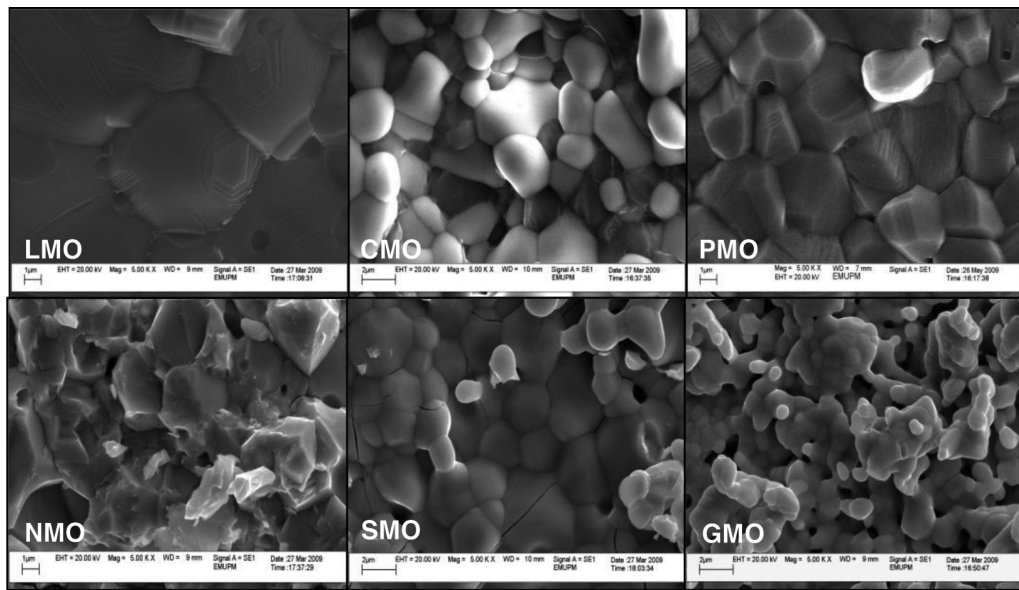


Fig. 1: SEM micrographs (5000X) of  $\text{AMnO}_3$  ( $A = \text{La}, \text{Ce}, \text{Pr}, \text{Nd}, \text{Sm}$  and  $\text{Gd}$ )

Tables 1 and 2. As observed, the crystal structure changed from trigonal (LMO) to orthorhombic (PMO, NMO, SMO, and GMO). Overall, the unit cell parameters  $a$ ,  $b$  and  $c$  decreased as smaller trivalent rare earth cation was substituted in the La site. This was probably due to the fact that the substitution of smaller ions in the La site shrunk the overall unit cell. As reported earlier, LMO was expected to be in orthorhombically distorted perovskite structure (Atsumi *et al.*, 1997), but in this work, LMO was found to have a trigonal crystal structure. This might due to the lack of oxygen or dissociation similar to that reported by Atsumi *et al.* (1996).

The changes in both bond length and bond angle of Mn-O-Mn long range order resulted from  $\text{MnO}_6$  octahedral were observed. Detailed studies on crystal structures are given in Table 2. Oxygen

TABLE 1  
Crystallographic data of perovskite manganites

Sample code	LMO	PMO	NMO	SMO	GMO
Chemical formula	$\text{LaMnO}_3$	$\text{PrMnO}_3$	$\text{NdMnO}_3$	$\text{SmMnO}_3$	$\text{GdMnO}_3$
Crystal System	Trigonal	Orthorhombic	Orthorhombic	Orthorhombic	Orthorhombic
Space Group	$R\bar{3}c$	$Pnma$	$Pnma$	$Pnma$	$Pnma$
Lattice parameter					
$a$ (Å)	5.5320 (2)	5.7970 (1)	5.7920 (1)	5.8412 (1)	5.8511 (2)
$b$ (Å)	5.5320 (2)	7.5892 (1)	7.5640 (1)	7.4838 (1)	7.4432 (3)
$c$ (Å)	13.3664 (7)	5.4496 (1)	5.4216 (7)	5.35866 (9)	5.3154 (2)
Volume of cell (Å <sup>3</sup> )	354.2529	239.7509	237.5216	234.251	231.4904
$R_{\text{expected}}$ (%)	4.5611	6.5695	3.6317	5.3531	2.7180
$R_{\text{profile}}$ (%)	8.1053	7.4170	9.4630	4.6500	3.1890
$R_{\text{weighed profile}}$ (%)	12.7308	9.6333	3.4608	5.9021	4.3941
Goodness of fit	8.4306	2.1501	3.7374	1.2156	2.6135

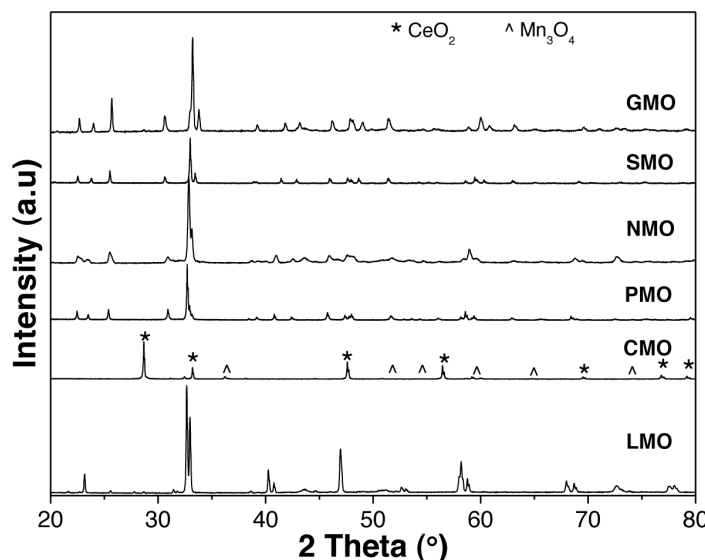


Fig. 2: X-ray diffraction pattern of Mn-based samples

atoms were found to be of different coordination which are classified as O(1) and O(2). However, this is not the case for LMO, since its crystal structure is trigonal and highly symmetric. Table 2 gives two different bond lengths between O(1) and Mn in the PMO, NMO, SMO and GMO samples. However, the Mn-O(2) bond length remains almost the same. On the other hand, the average bond angle of both Mn-O(1)-Mn and Mn-O(2)-Mn decreased as smaller ionic radii rare earth ions were substituted into the lattices. This was probably influenced by the diameter of the rare earth atoms which were located between  $\text{MnO}_6$  octahedra. When  $\text{MnO}_6$  was combined with rare earth elements of different ionic radii, it tended to deform to achieve a more stable shape. However, smaller ionic radii substitution not only drives  $\text{MnO}_6$  octahedra to display tilting, but elongation and compression as well. This occurs mainly due to attractive forces from the neighbouring  $\text{MnO}_6$  octahedra and at the same time, repulsion force was created to oppose that attraction force. Hence, the dimensions (bond length, Mn-O and Mn-O-Mn, bond angle) of  $\text{MnO}_6$  as discussed would be altered (Van Tendeloo *et al.*, 2004).

TABLE 2  
Interatomic distance and bond angle of  $\text{MnO}_6$  in  $\text{AMnO}_3$  ( $\text{A} = \text{La, Ce, Pr, Nd, Sm and Gd}$ )

Sample code	LMO	PMO	NMO	SMO	GMO
Chemical formula	$\text{LaMnO}_3$	$\text{PrMnO}_3$	$\text{NdMnO}_3$	$\text{SmMnO}_3$	$\text{GdMnO}_3$
$\angle \text{Mn-O(1)-Mn} (\circ)$	165.780 (3)	151.658 (6)	154.380 (6)	146.854 (5)	150.090 (1)
$\angle \text{Mn-O(2)-Mn} (\circ)$		152.340 (8)	148.200 (6)	147.621 (6)	144.080 (1)
Mn-O(1) ( $\text{\AA}$ )		$1.916 \times 2$	$1.941 \times 2$	$1.909 \times 2$	$1.852 \times 2$
	$1.962 \times 6$	$2.186 \times 2$	$2.127 \times 2$	$2.226 \times 2$	$2.238 \times 2$
Mn-O(2) ( $\text{\AA}$ )		$1.954 \times 2$	$1.966 \times 2$	$1.948 \times 2$	$1.956 \times 2$

From Fig. 3(a), the hysteresis loops of all the samples show a straight line crossing the origin, indicating either a paramagnetic or an anti-ferromagnetic behaviour. As depicted in Figure 3(b), however, drastic changes in magnetization values corresponding to the substituted magnetic trivalent rare earth ions at room temperature were clearly observed. The magnetization value of LMO is relatively much larger ( $\sim 8$  emu/g) compared to the other samples ( $< 1$  emu/g). Meanwhile, the magnetization value of each sample measured at 10 kG applied magnetic field decreased as magnetic trivalent rare earth ions (Ce, Pr, Nd, Sm and Gd) were substituted. This was probably due to the

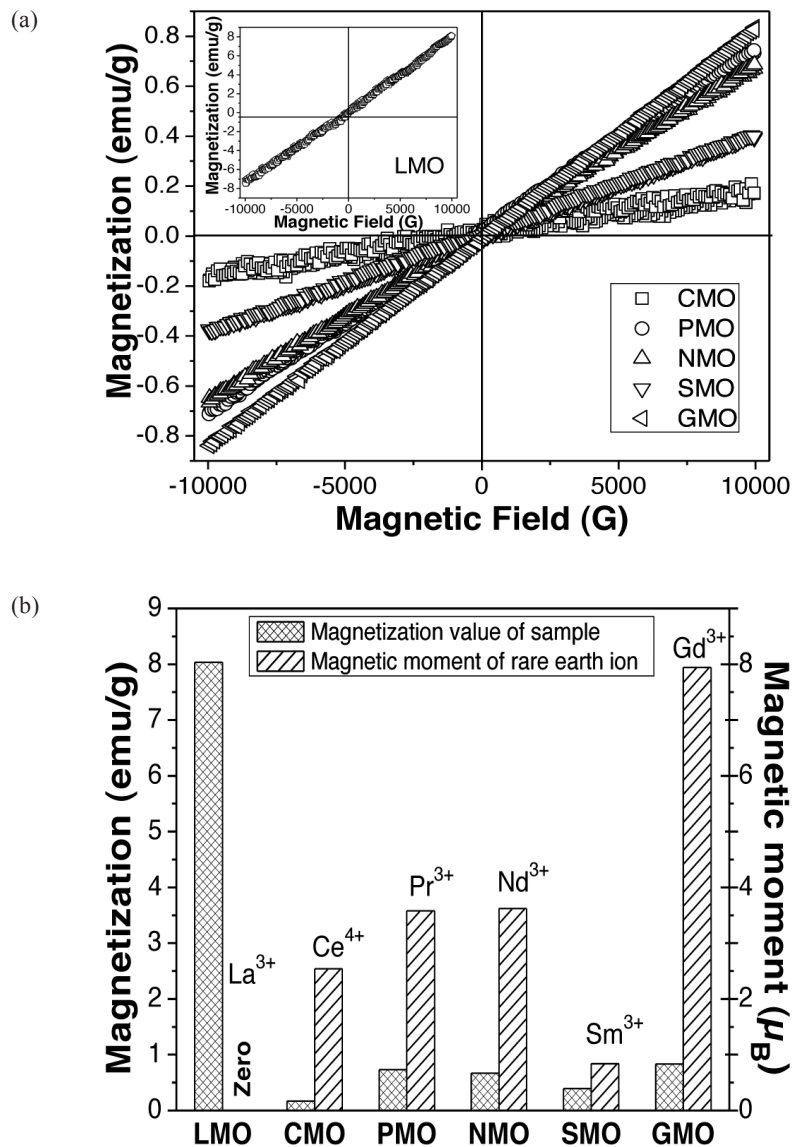


Fig. 3: (a) Hysteresis loops of  $AMnO_3$  ( $A = \text{La}, \text{Ce}, \text{Pr}, \text{Nd}, \text{Sm}$  and  $\text{Gd}$ ) (b) Magnetization value of the samples substituted by various rare earth ions at 10kG and magnetic moment of rare earth ions (Aspinall et al., 2001)

spins in the Mn sub-lattice which were pinned by the spins in the ‘A’ site sub-lattice. When an external magnetic field was applied, the pinned spins were unable to align with the direction of the applied magnetic field, and this subsequently decreased the net magnetization values. Since  $\text{La}^{3+}$  is a non-magnetic ion, it is reasonable that LMO exhibits the highest magnetization value, while CMO, PMO, NMO, SMO and GMO are smaller.

## CONCLUSIONS

It was found that the substitution of Ce, Pr, Nd, Sm and Gd for La site in  $\text{LaMnO}_3$  perovskite manganites greatly influenced their structures, especially the trivalent rare earth ions with small ionic radius.  $\text{MnO}_6$  can be invoked to deform and doing this stabilizes the systems. Nonetheless,  $\text{CeMnO}_3$  was not formed, but there were two different  $\text{CeO}_2$  and  $\text{Mn}_3\text{O}_4$  phases. The microstructure changed corresponding to the enthalpy of fusion of the substituted rare earth ion. Smaller enthalpy of fusion would lead to greater grain size. As observed in  $\text{LaMnO}_3$ , the substitution of La with other magnetic trivalent rare earth weakened their magnetic strength.

## ACKNOWLEDGEMENT

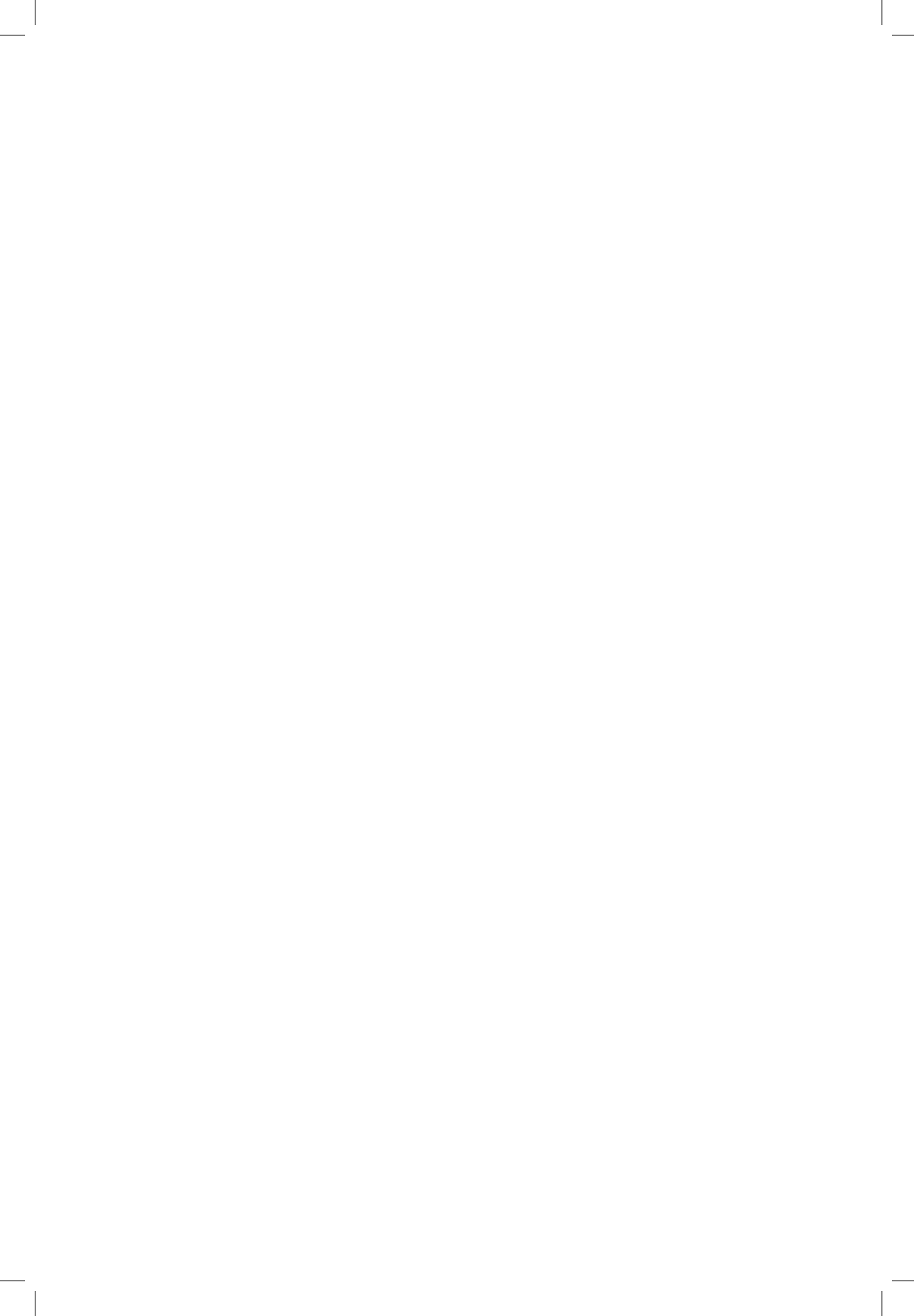
The authors gratefully acknowledge the support from the Ministry of Science, Technology and Innovation of Malaysia (MOSTI) for the grant under the Fundamental Research Grant Scheme (FRGS) 01-11-09-728FR, Research University Grant Scheme (RUGS) 91849 and the award of the National Science Fellowship (NSF).

## REFERENCES

- Aspinall, H. C. (2001). *Chemistry of the f-block Elements (Advanced chemistry texts; v. 5) 10-18*. United Kingdom: Gordon and Breach Science Publishers.
- Atsumi, T., Ohgushi, T., & Kamegashira, N. (1996). Studies on oxygen dissociation pressure of  $\text{LnMnO}_3$  ( $\text{Ln}$  = rare earth) with the e.m.f. technique. *Journal of Alloys and Compounds*, 238(1-2), 35-40.
- Atsumi, T., Ohgushi, T., Namikata, H., & Kamegashira, N. (1997). Oxygen nonstoichiometry of  $\text{LnMnO}_{3-\delta}$  ( $\text{Ln}=\text{La, Pr, Nd, Sm and Y}$ ). *Journal of Alloys and Compounds*, 252(1-2), 67-70.
- Barbalace, K. (2010). Periodic Table of Elements. Retrieved on September 8, 2010 from EnvironmentalChemistry.com. <http://EnvironmentalChemistry.com/yogi/periodic/>.
- Kobayashi, M., Tamura, H., Nakano, H., Satoh, H., & Kamegashira, N. (2008). Stability of phases in (Ba, Gd)  $\text{MnO}_3$  solid solution system. *Journal of Rare Earths*, 26(2), 233-236.
- Mahesh, R., Mahendiran, R., Raychaudhuri, A. K., & Rao C. N. R. (1995). Effect of the internal pressure due to the A-site cations on the giant magnetoresistance and related properties of doped rare earth manganites  $\text{Ln}_{1-x}\text{AxMnO}_3$  ( $\text{Ln}=\text{La, Nd, Gd, Y}$ ;  $\text{A}=\text{Ca, Sr, Ba, Pb}$ ). *Journal of Solid State Chemistry* 120, 160.
- Moreno, L. C., Valencia, J. S., Landínez Téllez, D. A., Arbej Rodríguez M., J., Martínez, M. L., Roa-Rojas, J., & Fajardo, F. (2008). Preparation and structural study of  $\text{LaMnO}_3$  magnetic material. *Journal of Magnetism and Magnetic Materials*, 320(14), e19-e21.
- Murakami, Y., Hill, J.P., Gibbs, D., Blume, M., Koyama, I., Tanaka, M., Kawata, H., Arima, T., Tokura, Y., Hirota, K., & Endoh, Y. (1998). Resonant X-Ray Scattering from Orbital Ordering in  $\text{LaMnO}_3$ . *Physical Review Letter*, 81, 582-585.

Effect of Rare Earth Elements Substitution in La site for LaMnO<sub>3</sub> Manganites

- Song, Q. X., Wang, G. Y., Yan, G. Q., Mao, Q., Wang, W. Q., & Peng, Z. S. (2008). Influence of substitution of Sm, Gd, and Dy for La in La<sub>0.7</sub>Sr<sub>0.3</sub>MnO<sub>3</sub> on its magnetic and electric properties and strengthening effect on room-temperature CMR. *Journal of Rare Earths*, 26(6), 821-826.
- Töpfer, J., & Goodenough, J. B. (1997). LaMnO<sub>3+δ</sub> Revisited. *Journal of Solid State Chemistry*, 130(1), 117-128.
- Van Tendeloo, G., Lebedev, O. I., Hervieu, M., & Raveau, B. (2004). Structure and microstructure of colossal magnetoresistant materials. *Report on Progress in Physics*, 67, 1315-1365.
- Yasuo, E. (2004). New scaling of spin excitations in ferromagnetic metals. *Physica B: Condensed Matter*, 345, 132-136.



## Exact Parallel Plurality Voting Algorithm for Totally Ordered Object Space Fault-Tolerant Systems

Abbas Karimi<sup>1\*</sup>, Faraneh Zarafshan<sup>1</sup>, Adznan Jantan<sup>2</sup>, Abdul Rahman Ramli<sup>2</sup>,  
M. Iqbal b. Saripan<sup>2</sup> and S. A. R. Al-Haddad<sup>2</sup>

<sup>1</sup>Department of Computer Engineering, Faculty of Engineering,  
Arak Branch, Islamic Azad University, Arak, Iran.

<sup>2</sup>Department of Computer and Communication Systems Engineering,  
Faculty of Engineering, Universiti Putra Malaysia,  
43400 UPM, Serdang, Selangor, Malaysia

\*E-mail: A-karimi@iau-arak.ac.ir

### ABSTRACT

Plurality voter is one of the commonest voting methods for decision making in highly-reliable applications in which the reliability and safety of the system is critical. To resolve the problem associated with sequential plurality voter in dealing with large number of inputs, this paper introduces a new generation of plurality voter based on parallel algorithms. Since parallel algorithms normally have high processing speed and are especially appropriate for large scale systems, they are therefore used to achieve a new parallel plurality voting algorithm by using  $(n/\log n)$  processors on EREW shared-memory PRAM. The asymptotic analysis of the new proposed algorithm has demonstrated that it has a time complexity of  $O(\log n)$  which is less than time complexity of sequential plurality algorithm, i.e.  $\Omega(n \log n)$ .

**Keywords:** Fault-tolerant, Parallel Algorithm, PRAM, Voting Algorithm

### INTRODUCTION

Fault-tolerance is the knowledge of manufacturing the computing systems which are able to function properly even in the presence of faults. These systems comprise a wide range of applications, such as embedded real-time systems, commercial interaction systems and e-commerce systems, Ad-hoc networks, transportation (including rail-way, aircrafts and automobiles), nuclear power plants, aerospace and military systems, and industrial environments in all of which, a precise inspection or correctness validation of the operations must occur (e.g. where poisonous or flammable materials are kept) (Latif-Shabgahi *et al.*, 2004). In these systems, the aims are to decrease the probability of the system hazardous behaviour and to keep the systems functioning even in the occurrence of one or more faults.

Redundancy is one of the important methods in achieving fault-tolerance and it can be implemented in three forms, including static (fault masking methods), dynamic (fault detection, fault diagnosis, fault isolation and fault location), and hybrid (masking faults and fault detection and location).

The aim of static redundancy is masking the effect of fault in the output of the system. *N*-Modular Redundancy (NMR) and *N*-Version Programming (NVP) are two principal methods of static redundancy in hardware and software, respectively. Three modular redundancy (TMR) is

---

Received: 1 October 2010

Accepted: 4 March 2011

\*Corresponding Author

the simplest form of NMR which is formed from  $N=3$  redundant modules and a voter unit which arbitrates among the modules' outputs (*Fig. 1*).

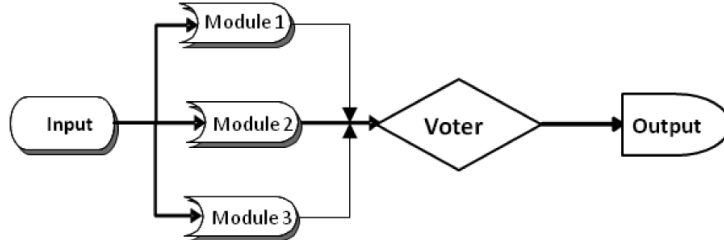


*Fig. 1: TMR System*

Voter performs a voting algorithm in order to arbitrate among different outputs of redundant modules or versions and to mask the effect of fault(s) from the system output. Many voting algorithms have been defined in the literature, each with particular strengths and weaknesses that make a particular voting algorithm more proper than the other one in a given application.

Plurality voter is one of several voting algorithms which is applied in the fault-tolerant control systems. The main advantages of this voter are high reliability (Blough *et al.*, 1990) and high availability (Yacoub *et al.*, 2002), in comparison with other popular voting algorithms. On contrary to some severe voters like majority and its extended forms, such as smoothing and predictive, plurality voter can operate flexibly if less than majority elements are in agreement (Latif-Shabgahi *et al.*, 2004).

In this paper, the parallel algorithms are used on the EREW shared-memory systems to present a new generation of voter – and this is known as Parallel Plurality Voter (PPV) – which provides the plurality voter extension without enlarging the calculations, and is suitable for large-scale systems and with optimal processing time.

The current paper is organized in the following manner. In the next section, background and related works are described, whereas the sequential and parallel plurality voting algorithms are presented in later sections. Result and discussion section deals with the performance analysis of the new algorithm and its comparison with the sequential algorithm. Finally, the conclusions and future works are explained.

## BACKGROUND AND RELATED WORKS

Voting algorithms have been extensively applied in situations where choosing an accurate result out of the outputs of several redundant modules is required. Generalized voters including majority, plurality, median and weighted average were first introduced by Lorcak *et al* (1989).

Majority voter is perhaps the most applicable voter that produces an output among  $n$  variant results, where at least  $\lfloor (n + 1)/2 \rfloor$  variant results agree (Latif-Shabgahi *et al.*, 2004). Meanwhile, plurality voter is a relax form of majority voter, in which even if less than  $\lfloor (n + 1)/2 \rfloor$  variant results are in agreement, voter can report consensus. Thus, plurality and majority are actually extended forms of  $m$ -out-of- $n$  voting, in which at least  $m$  modules out of  $n$  modules should be in agreement; otherwise, voter cannot produce the output. The  $m$ -out-of- $n$  voting method is a suitable choice for the systems where the number of the voter inputs is large. The other generalized voter is the median voter that always chooses the mid-value of voter inputs as the system output. The most significant limitation of this particular algorithm is that the number of the voter inputs is assumed

to be odd (Lorcak *et al.*, 1989). In the weighted average algorithm, the weighted mean of the input values is calculated as the voting result. The weight value is assigned to each voter input in various methods (Latif-Shabgahi, 2004; Latif-Shabgahi *et al.*, 2003; Lorcak *et al.*, 1989; Tong *et al.*, 1991), and then, the calculated weights,  $w_i$ , are used to provide the voter output,  $y = \sum w_i x_i / \sum w_i$ , where  $x_i$  refers to each voter inputs and  $y$  is the voter output. Average voter is a special case of the weighted average voter in which all the weights are assumed to be equal to  $1/n$ . Two latest methods amalgamate variant results to make the output (Latif-Shabgahi *et al.*, 2004); as a result, the output may be clearly different from the input values. Although this feature is useful in such applications as image processing filters (to merge the results of the adjacent pixels), in many safety critical and high reliable systems the voters like majority, plurality, and median are preferred, particularly due to their selecting strategy.

Based on the type of agreement, Plurality voter can be exact or inexact. In the exact voting, agreement achievement requires that the redundant results to be exactly the same, while in the inexact voting, agreement means that the multiple results might be different. Nevertheless, their difference from each other is smaller than a predefined, application specific threshold (Latif-Shabgahi *et al.*, 2004). Although inexact voting is closer to real conditions, to avoid the complexities due to selecting threshold, and to simply design parallel algorithm, the research is limited to the exact plurality voter.

The other important issue about all the above mentioned voters, including plurality, is their dependency on the structure of the input space (Parhami, 1992, 1994). Hence, while the number of voter inputs increases, there will be increases in the complexity of calculations, in addition to harmful effects on the speed of processing in the control system.

To address the problems of plurality voter mentioned, an effective parallel plurality algorithm was proposed based on the shared memory EREW by using the parallel algorithms.

### **PARALLEL ALGORITHM IN A SHAREDMEMORY SYSTEM**

So far, parallel voters have been taken into account in the studies by several authors (Karimi *et al.*, 2010; Lei *et al.*, 1993; Parhami, 1996). In addition, an optimal parallel average voter has been designed and analyzed in Karimi *et al.* (2010). It has also been demonstrated that the time complexity of the mentioned algorithm is  $O(\log n)$  with  $n/\log n$  processors in an EREW shared memory system. In Lei *et al.* (1993), an efficient parallel algorithm was proposed to find the majority element in shared-memory and message passing parallel systems and its time complexity was determined, while an approach for the parallelized  $m$ -out-of- $n$  voting through divide-and-conquer strategy was presented and analyzed in Parhami (1996).

Employing parallel algorithms is of the beneficial techniques to address the problems of sequential plurality voter for large object space applications such as public health systems, geographical information systems, Data Fusion, Mobile Robots, Sensor Networks, etc. Meanwhile, conducting large calculative operations using parallel algorithms is faster due to the modern processors, compared to when such operations are conducted by sequential algorithm. Moreover, multiple processing resources typically available in the applications dealing with a large number of inputs can be utilized for performing parallel voting algorithm (Parhami, 1996).

In this section, a new parallel plurality voting algorithm is presented on EREW shared-memory systems. First, sequential plurality voting is introduced and this is followed by introducing and describing the parallel plurality algorithm with inspirations from the functions of this algorithm and using divide-and-conquer method and Brent's theorem. Divide-and-conquer strategy and Brent's theorem are used in the designation and the optimization of the parallel plurality voting algorithm, respectively. To compare the new algorithm with plurality voter in this research, the asymptotic analysis was employed.

*Sequential Plurality Voting*

The algorithm for the sequential plurality voter in totally ordered space for  $n$  inputs is presented in Parhami (1994), as follows:

**Procedure Exact Sequential Plurality Voting (Totally Ordered)**

**Sort** (ascending order) in place the set of records  $(x_i, v_i)$  with  $x_i$  as key. Use the end -marker  $(x_{n+1}, v_{n+1}) = (\infty, 0)$ .

$y := z := x_1;$

$u := w := v_1;$

**For**  $i=2$  to  $n+1$  **do**

**While**  $x_i = z$  **do**

$u := u + v_i;$   
 $i := i + 1;$

**End While.**

**If**  $u > w$  **Then**

$w := u;$   
 $y := z;$

**End If.**

$z := x_i;$   
 $u := v_i;$

**End For.**

**End//end of procedure//**

*Parallel Plurality Voting*

Basically, there are two architectures for the multi-processor systems. One is the shared-memory multi-processor system and the other is message passing (Lei *et al.*, 1993). In a shared-memory parallel system, it is assumed that  $n$  processor has either shared the public working space or has a common public memory.

To present the parallel plurality voting (PPV) in the PRAM machines with EREW shared-memory technology, the following assumptions are taken into account:

- Array  $A [1 \dots n]$  with  $n$  elements, comprises  $a_1, a_2, \dots, a_n$ , where each  $a_i, i=1 \dots n$ , is the output of  $i^{\text{th}}$  module.
- The number of redundant modules,  $n$ , is considered as the power of 2.
- Array  $A$  is divided to  $p = (n/\log n)$  sub-arrays each of which contains at most  $\log n$  element.
- Divide-and-conquer method is used to implement the algorithm.
- For enhancing the algorithm, the number of required processors is assumed equal to the number of sub-arrays i.e.  $p$ .

The pseudo-code of our optimal parallel plurality voter (PPV) is presented as follows:

---

Pseudo-code of parallel plurality voter

---

**Procedure Exact Parallel-Plurality Voting (*Totally Ordered Space*)**

---

**Input:**  $X$  is an array of the  $n$  elements  $x_1, x_2, \dots, x_n$  where  $n=2^k$ .

**Output:** Return  $Y$  as the output of the Parallel Plurality Voting (PPV).

**Step 1.** // Partitioning  $X$  //

$X$  is subdivided into  $p = \frac{n}{\log n}$  subsequence's  $X_i$  of length  $\log n$  each, where  $1 \leq i \leq p$ ;

**Step 2.** // Find the number of iterative elements ( $k$ ) in each partition //

(2.1)  $k \leftarrow 1$

(2.2) **For**  $i=1$  to  $p$  **do in Parallel**

$Z_i \leftarrow X[(i-1)\log n + 1]$

$u_i \leftarrow 1$  // set tally for each element //

**For**  $j=((i-1)\log n + 2)$  To  $\min\{i \cdot \log n, n\}$  **Do**

**If**  $X_j = Z_i$  **Then**

            Find iterative Elements in each partition.

$u_i \leftarrow u_i + 1$  // update tally //

**Else**

$k \leftarrow k + 1$

$Z_k \leftarrow X_j$

$u_k \leftarrow v_j$

**End If.**

**End For.**

**End For.**

**Step 3.**

(3.1) **IF**  $k=n$  **Then** //  $n$  is the number of elements //

    "There is no plurality agreement"

**Else**

$Z$  is subdivided into  $p = \frac{k}{\log k}$  subsequence's  $Z_i$  of

    Length  $(\log k)$  each, where  $1 \leq i \leq p$ ;

  (3.2) **Broadcast**  $Z_i$  to processor  $P_i$

  (3.3)  $L \leftarrow 1$

  // Find Repetitive Elements in other partitions and update its tally //

  (3.4) **For**  $i=0$  to  $\lceil \log p - 1 \rceil$  **do**

**For**  $j=1$  to  $p$  **do in Parallel**

**IF** ( $j$  is Odd) **Then**

$T_j \leftarrow Z[(j-1) \cdot \log k + 1]$

$\forall S \in \{(j-1) \cdot \log k + 2\}$  **and**  $\min\{2(i+j) \cdot \log k, (j-1)k\}$

**Merge** each of pair subsequence  $(T_j, T_{j+1})$  **and do in Parallel.**

**IF**  $T_j = Z_s$  **Then**

$u_j \leftarrow u_j + 1$

```

Else
     $W(0,L) \leftarrow T_j; W(1,L) \leftarrow u_j;$ 
     $L \leftarrow L+1; T_j = Z_s; u_j \leftarrow u_s$ 
End IF.
End IF.
End for.
End for.
// Matrix  $W$  is an amalgamation of array  $X$  and the number of each element iteration(tally) //
Step4.

(4.1) For  $i=1$  to  $(L/\log L)$  do in Parallel
     $Y(0,i) \leftarrow W(0, (i-1)*\log L + 1)$ 
     $Y(1,i) \leftarrow W(1, (i-1)*\log L + 1)$ 
    For  $j=((i-1)*\log L + 2)$  To  $\min\{i*\log L, L\}$  do
        If  $Y(1,j) > Y(1,i)$  Then
             $Y(1,i) \leftarrow Y(1,j)$ 
             $Y(0,i) \leftarrow Y(0,j)$ 
        End If.
    End For.
    End For.
    End For.
// Return the Result if PPV exists //
(4.2) For  $i=0$  to  $\left\lceil \log\left(\frac{L}{\log L}\right) \right\rceil - 1$  do
    For  $j=1$  to  $(L/\log L)$  do in Parallel
        If ( $j$  is Odd) Then
            If  $Y(1,(j-1)*\log L + 1) > Y(1,(j*\log L + 1))$  Then
                 $Result \leftarrow Y(0,(j-1)*\log L + 1)$ 
            Else
                 $Result \leftarrow Y(0,(j*\log L + 1))$ 
            End If.
        End If.
    End For.
    End For.
End.

```

---

In next section, the four steps of the algorithm PPV are examined and compared with the time complexity of the sequential algorithm given in Sequential Plurality Voting section. In order to define an optimal parallel plurality voting with less time complexity and minimal number of processors, the Brent's theorem (Brent, 1973) was used to partition the input elements into predetermined groups in the PRAM systems with  $p$  processor.

## RESULTS AND DISCUSSION

In this section, both the parallel and sequential plurality voting algorithms introduced in previous sections were analyzed by computing the complexity of the algorithms and discussions on each step in order to highlight the efficiency of the new parallel algorithm. Hence, to do so,  $T_s(n)$  is

defined as the function of executing time of the sequential plurality voting algorithm and  $T_p(n)$  as the function of the executing time of the parallel voting algorithm in which  $p$  is the number of the processors. As mentioned in sub-section of Sequential Plurality Voting, the sequential plurality voter needs the time complexity  $T_s(n)=O(n \log n)$ , while parallel algorithm consumes the constant time of  $O(1)$  to divide array  $X$  into  $p$  sub-arrays (*partitioning X*) having the maximal length of  $(\log n)$  which has been indicated in step 1 of PPV.

In order to find the number of iterative elements in array  $X$ , i.e. the value of counter  $k$  in each partition,  $p$ , there is a need to time complexity of  $O(\log n)$  in step 2. In step 3, if value  $k$  is equivalent to the number of inputs of array  $X$ , the algorithm will no longer have any result because it does not achieve plurality agreement. The time complexity of step 3.1 is  $O(1)$ , other than if the value  $k$  is opposite to  $n$ , the number of the countered elements is arranged, which are stored as matrix  $Z$  in step 2, into  $p$  partitions by using the approach of step 1. The time complexities of the procedures in steps 3.2, 3.3 and 3.4 are respectively  $O(1)$ ,  $O(1)$  and  $O\left(\log \frac{k}{\log k}\right)$  or  $O(\log k)$ , which is smaller than or equal to  $O(\log n)$ .

The result of step 3 is matrix  $W$  in which row zero refers to the *value* of algorithm's input, and the first row represents the *tally* of each element in the partition. In step 4, the later row in several partitions should be compared to find the iterative elements (step 4.1). Finally, the plurality element in step 4.2 is possibly considered. The procedures in step 4 totally require  $O(\log l) < O(\log k) < O(\log n)$ , and therefore:

$$T_p(n) = O(1) + O(\log n) + O(\log k) + O(\log l). \quad (1)$$

It is concluded that the totally complexity of the parallel plurality voting for  $1 \leq k \leq n$  is:

$$T_p(n) = O(\log n). \quad (2)$$

Since the execution time of the parallel plurality voter is  $O(\log n)$ , it is able to run faster than the sequential plurality voter with the complexity of  $\Omega(n \log n)$ . Furthermore, it can be obviously seen that the total number of the required processors in the parallel algorithm does not exceed  $(n/\log n)$ . Hence, taking into account the execution time and number of processors needed, the cost and time complexity of the proposed algorithm are optimal.

## CONCLUSIONS

In this paper, an optimal parallel algorithm has been proposed to find the plurality agreement among the results of  $n$  redundant modules in the parallel shared-memory systems in the EREW model. As seen in results and discussion, the execution time of the sequential algorithm is  $\Omega(n \log n)$ , whereas it is  $O(\log n)$  in the proposed parallel algorithm. Hence, the time complexity of the parallel plurality voter is less than its sequential peer.

The parallel plurality voter has also been shown to resolve the problem associated with sequential plurality voter in dealing with a large number of inputs. This parallel algorithm can be extended to unordered arrays that are implemented in future on Bus, Hyper Cube and Mesh typologies in the message passing systems.

## REFERENCES

- Blough, D. M., & Sullivan, G. F. (1990). *A Comparison of Voting Strategies for Fault-tolerant Distributed Systems*. Paper presented at the Ninth Symposium on Reliable Distributed Systems.

- Brent, R. P. (1973). *Algorithms for Minimization without Derivatives*. Englewood Cliffs, NJ.: Prentice-Hall.
- Karimi, A., Zarafshan, F., Jantan, A. B., Ramli, A. R. B., & Saripan, M. I. B. (2010). *An Optimal Parallel Average Voting for Fault-tolerant Control Systems*. Paper presented at the 2010 International Conference on Networking and Information Technology (ICNIT).
- Latif-Shabgahi, G. (2004). A Novel Algorithm for Weighted Average Voting Used in Fault-Tolerant Computing Systems. *Microprocessors and Microsystems*, 28(7), 357-361.
- Latif-Shabgahi, G., Bass, J. M., & Bennett, S. (2004). A Taxonomy for Software Voting Algorithms Used in Safety-Critical Systems. *IEEE Transactions on Reliability*, 53(3), 319- 328.
- Latif-Shabgahi, G., Hirst, A. J., & Bennett, S. (2003). *A Novel Family of Weighted Average Voters for Fault Tolerant Computer Systems*. Paper presented at the Proceedings of ECC03: European Control Conference, Cambridge, UK.
- Lei, C. L., & Liaw, H. T. (1993). Efficient Parallel Algorithms for Finding the Majority Element. *Journal of Information Science and Engineering*, 9, 319-334.
- Lorczak , P. R., Caglayan, A. K., & Eckhardt, D. E. (1989). *A Theoretical Investigation of Generalized Voters for Redundant Systems*. Paper presented at the FTCS-19. Digest of Papers. Nineteenth International Symposium on Fault-Tolerant Computing, chicago, USA.
- Parhami, B. (1992). *Optimal Algorithms for Exact, Inexact and Approval Voting*. Paper presented at the 22nd International Symposium on Fault-Tolerant Computing (FTCS-22), Boston, N.A, USA.
- Parhami, B. (1994). Voting Algorithms. *IEEE Transactions on Reliability*, 43, 617-629.
- Parhami, B. (1996). Parallel Threshold Voting. *The Computer Journal*, 39(8), 692-700.
- Tong, Z., & Kain, R. Y. (1991). Vote Assignments in Weighted Voting Mechanisms. *IEEE Transactions on Computers*, 40(5), 664-667.
- Yacoub, S., Lin, X., & Burns, J. (2002). Analysis of the Reliability and Behavior of Majority and Plurality Voting Systems. Palo Alto: Hewlett-Packard Company.

## An Audit of Type 2 Diabetes Care in a Malaysian Public Community Polyclinic

**Chew, B. H.<sup>1\*</sup>, Palikat, J. M.<sup>2</sup>, Nur Syamimi, A.<sup>2</sup>, Nor Azillah, A.<sup>2</sup>,  
See, J. K.<sup>2</sup>, Hafiz, A. R.<sup>2</sup>, Siti Nazira, A.<sup>2</sup>, Aienum, Y.<sup>2</sup>, Muhamad Zaid, M.<sup>2</sup>,  
Palaniappan, K.<sup>2</sup> and Tan, Y. Y.<sup>2</sup>**

<sup>1</sup>*Department of Family Medicine,*

<sup>2</sup>*Medical Students,*

*Faculty of Medicine and Health Sciences, Universiti Putra Malaysia,  
43400 Serdang, Selangor, Malaysia*

*\*E-mail: chewboonhow@yahoo.com*

### ABSTRACT

Adequate and proper diabetes care in any practice is paramount and deems to be the fundamental requirement for good diabetes control. This is an audit of type 2 diabetes care process in a public Polyclinic, with the objectives of studying the quality of diabetic care provided in terms of clinical and managerial performance and also to give recommendations on improving its diabetes care delivery. The audit was done on patients' medical records selected via systematic random sampling. Patients who have been diagnosed with type 2 diabetes mellitus for more than 2 years, and those who have come for follow-up at least twice in between 1<sup>st</sup> October 2008 and 30<sup>th</sup> September 2009 by the medical officer and/or family medicine specialist. Patients with gestational diabetes mellitus and Type 1 diabetes mellitus were excluded. A total of 100 medical records were audited. 51% were female and 82% were in the 40-69 age group. Measurements of blood glucose and blood pressure were done at each follow-up at the polyclinic at 96% and 93% of the times, respectively. Within the past one year, HbA1c was performed in 46% of the patients, while renal profile was screened in 66% of the patients and urine protein was tested in 59% of the diabetics. Only 15% had their eyes screened by fundus camera. The diabetes care process at this public polyclinic was unsatisfactory, as many annual blood tests were not done and complications screening were also omitted. Thus, an urgent intervention is recommend in order to rectify these inadequacies.

**Keywords:** Type 2 Diabetes mellitus, health care deliveries, medical audit, community polyclinic

### INTRODUCTION

According to the Altman Committee in the United Kingdom, the term medical audit means "sharing by a group of peers of information gained from personal experience and/or medical records in order to assess the care provided to their patients to improve their learning and to contribute to the medical knowledge" (Piterman & Yasin, 1997, p. 531). Meanwhile, the concept of clinical audit, as adopted by Healthcare Commission and National Institute for Clinical Excellence (NICE) in United Kingdom (UK), is "... a quality improvement process that seeks to improve the patient care and outcomes through systematic review of care against explicit criteria and the implementation of change. Aspects of the structures, processes and outcomes of care are selected and systematically evaluated against explicit criteria. Where indicated, changes are implemented at an individual team, or service level and further monitoring is used to confirm improvement in healthcare delivery" (Clinical Governance Support Team, 2005, p. 3; Yasin & Piterman, 1997).

---

Received: 22 April 2010

Accepted: 22 January 2011

\*Corresponding Author

Type 2 diabetes mellitus (T2D) is an important public health concern for both patients and health care providers, as it could lead to varied complications, reduced quality of life and life expectancy, and yet T2D with the aforementioned impediments are preventable (International Diabetes Federation, 2004; American Diabetes Association, 2001; American Diabetes Association, 1998; Stamler *et al.*, 1993; Garcia *et al.*, 1974). The Third National Health and Morbidity Survey (NHMS III, 2006) reported a prevalence of 14.9%, and this marked a significant increase of the diabetes mellitus prevalence of 82% from NHMS II, which recorded only 8.2% (National Health and Morbidity Survey II, 1997). Hence, prompt and efficient treatments are needed to curb this epidemic and these have been proven to be important in order to delay complication (The UK Prospective Diabetes Study Group, 1998; Kuusisto *et al.*, 1994). The four components of the standard care for T2D encompass diet, exercise, medication and education (Malaysian Clinical Practice Guidelines for the Management of Type 2 Diabetic Mellitus, 2009; American Diabetes Association, 2009). This is greatly enhanced by a regular self-monitoring of diabetes control and an early management of complications by health care providers. Thus, a good diabetes care in a practice is essential to ascertain a proper delivery of medical care for the diabetic patients, which will in turn improve the level of control and reduce complications associated with diabetes, such as diabetic retinopathy, coronary heart diseases, stroke, diabetic nephropathy, and foot complications (American Diabetes Association, 2009).

Studies revealed that the quality of diabetes management in primary care is on par or even better than hospital out-patient settings (Griffin *et al.*, 1998). Nevertheless, recent systematic meta-analysis reported outcomes of diabetic care were equivocal between the sub-specialist centres and primary care centres (Piet *et al.*, 2009). In particular, the quality of the diabetes care delivered by the local general practice has showed improvement over the years, while the quality of diabetes management in some other countries like Cyprus remained suboptimal (Lee *et al.*, 2004; Zachariadou *et al.*, 2006). However, there are a few similar studies conducted in the local public health clinics, where majority of the people obtain their diabetic care (National Health and Morbidity Survey II, 1997; National Health and Morbidity Survey III, 2006). In view of this, the researchers set out to study the diabetes care process at one of the public health clinics via a medical audit exercise focusing on the care process.

## MATERIALS AND METHODS

This was a retrospective study using patients' medical records or diabetic books. The records chosen were those of the patients diagnosed with T2D for more than 2 years and have come for follow-up at least twice between 1<sup>st</sup> October 2008 and 30<sup>th</sup> September 2009 with the medical officers and/or family medicine specialist. Nonetheless, patients with Type 1 diabetes mellitus and gestational diabetes mellitus were excluded. The sample size was estimated based on the table of sample size calculations provided in the 2009 Indian Health Services Diabetes Audit Instructions, which stated that the minimum number of charts (records) needed to be reviewed to be reasonably sure (95% confidence) that a 10% difference noted from a previous or a subsequent audit is a real change and not just due to the chance for about 3000 population is 93. Thus, the sample size estimated was rounded up to 100. The records were chosen using the systematic random sampling method. From a total of 3092 diabetic records available at the health centre, 100 records were selected. Thus, the constant  $k$  is equal to 31. This means that one record was picked after every 31 medical or diabetic books. The first number selected from 1 to 31 was 6, and the process was continued by selecting the next 31<sup>st</sup> record on the list until 100 records were obtained. Each of the records was screened for the inclusion and exclusion criteria before the data were captured and recorded into a structured

An Audit of Type 2 Diabetes Care in a Malaysian Public Community Polyclinic

pro-forma. The structured pro-forma was the standardized case record forms used by the researchers to capture data from the patients' medical records. All the indicators of the process were recorded as done or not done to evaluate the standard of diabetes care process in this polyclinic. All the targets of the performance were arbitrarily set as they were deemed reasonable by the family medicine specialists and other staff involved in providing diabetes care. Blood glucose, either fasting or casual, and blood pressure measurement at each clinic visit were set at 98% target of performance as the researchers felt that they are important for the management of T2D (see Table 2). The gathered data were analysed using SPSS version 15.

TABLE 1  
Demographic and clinical characteristics of 100 patients included in the clinical audit

Characteristics	Percentage of the patients (%)
Female	51
Male	49
<b><i>Age groups (years)</i></b>	
< 29	1
30 – 39	10
40 – 49	26
50 – 59	29
60 – 69	27
> 70	7
<b><i>Duration of diagnosis (years)</i></b>	
2 to 5	47
6 to 10	35
> 10	18

TABLE 2  
Percentage of the completed processes of care as compared to the target level of performance

Processes	Percentage of completed processes (%)	Target level of performance (%)
<b>Performed at each visit</b>		
Blood glucose (fasting or random)	96%	98%
Blood pressure	93%	98%
<b>Performed at least once a year</b>		
Glycated haemoglobin (HbA <sub>1c</sub> )	46%	60%
Renal profile	66%	80%
Urine protein	59%	80%
Lipid profile	62%	60%
Electrocardiogram	35%	10%
Body mass index (BMI)	40%	30%
Foot inspection	44%	60%
Visual acuity	27%	60%
Fundus camera	15%	60%

## RESULTS

Out of the 100 patients with T2D, 51 were women. The majority of the subjects (82%) were in the 40-69 age group and most (47%) have been diagnosed with T2D for 1 to 5 years (see Table 1). Blood glucose (either fasting or random) and blood pressure measurements were done at each follow-up at the clinic 96% and 93% of the times, respectively. Within the past one year, HbA<sub>1c</sub> was performed in 46% of patients, while renal profile was screened in 66% of the patients and urine protein was tested in 59% of the diabetics. Only 15% had their eyes screened by fundus camera (see Table 2).

## DISCUSSION

The demography of the diabetes patients at this clinic was mostly of younger age groups, i.e. from about equal gender proportion, with two thirds of them below 60 years old, and have been diagnosed for less than a decade ago.

Fasting blood glucose (FBG) and random blood glucose (RBG) were usually carried out during each follow-up visit at this clinic. Having this state level of performance was not unexpected of a government polyclinic, where there is an established medical laboratory on-site manned by a medical laboratory technician. However, HbA<sub>1c</sub> was not done even once a year for the majority (54%) of T2D patients. This was worse than the England and Wales (E&W) general practices (GP) diabetes care about 10 years ago, whereby 72.5% of the patients had an HbA<sub>1c</sub> or fructosamine at least once in the past one year (Khunti *et al.*, 1999). The most likely reason for this was the unavailability of reagent for the test at this clinic, which was frequently affected by budget constraint. A similarly less desirable performance was also observed in the annual screening for nephropathy and dyslipidaemia, where there were less than two third of the patients had them done. These were comparable to (E&W) GP practices, 65.8% checked their patients' urine and 49% tested their patients' serum creatinine annually (Khunti *et al.*, 1999).

Nonetheless, lipid profile test was found to be better than the expectation, whereby it achieved the target of the performance set most probably improvement in the availability of the test's reagent at the clinic's medical laboratory. The annual foot examination and body weight measurement were largely omitted even though the later and electrocardiography attained the target of performance. In more specific, foot examination practice was comparable to local GP; however, 40.5% of them improved their inspection of the diabetic feet to more than 70% of their total past visits post-intervention (Lee *et al.*, 2004). The worst performance was the fundus examination amongst these diabetic patients, with only 15% had a proper fundus examination using a fundus camera. Funduscopic examination is a performance indicator that was found to be observed as much better amongst the local GP than this clinic, who managed to check 19.1% of their patient's fundus at least once in the past one year and this frequency increased to 51.7% after improvement exercise by intention (Lee *et al.*, 2004).

## RECOMMENDATIONS

In order to rectify these inadequacies of diabetes care at this clinic, the researchers have put forward the following recommendations. First, a dedicated team consisting of paramedic staff is to be trained to regularly carry out the test for blood glucose, blood pressure, weight measurement and foot examination at the pre-designated time. They could also be trained to maintain detailed diabetes registry and to post reminders for the doctor seeing the diabetes patients at the clinic about the annual blood tests HbA<sub>1c</sub>, screening for dyslipidaemia and nephropathy (Khunti *et al.*, 2001; Feder *et al.*, 1995). Meanwhile, education classes for the patients are to be conducted both by the pre-trained paramedics as well as the doctors. Similarly, a regular continuous medical education (CME) for the

## An Audit of Type 2 Diabetes Care in a Malaysian Public Community Polyclinic

doctors and the staff is crucial for a better standard of diabetes care, a more proper documentation in the diabetic book and strengthen the effort of screening for complications (Feder *et al.*, 1995).

Funding is not to be lacking for regular maintenance of medical equipment and the availability of reagents in the laboratory, especially for the HbA1c and lipid profiles. Staffing of the clinic must be adequate and in congruent with the workload, specifically for the doctor-patient ratio per day as it has been reported a higher volume of patients causes reduced adherence to the process measures recommended by clinical practice guidelines (Khunti *et al.*, 2001; Turchin *et al.*, 2007). In the present situation of staff shortages, they are to be more efficiently managed by the administration. Last but not least is to repeat a similar audit exercise on the diabetes care process after a lapse of about three to four months.

### LIMITATIONS

This audit involved reading of patients' records, which entailed with it the limitations of missing laboratory results, as well as illegible and incomplete documentation. Furthermore, filing of the test results is often erroneous and this makes them very difficult to be traced. In this study, this was overcome through an extra effort of looking into the patient's medical records and the central filing system, which subsequently led to the researchers having minimal difficulty with the lost laboratory reports.

### CONCLUSION

Type 2 diabetes care in this urban community polyclinic is good at blood pressure, lipid profiles and office glucose monitoring but poor at regular HbA1c testing, and worse at the regular annual screening practice for diabetic complications. As a result, urgent measures are needed to rectify and improve the current standard of diabetes care delivery in order to confer the greatest benefits to the patients.

### ACKNOWLEDGEMENTS

The researchers wish to express their gratitude to the Director General of the Ministry of Health for his permission to publish this article using the data from public health clinics. Our sincere appreciation also goes to Dr. Zaiton Ahmad for helping us in the planning phase of this project. A special acknowledgement is also owed to Dr. Sanidah Md Ali who had given her valuable input and supervision of this audit project during her tenancy as a family medicine specialist at Seri Kembangan Community Polyclinic. We extend our appreciation to all the staff at the clinic who had assisted us in one way or another in this study.

### REFERENCES

- American Diabetes Association. (1998). Economic Consequences of Diabetes Mellitus in the U.S. in 1997. *Diabetes Care*, 21(2), 296-309.
- American Diabetes Association. (2001). *Diabetes 2001 Vital Statistics* (p. 77-85). Alexandria, VA: American Diabetes Association.
- American Diabetes Association. (2009). Standards of Medical Care in Diabetes—2009. *Diabetes Care*, 32(Supplement 1), S13-S61.
- Clinical Governance Support Team. (2005). *A Practical Handbook for Clinical Audit*. National Health Service.

- Feder, G., Griffiths, C., Highton, C., Eldridge, S., Spence, M., & Southgate, L. (1995). Do clinical guidelines introduced with practice based education improve care of asthmatic and diabetic patients? A randomised controlled trial in general practices in east London. *BMJ British Medical Journal*, 311(7018), 1473-1478.
- Garcia, M. J., McNamara, P. M., Gordon, T., & Kannel, W. B. (1974). Morbidity and mortality in diabetics in the Framingham population. Sixteen year follow-up study. *Diabetes*, 23(2), 105-111.
- Griffin, S. (1998). Diabetes care in general practice: meta-analysis of randomised control trials. *BMJ British Medical Journal*, 317(7155), 390-396.
- International Diabetes Federation. (2004). *Diabetes Atlas* (2<sup>nd</sup> ed.). Brussels, Belgium: International Diabetes Federation.
- Khunti, K., Baker, R., Rumsey, M., & Lakhani, M. (1999). Quality of care of patients with diabetes: collation of data from multi-practice audits of diabetes in primary care. *Family Practice*, 16(1), 54-59.
- Khunti, K., Ganguli, S., Baker, R., & Lowy, A. (2001). Features of primary care associated with variations in process and outcome of care of people with diabetes. *British Journal of General Practice*, 51(466), 356-360.
- Kuusisto, J., Mykkänen, L., Pyörälä, K., & Laakso, M. (1994). NIDDM and its metabolic control predict coronary heart disease in elderly subjects. *Diabetes*, 43(8), 960-967.
- Lee, T. W., Chan, S. C., Chua, W. T., Harbinder, K., Khoo, Y. L., Ow Yeang, Y. L., Sethuraman, K., & Teoh, L. C. (2004). Audit of diabetes mellitus in general practice. *Medical Journal of Malaysia*, 59(3), 317-322.
- Ministry of Health Malaysia (2006). *National Health and Morbidity Survey III – Diabetes Epidemic in Malaysia*, 2006. Kuala Lumpur: Ministry of Health Malaysia.
- Ministry of Health Malaysia. (1997). *National Health and Morbidity Survey II – Diabetes Epidemic in Malaysia*. Kuala Lumpur: Ministry of Health Malaysia.
- Ministry of Health Malaysia (2009). *Malaysian Clinical Practice Guidelines for the Management of Type 2 Diabetic Mellitus* (4<sup>th</sup> ed.). Putrajaya: Ministry of Health Malaysia.
- Piet, N. P., Jolanda, W., & Jako, S. B. (2009). Do specialized centers and specialists produce better outcomes for patients with chronic diseases than primary care generalists? A systematic review. *International Journal of Health Care Quality*, 21, 387-96.
- Piterman, L., & Yasin, S. (1997). Medical audit-Why Bother. *Hong Kong Practitioner*, 19(10), 530-534.
- Stamler, J., Vaccaro, O., Neaton, J. D., & Wentworth, D. (1993). Diabetes, other risk factors, and 12-year cardiovascular mortality for men screened in the Multiple Risk Factor Intervention Trial. *Diabetes Care*, 16, 434-44.
- The UK Prospective Diabetes Study Group. (1998). Tight blood pressure control and risk of macrovascular and microvascular complications in type 2 diabetes: UKPDS 38. *British Medical Journal*, 317(7160), 703-713.
- Turchin, A., Shubina, M., & Pendergrass, M. L. (2007). Relationship of physician volume with process measures and outcomes in diabetes. *Diabetes Care*, 30, 1442-1447.
- Yasin, S., & Piterman, L. (1997). How to Do Medical Audits. *Hong Kong Practitioner*, 19(11), 591-600.
- Zachariadou, T., Makri, L., Stoffers, H. E., Philalithis, A., & Lionis, C. (2006). The need for quality management in primary health care in Cyprus: results from a medical audit for patients with type 2 diabetes mellitus. *Quality Management in Healthcare*, 15, 58-65.

## Residence Time Distribution of Tapioca Starch-Poly(lactic acid)-Cloisite 10A Nanocomposite Foams in an Extruder

Lee, S. Y.

*Mechanisation and Automation Research Centre,  
MARDI Headquarters, 43400 Serdang, Selangor, Malaysia  
E-mail: sylee@mardi.gov.my*

### ABSTRACT

Tapioca starch, poly(lactic acid) and Cloisite 10A nanocomposite foams were prepared by twin screw extrusion. Residence time distribution (RTD) in an extruder is a useful means of determining optimal processing conditions for mixing, cooking and shearing reactions during the process. RTD was obtained by inputting a pulse-like stimulus and measuring its profile at the exit or other point in the extruder. During processing, after the steady state had been reached, a fixed amount of tracer was instantaneously fed into the extruder and its concentration was measured from the samples collected at fixed time intervals in the extruder exit. The tracer concentration was the value of the redness,  $a^*$  was used as a measure of red colour intensity of the concentration of tracer in the extrudate. Meanwhile, the effects of two screw configurations (compression and mixing screws) and two barrel temperatures (150 and 160°C) on RTD of nanocomposite foams were also studied. The influences of screw configurations and barrel temperatures on RTD were analyzed using the mean residence time (MRT) and variance. Screw configurations and temperatures had significant effects ( $P<0.05$ ) on MTR. Mixing screws and lower temperature resulted in higher MRT and variance of RTD.

**Keywords:** Mean residence time, variance, screw configuration, temperature

### INTRODUCTION

Extrusion process is composed of a series of physical, thermal and chemical changes occurring in a simultaneous or consecutive manner inside the extruder barrel. The characteristic of the product is related to the time that a particle spends in the extruder. The degree of mixing or the extent of degradation of the material depends on how long it is exposed to the processing conditions. RTD in an extruder is a useful means of determining optimal processing conditions for mixing, cooking and shearing reactions during the process. From the RTD functions, one can estimate the degree of mixing, the life expectancy of mass flow, and the average total strain exerted on the mass during its transition, which thus provides a clear picture of how an extruder behaves as a chemical reactor (Fichtali & van de Voort, 1989). These results, coupled with the knowledge of the operating variables (such as temperature, screw speed and screw configuration) can provide sufficient information to predict the fraction of the material that will undergo specific reactions. Meanwhile, the RTD data also are used for scale-up and to improve equipment design (Todd, 1975). In addition, RTD can also be used to characterize and predict the extrusion process (Chen *et al.*, 1995; Gao *et al.*, 1999). RTD can be measured by introducing an inert tracer as a pulse at a chosen location of the extruder, and its concentration at another location downstream (usually at the die exit), which is determined by taking samples in a discrete manner (Gogoi & Yam, 1994; Wolf *et al.*, 1986).

Polymer-clay nanocomposites are a class of reinforced polymers containing small quantities

---

Received: 15 January 2011

Accepted: 1 April 2011

(1-5wt%) of nanometric-sized clay particles. The objectives of this study were to investigate the influence of screw configurations and barrel temperatures on the RTD and to analyze the influence of extrusion variables on the MRT and variance of RTD affecting the properties of the nanocomposite foams. In this article, emphasis is given on the RTD results and the influence on MRT and variance, whilst the properties are not discussed.

## MATERIALS AND METHODS

### *Materials*

Semicrystalline poly(lactic) acid (PLA) resin of MW<sub>n</sub> 85,000 was produced by Cargill, Inc. (Minneapolis, MN, USA). Commercially available tapioca starch was purchased from Starch Tech, Inc. (Golden Valley, MN, USA). Organoclay, under the trade name of Cloisite 10A, was purchased from Southern Clay Co. (Gonzales, TX, USA) and used as nanofiller. The organoclay was organically-modified montmorillonite (MMT). Tapioca starch was agglomerated into spherical granules of 2-4mm diameter to facilitate feeding into the extruder. The moisture content of the tapioca starch was adjusted to 20%, dry basis, with distilled water prior to extrusion. Tapioca starch and PLA (90:10 weight ratio) were blended with 3% Cloisite 10A in a Hobart mixer (Model C-100, Horbart Corp., Troy, OH, USA) and stored in plastic bottles prior to extrusion.

### *Extrusion*

A twin-screw extruder (model DR-2027-K13, C. W. Brabender, Inc., S. Hackensack, NJ, USA), with two types of corotating screws (namely, compression and mixing screws, model CTSE-V, C. W. Brabender, Inc., S. Hackensack, NJ, USA) was used to conduct the extrusions. The conical screws had diameters decreasing from 43mm to 28mm along their length of 365mm from the feed end to the exit end. The compression screws were universally single flighted corotating intermeshing screws with interrupted flight mixing zones. The mixing screws had a mixing section, in which small portions of the screw flights were cut away. The mixing section enhanced the mixing action and also increased the residence time of the sample in the barrel. A 90-rev/min screw speed was used for all the extrusions. The temperature at the feeding section was maintained at 50°C, while the second barrel section at 120°C and the third barrel section and die section were maintained at 150°C. Die nozzle of 3mm diameter was used to produce extrudates which were cut by a rotating cutter. The extruder was controlled by a Plasti-Corder (Type FE 2000, C. W. Brabender, Inc. S. Hackensack, NJ, USA). Data including barrel temperature profiles, pressure profiles and torque reading were recorded by a computer for subsequent analyses. Extrusion conditions selected were based on the preliminary studies and previous experiments.

### *Determination of RTD*

The RTD study was performed using a dye technique (Lin & Armstrong, 1990). The tracer used for determining the RTD was prepared by mixing 0.05g of red dye sodium erythrosine (Sigma Chemical Co., St. Louise, MO, USA) with 5g of tapioca starch and the amount of water needed to bring the moisture content of the tracer to that of the feed material (20%) (Lee & McCarthy, 1996). The tracer was added as a pulse input through the inlet port of the extruder when steady state conditions were achieved. Foam samples were collected every 5s for 3 min after adding the tracer.

### Colorimeter

The 5 s samples were ground in a mill to pass through a 50 US standard sieve. The values of  $L^*$ ,  $a^*$ ,  $b^*$  were measured three times for each ground sample using a Chroma meter (Model CR-300, Minolta, Japan). The red colour intensity,  $c$  was calculated as:

$$c = \sqrt{(a^*)^2 + (b^*)^2} \quad [1]$$

where  $a^*$  represents the value of redness and  $b^*$  is the value of blueness. However, the value of  $b^*$  did not contribute to the red colour intensity (Seker, 2005), so  $c$  was simplified as:

$$c = a^* \quad [2]$$

Thus, the value of the redness,  $a^*$ , was used as a measure of red colour intensity of the tracer concentration in the extrudate (Bi *et al.*, 2007).

### RTD Functions

In general, RTD can be described with two functions, namely,  $E(t)$  and  $F(t)$  diagrams, which are closely related (Levenspiel, 1972). The response of the extruder to a pulse at the inlet is given by the  $E(t)$  diagram, which represents the age distribution of the material in the extruder. Since it is difficult to ensure that the same amount of tracer is used in all the experiments, it is common to normalize the tracer concentrations at each point in time by dividing them by the total amount of tracer passing through the system. Thus, the  $E(t)$  diagram can be obtained by dividing the concentration, at any time interval, by the total amount of tracer injected, as given in the following equation:

$$E(t) = \frac{c_i}{\int_{i=0}^{\infty} c_i dt} \approx \frac{c_i}{\sum_{i=0}^{\infty} c_i \Delta t} \quad [3]$$

where  $c$  is the tracer concentration at time  $t$ .

The  $F(t)$  diagram is related to the  $E(t)$  diagram and it represents the cumulative distribution function in the exit stream at any time.

$$F(t) = \int_{i=0}^{i=t} E(t) dt \approx \frac{\sum_{i=0}^{i=t} c_i \Delta t}{\sum_{i=0}^{\infty} c_i \Delta t} \quad [4]$$

The mean residence time (MRT) or  $\bar{t}$  which represents the mean time that a particle spent in the extruder can be described as:

$$\bar{t} = \int_{i=0}^{i=t} t_i E(t) dt \cong \frac{\sum_{i=0}^{\infty} t_i c_i \Delta t}{\sum_{i=0}^{\infty} c_i \Delta t} \quad [5]$$

While the variance ( $\sigma^2$ ) can be described as:

$$\sigma^2 \cong \frac{\sum_{i=0}^{\infty} (t_i - \bar{t})^2 c_i \Delta t}{\sum_{i=0}^{\infty} c_i \Delta t} \quad [6]$$

#### *Experimental Design and Statistical Analyses*

A 2 x 2 factorial design (with three replications) was used to analyze the effects of screw configurations (compression and mixing screws) and barrel temperatures (150 and 160°C) on the RTD. The results for the measurements were analyzed using the general linear models (GLM) in the SAS analysis program (SAS Institute Inc., Cary, NC, USA). Duncan's multiple range tests were conducted to check for significant ( $p < 0.05$ ) differences between the treatment groups.

#### **RESULTS AND DISCUSSION**

RTD is a key parameter for characterizing the performance of an extruder reactor. A twin screw extruder often works under starved conditions. Thus, screw configurations and temperature are two independent operating parameters. Their respective influences on the RTD measured by the above described method are shown in *Fig. 1*. As expected, for a given screw configuration, an increase in temperature shifted the RTD function to the short time domain. For a given temperature, the mixing screw displayed a similar effect. All the RTD curves were of good quality, regardless of the screw configurations and/or temperature. This implies that the extruder is able to work under a relatively large processing window. Meanwhile, the reproducibility of the experiments carried out in the present study was found to be very good, as shown in *Fig. 2*. The figure shows that the RTD for two experimental runs at the same operating conditions were almost identical.

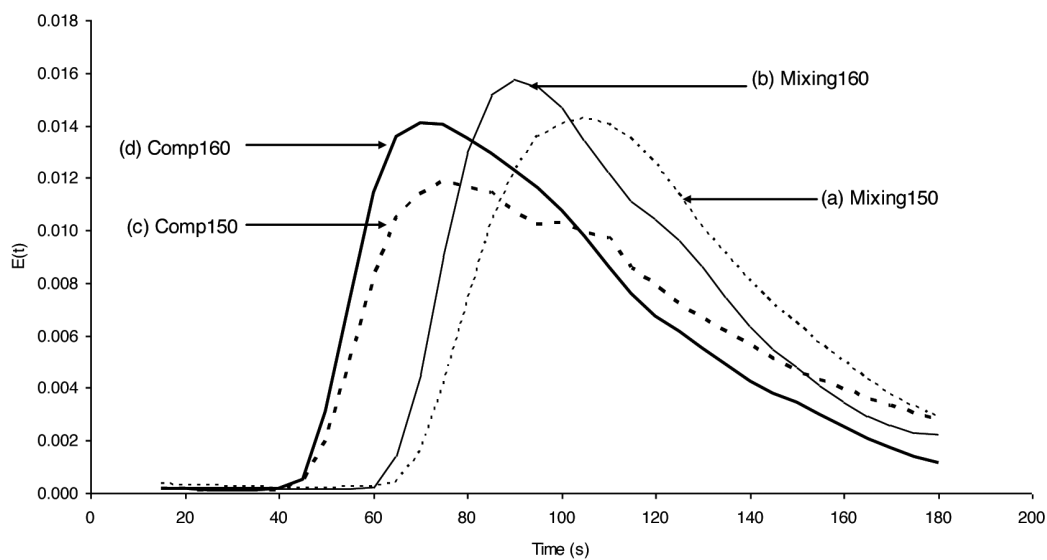


*Fig. 1: Residence time distribution of (a) mixing screws at 150°C, (b) mixing screws at 160°C, (c) compression screws at 150°C, and (d) compression screws at 160°C.*

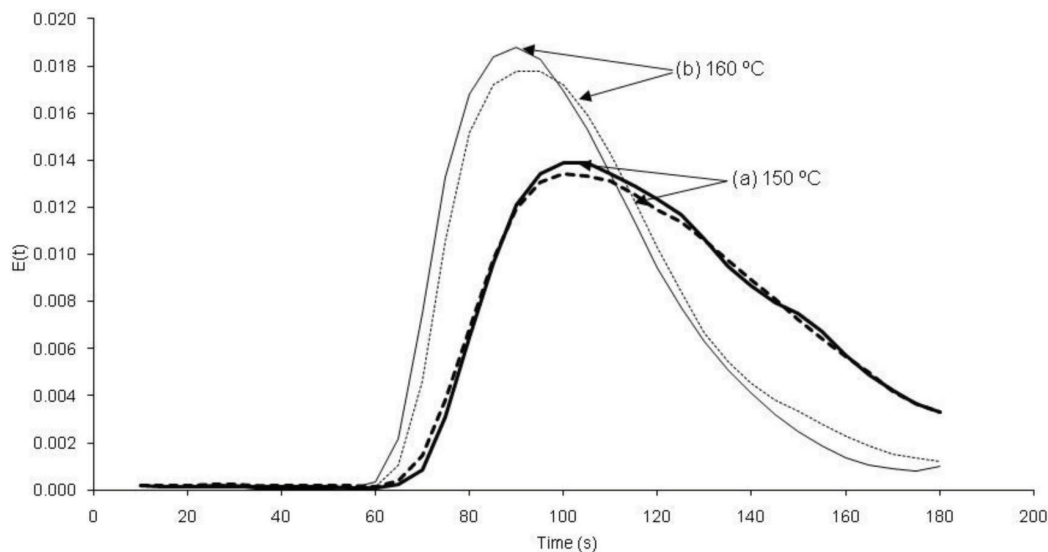


Fig. 2: Residence time distribution of mixing screws obtained at the same operating conditions (a) 150°C and (b) 160°C for two experimental runs.

The influences of screw configurations and temperature on MRT are shown in Table 1. The MRTs were significantly different ( $p < 0.05$ ) for mixing and compression screws at 150°C and 160°C, respectively. As expected, the mixing screws had longer MRT than the compression screws. In addition, lower temperature resulted in longer MRT for both screws, as expected. On the other hand, higher temperature produced more heat energy which decreased the viscosity of the mass, resulting in a more flowable material. Similar results were also reported by Altomare *et al.* (1986). Data from mixing screws at 150°C had significantly higher variance. However, the MRTs were not significantly different for the compression screws at 150°C and 160°C. Similarly, the variances were not significantly different for both sets of screws at 150°C and 160°C.

TABLE 1  
Mean residence time (MRT) and variance for mixing and compression screws at two temperatures

	Temperature [°C]	MRT [s]	Variance [s <sup>2</sup> ]
Mixing	150	110.7a	1008a
Mixing	160	98.74b	750.2b
Compression	150	91.74c	734.5b
Compression	160	83.43d	658.5b

a-d means with same letter within a column indicate no significant ( $P>0.05$ ) difference by Duncan multiple range test.

## CONCLUSIONS

In this study, the RTD results produced curves with good distribution, which is related to the MRT of the process. The influences of screw configuration and temperature on RTD were predicted well using the process. Mixing screws had longer MRT compared to the compression screws. Lower

temperatures resulted in longer MRT for both the screws. Mixing screws at 150°C had significantly higher variance. Nevertheless, the variances were not significantly different for both sets of the screws at 150°C and 160°C.

### ACKNOWLEDGEMENTS

This research was funded by University of Nebraska Agricultural Research Division, supported in part by the funds provided through the Hatch Act, USDA. Our sincere thanks are due to Prof. Dr. Milford Hanna of University of Nebraska, Lincoln and Malaysian Agricultural Research and Development Institute (MARDI) for supporting this work.

### REFERENCES

- Altomare, R. E., & Ghossi, P. (1986). An analysis of residence time distribution patterns in a twin screw extruder. *Biotechnology Progress* 2(3), 157-163.
- Bi, C., Jiang, B., & Li, A. (2007). Digital image processing method for measuring the residence time distribution in a plasticating extruder. *Polymer Engineering Science* 47, 1108-1111.
- Chen, L.G. Hu, H., & Lindt, J. T. (1995). Residence time distribution in non-intermeshing counter-rotating twin-screw extruders. *Polymer Engineering Science*, 35, 598-603.
- Fichtali, J., & van de Voort, F. R. (1989). Fundamental and Practical Aspects of Twin Screw Extrusion. *Cereal Foods Worlds* 34, 921-929.
- Gao, J., Walsh, G., Bigio, C. D., Briber, R. M., & Wetzel, M. D. (1999) Residence-time distribution model for twin-screw extruders. *AICHE Journal* 45(12), 2541-2549.
- Gogoi, B. K., & Yam, L. K. (1994). Relationship between residence time and process variables in a corotating twin-screw extruder. *Journal of Food Engineering*, 21, 177-196.
- Lee, S. Y., & McCarthy, K. L. (1996). Effect of screw configuration and speed on RTD and expansion of rice extrudate. *Journal of Food Process Engineering*, 19, 153-170.
- Levenspiel, O. (1972). *Chemical Reaction Engineering (2<sup>nd</sup> Ed.)*. N.Y.: Wiley.
- Lin, J. K., & Armstrong, D. J. (1990) Process variables affecting residence time distributions of cereals in an intermeshing, rountner rotating twin screw extruder. *Transaction of ASAE*, 33, 1971-1978.
- Seker, M. (2005) Residence time distributions of starch of high moisture content in a single screw extruder. *Journal of Food Engineering*, 67, 317-324.
- Todd, D. B. (1975) Residence Time Distribution in Twin-Screw Extruders. *International Polymer Processing*, 6, 143-147.
- Wolf, D., Holin, N., & White, D. H. (1986) Residence time distribution in a commercial twin-Screw Extruder. *Polymer Engineering Science*, 26, 640-646.

## Ex-Situ Experimental Set-Up for Pink Guava Juice Fouling Deposit Study

Ong C. A., Abdul Aziz, N.\* , Taip, F. S. and Ibrahim M. N.

*Department of Process and Food Engineering,  
Faculty of Engineering, Universiti Putra Malaysia,  
43400 Serdang, Selangor, Malaysia  
\*E-mail: shekeen@eng.upm.edu.my*

### ABSTRACT

A study has been conducted on pink guava juice (PGJ) fouling deposit. Several ex-situ experimental rigs were set-up to obtain PGJ fouling deposit, while the best ex-situ experimental rig was also selected. PGJ was heated at 93°C and its fouling deposit was obtained after 1 hour of heating. Then, it was used for the ex-situ cleaning study at 1 litre min<sup>-1</sup>, at several temperatures (70, 80 and 90°C), and in some chemical concentrations (1.6 v/v% of Maxiclean CP6 or 0.325 % OH<sup>-</sup>; 1.8 v/v% of Maxiclean CP6 or 0.369 % OH<sup>-</sup>; 2.0 v/v% of Maxiclean CP6 or 0.44 % OH<sup>-</sup>). The best cleaning combinations were investigated. Carbohydrate is the main content in the fouling deposit. The morphology of the deposit was studied using SEM and it showed an aggregated structure. The cleaning process improved as the temperature increased with the increasing of the chemical solution concentration. The shortest cleaning time was 40 minutes, for cleaning using 2.0 v/v% of Maxiclean CP6 (0.44 % OH<sup>-</sup>) at 90°C.

**Keywords:** Pink guava juice, fouling deposit, cleaning, ex-situ method

### INTRODUCTION

In many processing industries, fouling deposit is an unwanted by-product that attaches to the inner surfaces of processing equipment (Bott, 1995). Fouling deposit can hamper the process performance, both technically and economically. It is important to note that fouling deposit can reduce equipment performance and product output, as well as increase maintenance cost, energy cost and affect the environment. The formation of fouling deposit is caused by the effect of processing condition and processing raw material properties. In food industries, the formation of fouling deposit is common because food substances are heat sensitive and heating process is a typical technique to preserve the food. Thus, it is almost impossible to terminate formation of fouling deposit in the food industry.

Pasteurisation is a common technique used to preserve food products in the food industry. High temperature is required to deactivate enzyme and kill harmful bacteria. However, food substances are heat sensitive. Exposure to high temperature will denature food substances and promote formation of fouling deposit. Heat exchanger is a common unit operation use in the food industry to pasteurize and sterilize food products (Earle, 1983). As formation of fouling deposit is presumed to occur, most heat exchanger designers take into consideration the fouling factor in designing it to ensure that its usage can be prolonged (Saunders, 1988). Meanwhile, the application of fouling factor is one of the precaution methods to delay the fouling removal procedure. Each material should have its own fouling factor as it depends on the raw material properties and the

---

Received: 15 January 2011

Accepted: 1 April 2011

\*Corresponding Author

fouling deposition mechanism (Krause, 1993). Nonetheless, only few fouling factors have been discovered, and these are mostly for the petroleum industry (Müller-Steinhagen, 2000). Therefore, an in-depth empirical study is required to quantify the fouling factor of undefined fouling deposit.

Cleaning-in-place (CIP) is a common method used in food plants to remove fouling deposit and regain the original condition of heat exchanger. Cleaning procedure needs to be done frequently as food fouling deposit reduces processing performance, and product quality, as well as provides a medium for bacteria growth. Meanwhile, cleaning agent, procedure and condition are generally dependent on the type of food substances; for instance, alkaline-based cleaning agent is best suited with protein-based and fat-based fouling deposit (Watkinson, 2008). However, an empirical study is still needed to set the right duration for cleaning, to ensure short downtime and less consumption of water and chemical during the cleaning process. Many studies on fouling and cleaning have been focussing on dairy-based products (Fryer & Bird, 1994; Changani *et al.*, 1997; Chen *et al.*, 2004; Swartzel, 1983), which provide important knowledge for mitigating the fouling problem. Thus, studies on fouling and cleaning are still limited, particularly on tropical-based food products.

Therefore, this study investigated pink guava juice (PGJ) fouling deposit, which is an undefined fouling deposit. Pink guava is also among the main natural resources of tropical countries. Furthermore, Malaysia is among the main producers of pink guava puree. Zainal *et al.* (1999) studied the effect of temperature on pink guava juice, but the researchers did not include the aspect of fouling deposit formation in their work. The objectives of this study were to set-up a simple ex-situ experimental rig to obtain PGJ fouling deposit in a short processing time and to provide basic knowledge on cleaning requirement. The reason to use an ex-situ experimental set-up was to reduce the consumption of raw material, labour work and processing time. The findings from this work are essential for further investigations on the fouling factor of the PGJ fouling deposit and the best cleaning procedure for the PGJ industry.

## MATERIALS AND METHODS

### *Preparation of Pink Guava Juice (PGJ)*

Pink guava juice was prepared according to the basic formulation provided by Sime Darby Food and Beverages Marketing Sdn. Bhd. Filtered water and sugar were added to the puree at the ratio of 1:3:7 (sugar: pink guava puree: water) to produce PGJ. The puree was sponsored by Sime Darby Food and Beverages Marketing Sdn. Bhd. This PGJ had the viscosity of 11.2 mPas and the pH value ranging from 3.8 to 4.5, which is classified as acidic food. The total soluble solid tested with refractometer is 11° Brix.

### *Preparation of Ex-Situ PGJ Fouling Deposit*

The ex-situ PGJ fouling deposit was prepared by adapting the method proposed by Chen *et al.* (2004), in which the ex-situ milk fouling deposit was prepared by boiling the milk. A small stainless steel plate was placed at the bottom of heated beaker to form milk fouling. In this study, the juice was heated at 93°C inside a stainless steel petri dish by using hot plate, static water bath (Heidolph, Germany) and shakeable water bath (Hotech 903D, Taiwan) until the ex-situ fouling deposit was formed. The heating temperature is a recommended temperature for pasteurising foods in acidic class (Lewis & Heppell, 2000). The speed for the shaker of the shakeable water bath was set at 50 rpm. Equation 1 was used to convert the rotation-based speed,  $S$  (unit is rpm), of the shaker to distance-based speed,  $v$  (unit is  $\text{ms}^{-1}$ ). The distance-based speed was used to represent the velocity flow of the PGJ.

$$\text{Velocity of liquid flow, } v \text{ (ms}^{-1}\text{)} = \frac{25\pi r}{60} \quad [1]$$

The radius,  $r$ , of the rotary shaft in shakeable water bath was 0.025 m. Meanwhile, the cross sectional area of the flow was  $1.253 \times 10^{-4} \text{ m}^2$ . Thus, the flow rate of the PGJ on the moving shaker (at 50rpm) was equivalent to 1 litre min $^{-1}$ .

Heating by hot plate and static water bath represents non-flowing system while shakeable water bath represents flowing system. Fig. 1 illustrates the experimental set-up for obtaining fouling deposit and cleaning using hot water bath. The ex-situ fouling deposits from each method were then compared and the best method was selected to obtain the samples of the ex-situ fouling deposit, which were then used for finding their cleaning requirement.

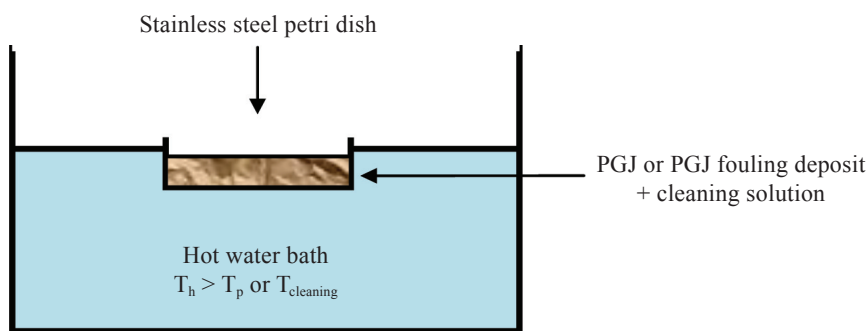


Fig. 1: Experimental set-up for obtaining fouling deposit and for cleaning

#### *Analyses of the PGJ Samples*

Proximate analyses were done to obtain PGJ and the ex-situ PGJ fouling deposit compositions. Water content was measured using the oven method, while the fat content was determined using the Soxhlet method and the protein content was examined using the Kjeldahl method (AOAC, 1990). The determination of ash was measured by drying the sample in a muffle furnace up to 550°C. Environmental scanning electron microscopy (ESEM - Philips XL30) was used to observe the microstructure of the fouling deposit surface.

#### *Cleaning*

Cleaning chemical or detergent was used to remove the deposit. The food industrial detergent, Maxiclean CP6 was donated by Averex Chemicals Sdn. Bhd. The detergent is an alkaline based-chemical solution. The main components in the detergent are NaOH and KOH. The detergent was diluted prior to use (1.6 v/v% of Maxiclean CP6 or 0.325 % OH $^-$ ; 1.8 v/v% of Maxiclean CP6 or 0.369 % OH $^-$ ; 2.0 v/v% of Maxiclean CP6 or 0.44 % OH $^-$ ). The ex-situ cleaning method was done by using shakeable water bath at different temperatures (namely, 70, 80 and 90°C) and at 50rpm (equivalent to 1 litre min $^{-1}$ ). The diluted detergent was preheated to the required temperature, and it was later added into the fouled stainless steel petri dish. The petri dish was placed into the shakeable water bath that had been heated to the desired cleaning temperature. The liquid inside the petri dish was drained and refilled after every 5 minutes to observe the remaining of the fouling deposit. This particular step was repeated until the petri dish was clear from the fouling deposit. Photographs were taken and the cleaning time was also noted.

## RESULTS AND DISCUSSION

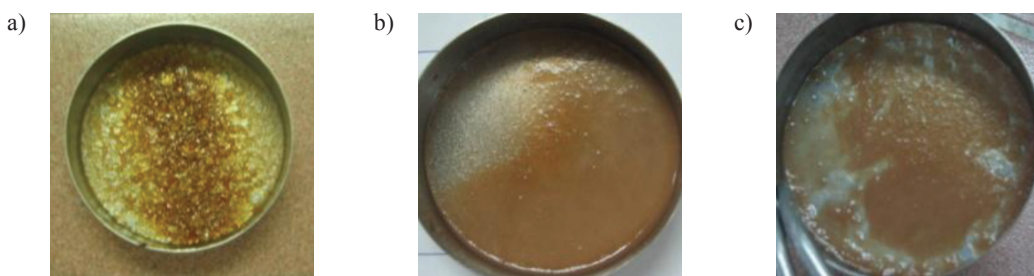
### *Ex-situ PGJ Fouling Deposits*

Table 1 shows the characteristics of the ex-situ PGJ fouling deposits from different methods, which were using hot plate, static water bath and shakeable water bath, respectively. The hot plate method is not a suitable method because the direct heating concept can cause overheating process and promote dehydration. Thus, any experiment carried out cannot be done for a period of more than 20 minutes. The hot plate method can be classified as a rapid fouling deposit preparation. Fig. 2 shows the ex-situ fouling deposits gained from the hot plate, static water bath and shakeable water bath method. The fouling deposit from the hot plate method appeared to be slightly burned in colour, which is not appropriate to be a physical model for the cleaning study. This could be due to the caramelization effect (non-enzymatic browning of sugar) as the preparation was done at high temperature and the moisture was decreasing with time. According to Ab. Aziz (2007) and Christian (2003), there is a weakness in the rapid preparation of fouling deposit; for instance, using an oven to dehydrate the fluid of study. One of the weakness is the structure of the fouling deposit is not fully developed as compared to the fouling deposit obtained from industrial environment. The fouling deposit from industrial environment is gradually formed due to the effect of the process condition (i.e. temperature, flow rate, pressure) on its compound (Müller-Steinhagen, 2000; Bott, 1995). Meanwhile, the concept of heat transfer between hot and cold fluid is the best as it can mimic the heat transfer in commercial heat exchanger. The application of water bath to set-up the simple fouling deposit preparation was done to revamp the weakness of the hot plate method. However, the fouling deposit obtained from the static water bath could be due to the sedimentation of the PGJ solid compound. The fouling deposit from this particular method had a weak attachment as it could be easily removed by rinsing with water alone. On the contrary, shakeable water bath is preferred due to the motion condition, which approximates the flowing system in commercial heat exchanger. However, the deposit was not evenly formed on the surface and the covered area was not similar after each preparation of the fouling deposit. This could be due to the unstable rotation effect which further creates vortex within the medium of study, and thus promoting rapid de-attachments of the fouling deposit. For Ab. Aziz (2007) and Christian (2003), their samples of the fouling deposits were evenly spread on the surface and the covered areas were similar for every preparation. It is crucial to highlight that this particular standard is important for a repetitive study. Thus, the tests in this work were not repeated. Despite the fact that the repeated tests were not performed, the findings from this work have provided a basis for future studies on PGJ fouling deposit, particularly in term of the experimental set-up to obtain a physical model of the PGJ fouling deposit, their characteristics and the cleaning requirements.

TABLE 1  
Comparison of ex-situ PGJ fouling deposits characteristics obtained from different ex-situ methods

Characteristics of Different Ex-situ PGJ Fouling Deposits		
Hot plate	Static water bath	Shakable water bath
1. Direct heating process	1. Heat transfer between hot and cold fluids, simulation of simple heat exchanger condition	1. Heat transfer between hot and cold fluids, simulation of simple heat exchanger condition
2. Fast heating process and can get overheated easily	2. Less prompt to overheat	2. Less prompt to overheat
3. Non-flowing system	3. Non-flowing system	3. Flowing system
4. "Batch" processing	4. "Batch" processing	4. "Batch" processing

### Ex-Situ Experimental Set-Up for Pink Guava Juice Fouling Deposit Study



*Fig. 2: Ex-situ PGJ fouling deposit obtained from: a) hot plate, b) static hot water bath, and c) shakeable hot water bath methods*

#### *PGJ and Its Fouling Deposit*

Table 2 shows the components in PGJ and its fouling deposit. PGJ differs from dairy-based fouling deposits because their main component is protein, while PGJ consists of mainly carbohydrate. Thus, the formation of the PGJ fouling deposit is due to the deformation of the carbohydrate configuration at high temperature which forms carbonised deposits that are difficult to remove (Tamime, 2008). Alkaline-based detergent is required to remove protein-based fouling deposit in normal practice (Watkinson, 2008), while for carbohydrate-based deposit, water alone can be used as a cleaning agent, although it is not efficient. The existence of dispersed particles, which are also known as “seedstone” in PGJ, can also harden the PGJ fouling deposit, and hence, a suitable cleaning procedure is required. The dispersed particles in the PGJ are referred to as insoluble solids (fibres). These particles are the ruptured seeds of pink guava fruit that were produced after the filter press operation during the production of the pink guava puree. The size of the dispersed particles ranged from 168 to 200 $\mu\text{m}$  (Ho *et al.*, 2010). The surface microstructure of the ex-situ PGJ fouling deposit is shown in *Fig. 3*. The deposit consisted of small groups of 10-50 $\mu\text{m}$  aggregates. Each group comprises smaller aggregates in the sizes of 2-5 $\mu\text{m}$ . Table 2 shows that the main solid composition of the PGJ deposit is carbohydrate. Thus, it is presumed that the carbohydrate constitutes the aggregates. The formation of the aggregates is due to the heat-denaturation of the carbohydrate structure. The distribution of these aggregates can be further validated by performing elemental map analysis.

TABLE 2  
Results from the proximate analysis of PGJ and its fouling deposit

Component (%)	Pink guava juice	Ex-situ deposit
Moisture Content	88.64	48.825
Ash	0.568	0.750
Protein	1.112	0.886
Fiber	0.972	1.684
Fat	0.112	0.094
Carbohydrate	8.602	47.761

#### *Cleaning*

The ex-situ cleaning method was utilized in this study. *Fig. 4* shows the influences of temperature and detergent concentration on cleaning time. The result has shown that short cleaning time can be obtained when the cleaning condition is set at high temperature and at high chemical concentration.

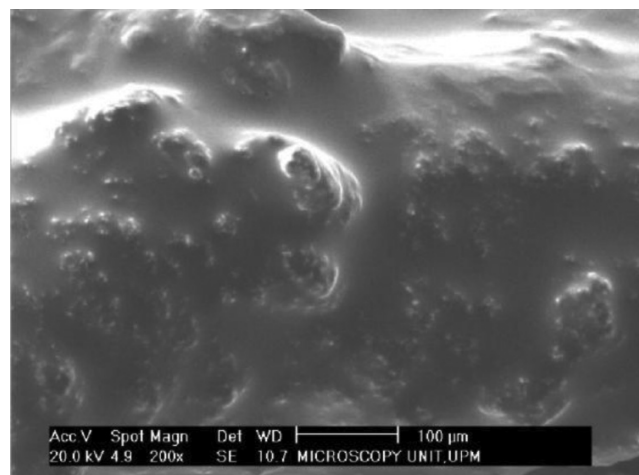


Fig. 3: SEM micrograph of the ex-situ PGJ fouling deposit

This finding is in agreement with the findings of Fryer and Bird (1994), Changani *et al.* (1997), Ab. Aziz (2007), and Christian (2003). Meanwhile, the shortest cleaning time (i.e. 40 minutes) was obtained for the cleaning at 90°C and 2.0 v/v% of Maxiclean CP6, in which alkaline detergent was used as it is one of the agents for dissolving organic compound. Tables 3 to 5 illustrate the changes on the fouling deposit that occurred during cleaning in different conditions. From the series of the pictures, the removal of the fouling deposit was started with the wetting process, which softened the deposit to further assist the next removal action. The effect of rotation was also contributed to the removal, as there were sequences of the removal of pieces of the deposit. It is presumed that for the in-situ cleaning, the cleaning time is shorter than that found in this study due to the effect of the existing high flow rate. According to Eggleston and Monge (2007), a study on cleaning time required for each food processing plant is important as it can affect the production performance which further contributes to economic losses.

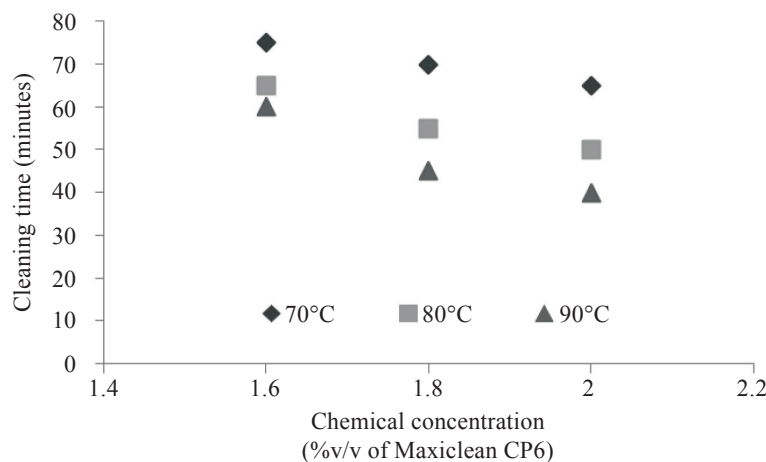


Fig. 4: Cleaning time profile for the removal of PGJ fouling deposit at different chemical concentrations and temperatures

Ex-Situ Experimental Set-Up for Pink Guava Juice Fouling Deposit Study

TABLE 3  
Cleaning progress during cleaning at 70°C

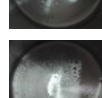
Time (minute)	Concentration of the cleaning solution		
	1.6 v/v% Maxiclean CP6 (0.352% OH <sup>-</sup> )	1.8 v/v% Maxiclean CP6 (0.396% OH <sup>-</sup> )	2.0 v/v% Maxiclean CP6 (0.44% OH <sup>-</sup> )
0			
10			Not significant
20			
30			
40			
45			
50			
55			
60			
65			
70			
75			

TABLE 4  
Cleaning progress during cleaning at 80°C

Time (minute)	Concentration of the cleaning solution		
	1.6 v/v% Maxiclean CP6 (0.352% OH <sup>-</sup> )	1.8 v/v% Maxiclean CP6 (0.396% OH <sup>-</sup> )	2.0 v/v% Maxiclean CP6 (0.44% OH <sup>-</sup> )
0			
10	Not significant		
20			
30			
35		Not significant	Not significant
40			
45			
50			
55			
60			
65			

Ex-Situ Experimental Set-Up for Pink Guava Juice Fouling Deposit Study

TABLE 5  
Cleaning progress during cleaning at 90°C

Time (minute)	Concentration of the cleaning solution		
	1.6 v/v% Maxiclean CP6 (0.352% OH <sup>-</sup> )	1.8 v/v% Maxiclean CP6 (0.396% OH <sup>-</sup> )	2.0 v/v% Maxiclean CP6 (0.44% OH <sup>-</sup> )
0			
10			
20			
30			
35	Not significant		
40			
45			
50			
55			
60			

### CONCLUSIONS

This work has shown several simple experimental set-ups to form PGJ fouling deposit, which can be used as a physical model for further studies on fouling and cleaning. In this study, the shakeable water bath method was found to be the best method to obtain the PGJ fouling deposit samples. This particular ex-situ method was observed to require less raw material and short processing duration (i.e. within 1 hour). However, some improvements on the method need to be done for future studies

as it is quite difficult to obtain similar covered area of fouling deposits for each preparation. It has been proven that the PGJ fouling deposit would form on the heat transfer surface and the deposit is carbohydrate-based deposit. Thus, the preliminary cleaning study was performed using the ex-situ cleaning method. Cleaning can be done using alkaline detergent to shorten the cleaning time. The best ex-situ cleaning process was obtained at the concentration of 2.0 v/v% Maxiclean CP6 (0.44% OH<sup>-</sup>) and at the temperature of 90°C. The effect of rotation may also promote the removal of the deposit, due to shear stress flow effect. Therefore, the findings of this work have provided essential basic knowledge of PGJ fouling deposit, which can assist future work on the reduction of PGJ fouling deposit formation and finding the optimum cleaning procedure. However, more work is still needed to characterize the PGJ fouling deposit in order to obtain its fouling factor and to formulate a better cleaning procedure.

### ACKNOWLEDGEMENTS

This work was supported by Universiti Putra Malaysia (Research University Grant, 05-03-08-0483RU). The authors acknowledge Sime Darby Foods and Beverages Marketing Sdn. Bhd. for supplying pink guava puree and Averex Chemicals Sdn. Bhd. for supplying chemical solution.

### REFERENCES

- AOAC (1990). *Association of Official Analytical Chemists. Official Methods of Analysis*. 15<sup>th</sup> Ed., Washington, DC.
- Ab. Aziz, N. (2007). *Factors that affect cleaning process efficiency*. PhD Thesis. University of Birmingham, UK.
- Bott, T. R. (1995). *Fouling of Heat Exchangers*. New York: Elsevier Science.
- Changani, S. D., Belmar-Beiny, M. T., & Fryer, P. J. (1997). Engineering and Chemical Factors Associated with Fouling and Cleaning in Milk Processing. *Experimental Thermal and Fluid Science*, 14, 392-406.
- Chen, X. D., Ozkan, N., Xin, H., & Lin L. (2004). An Effective CIP Procedure for Removing Dairy Protein Based Deposit – A Laboratory Investigation. In *2003 ECI Conference in Heat Exchanger Fouling and Cleaning: Fundamentals and Applications*. Santa Fe, New Mexico, USA.
- Christian G. K. (2003). *Cleaning of carbohydrate and dairy protein deposits*. PhD Thesis, University of Birmingham, Birmingham, UK.
- Earle, R. L. (1983). *Unit Operations in Food Processing*, 2nd Edition, Pergamon Commonwealth and International Library.
- Eggleston, G., & Monge A. (2007). How Time Between Cleanings Affects Performance And Sucrose Losses In Robert's Evaporators. *Journal of Food Processing and Preservation*, 31(1), 52-72.
- Fryer, P. J., & Bird, M. R. (1994). Factors which affect the kinetics of cleaning dairy soils. *Food Sci. Tech. Today*, 8, 36-42.
- Ho, A. L., Tan, V. C., Ab. Aziz, N., Taip, F. S., & Ibrahim, M. N. (2010). Pink Guava Juice Pasteurization: Fouling Deposit and Cleaning Studies. *Journal - The Institution of Engineers, Malaysia*, 71(4), 50-62.
- Krause, S. (1993). Fouling of heat-transfer surfaces by crystallization and sedimentation. *International Chemical Engineering*, 33(3), 355-401.
- Lewis, M., & Heppell, N. (2000). *Continuous Thermal Processing of Foods: Pasteurization and UHT Sterilization*. Gaithersburg: An Aspen Publication.

Ex-Situ Experimental Set-Up for Pink Guava Juice Fouling Deposit Study

- Müller-Steinhagen, H. (2000). *Heat Exchanger Fouling: Mitigation and Cleaning Techniques*. Germany: IEEE.
- Saunders, E. A. D. (1988). *Heat Exchangers: Selection, Design & Construction*. United Kingdom: Longman Scientific & Technical.
- Swartzel, K. R. (1983). The Role of Heat Exchanger Fouling in the Formation of Sediment in Aseptically Processed and Packaged Milk 1. *Journal of Food Processing and Preservation*, 7(4), 247-257.
- Tamime, A. (2008). *Cleaning-in-Place: Dairy, Food and Beverage Operations*, 3rd Edition. Oxford: Blackwell Publishing Ltd.
- Watkinson, W. J. (2008). Chemistry of Detergents and Disinfectants. In A. Y. Tamime (Ed.), *Cleaning-in-Place: Dairy, Food and Beverage Operations* (pp. 56-79). Oxford: Blackwell Publishing Ltd.
- Zainal, B. S., Abdul Rahman, R., Ariff, A. B., Saari, B. N., & Asbi, B. A. (1999). Effect of Temperature on the Physical Properties of Pink Guava Juice at Two Different Concentrations. *Journal of Food Engineering*, 43, 50-59.



## Effect of Solid Solution Treatment on Semisolid Microstructure of Zn-22Al Alloy

M. A. M. Arif, M. Z. Omar\* and N. Muhamad

Department of Mechanical and Materials Engineering,

Faculty of Engineering and Built Environment,  
Universiti Kebangsaan Malaysia, Malaysia.

\*E-mail: zaidi@eng.ukm.my

### ABSTRACT

The effect of solid solution treatment on semisolid microstructure of Zn-22Al with developed dendrites was investigated. Zn-22Al is a zinc-based alloy with aluminium as its main alloying element. Producing Zn-22Al product by semisolid metal processing (SSM) offers significant advantages, such as reduction of macrosegregations, porosity and low forming efforts. Meanwhile, thermal and microstructure analyses of Zn-22Al alloy were studied using differential scanning calorimeter (DSC) and Olympus optical microscope. Solidus and liquidus of the alloy can be determined by DSC analysis. In addition, changes to the microstructures in response to solid solution treatments were also analyzed. The major effort of all the semi-solid technologies is the generation of small and spherical morphologies. Prior to the generation of spherical morphologies, the fine grains should be first produced. The as-cast samples were isothermally held at 315°C, ranging from 0.5 to 5 hours before they were partially re-melted at semisolid temperature of 438°C to produce solid globular grains structure in liquid matrix. The results indicated that a non-dendritic semisolid microstructure could not be obtained if the traditionally cast Zn-22Al alloy with developed dendrites was directly subjected to partial remelting. After solid solution treatment at 315°C, the black interdendritic eutectics were dissolved and gradually transformed into  $\beta$  structure when the treatment time was increased. The microstructure of the solid solution treated sample changed into a small globular structure with the best shape factor of 0.9 and this corresponded to  $40 \pm 16 \mu\text{m}$  when the sample was treated for 3 hours, followed by directly partial remelting into its semi solid zone.

**Keywords:** Semisolid metal processing (SSM), solidus; liquidus; dendritic; spherical morphologies

### INTRODUCTION

The initial work that led to the interest in semi-solid metal processing (SSM) could be traced back to the studies by researchers at the Massachusetts Institute of Technology in the early 1970s. This work was originally directed at the problem of hot tearing in alloy castings, but it was later realised that a new technology for near-net shaping of complex shapes had been discovered (Flemings, 1991). This SSM technology can be generally defined as a forming process that shapes metal components in their semi-solid state (Flemings, 1991; Kirkwood, 1994; Omar *et al.*, 2005, 2009).

Semi-solid metal forming (SSM) has become a widely accepted metal processing technique because it combines the elements of both casting and forging, offering significant advantages, such as the reduction of macrosegregations, porosity and low forming efforts (Kirkwood, 1994; Chen *et al.*, 2002; Omar *et al.*, 2005, 2009). Other major advantages include prolonged die life

---

Received: 15 January 2011

Accepted: 1 April 2011

\*Corresponding Author

due to decreased thermal shock (forging below liquidus as against castings), weight savings in components with less porosity than conventional, plus improved usage of feedstock materials because of improved designs (Omar *et al.*, 2009).

Continuous searches have been carried out for alternative materials in engineering applications to reduce the cost of production without sacrificing the functional requirements of the components. Zinc-based alloys are of recent interest in this regard, offering a number of benefits over their conventional counterparts like aluminium casting alloys, copper-based alloys, bearing bronzes and cast iron in various engineering applications. These alloys feature clean, low-temperature, energy-saving melting, excellent castability, as well as high strength and equivalent or often superior bearing and wear properties as compared to standard bronze bearing. Meanwhile, cast Zn-Al (ZA) alloys have been widely used for engineering components, including those in the automotive industry (Abou El-khair *et al.*, 2004).

The main requirement for alloys to be shaped in the semi-solid state is that they should exhibit a fine spheroidal or non-dendritic grain structure (Chen *et al.*, 2002). From the previous research, non-dendritic semisolid microstructure could not be obtained if the traditional cast alloy with developed dendrites was directly subjected to partial remelting. The alloy must be pretreated, such as by mechanical stirring during solidification, modifying prior to pouring, or subjected to deformation prior to remelting. These pre-treatments not only brought about melt contamination and gas absorption during mechanical stirring or melt contamination from refine, but also needed some special high-cost equipments (e.g. stirring equipment for magnetohydrodynamic stirring and rolling or pressing machine for predeformation) (Chen *et al.*, 2006). In this study, the development of non-dendritic microstructures of Zn-22Al was investigated by applying isothermal heat treatments in a single phase area at various holding times, followed by a direct partial remelting into its semi-solid zones.

## EXPERIMENTAL PROCEDURES

### Materials

Zn-22Al is zinc based metal alloy with the alloying elements of aluminium, magnesium and copper. Adding copper and magnesium was found to increase strength and inhibit intergranular corrosion, respectively. Typical uses are automotive parts, household appliances and fixtures, office and computer equipment, as well as building hardware (Robert, 1984). The chemical composition of the as-cast material is given in Table 1.

TABLE 1  
Chemical composition of the Zn-22Al alloy compared to the nominal

Zn-22Al	Chemical composition (wt%)							
	Al	Cu	Mg	Cd	Pb	Fe	Sn	Zn
Nominal	21 – 23	0.4 – 0.6	0.008 – 0.012	0.01 max	0.01 max	0.002 max	0.001 max	balance
Analysis	21.46	0.5	0.004	-	-	-	-	balance

### Differential Scanning Analysis (DSC)

DSC analysis was carried out primarily to estimate the solidus, liquidus and liquid fraction within the semi-solid zone of the supplied material. The alloy was cut into small pieces (less than 20 mg) for the DSC test using Mettler Toledo DSC 822e. The heating rate employed is 10°C per minute.

## Effect of Solid Solution Treatment on Semisolid Microstructure of Zn-22Al Alloy

Heating was carried out in a nitrogen atmosphere to prevent oxidation. From the heating curve, phase transformation reactions were also observed.

### Solid Solution Treatment and Partial Remelting

Solid solution treatment and partial remelting procedures were carried out using an electric furnace. Zn-22Al samples were solution treated at 315°C in  $\beta$  zone, for a range of holding times from 0.5 to 5 hours. Subsequently, the samples of solution treated were quickly removed from the furnace and water quenched before the partial remelting treatment was carried out at 438°C (i.e. in the semi-solid temperature of Zn-22Al) for 1 hour.

### Image Analysis

The microstructural characterisation was carried out using Olympus optical microscope and Philips XL30 scanning electron microscope prior to the analysis using imageJ software. All the samples were etched in a solution of 100ml water + 0.5-5ml HNO<sub>3</sub> (Frank 1991).

## RESULTS AND DISCUSSIONS

The equilibrium phase diagram of zinc-aluminum alloy is shown in Fig. 1. Zn-22Al alloy with aluminium content of about 22% has a single  $\beta$  phase when it is heated above the eutectoid temperature. The microstructures of the as-cast and solid solution treated Zn-22Al alloy are presented in Fig. 2. Meanwhile, the as-cast microstructure of Zn-22Al [shown in Fig. 2(a)] consists of developed dendrites and interdendritic eutectics. Solid solution treatment procedure was carried out at 315°C in  $\beta$  zone, with various holding times between 0.5 to 5 hours. The black interdendritic eutectics (mainly Al rich) shown in Fig. 2(a) gradually dissolved into the primary dendrite structures

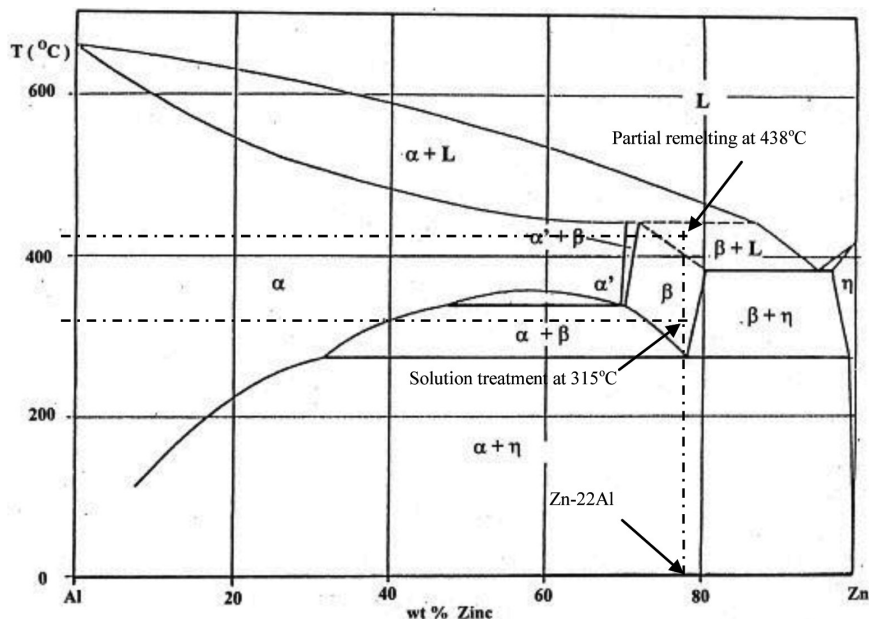
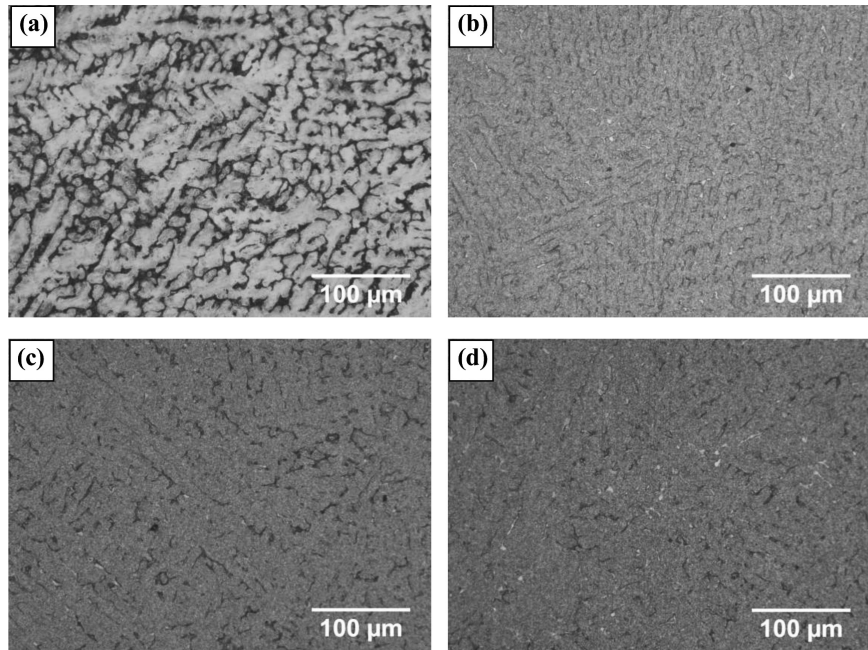


Fig. 1: Binary phase diagram of Zn-Al system (Zhu et al., 1999)

(as shown in *Fig. 2(b), 2(c) and 2(d)*) during solid solution treatment. It resulted in a decrease of the eutectic phases which gradually evolved into  $\beta$  phase until no obvious dendritic structures were observed when the treatment time was long enough (*Fig. 2(d)*).



*Fig. 2: Microstructures of Zn-22Al (a) as-cast, and after solution treatment for (b) 1.5 hrs, (c) 3 hrs, (d) 5 hrs*

The DSC heating curve, together with its corresponding liquid distribution of the as-cast Zn-22Al, is shown in *Fig. 3*. The solidus is estimated at 380°C, and this is at 468°C for the liquidus, while 20% and 50% liquid fractions correspond to 419°C and 438°C, respectively. Note that thixoforming is normally carried out at liquid fraction between 20-50% (Kirkwood, 1994). Hence, when the solution treated Zn-22Al alloy was partially re-melted at 438°C, the corresponding liquid fraction is approximately 50%. *Fig. 4* shows some of the typical semi-solid microstructures of Zn-22Al alloy after the solid solution treatment for different periods. Meanwhile, *Fig. 4(a)* shows the as-cast microstructure after direct partial re-melting. It could be seen that the liquid phase appeared along the grain boundaries as well as entrapped within large solid agglomerates of  $\beta$  phase. When the sample was solution treated at 315°C for 1.5 hours before partially re-melted, however, the number of irregular grains was relatively higher and the size was smaller than the semi-solid microstructure of the re-melted as-cast sample (see *Fig. 4(b)*). Large and irregular structures gradually transformed into a structure of spheroidal particles when the holding time of solid solution treatment was increased to 3 and 5 hours (*Fig. 4(c)* and *Fig. 4(d)*, respectively).

The microstructure evolution is focused on the change of shape and size of grains as a function of time in the semi-solid state. To quantitatively represent the shape of grains, shape factor was commonly used to characterize SSM microstructures. Shape factor is defined as  $P^2/4\pi A$ , where  $P$  is the perimeter and  $A$  is the area of the particle (shape factor of a circle is equivalent to 1). For optimum semi-solid processing characteristics, the shape factor should be as close to 1 as possible (Legoretta *et al.*, 2008). The average size of the primary particles is defined as  $[\sum 2(A_i/\pi)^{1/2}]/N$ ,

## Effect of Solid Solution Treatment on Semisolid Microstructure of Zn-22Al Alloy

where  $A_i$  is the area of each particle and  $N$  is the total particle numbers in each image (Chen *et al.*, 2008). It can be observed that the shape factor has changed to be as close to 1 and the particle size has gradually reduced with an increase in the treatment time.

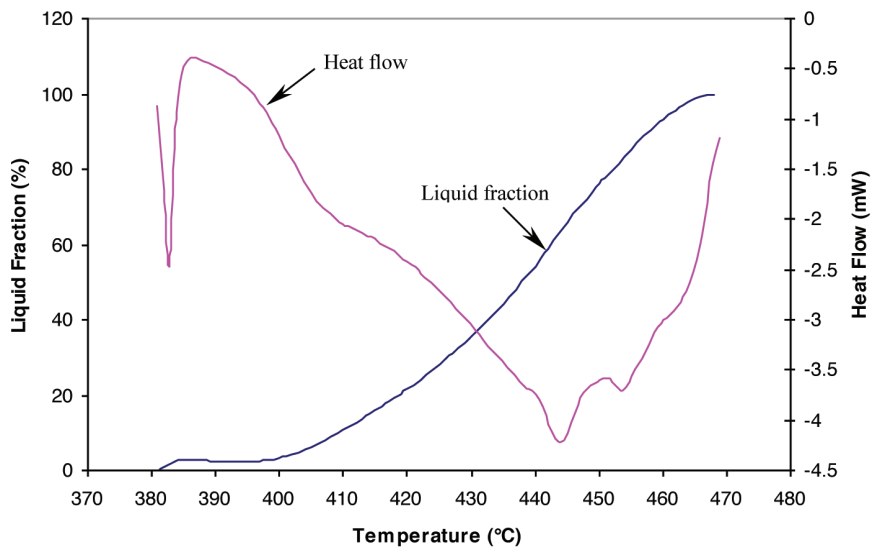


*Fig. 3: DSC and liquid fraction curve of Zn-22Al*

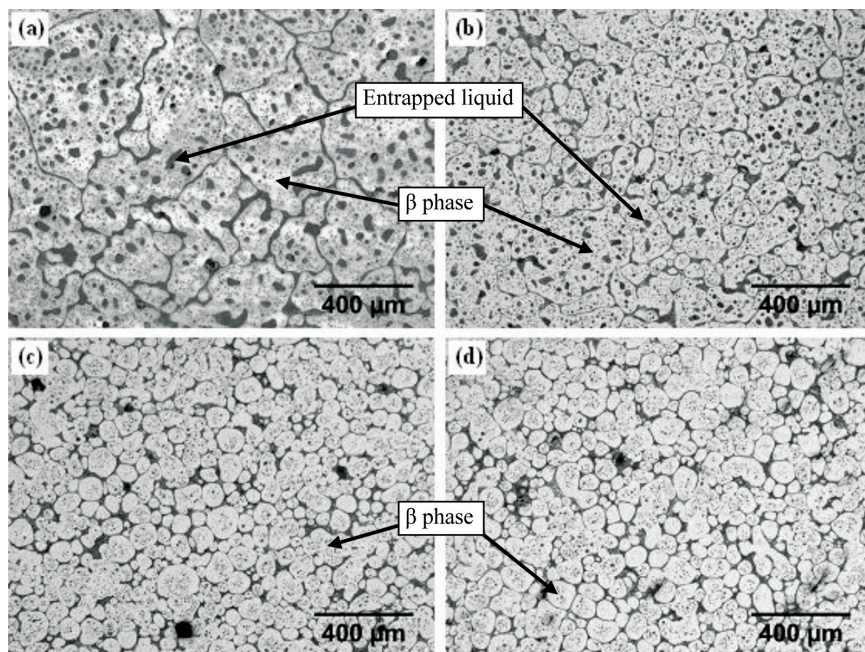


*Fig. 4: Microstructure of Zn-22Al subjected to partial re-melting at 438°C for 1 hour on (a) as-cast sample, and on the samples which have previously solution treated at 315°C for (b) 1.5hrs, (c) 3 hrs, and (d) 5 hrs.*

Meanwhile, the variations of shape factor and primary grain size of Zn-22Al subjected to partial re-melting are shown in *Fig. 5*. After the partial remelting at 438°C (i.e. semi-solid condition with 48% liquid fraction) for 1 hour for the samples that have previously been solution treated at 315°C, the average shape factor has continuously increased with further increases of treatment time. However, the shape factor of the semi-solid Zn-22Al has significantly decreased after 1.5 hours of holding time. Subsequently, the shape factors continued to increase with the increasing holding time until a maximum value of about 0.9 was achieved at 3 hours.

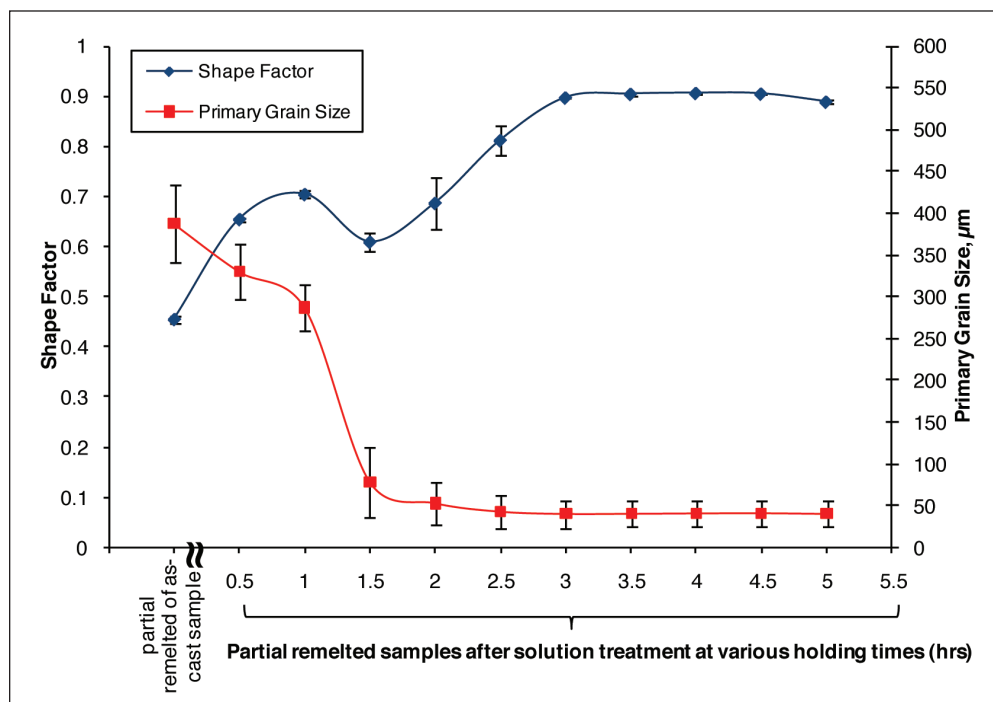


*Fig. 5: Variations of shape factor and primary grain size of Zn-22Al subjected to partial re-melting at 438°C for 1 hour on the as-cast sample, and on the samples which had previously solution treated at 315°C (at various holding times).*

The curve of the primary particle size in the semi-solid condition proved that the particles had become smaller when the treatment time was increased. It could be noted that the primary particle size decreased significantly when the sample was previously heated for 1.5 hours. Semi-solid non-dendrites, with the best shape factor of 0.9 and the smallest average primary particle size of about  $40 \pm 16 \mu\text{m}$  in the eutectic matrix, were achieved when the sample was solution treated for 3 hours. The shape factor and size of primary particles in the semi-solid condition have now remained almost constant when the solution treatment was carried out for more than 3 hours (i.e. up to 5 hours). These observations indicate that the solid solution treatment has a great influence on microstructural spheroidisation during partial remelting procedures.

It can be speculated that when the solution treatment holding time was increased, the original dendritic microstructure coarsened through the merging of the dendritic arms and the dendrites due to the dissolution of the interdendritic eutectics, a phenomenon which has also been observed by Chen *et al.* (2006). When the solutionised samples were subjected to partial re-melting, the liquid

phase was first formed by melting residual eutectic along the sites at the former grain boundaries, arm boundaries, and arm roots during partial re-melting, resulting in a separation of the coarsened arms from the original dendrites into smaller truncated grains (Flemings, 1991; Chen *et al.*, 2006). The truncated grains could perhaps further ripened into spheroidal grains resulting in the non-dendritic microstructures that are probably now suitable for the semi-solid metal processing application. Work on the disintegration of these solutionised dendrites and the dissolution of the interdendritic eutectics (for example by EDAX line scan) is still ongoing.

## CONCLUSION

A semisolid microstructure with small and spherical morphologies could be obtained if a traditionally cast Zn-22Al alloy with developed dendrites was solid solution treated for 3 hours at 315°C, followed by partially re-melted at 438°C for 1 hour. In this study, the solid solution treatment was found to have resulted in the dissolution of the interdendritic eutectic structures and the coarsening of the dendritic structures through the merging of the dendritic arms and the dendrites. Partial re-melting has transformed these structures into non-dendritic microstructures which are probably suitable for the semi-solid metal processing application.

## ACKNOWLEDGEMENT

The authors would like to thank Universiti Kebangsaan Malaysia (UKM) and the Ministry of Science, Technology and Innovation (MOSTI) Malaysia for the financial assistance.

## REFERENCES

- Abou El-khair, M. T., Daoud, A., & Ismail, A. (2004). Effect of Different Al Contents on the Microstructure, Tensile and Wear Properties of Zn-based Alloy. *J. Mater. Lett.*, 58, 1754 -1760.
- Chen, T. J., Hao, Y., & Sun, J. (2002). Microstructural Evolution of Previously Deformed ZA27 Alloy During Partial Remelting. *J. Mater. Sci. Eng. A*, 337, 73-81.
- Chen, T. J., Li, Y. D., & Hao, Y. (2006). A New Method for Production of Nondendritic Semisolid ZA27 Alloy. *J. Mater. Manuf. Process.* 21, 464-468.
- Chen, T. J., Hao, Y., Li, Y. D., & Ma, Y. (2008). Effect of Solid Solution Treatment on Semisolid Microstructure of Dendritic Zinc Alloy ZA27. *J. Mater. Sci. Tech.* 24, 1313-1320.
- Flemings, M. C. (1991). Behavior of Metal Alloys in the Semisolid State. *Metall. Trans. A* 22, 957-980.
- Frank, C. P. (1991). *Zinc Handbook Properties, Processing, and Use in Design*. Marcel Dekker, Inc. New York.
- Kirkwood, D. H. (1994). Semisolid Metal Processing. *Int. Mater. Rev.* 39(5): 173.
- Legoretta, E. C., Atkinson, H. V., & Jones, H. (2008). Cooling Slope Casting to Obtain Thixotropic Feedstock II: Observations With A356 Alloy. *J. Mater. Sci.* 43, 5456–5469.
- Omar, M. Z., Palmiere, E. J., Howe, A. A., Atkinson, H. V., & Kaprinos, P. (2005). Thixoforming of a High Performance HP9/4/30 Steel. *J. Mater. Sci. Eng. A* 395, 53-61.
- Omar, M. Z., Atkinson, H. V., Howe, A. A., Palmiere, E. J., Kaprinos, P., & Ghazali, M. J. (2009). Solid-liquid Structural Break-up in M2 Tool Steel for Semi-solid Metal Processing. *J. Mater. Sci.* 44(3), 869-874.
- Robert, J. B. (1984). *Zinc and Zinc Alloys. ASM Handbook Vol. 2*, American Society International.
- Zhu, Y. H., Man, H. C., & Lee, W. B. (1999). Exothermic reaction in eutectoid Zn-Al based alloys. *J. Mater. Sci. Eng. A*, 268, 147-153.



## Effect of Epoxidized Natural Rubber on Mechanical Properties of Epoxy Reinforced Kenaf Fibre Composites

Abu Bakar, M. A.<sup>1\*</sup>, Ahmad, S.<sup>2</sup> and Kuntjoro, W.<sup>1</sup>

<sup>1</sup>Faculty of Mechanical Engineering, Universiti Teknologi MARA,  
40450 Shah Alam, Selangor, Malaysia

<sup>2</sup>Polymer Research Centre (PORCE), Faculty of Science and Technology,  
Universiti Kebangsaan Malaysia, 43600 Bangi, Selangor, Malaysia

\*E-mail: mimi\_azlina@salam.uitm.edu.my

### ABSTRACT

Kenaf fibre that is known as *Hibiscus cannabinus*, L. family *Malvaceae* is an herbaceous plant that can be grown under a wide range of weather conditions. The uses of kenaf fibres as a reinforcement material in the polymeric matrix have been widely investigated. It is known that epoxy has a disadvantage of brittleness and exhibits low toughness. In this research, liquid epoxidized natural rubber (LENR) was introduced to the epoxy to increase its toughness. Kenaf fibres, with five different fibre loadings of 5%, 10%, 15%, 20% and 25% by weight, were used to reinforce the epoxy resins (with and without addition of epoxidized natural rubber) as the matrices. The flexural strength, flexural modulus and fracture toughness of the rubber toughened epoxy reinforced kenaf fibre composites were investigated. The results showed that the addition of liquid epoxidized natural rubber (LENR) had improved the flexural modulus, flexural strength and fracture toughness by 48%, 30%, and 1.15% respectively at 20% fibre loading. The fractured surfaces of these composites were investigated by using scanning electron microscopic (SEM) technique to determine the interfacial bonding between the matrix and the fibre reinforcement.

**Keywords:** Biocomposite, kenaf fibre, natural rubber, mechanical properties, toughened

### INTRODUCTION

Conventional fibre reinforced composites, such as carbon fibres and glass fibres, can contribute to environmental problems in disposal through incineration. To overcome these problems, environmentally friendly composites are required by utilizing natural fibres as reinforcement in the composites (Marthur, 2006). Mechanical properties of the fabricated composites are governed by reinforcement and matrix properties, as well as the interfacial adhesion between them. Fibre reinforced polymer receives considerable demands in structural application, automotive, recreation and sports tool, as well as furniture and aerospace. Meanwhile, natural fibres such as jute, sisal, coir and banana are major renewable resource materials that are abundantly available throughout the world, especially in the tropical region such as India, Sri Lanka, Thailand, Indonesia, Bangladesh and Philippines. These plant fibres have a great potential to be used as reinforcement in polymer composites (Saheb & Jog, 1999). The attractive features of these fibres include low cost, light weight, high specific modulus, renewability and biodegradability (Ray *et al.*, 2001a; Ray *et al.*, 2001b). For example, kenaf (*Hibiscus cannabinus*, L. family *Malvaceae*) is an herbaceous annual plant that can be grown under a wide range of weather conditions, and kenaf is economically not expensive

---

Received: 15 January 2011

Accepted: 1 April 2011

\*Corresponding Author

and it is also ecologically biodegradable (Nishino *et al.*, 2003). However, kenaf fibres have low strength to resist the failure. This particular behaviour causes fracture in the composite materials to catastrophically occur without any warning. Therefore, composite based rubber-toughened polymer matrix provides extra toughness and delays the failure through dispersion mechanism in the material (Hazleen, 2007).

Epoxy resins are a large family of resins that represent some of the high performance resins available in the market; they are characterized by high chemical and corrosion resistance as well as good mechanical and thermal properties once cured (Ray & Rout, 2005; Saadati *et al.*, 2005). In many applications, however, they have disadvantages of brittleness with poor resistance to crack propagation, low impact strength and low toughness. A number of research have been carried out to increase the toughness, and these include using glass beads, alumina trihydrate and silica. The most successful work involved the addition of a suitable rubber, such as liquid amine-terminated (ATBN) (Saadati *et al.*, 2005), carboxyl-terminated (CTBN) (Calabrese & Valenza, 2003; Thomas *et al.*, 2007); Auad *et al.*, 2001; Jang & Yang, 2000), hydroxyl-terminated (HTBN) (Ozturk *et al.*, 2001; Thomas *et al.*, 2008; Kaynak *et al.*, 2005), epoxy-terminated (ETBN) copolymers of butadiene and acrylonitrile (Thomas *et al.*, 2007), and hydroxyl-terminated and epoxy-terminated polybutadiene to interpenetrating the polymer networks (IPN) structures (Saadati *et al.*, 2005). Another potential method is by addition of suitable rubbers that are copolymers with variable acrylonitrile contents to the uncured epoxy resins. The effects of the acrylonitrile content of the copolymer type, the molecular weight, the concentration and the solubility parameter of the rubber and its functional end groups on the fracture toughness and impact strength have been studied. It has been reported that the modification of epoxy resins by the addition of rigid particle leads to a significant reduction in cost and a considerable improvement in the mechanical, thermal and electrical properties of resin (Saadati *et al.*, 2005; Jayle *et al.*, 1996). Meanwhile, the variation of parameters such as volume fraction of the filler, particle size, modulus and strength of the filler, as well as resin-filler adhesion and toughness of the matrix, leads to improvement in the toughness of resins.

## MATERIALS AND METHODS

### *Materials*

The epoxy (Morcote BJC 39) materials used in this study were supplied by Vistec Technology Sdn. Bhd. The kenaf fibres were supplied by Symphony Advance Sdn. Bhd., sieved with sizes ranging from 125 - 355 µm. Polymer used was epoxidized natural rubber (ENR) which was supplied by Rubber Research Industries Malaysia (RRIM). Liquid epoxidized natural rubber (LENR) was prepared using photochemical degradation technique in the polymer laboratory, UKM, according to the method described by Abdullah and Zakaria (1989).

### *Composite Preparation*

Kenaf fibre-epoxy composites were fabricated in the form of plate using a stainless steel mould measuring 165 × 165 × 3 mm. Firstly, the kenaf fibre and the epoxy (with and without LENR) were mixed using mechanical stirrer and with the hardener for a few minutes after that. The mixture was poured into the mould. The mould was then placed between the heated platens of a hot press of 8 MPa pressure at 100°C for 25-50 minutes, depending on the percentages of the fibres used. Then, the plates were cut into the sizes, depending on the types of testing to do, using a diamond blade cutter.

## TEST METHODS

### *Flexural Test*

The flexural strength and flexural modulus were determined according to ASTM D790-96. A gauge length of 100 mm was employed with a cross-head speed of 5 mm/min using Shimadzu Universal Testing Machine (model: Autograph AG-X 50kN). The value of the flexural strength and flexural modulus would be determined from the graph of stress-strain curve.

### *Fracture Toughness Test*

The composites were tested for fracture toughness according to ASTM D5045. A span of 80 mm was employed maintaining a cross-head speed of 2 mm/min using Shimadzu Universal Testing Machine. The fracture toughness of the kenaf fibre reinforced epoxy composites can be calculated using Equations 1 and 2.

$$K_{IC} = \frac{PS}{BW^{3/2}} \cdot y \quad (\text{Equation 1})$$

$$y = 3\sqrt{(a/w)} \cdot \frac{1.99 - (a/w)[1-(a/w)][2.15 - 3.93(a/w) + 2.7(a/w)^2]}{2[1 + 2(a/w)][1 - (a/w)]^{3/2}} \quad (\text{Equation 2})$$

where P is the maximum load, S is the span length, a is the notch length, B is the specimen thickness, w is the specimen width, and y is the geometry correction factor.

### *Morphological Examination*

The surface morphology was examined using scanning electron microscope (Philips XL 30) on the impact fractured samples. The fractured samples were coated with a thin layer of gold to avoid electrostatic charging during examination.

## RESULTS AND DISCUSSION

### *Flexural Properties of the Kenaf Fibre Reinforced Epoxy Composite*

The flexural strength and flexural modulus for the composites, with and without addition of LENR are shown in Fig. 1 and 2, respectively. In general, the flexural strength for kenaf fibre reinforced epoxy composites with the addition of LENR seems to be improved with increasing of fibre content up to 20wt%. For the kenaf fibre reinforced epoxy composites, without addition of LENR, there is an increment in the flexural strength up to 10 wt% of the fibre loadings. Higher fibre loading causes a decrease in the flexural strength of the composites. John and Venkata (2004) have reported that decreases in the mechanical properties for higher fibre loading are due to the poor adhesion between the matrix and the fibre and the presence of voids at the resin-fibre interface (John & Venkata, 2009).

In comparison, flexural strength and flexural modulus for the kenaf fibre reinforced LENR modified epoxy composites were higher than the composite without LENR, except at low wt%. It was observed that the optimum flexural strength was obtained at 20wt% fibre loading for the kenaf fibre reinforced epoxy with the addition of LENR. Meanwhile, the flexural strength of 20wt% of

kenaf fibre reinforced epoxy, with the addition of LENR composite, was found to be 25% higher than that of the neat epoxy, whilst the flexural modulus was 60% higher than that of the neat epoxy composite.

As shown in *Fig. 1*, the flexural strength of the composites at 20wt% of fibre loading for kenaf fibre reinforced epoxy with the addition of LENR composite was 56.33 MPa as compared to 43.42 MPa for kenaf fibre reinforced epoxy without addition of LENR composites. The improvement was about 30%. The interfacial strength of the composites and the flexural strength of the matrix are the important factors that determine the flexural strength of a composite. In the case of the kenaf fibre reinforced epoxy with LENR composite, the modification of epoxy with LENR contributed to a strong interface and hence improved the flexural strength of the composite. This could be seen from the SEM micrograph shown in *Fig. 4*.

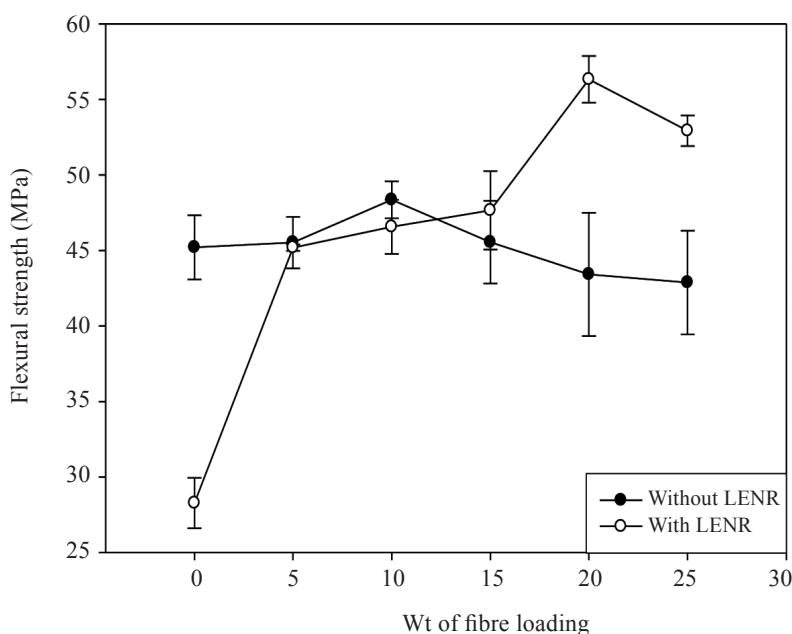


*Fig. 1: Flexural strength versus weight percentage of fibre loading used for kenaf fibre reinforced epoxy composite (with and without LENR)*

As illustrated in *Fig. 2*, the optimum flexural modulus of the composites at 25wt% of fibre loading for the kenaf fibre reinforced epoxy with the addition of LENR composite was 3.4 GPa compared to merely 2.3 GPa for the kenaf fibre reinforced epoxy composites without the addition of LENR. The improvement was about 48%, and this was mainly due to toughening caused by the LENR modification of the epoxy matrix, which gave rise to good energy absorbing capacity. Rubber domains were formed after the addition of LENR had been found to improve flexibility and toughness. The reactions of LENR used to modify the epoxy matrix, the ring opening reaction between the LENR hydroxyl end group, and hardener may lead to chain extension leading to flexibility and toughness (Kaynak *et al.*, 2005). Furthermore, cross linking during the reaction produces higher chain extensions, and therefore, specimens containing both kenaf fibre and LENR should show better mechanical performances at the same extent of cross linking.

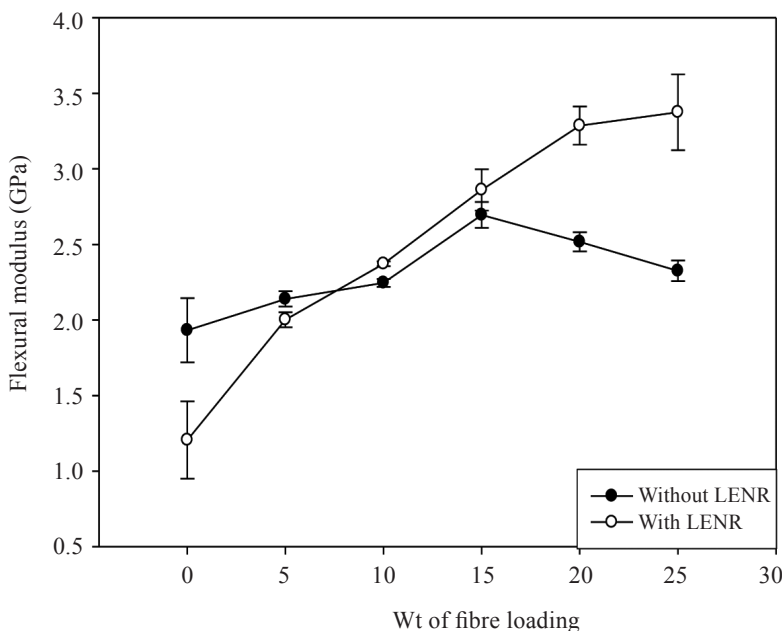


*Fig. 2: Flexural modulus versus weight percentage of fibre loading used for kenaf fibre reinforced epoxy composite (with and without LENR)*

#### *Fracture Toughness Properties of the Kenaf Fibre Reinforced Epoxy Composite*

The fracture toughness properties of the composites are stipulated in *Fig. 3*. The composites, which were prepared with epoxy and addition of LENR as a matrix, showed improvement of the fracture toughness at all weight percentages of fibre loadings. The fracture toughness was relatively higher for the kenaf fibre reinforced epoxy composite as compared to the neat epoxy. The optimum fracture toughness of the kenaf fibre reinforced epoxy, with addition of LENR composite at 20wt% fibre loading, was  $2.64 \text{ MPa} \cdot \text{m}^{1/2}$  as compared to  $2.61 \text{ MPa} \cdot \text{m}^{1/2}$  for the kenaf fibre reinforced epoxy composite without the addition of LENR. This indicated an improvement of 1.15 %. It could also be clearly seen that the fracture toughness for 20wt% fibre loading of the kenaf fibre reinforced epoxy with the addition of LENR composite was 10.9 % higher than the neat epoxy. It could be expected that the composites made using rubber modified epoxy showed improvement in the fracture toughness. This improvement in the toughness was attributed to the rubber particles that enhanced shear localization by acting as stress concentrators. Meanwhile, hydrostatic tension ahead of the crack tip caused rapid cavitations of the rubber. The voided damage zone then blunts the crack, which behaves as if it possesses a much larger crack tip radius. Thus, a larger plastic zone gets associated with this crack and this is the source of toughening effect. The rubber particles that are bonded to the matrix can bear the load in triaxial tension. Thus, the interfacial interaction of rubber particles with the matrix epoxy is desirable for the toughness property which can be attributed by the pre-reaction of the rubber, and thereby improves the toughness by increasing the miscibility of rubber into the epoxy matrix. Hence, some amount of rubber goes into the epoxy matrix and act as plasticizer. If rubber is incorporated into the epoxy network, it will act as a flexibilizer. Both these effects will increase the ability of the matrix to deform under shear (Thomas *et al.*, 2008).

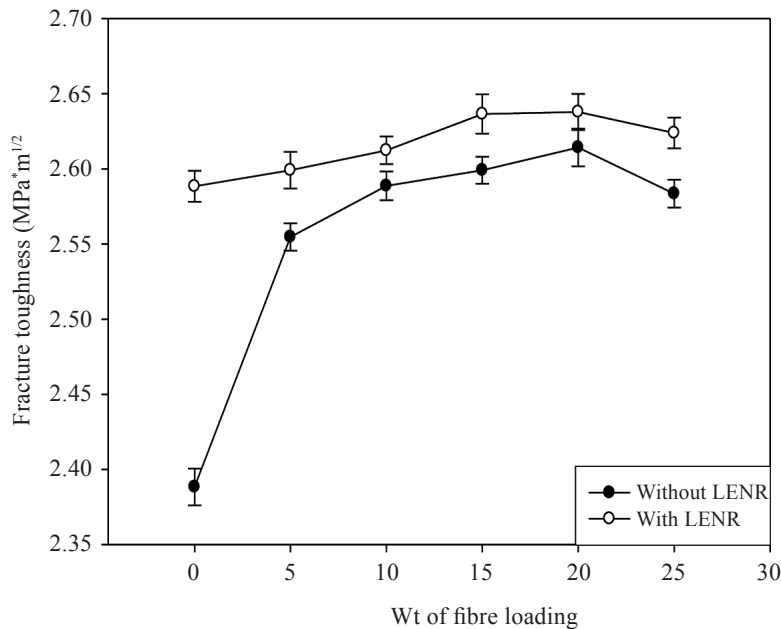


*Fig. 3: Fracture toughness versus weight percentage of fibre loading used for kenaf fibre reinforced epoxy composite (with and without LENR)*

#### *Morphology of Impact Fractured Surfaces*

The fractured surfaces of the specimens were examined using the scanning electron microscope (SEM). The typical fracture surfaces of the kenaf fibre reinforced, with and without LENR modified epoxies, are shown in *Fig. 4*. The composites epoxy without the addition of LENR showed smooth and rivery fractured surfaces with ripples. The relative smoothness of the fractured surface indicates that no significant plastic deformation had occurred irrespective of the presence of some shear deformation lines. The morphology of the LENR modified epoxy shows that the rubber particles are well dispersed in the epoxy matrix. Nonetheless, the fractured surfaces are not very smooth, indicating a ductile manner of the fracture. Yang and Li (1987) have reported that the size of the stress-whitened zone or the amount of deformation lines is proportional to the increase of toughness in the material. The relatively distorted shape of rubber domains in these epoxy resin matrices is supposed to be attributed to the higher amount of plastic deformation. The deformation lines are propagated through rubber domains, promoting stress transfer between the particles and the epoxy matrix. The same finding has also been reported by Thomas *et al.* who operated the yielding process throughout the matrix, whereby, a homogenous distribution of smaller particles is necessary (Thomas *et al.*, 2008). This morphological structure in *Fig. 4* is believed to be responsible for the higher toughness performance of the kenaf fibre reinforced LENR modified epoxy composites. Thus, the uniformly distributed rubber particles act as stress concentrators and exhibit higher toughness than the kenaf fibre reinforced unmodified epoxy composites.

#### **CONCLUSIONS**

This work clearly shows that introducing LENR to epoxy matrix can improve the mechanical performance of the kenaf fibre reinforced epoxy composites. The results have shown that the

## Effect of Epoxidized Natural Rubber on Mechanical Properties of Epoxy Reinforced Kenaf Fibre Composites

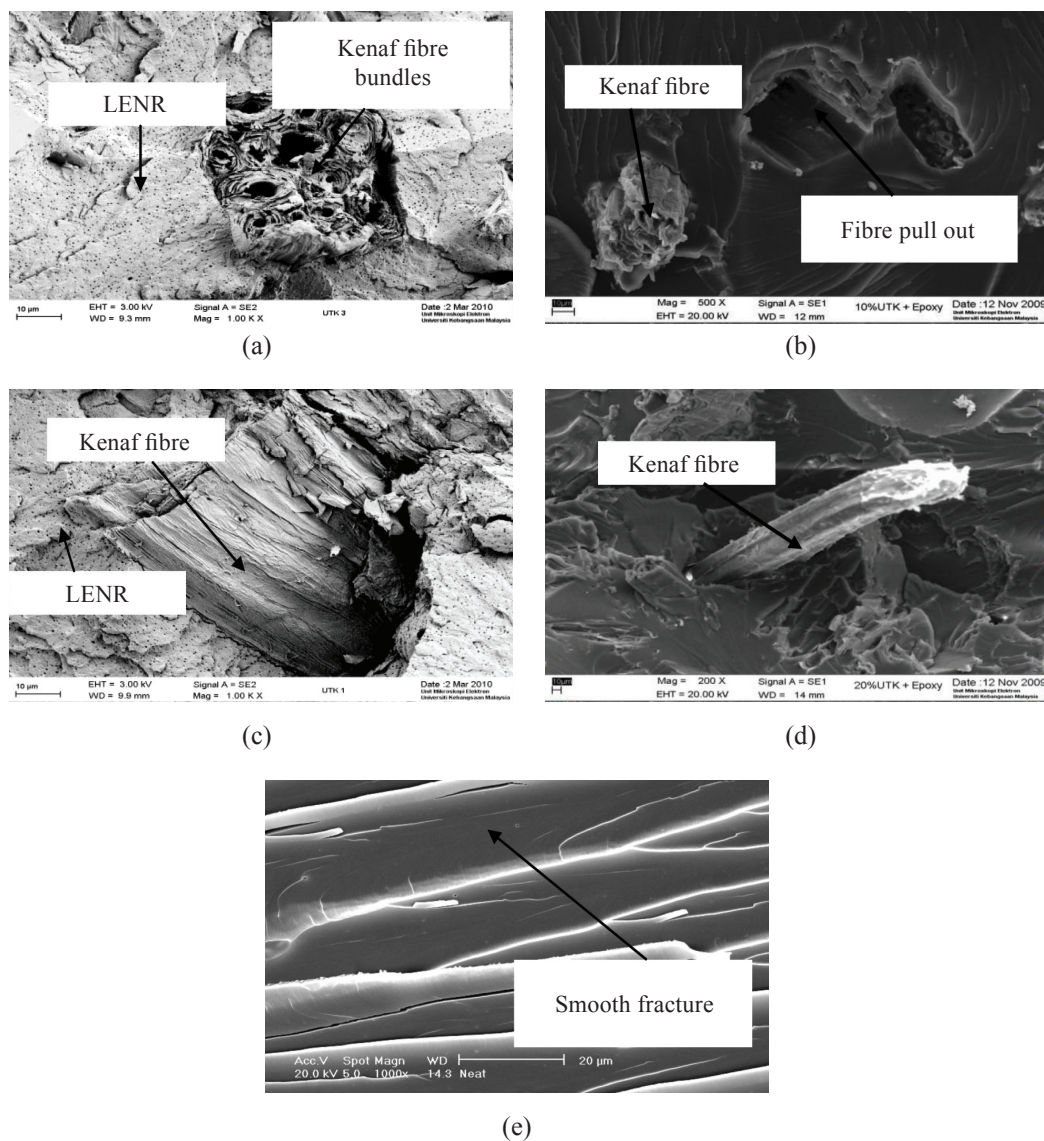


*Fig. 4: The SEM micrographs of the fractured surface of kenaf fibre-epoxy composites for; (a) 10% fibre loadings with LENR; (b) 10% fibre loadings without LENR; (c) 25% fibre loadings with LENR; (d) 20% fibre loadings without LENR, and (e) neat epoxy*

addition of liquid epoxidized natural rubber (LENR) improved the flexural modulus, flexural strength and fracture toughness by 31%, 30% and 28%, respectively, at 20wt% of the fibre loadings. When LENR reacted with epoxy during mixing process, the path of the reaction could change. This reaction could cause the flexibility and toughness to increase. Furthermore, the formations of rubber domains in the epoxy matrix led to flexibility and improved toughness. The distorted shape of rubber domains in the epoxy resin matrices was attributed to the higher amount of plastic deformation. These deformation lines are propagated through rubber domains, promoting stress transfer between the particles and epoxy matrix, and this consequently increases its toughness.

### ACKNOWLEDGEMENT

This work was supported by the MOSTI under grant 03-01-02-SF0223. The authors are grateful to the KPT, Universiti Kebangsaan Malaysia and Universiti Teknologi MARA for sponsoring this research.

### REFERENCES

- Abdullah, I., & Zakaria, Z. (1989). Pendopolimeran fotokimia getah asli. *Sains Malaysiana*, 18(2), 99-109.
- Auad, M. L., Frontini, P. M., Borrajo, J., & Aranguren, M. I. (2001). Liquid rubber modified vinyl ester resins: fracture and mechanical behaviour. *Polymer*, 42, 3723-3730.
- Calabrese, L., & Valenza, A. (2003). Effect of CTBN rubber inclusions on the curing kinetic of DGEBA-DGEBA epoxy resin. *European Polymer Journal*, 39, 1355-1363.
- Hazleen Anuar. (2007). D.Phil Thesis, Department of Applied Physics, Universiti Kebangsaan Malaysia, Bangi Selangor.
- Jang, J., & Yang, H. (2000). Toughness improvement of carbon-fibre/polybenzoxazine composites by rubber modification. *Composites Science and Technology*, 60, 457-463.
- Jayle, L., Bucknall, C. B., Partridge, I. K., Hay, J. N., Farnyough, A., & Nozue, I. (1996). Ternary blends of epoxy, rubber and polycarbonate: phase behaviour, mechanical properties and chemical interactions. *Polymer*, 37(10), 1897-1996.
- John, K., & Venkata, N. S. (2009). Sisal fiber/glass fiber hybrid composites: The impact and compressive properties. *Journal of Reinforced Plastics and Composites*, 23, 1253-1258.
- Kaynak, C., Orgun, O., & Tincer, T. (2005). Matrix and interface modification of short carbon fiber-reinforced epoxy. *Polymer Testing*, 24, 455-462.
- Mathur, V. K. (2006). Composite materials from local resources. *Construction and Building Materials*, 20, 470-477.
- Nishino, T., Hirao, K., Kotera, M., Nakamae, K., & Inagaki, H. (2003). Kenaf reinforced biodegradable composite. *Composites Science and Technology*, 63, 1281-1286.
- Ozturk, A., Kaynak, C., & Tincer, T. (2001). Effects of liquid rubber modification on the behavior of epoxy resin. *European Polymer Journal*, 37, 2353-2363.
- Ray, D., & Rout, J. (2005). *Natural Fibers, Biopolymers and Biocomposites* (p. 291-341). USA: CRC Press.
- Ray, D., Sarkar, B. K., Rana, A. K., & Bose, N. R. (2001a). Effect of alkali treated jute fibres on composite properties. *Bull Mater Science*, 24(2), 129-135.
- Ray, D., Sarkar, B. K., Rana, A. K., & Bose, N. R. (2001b). The mechanical properties of vinylester resin matrix composites reinforced with alkali-treated jute fibres. *Composites Part A*, 32, 119-127.
- Saadati, P., Baharvand, H., Rahimi, A., & Morshedian, J. (2005). Effect of modified liquid rubber on increasing toughness of epoxy resins. *Iranian Polymer Journal*, 14 (7), 637-646.
- Saheb, D. N., & Jog, J. P. (1999). Natural Fiber Polymer Composites: A review. *Advances in Polymer Technology*, 18(4), 351-363.
- Thomas, R., Durix, S., Sinturel, C., Omonov, T., Goossens, S., Groninckx, G., Moldenaers, P., & Thomas, S. (2007). Cure kinetics, morphology and miscibility of modified DGEBA-based epoxy resin – Effects of a liquid rubber inclusion. *Polymer*, 48, 1695-1710.

Effect of Epoxidized Natural Rubber on Mechanical Properties of Epoxy Reinforced Kenaf Fibre Composites

- Thomas, R., Yumei, D., Yuelong, H., Le, Y., Moldenaers, P., Weimin, Y., Czigany, T., & Thomas, S. (2008). Miscibility, morphology, thermal and mechanical properties of a DGEBA based epoxy resin toughened with a liquid rubber. *Polymer*, 49, 278-294.
- Yang, W. F., & Li, S. (1987). Structures and properties of a rubber-epoxy resin dual-phase system. *Materials Chemistry and Physics*, 15, 443-450.



## Catalytic Gasification of Empty Fruit Bunch for Enhanced Production of Hydrogen Rich Fuel Gas

Mohammed M. A. A.<sup>1</sup>, Salmiaton A.<sup>1\*</sup>, Wan Azlina W. A. K. G.<sup>1</sup>, Mohamad Amran M. S.<sup>1</sup>, Omar R.<sup>1</sup>, Taufiq-Yap Y. H.<sup>2</sup> and Fakhru'l-Razi A.<sup>1</sup>

<sup>1</sup>*Department of Chemical & Environmental Engineering,  
Faculty of Engineering, Universiti Putra Malaysia,  
43400 Serdang, Selangor, Malaysia.*

<sup>2</sup>*Centre of Excellence for Catalysis Science and Technology; and Department of Chemistry,  
Faculty of Science, Universiti Putra Malaysia,  
43400 Serdang, Selangor, Malaysia.*

\*E-mail: mie@eng.upm.edu.my

### ABSTRACT

Oil palm is widely grown in Malaysia. There has been interest in the utilization of oil palm biomass for production of environmental friendly biofuels. The gasification of empty fruit bunches (EFB), a waste of the palm oil industry, was investigated in this study to effectively and economically convert low value and highly distribution solid biomass to a uniform gaseous mixture mainly hydrogen ( $H_2$ ). The effects of temperature, equivalence ratio (ER) and catalyst adding on the yields and distribution of hydrogen rich gas products were also investigated. The main gas species generated, as identified by GC, were  $H_2$ , CO,  $CO_2$ ,  $CH_4$  and trace amounts of  $C_2H_4$  and  $C_2H_6$ . With temperature increasing from 700 to 1000 °C, the total gas yield was enhanced greatly and reached the maximum value (~ 90 wt. %) at 1000°C with a big portion of  $H_2$  (38.02 vol. %) and CO (36.36 vol. %). Equivalence ratio (ER) showed a significant influence on the upgrading of hydrogen production and product distribution. The optimum ER (0.25) was found to attain a higher  $H_2$  yield (27.42 vol. %) at 850°C. The effect of adding catalysts (Malaysian dolomite1, P1), Malaysian dolomite2 (GML), NaOH, NaCl, CaO, ZnO, NiO) as a primary catalyst on gas product yield was investigated, and it was found that adding dolomite showed the greatest effect with the maximum  $H_2$  yield achieved (28.18 vol.%) at 850°C.

**Keywords:** Biomass, hydrogen, gasification, catalyst adding

### INTRODUCTION

Biomass is an important contributor to the world economy. Today, various forms of biomass energy are consumed all over the world. Biomass provides a clean, renewable energy source that could dramatically improve the environment, economy and energy security. In particular, conversion of non-edible biomass, such as agriculture residues, wood chips, and fruit bunches, stalks, industrial and municipal wastes, into fuels and useful chemicals would solve waste disposal and energy issues (Baratieri *et al.*, 2008). Palm oil wastes are the main biomass resources in ASEAN countries. In Malaysia alone, there were 9.66, 5.20 and 17.08 million tons for fibres, shell and empty fruit bunches, respectively (Nasrin *et al.*, 2008). Thus, to treat this tremendous amount of wastes, novel technologies with improved efficiencies and reduced environmental impacts need to be established timely.

---

Received: 18 April 2011

Accepted: 12 September 2011

\*Corresponding Author

Biomass gasification is one of the most promising thermo-chemical conversion routes to recover energy from biomass. During gasification, biomass is thermally decomposed to solid charcoal, liquid bio-oil and bio-gases under partial oxidation condition. The yields of end products of gasification are dependent on several parameters which include temperature, biomass species, particle size, equivalence ratio and reactor configuration, as well as extraneous addition of catalysts (Demirbas, 2002). As two most important parameters, temperature and equivalence ratio (ER) (Wang *et al.*, 2008) have been investigated widely in bench scale reactors including fixed beds (Yang *et al.*, 2006), fluidized bed (Cao *et al.*, 2006; Lv *et al.*, 2004) and others (Sheth & Babu, 2009). Generally, H<sub>2</sub>-rich gas products are favoured at high temperature and the H<sub>2</sub> yield from the gasification of biomass is acceptable as compared to fast pyrolysis, but they still contain high quantity of tar. It is known that the gas yield, especially H<sub>2</sub>, could be improved by catalyst adding and at the same time, reducing the tar content in the gas yield. So far, various types of chemicals (such as dolomite, oxides and inorganic compounds) have been selected as catalysts to improve the overall efficiency of the system used in producing high quality fuel gases so as to increase the economic feasibility of the biomass gasification process. Furthermore, the humid weather in Malaysia could also show a great effect on gaseous products from biomass gasification when air is used as a gasification agent.

In this study, the catalyst effect on air gasification of EFB was investigated using a fluidized bed reactor in the attempt to achieve an improved performance of EFB conversion to energy with higher yield of H<sub>2</sub>-rich gas and minimum tar content. The biomass gasification technologies used to produce hydrogen-rich fuel gas were found to present highly interesting possibilities for biomass utilization as a sustainable energy. In more specific, biomass used as an energy source can reduce CO<sub>2</sub> greenhouse effect, as well as SO<sub>2</sub> and NO<sub>x</sub> atmospheric pollution (McKendry, 2002), due to its characterization of natural carbon and less sulphur and nitrogen contents.

## MATERIALS AND METHODS

### *Biomass Samples and Catalysts*

The feedstock used was empty fruit bunches (< 1mm, ~5.18 moisture). The physical and chemical properties of the EFB are presented in Table 1. The molecular formula of EFB can be expressed as CH<sub>1.66</sub>O<sub>0.73</sub> based on the ultimate analysis. Meanwhile, particle size reduction was required to allow gasification of the EFB on the available reactor. First, the bunches were manually chopped into small pieces that could be fed in a shredder. After that, a Fritsch grinder with a screen size of 1.0 mm was used to obtain the feedstock size of less than 1.0 mm. The cellulose, hemicelluloses and lignin contents of EFB were sent to MARDI for analysis. Acid detergent fibre (ADF), neutral detergent fibre (NDF) and acid detergent fibre (ADL) analyses were also carried out. The percentages of the cellulose, hemicelluloses and lignin of EFB are also given in Table 1. Among the EFB components, lignin is the most thermally stable and also the main source of tar.

Seven types of catalysts, including Malaysian dolomites P1 and GML, NaOH, NaCl, CaO, ZnO, NiO, were introduced into the thermal system as the catalysts to improve the yields of gas product from EFB gasification. The catalysts' surface areas were measured using nitrogen adsorption (BET) analysis by Quantachrome AS1Win with liquid N<sub>2</sub> at 77.3 K. It was found that NaOH and NaCl contain very low surface area (< 1 m<sup>2</sup>/g) while those of GML, CaO, ZnO and NiO are higher (2-9 m<sup>2</sup>/g), and Malaysian dolomite P1 shows the highest surface area (15.2 m<sup>2</sup>/g). The catalysts were directly dry-mixed with the EFB samples (Sutton, *et al.* 2001) and their weight ratio to EFB (C/W) was kept at 0.1.

Catalytic Gasification of Empty Fruit Bunch for Enhanced Production of Hydrogen Rich Fuel Gas

TABLE 1  
Properties of EFB

Component	Measured (wt. %)
Cellulose	22.24
Hemicellulose	20.58
Lignin	30.45
Elemental analysis	
C	46.62
H	6.45
N	1.21
S	0.035
O <sup>a</sup>	45.66
Proximate analysis	
$M_{ad}$	5.18
$V_{ad}$	82.58
$A_d$	3.45
$FC_{ad}$	8.79
Calorific value (MJ/Kg)	17.02

$M$ : moisture content;  $V$ : volatile matters;  $A$ : ash;  
 $FC$ : fixed carbon;  $ad$ : on air dried basis;  $d$ : on dry basis.

<sup>a</sup> the oxygen (O) content was determined by difference.

### Experimental Set-up

A fluidized bed bench scale gasification unit, operating at atmospheric pressure, was employed for all the runs. Fig. 1 shows a schematic diagram of this particular unit, which consists of three main systems, namely, reactor (gasifier and heating furnace), condenser and purification (condenser, glass wool filter and dryer) and gas storage (gasbags). The reactor is a cylindrical configuration that is made of stainless steel with a length of 600 mm and a diameter of 40 mm. Three thermocouples were inserted in the middle of the heating furnace, middle of the reactor tube and bottom of the reactor tube, respectively. Biomass was fed into the reactor by a feeder on the top of the reactor, which was continuously carried out at a constant flow rate. The feeding capacity of biomass was 10 g/min. The heating medium in fluidized bed gasifier was silica sand of a mean size of 0.1-0.15 mm. The density of sand material is approximately 1470 kg/m<sup>3</sup>. It is approximately 69.3% SiO<sub>2</sub>, 26.5% CaO, and 1.7% Fe<sub>2</sub>O<sub>3</sub> with the balance of the other trace amounts of oxides. The minimum fluidization velocity at atmospheric pressure for the sand material was measured to be 0.04 m/s.

Initially, the fluidized bed reactor was loaded with 100 g of inert sand as bed material. The air was injected from the bottom distributor to maintain the sand material to be fluidized. When the desired temperatures were achieved, a 20 min waiting time was allowed so as to make the system stable and to achieve a steady state, before the biomass feeding was started. The fuel gas produced was passed to the downstream cooling system, where the condensable vapours were collected by ice water condenser and caught by dichloromethane inside the neck flask, whereas the incondensable part of product gas left the cooling system and passed through a fibre glass-wool filter for more tar trapping and dried by silica gel before it was collected by 12 L gas sampling bags and taken every 1 min for gas chromatography (GC) analysis.

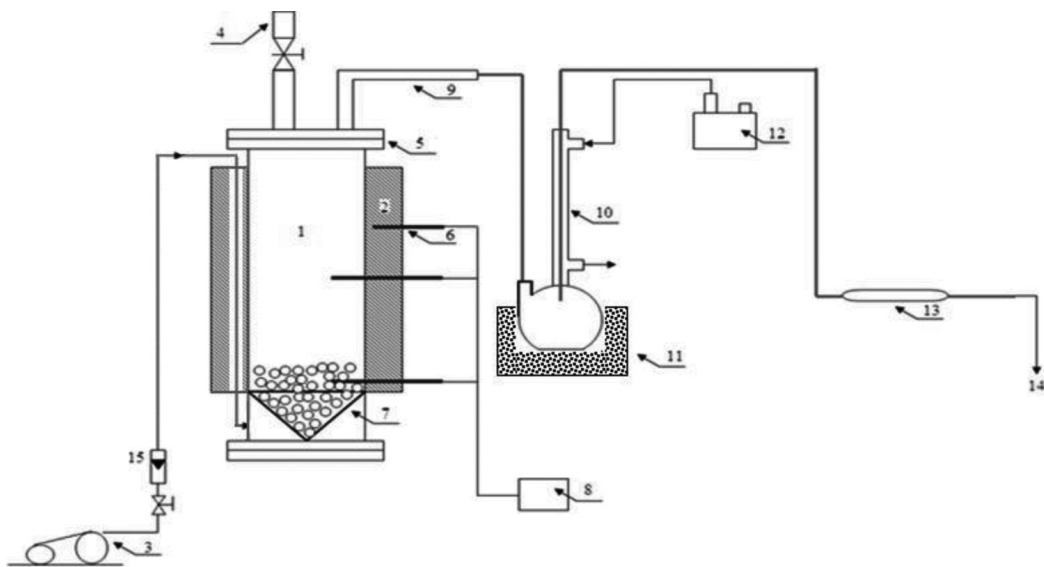


*Fig. 1: The schematic of lab-scale fluidized bed biomass gasifier; (1) lab-scale grater, (2) electric furnace, (3) air pump, (4) biomass feeder, (5) flange, (6) thermocouples, (7) air distributor, (8) furnace controller, (9) gas discharge, (10) water cooler, (11) ice trap, (12) cooling water pump, (13) glass wool filter, and (14) fuel gas*

#### *Fuel Gas Sampling and Measuring Procedures*

After a steady state was achieved, the fuel gas stream was switched to downstream cooling system and glass wool filter. Then, the dry gas was sampled by a gas sampling bag and taken every 1 min. The permanent gas compositions and light hydrocarbon constituents (mainly C<sub>2</sub>-C<sub>6</sub>) of the fuel gas were analyzed by a gas chromatograph (Agilent HP6890N) with TCD and FID detectors using argon as a carrier gas. The standard gas mixture of H<sub>2</sub>, CO, O<sub>2</sub>, N<sub>2</sub> and CH<sub>4</sub> was used as a quantitative calibration of GC. Generally, 10 gas samples were taken for each test condition. The tar product was trapped in the cooling system condenser and fibre-glass wool filter. Dichloromethane (99.8 %) was used to dissolve the tar from the condenser walls and fibre-glass wool filter. The dissolved product was transferred to a ceramic tray and heated in an oven at 100 °C for about 12 hours to evaporate any water and solvent fractions and later weighted to get the tar mass.

## RESULTS AND DISCUSSION

The goal of this study was to produce H<sub>2</sub>-rich gas with less tar formation from the air gasification process of a biomass. The experiments were conducted to investigate the impacts of the parameter variation, such as temperature profiles in the reactor, the equivalence ratio (ER) and catalysts that were adding on to gas composition and tar formation.

#### *The Influence of Gasifier Temperature on EFB Gasification*

The yields of the final products from the EFB gasification under different temperatures are illustrated in *Fig. 2*. With the temperature increasing from 700 to 1000 °C, the total gas yield increased sharply from 62.68 to 91.70 wt. %, while liquid, char and tar yields were found to have constantly reduced.

Meanwhile, varying the temperature showed a great influence on the gas product components. As shown in *Fig. 3*, the main gas products are H<sub>2</sub>, CO, CO<sub>2</sub>, CH<sub>4</sub> and some C<sub>2</sub> hydrocarbons traces (C<sub>2</sub>H<sub>4</sub> and C<sub>2</sub>H<sub>6</sub>). Among them, the H<sub>2</sub> content increased steadily from 10.27 to 38.02 vol. % as the temperature was increased from 700 to 1000 °C. Meanwhile, the yield of CH<sub>4</sub> was also increased from 5.84 to 14.72 vol. %, whilst the CO<sub>2</sub> content generally decreased with the increase of the temperature, particularly at 1000 °C. The CO yield was initially increased from 21.87 to 33.35 vol. % as the temperature increased to 800 °C, before it decreased to 33.08 vol. % at 900 °C, and later increased again to 36.36 vol. % as the temperature continuously increased to 1000 °C. On the contrary, the C<sub>2</sub>H<sub>4</sub> and C<sub>2</sub>H<sub>6</sub> yields were relatively small and the influence of temperature was insignificant. As the temperature of the reactor increased, the tar content in the fuel gas produced decreased sharply from 8.05 wt. % at 700 °C to less than 2.12 wt. % at 1000 °C. The thermal cracking of gas-phase hydrocarbons at the high temperature might explain the variation of the gas product distribution observed (Dai *et al.*, 2000). At a high furnace temperature, the gas species generated from the biomass at pyrolysis zone could undergo further reactions (secondary reactions), such as tar cracking and shifting reaction, leading to much more incondensable gases (including H<sub>2</sub>) generated. Therefore, the total yield of gas products increased significantly as the temperature increased from 700 to 1000 °C. The main reactions involved could be expressed using equations (1) - (10) (Dai *et al.*, 2000; Demirbas, 2001). Among them, equations (1) – (5) are the principle or heterogenous gasification reactions whilst equations (6) – (10) are homogenous and secondary reactions. In terms of increasing H<sub>2</sub> production, equations (6) to (10) are the main reactions of interest for the EFB gasification at atmospheric pressure and temperature between 700 and 1000 °C. The other gas components might increase or decrease with the occurring of secondary reactions. As a result, more H<sub>2</sub> could be obtained when secondary reactions occurred significantly. From the above analysis, it could be concluded that higher temperature (1000 °C) is favourable for thermal cracking of tar and shift reaction.



The lower heating value (LHV, MJ/m<sup>3</sup>) of the gas products can be calculated using the following equation (Dai *et al.*, 2000; Yang *et al.*, 2006):

$$LHV = (30xCO + 25.7xH_2 + 85.4xCH_4 + 151.3xC_nH_m)x4.2 \quad (11)$$

CO, H<sub>2</sub>, CH<sub>4</sub> and C<sub>n</sub>H<sub>m</sub> in the above equation are the molar ratios of the CO, H<sub>2</sub>, CH<sub>4</sub> and other hydrocarbon (C<sub>2</sub>H<sub>2</sub> and C<sub>2</sub>H<sub>6</sub>) in the gas product. As shown in *Fig. 2*, the heating value of the total gas products increased steadily as the temperature increased. At 1000 °C, the LHV of gas products reached 15.55 MJ/m<sup>3</sup>, which could be grouped in the medium level of the heat values for gas fuels.

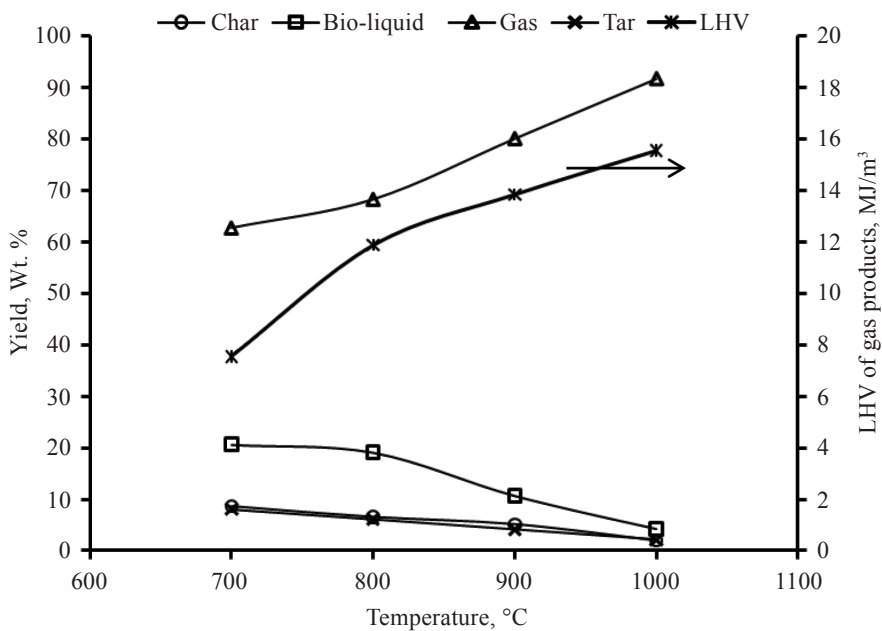


Fig. 2: The effect of gasifier temperature on the EFB gasification yields

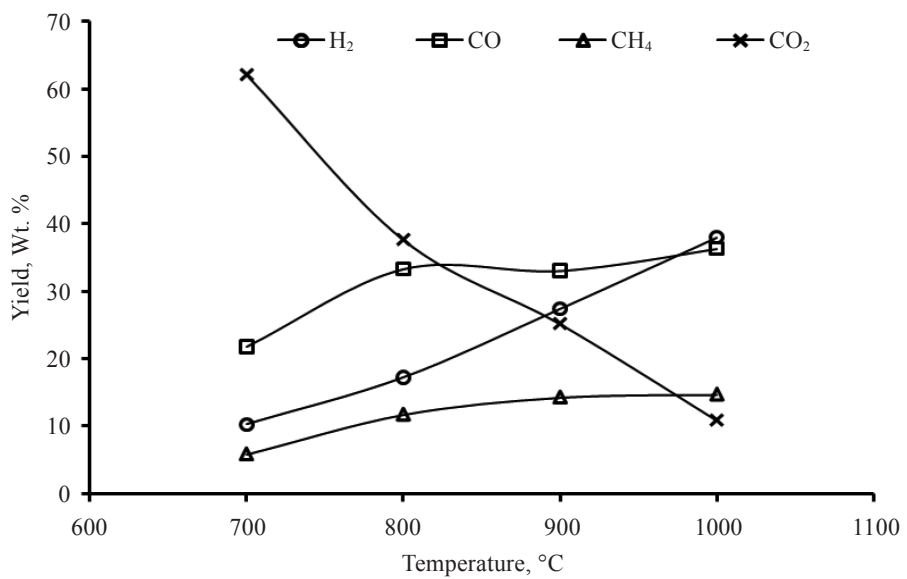


Fig. 3: The effect of gasifier temperature on the gas composition of EFB gasification

This LHV group can be directly used for gas engine, gas turbine or boiler for power generation. In addition, this group can also be applied for the chemical formation of methanol and methane (McKendry, 2002).

#### *The Influence of Equivalence Ratio (ER) on Product Yields*

The equivalence ratio (ER) is defined as the ratio of oxygen (air) that is required for gasification to oxygen (air) required for stoichiometric combustion of a given amount of biomass (Narvaez *et al.*, 1996). In this work, ER varied from 0.15 to 0.35 in an increment of 0.05, keeping the final temperature of the reactor at 850°C, and the feedstock particle size in the range of 0.3-0.5 mm. The air flow rate entering the reactor was varied to investigate the effect of ER. As shown in Fig. 4, with increased in ER, char and tar yield decreased from 13.65 to 2.12 wt. % and 9.83 to 2.82 wt. % respectively, while gas yield increased from 70.75 to 86.46 wt. %. The lower heating value (LHV) of the gases decreased slightly from 15.38 to 12.35 MJ/m<sup>3</sup>. The increase in ER increased oxidation reaction and decreased the product gas quality. However, too high ER causes low concentrations of H<sub>2</sub> and CO with a high CO<sub>2</sub> content in the product gas. As shown in Fig. 5, with ER varied from 0.15 to 0.35, the H<sub>2</sub> content increased to and reached the maximum value of 27.42 vol. % at ER of 0.25 and then dropped to 18.37 vol. % with a further increase in ER, while the CO<sub>2</sub> content increased steadily from 16.66 vol. % to 36.05 vol. %; however, CH<sub>4</sub> and other hydrocarbons traces content were found to have the contrary results. It can be explained that in the gasification process, the oxidation reactions are always strong, and oxidization reactions of combustible product gases

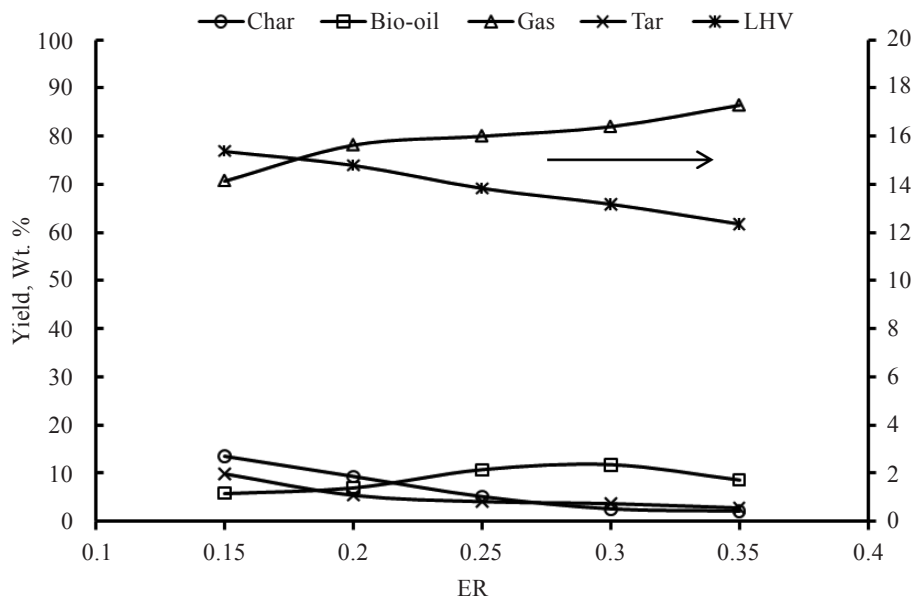


Fig. 4: The effect of ER on the EFB gasification yields

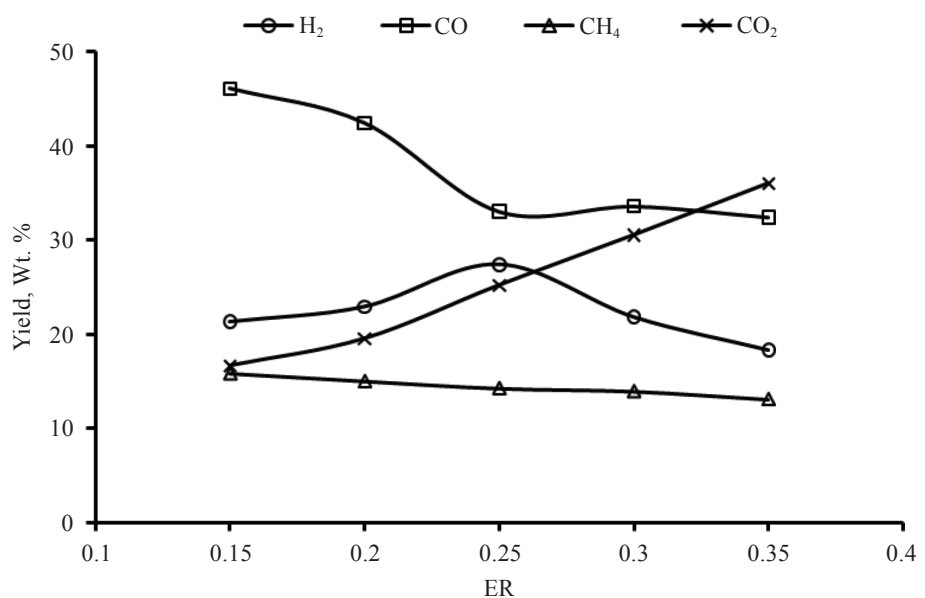


Fig. 5: The effect of ER on the gas composition of the EFB gasification

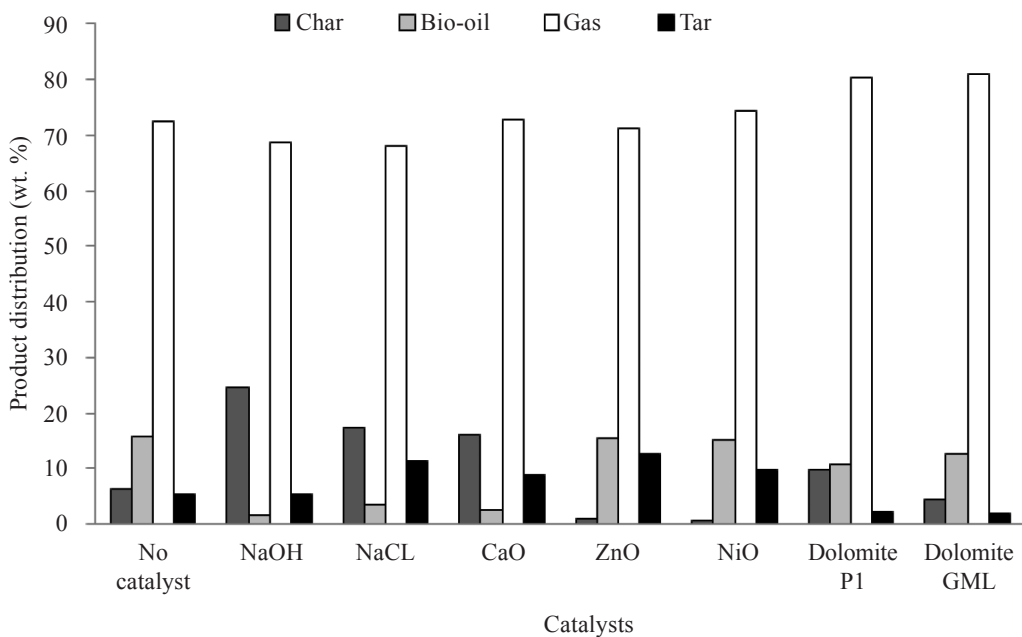


Fig. 6: Product distribution from the EFB gasification with different catalysts at 850 °C, ER=0.25 and C/W = 10 wt. %.

strengthen with ER, which results in more CO<sub>2</sub>. Several research groups, such as Mansaray *et al.* (1999), Manya *et al.* (2006) and Xiao *et al.* (2007), investigated the effect of ER in the air gasification of biomass in a fluidized bed gasifier, and found that with the increase in ER, H<sub>2</sub> and CO initially increased but later decreased, whereas CO<sub>2</sub>, CH<sub>4</sub> and other hydrocarbon contents were progressively decreased, which are similar with the findings obtained in the current study. Through the analysis on the experimental results of varying ER, it could be understood that the optimum value for ER is 0.25, in which the maximum hydrogen content was obtained.

### *The Influence of Adding Catalyst*

The results of the catalytic gasification of EFB at 850 °C and ER= 0.25 are reported in Fig. 6 and Fig. 7. All the catalysts with C/W of 10 wt. % showed a more or less positive influence on gasification yields and the total volume of gases produced. Malaysian dolomite P1 appeared to have the strongest catalytic effect than others; with the presence of dolomite, the total gas yield from EFB gasification was increased to reach 28.18 vol. % as compared with 24.78 vol. % without any catalyst. Meanwhile, the Malaysian dolomite GML and pure catalyst NiO showed less effect compared to dolomite P1. The sodium compounds (NaOH and NaCl) showed the lowest effect on EFB gasification, and this was possibly due to the strong sodium base which could extract some low molecular compounds in the biomass and also break the intermolecular hydrogen bridges under swelling or heating (Wang *et al.*, 2006). It could also react with cellulose, hemicellulose and lignin to make the devolatilization of biomass to occur earlier at a low temperature and that can increase

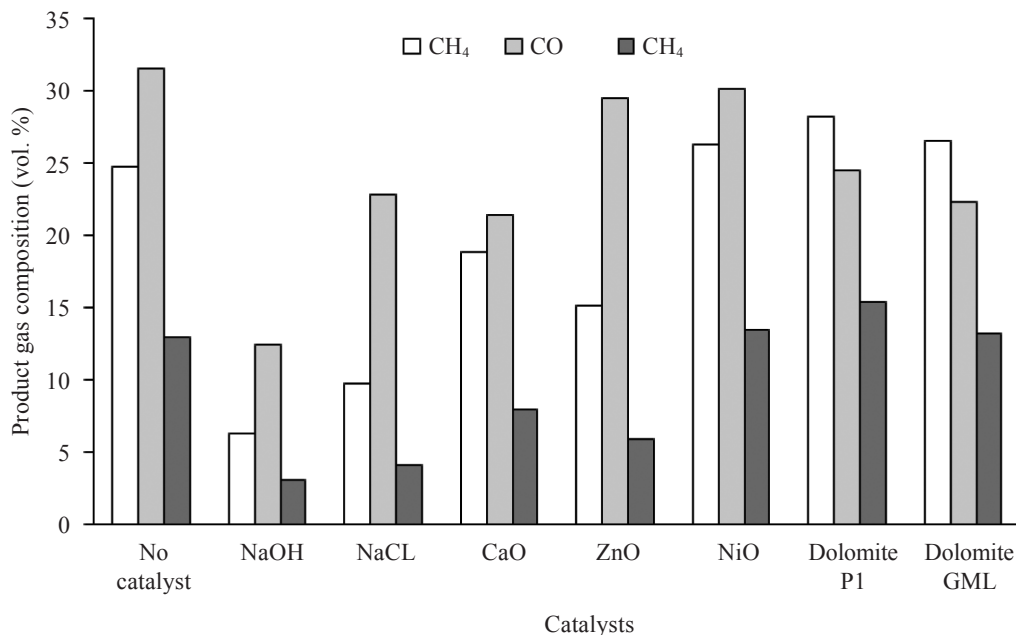


Fig. 7: Product gas composition (N<sub>2</sub>free) from the EFB gasification with different catalysts at 850 °C, ER=0.25 and C/W = 10 wt. %

char formation during gasification. The catalytic gasification of EFB, in terms of the yield of H<sub>2</sub> production, was Malaysian dolomite P1 > Malaysian dolomite GML > pure catalyst NiO > no catalyst > CaO > ZnO > sodium based catalysts NaCl and NaOH. Adding the catalysts to biomass (except for the sodium compounds) could improve the H<sub>2</sub> content, whilst the CO contents were found to have decreased in all the cases, and these were attributed possibly to the shifting reactions. This changing trend is consistent with that observed from the gasification process in some previous research (Haiping *et al.*, 2006; Perez *et al.*, 1997).

## CONCLUSION

The main products of EFB gasification were solid charcoal, bio-oil liquids and gas products. Gas yield increased greatly whilst solid and liquid yields decreased constantly as the temperature was increased from 700 to 1000°C. The gas products mainly consist of H<sub>2</sub>, CO, CO<sub>2</sub> and CH<sub>4</sub> and some C<sub>2</sub> hydrocarbons. The high temperature was found to be favourable for higher hydrogen/syngas production and for the enhancement of LHV of gas products. The optimum equivalence ratio was 0.25 for the fluidized bed gasifier studied. Several potential catalysts have been investigated on improving gas yield and quality. The Malaysian dolomites P1 and GML appeared to have the strongest effects on H<sub>2</sub> yield and tar removal. With the addition of dolomite P1 (10%), the total gas yield from the EFB gasification was improved and gas quality was upgraded, in addition to the great reduction of the tar yield.

## REFERENCES

- Baratieri, M., Baggio, P., Fiori, L., & Grigiante, M. (2008). Biomass as an energy source: Thermodynamic constraints on the performance of the conversion process. *Bioresource Technology*, 99(15), 7063-7073.
- Cao, Y., Wang, Y., Riley, J. T., & Pan, W.P. (2006). A novel biomass air gasification process for producing tar-free higher heating value fuel gas. *Fuel Processing Technology*, 87(4), 343-353.
- Dai, X., Wu, C., Li, H. P., & Chen, Y. (2000). The fast pyrolysis of biomass in CFB reactor. *Energy and Fuels*, 14, 552-557.
- Demirbas, A. (2001). Yields of hydrogen-rich gaseous products via pyrolysis from selected biomass samples. *Fuel*, 80(13), 1885-1891.
- Demirbas, A. (2002). Gaseous products from biomass by pyrolysis and gasification: Effects of catalyst on hydrogen yield. *Energy Conversion and Management*, 43(7), 897-909.
- Haiping, Y., Rong, Y., Hanping, C., Dong, H., David, T., & Chuguang, Z. (2006). Pyrolysis of palm oil wastes for enhanced production of hydrogen rich gases. *Fuel Processing Technology*, 87, 935-942.
- Lv, P. M., Xiong, Z. H., Chang, J., Wu, C. Z., Chen, Y., & Zhu, J. X. (2004). An experimental study on biomass air-steam gasification in a fluidized bed. *Bioresource Technology*, 95(1), 95-101.
- Mansaray, K. G., Ghly, A. E., Al-Tawee, A. M., Hamdullahpur, F., & Agursal, V. I. (1999). Air gasification of rice husk in a dual distributor type fluidized bed gasifier. *Biomass and Bioenergy*, 17, 315-332.
- Manya, J. J., Sanchez, J. L., Abrego, J., Gonzalo, A., & Arauzo, J. (2006). Influence of gas residence time and air flow on the air gasification of dried sewage sludge in a bubbling fluidized bed. *Fuel*, 85, 2027-2033.
- McKendry, P. (2002). Energy production from biomass (part 1): Overview of biomass. *Bioresource Technology*, 83(1), 37-46.

Catalytic Gasification of Empty Fruit Bunch for Enhanced Production of Hydrogen Rich Fuel Gas

- Narvaez, I., Orio, A., Aznar, M. P., & Corella, J. (1996). Biomass gasification with air in an atmospheric bubbling fluidized bed-effect of six operating variables on the quality of produced raw gas. *Industrial & Engineering Chemistry Research*, 35, 2110-2120.
- Nasrin, A. B., Ma, A. N., Choo, Y. M., Mohamad, S., Rohaya, M. H., & Azali, A. (2008). Oil palm biomass as potential substitution raw materials for commercial biomass Briquettes production. *American Journal of Applied Sciences*, 5(3), 179-183.
- Perez, P., Aznar, P. M., Caballero, M. A., Gil, J., Martin, J. A., & Corella, J. (1997). Hot gas cleaning and upgrading with a calcined dolomite located downstream a biomass fluidized bed gasifier operating with steam-oxygen mixtures. *Energy and Fuels*, 11(6), 1194-1197.
- Sheth, P. N., & Babu, B. V. (2009). Experimental studies on producer gas generation from wood waste in a downdraft biomass gasifier. *Bioresource Technology*, 100(12), 3127-3133.
- Sutton, D., Kelleher, B., & Ross, J. R. H. (2001). Review of literature on catalysts for biomass gasification. *Fuel Processing Technology*, 73(3), 155-173.
- Wang, J., Zhang, M., Chen, M., Min, F., Zhang, S., & Ren, Z. (2006). Catalytic effects of six inorganic compounds on pyrolysis of three kinds of biomass. *Thermochimica acta*, 444, 110-114.
- Wang, L., Weller, C. L., Jones, D. D., & Hanna, M. A. (2008). Contemporary issues in thermal gasification of biomass and its application to electricity and fuel production. *Biomass and Bioenergy*, 32(7), 573-581.
- Xiao, R., Jin, B., Zhou, Z., & Zhang, M. (2007). Air gasification of polypropylene plastic waste in fluidized bed gasifier. *Energy Conversion and Management*, 48, 778-786.
- Yang, H., Yan, R., Chen, H., Lee, D., Liang, D., & Zheng, C. (2006). Pyrolysis of palm oil wastes for enhanced production of hydrogen rich gases. *Fuel Processing Technology*, 87(10), 935-942.
- Yang, W., Ponzio, A., Lucas, C., & Blasiak, W. (2006). Performance analysis of a fixed-bed biomass gasifier using high-temperature air. *Fuel Processing Technology*, 87(3), 235-245.



## Earthquake and Tsunami Research in USM: The Role of Disaster Research Nexus

Hock Lye Koh<sup>1</sup>, Su Yean Teh<sup>2\*</sup>, Taksiah A. Majid<sup>1</sup>, Tze Liang Lau<sup>1</sup>  
and Fauziah Ahmad<sup>1</sup>

<sup>1</sup>*Disaster Research Nexus, School of Civil Engineering, Engineering Campus,  
Universiti Sains Malaysia, 14300 Nibong Tebal, Penang, Malaysia*

<sup>2</sup>*School of Mathematical Sciences, Universiti Sains Malaysia,  
11800 Penang, Malaysia*

\*E-mail: hlkoh@cs.usm.my

### ABSTRACT

The 2004 Banda Aceh earthquake and ensuing Andaman mega tsunami that killed a quarter million people worldwide is a wake-up call to many. Active research was initiated in Universiti Sains Malaysia (USM) immediately after the infamous event with the aims to help develop human capacity and resources, and to mitigate any future earthquake and tsunami. The Disaster Research Nexus (DRN) was formed recently within the School of Civil Engineering, USM, to facilitate active collaborative research on earthquakes and tsunamis, as well as on other natural disasters, such as landslides. This paper begins with an introduction to DRN. This is followed by a description of some research achievements undertaken by DRN staff. A concise exposition on the tsunami simulation model TUNA developed by the authors and its application to the 2004 Andaman tsunami are given to illustrate the capability of TUNA. The role of mangrove in reducing the impact of tsunami is then modelled. Tsunami may inundate coastal plain with large quantity of saline water, changing the salinity regimes in the soil and inducing vegetative succession changes. A model called MANHAM was developed to simulate the salinity changes and its associated vegetative evolution to assist in the rehabilitation of vegetation destroyed by tsunami. Meanwhile, an earthquake risk analysis for the Upper Pandas Dam in Sabah is then presented, and this is followed by a model estimation of tsunami forces on the coastal structures. The main objective of this paper is to reach out to research scientists and onsite risk reduction professionals to collaborate towards the development of a vibrant research culture to face future natural disasters such as earthquakes and tsunamis. It is hoped that DRN will move forward to further enhance active collaborations with other research and operational institutions worldwide towards developing earthquake and tsunami resilient communities.

**Keywords:** DRN, TUNA, MANHAM, tsunami simulation, mangrove, earthquakes, coastal structures

### INTRODUCTION TO DRN

The mission of the recently established Disaster Research Nexus (DRN) in Universiti Sains Malaysia (USM) is to advance and to communicate knowledge on natural disasters mitigation, research and community preparedness, response, and recovery. Using an interdisciplinary framework, the DRN fosters information sharing and promotes integration of activities among researchers, practitioners, and policy makers from around the nation. It supports and conducts research on various aspects of natural disasters and provides educational opportunities for the next generation of natural hazard scholars and professionals. The prime objectives consist of conducting fundamentally sound research of deep scientific interest, and producing results which are reliable, accurate and of

---

Received: 18 April 2011

Accepted: 12 September 2011

\*Corresponding Author

practical application to both society and industry. Working closely with other centres and institutes within and outside USM, DRN creates opportunities for collaboration with both private and public institutions, locally and internationally, to advance the science of natural disasters, strengthen the communication between the hazard academic scientists and on-site application communities, and improve the implementation of hazards prediction, preparedness and mitigation leading to effective emergency management programmes. It is a recognized resource centre for researchers and practitioners who wish to obtain the most current scientific knowledge and the best practices available to solve hazard-related problems. It accomplishes its work through four major activities, namely, information dissemination and services, regular training workshops, basic scientific research and dedicated consultancy services. In summary, the missions of DRN are:

- to coordinate the development of technology and expertise to deal with a broad spectrum of issues arising from natural disasters;
- to conduct rigorous and cutting-edge research on natural disasters, damage monitoring, risk assessment and risk reduction;
- to collaborate with other research centres and institutes to extend the research to a broad social, economic and financial context;
- to provide resources and support services for national and international projects that require natural disaster considerations.

Guided by the missions and goals of DRN, the researchers devote their full attention to the fields within the scope of the nexus and within their core research interest and competence to achieve the objectives. In this short paper, the researchers limit the exposition to merely two fields of earthquake and tsunamis, leaving the other fields to a later occasion.

### **TSUNAMI SIMULATION BY TUNA**

An earthquake with magnitude of  $M_w = 9.3$  erupted off the western coast of Banda Aceh, North Sumatera at 00:58:53 UTC (08:58:53 Malaysian time) on 26 December 2004. The earthquake occurred on the tectonic boundaries of the subduction zones, between the Indian plate and the Sunda plate. The instantaneous uplift of the sea floor caused the sea level to be lifted upward by as much as 12 meters at the source, triggering a mega tsunami that killed 200,000 people worldwide. This undersea earthquake lifted upwards a large volume of water, in the order of two hundred trillion tons. Mindful of the deadly potential of future tsunamis inflicting devastating toll on Malaysian coastal communities, Universiti Sains Malaysia (USM) immediately initiated a tsunami research programme to understand the mechanism of tsunami generation, propagation and runup, develop the capability of predicting the impacts of potential tsunamis on the Malaysian coastal communities and establish mitigation measures for reducing these impacts. Two field surveys were conducted along the affected beaches in Penang and Kedah to assess the runup heights and inundation distances as well as to document the damage to properties. The survey data were then collated for calibrating and validating a tsunami simulation model TUNA developed in-house in USM (Koh *et al.*, 2009; Koh *et al.*, 2010). The survey locations are indicated in *Fig. 1*. A series of international workshops, conferences and roundtables were also held in Malaysia and other affected countries in Asia, including Thailand, Indonesia, Singapore, Philippines, Taiwan, China, Australia, Sri Lanka and India, to report research findings, coordinate collaboration and also establish effective early warning systems. This series of activities and achievements has been reported briefly in an article published by the United Nations Asian and Pacific Centre for Transfer of Technology (UN-APCTT) to provide guidelines and resource for policy makers (Koh *et al.*, 2007).

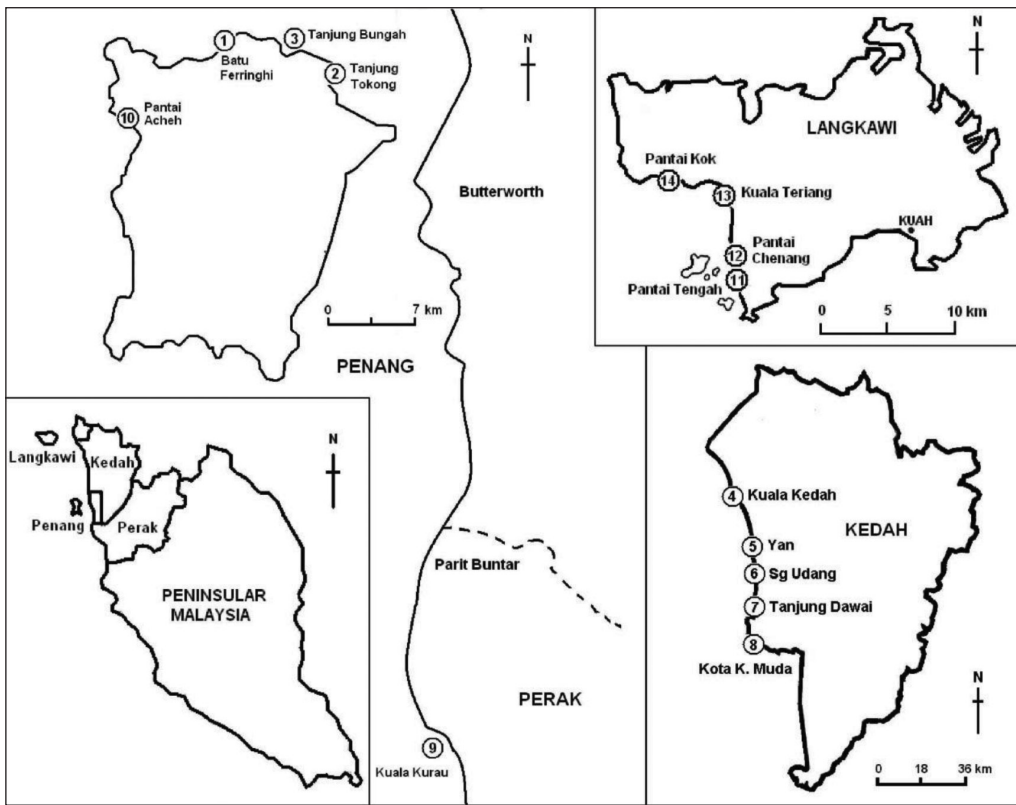


Fig. 1: Survey locations in Malaysia (Koh *et al.*, 2009)

TUNA is a simulation model that is based on Shallow Water Equation (SWE), as briefly described below. The model consists of a conservation of mass and momentum equations that have been depth averaged. Tsunami propagation fulfils the requirements that are necessary to permit the use of the SWE (Herbert *et al.*, 2005; Koh *et al.*, 2009) and hence may be described by the following SWE equations (Equations 1 to 3).

$$\frac{\partial \eta}{\partial t} + \frac{\partial M}{\partial x} + \frac{\partial N}{\partial y} = 0 \quad (1)$$

$$\frac{\partial M}{\partial t} + \frac{\partial}{\partial x} \left( \frac{M^2}{D} \right) + \frac{\partial}{\partial y} \left( \frac{MN}{D} \right) + gD \frac{\partial \eta}{\partial x} + \frac{gn^2}{D^{2/3}} M \sqrt{M^2 + N^2} = 0 \quad (2)$$

$$\frac{\partial N}{\partial t} + \frac{\partial}{\partial x} \left( \frac{MN}{D} \right) + \frac{\partial}{\partial y} \left( \frac{N^2}{D} \right) + gD \frac{\partial \eta}{\partial y} + \frac{gn^2}{D^{2/3}} N \sqrt{M^2 + N^2} = 0 \quad (3)$$

Here, the volume fluxes per unit length ( $M, N$ ) in the  $x$ - and  $y$ - directions are related to depth averaged velocities  $u$  and  $v$  by the expressions  $M = u(h+\eta) = uD$ , and  $N = v(h+\eta) = vD$ , where  $h$  is the mean sea depth and  $\eta$  is the water elevation associated with tsunami. Note that  $g$  is the gravitational acceleration and  $D$  is the total water depth ( $D = h+\eta$ ). Further details are available elsewhere (IOC 1997; Teh *et al.*, 2009). TUNA was successfully applied to simulate the impact of the 2004 Andaman tsunami. Fig. 2 illustrates snapshots of the 2004 Andaman tsunami propagation,

beginning at the coast off Banda Aceh propagating to Penang and Langkawi and into the Straits of Malacca. At the initialization of the tsunami (the first frame of *Fig. 2*), the initial tsunami waves split into two fronts, one moving eastwards towards Malaysia and Thailand, while the second propagating westwards towards Sri Lanka and India. The waves moving eastwards are the leading depression N waves, while those moving westwards are the leading elevation N waves. One and a half hour after the earthquake (frame 2 in *Fig. 2*), the waves reached the offshore of Phuket at the depth of about 50 m, with a leading depression and a surface elevation soon behind. These waves continued to move closer to land, propagating into the Straits of Malacca and moving closer to Langkawi. Three hours after the initiation of the tsunami, the waves reached the coast of Langkawi (frame 3) and propagated towards Penang Island. Four hours after the occurrence of the tsunami (frame 4), the waves propagated almost halfway through the Straits of Malacca.

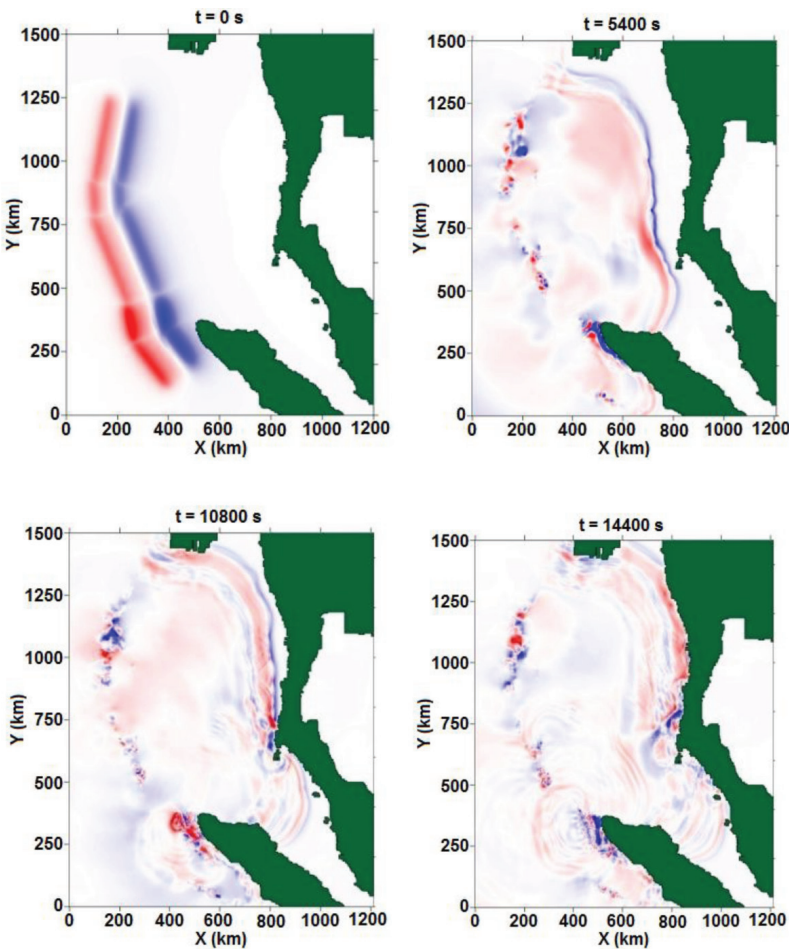


*Fig. 2: Tsunami snapshots by TUNA for 2004 Andaman tsunami*

To simulate the wave runup along the dry beaches, the Non-Linear Shallow Water Equations (NLWE) are used (Equations 4 and 5). Extensive simulations of TUNA indicate that the tsunami wave heights might be amplified as the waves propagated up the shallow seas and onto the dry

beaches. The maximum amplification factor of 3.3 to 3.5 was observed in the simulation results, with the maximum inundation distance of about 60 m to 80 m recorded, depending on the bathymetry and other parameters used in these simulations. In general, the simulated wave heights off the coast of Penang at a depth of around 50 m might reach a maximum of 1.0 to 1.2 m, while the runup wave heights might achieve the maximum of 3.3 to 4.0 m. These TUNA simulated runup wave heights are consistent with the range of the runup wave heights recorded, being in the range of 2.3 to 4.0 m surveyed along the beaches in Penang and Kedah after the 26 December 2004 tsunami. The simulated inundation distance of about 60 to 80 m is consistent with the recorded range of the measured inundation distances of 20 to 100 m, which was surveyed after the 2004 Andaman tsunami.

### THE ROLE OF MANGROVE

Mangrove forests have been observed to play a role in reducing tsunami wave heights if the heights are not too high, or are less than 3 m. Hence, these motivated the numerical analysis on the role of mangrove in reducing the adverse impact of tsunamis. For this purpose, a numerical simulation model was developed within the framework of TUNA (Koh *et al.*, 2009). The 1D continuity and momentum equations in flux forms in the x-direction are expressed as Equations (4) and (5), respectively. The last term in Equation (5) is the resistance force used to model the effects of coastal vegetation, such as mangroves (Mazda *et al.*, 1997; Massel *et al.*, 1999). The drag coefficient  $C_D$  used in the model of the present study is estimated by using Equation (6) while inertia coefficient  $C_M = 1.7$  is used (Harada & Imamura, 2000; Hiraishi & Harada, 2003; Harada & Kawata, 2004). There are other estimates of the drag coefficient  $C_D$  used (Quartel *et al.*, 2007). Equations (4) and (5) are then solved by the finite difference approximation in the runup model TUNA-RP, with the inclusion of mangrove friction term.

$$\frac{\partial \eta}{\partial t} + \frac{\partial M}{\partial x} = 0 \quad (4)$$

$$\frac{\partial M}{\partial t} + \frac{\partial}{\partial x} \left( \frac{M^2}{D} \right) + gD \frac{\partial \eta}{\partial x} + \frac{gn^2 M |M|}{D^{1/3}} + \frac{C_D}{2} A_0 \left( \frac{M |M|}{D^2} \right) + C_M \frac{V_0}{V} \frac{\partial M}{\partial t} = 0 \quad (5)$$

$$C_D = 8.4 \frac{V_0}{V} + 0.66 \left( 0.01 \leq \frac{V_0}{V} \leq 0.07 \right); \quad (6)$$

In the above,

$M$  = flow flux,  $m^2/s$ ;

$D = (\eta+h)$  = total water depth, m;

$h$  = still water depth, m;

$n$  = Manning coefficient;

$g$  = gravitational acceleration,  $m/s^2$ ;

$C_D$  = drag coefficient;

$A_0$  = projected area of trees under water surface, per 100 m<sup>2</sup>;

$V_0$  = total volume of tree under water surface (m<sup>3</sup>);

$V$  = control volume (m<sup>3</sup>);

$C_M$  = inertia coefficient.

The role of mangrove forests in reducing the impacts of tsunami waves is demonstrated in this section. The incident solitary wave is a positive half sine curve with a wavelength  $L = 12000$  m, period  $T = 0.15$  hr and amplitude  $a = 1$  m. This wave enters the computational domain at 0 hour

and distance 0 m from the left, with a depth  $h = 50$  m, and travels a distance of 10000 m along this flat seabed before it begins its climb at the toe of the slope at 10000 m. The concave slope, with an average slope of 1:40, has a horizontal length of 2000 m, climbing 49 m along this stretch. A healthy and vibrant mangrove forest is located between 12000 m and 13000 m. Fig. 3 shows snapshots of wave heights  $\eta$  at the interval of 0.05 hour. The wave propagates into the computational domain at 0.15 hours (Fig. 3a) and amplifies to 1.8 m at 0.20 hours (Fig. 3b). The presence of a patch of mangrove amplifies the wave heights to 2.5 m in front of the mangrove due to reduced velocity but with a much-reduced wave behind the forests (Fig. 3c). A sharp gradient subsequently causes strong back flows that reduce the height to merely 1.2 m (Fig. 3d), with smaller waves behind the mangroves. This result is consistent with the reported findings.

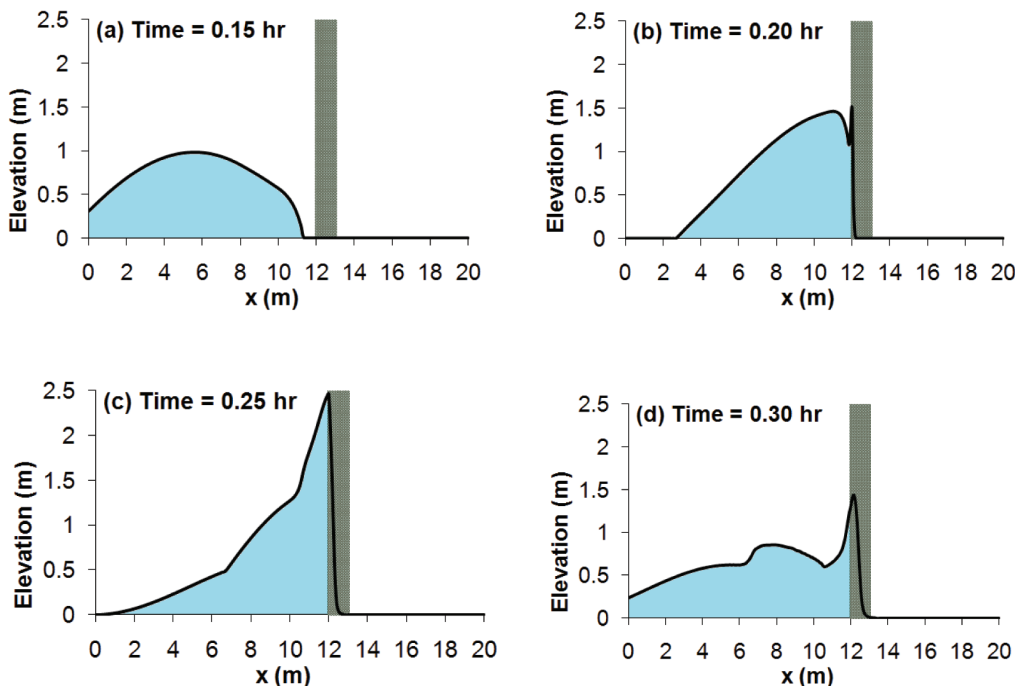


Fig. 3: Waveforms at an interval of 0.05 hr with mangrove forest between 12 and 13 km

#### MANHAM

It was observed during the surveys that significant stretches of coastal land in Kedah were extensively exposed to saline seawater brought to coastal lane by the Andaman tsunami. This seawater inundation has resulted in a sharp increase in the salinity of the coastal soil, leading to the land being unsuitable for cultivation of crops such as rice. This salinity inundation is clearly observed in Aceh of Indonesia after the 2004 Andaman tsunami, as it is also commonly seen in other places as well, following large storm surges or inundation by hurricanes. Hence, the study team initiated a research programme on simulating salinity intrusion and its impacts on coastal vegetation. For this purpose, a simulation model known as MANHAM was developed with a collaboration with the scientists from South Florida (Koh *et al.*, 2011; Teh *et al.*, 2008; Sternberg *et al.*, 2007). The results are briefly presented in the subsequent paragraph.

A large tsunami may and will often inundate vast tracks of coastal lands with large volumes of highly saline seawater, thereby changing the salinity regimes. Changes in salinity regimes may induce changes in the coastal vegetation types. Further, mega tsunami may destroy coastal vegetations instantly, giving rise to coastal vegetative successions. This will lead to alteration to coastal ecosystem dynamics. In Malaysia and Indonesia, the 2004 Andaman tsunami has destroyed the stretches of the coastal mangrove forests, exposing the coastal regions to the vagaries of the seas. Thus, rehabilitation and recovery of these coastal mangrove forests is an important element in any effort to develop tsunami resilient communities (Levy & Gopalakrishnan, 2005). Hence, the current research was extended to the study and analysis, via modelling and simulation, on the recovery and succession dynamics of the coastal mangrove forests. To investigate the effects of the increased salinity in the vadose zone, due to storm surge on mangroves and hardwood hammocks, a storm surge was assumed to take place, flooding the entire study domain for one day. Several intensities of the storm surge were also employed in the simulations, ranging from a light surge that saturates the vadose zone homogeneously at 7.5 ppt to a heavy surge event that saturates the vadose zone at 30 ppt. A medium surge saturates the vadose zone at 15 ppt. After the inundation, natural processes of precipitation, tides, and evapotranspiration interact to affect salinity in the soil, and thus, inducing vegetation to undergo succession.

Under stable environmental conditions, where there were no major disturbances, such as storm surges that would cause a catastrophic shift of vegetation, the freshwater hardwood hammocks (white) occupied the higher elevation cells, while mangroves (green) occupied the lower elevation cells (which were frequently inundated by tides), except for some patches of mangroves at higher elevations (*Fig. 4a*). However, small amounts of biomass of the subdominant species remained in every spatial cell which could act like seeds in the event of an environmental change, such as a storm surge. In the event of a light surge, hardwood hammocks were able to restore the salinity to low levels in a short time period. Twenty years after the storm surge, hardwood hammocks still dominate the cells at higher elevation (*Fig. 4b*) compared to the case without a storm surge event (*Fig. 2a*). A medium surge event that saturates the vadose zone at 15 ppt causes the mangroves to invade the cells at higher elevation, which were initially dominated by hardwood hammocks (*Fig. 4c*). A heavy surge causes the mangroves to take over the entire study domain 20 years after the surge (*Fig. 4d*). Such vegetation succession patterns have been observed in many coastal zones co-occupied by freshwater and saltwater vegetations such as mangrove and hardwood hammock, respectively.

## SEISMIC RISK ANALYSIS

Sabah is affected by both regional and local earthquakes. Significant earthquakes from the Sulu and Celebes seas are periodically felt as slight tremors in Sabah. The USGS earthquake database shows a total of 221 with  $M>6$  within 1000 Km from Kota Kinabalu since 1973 (*Fig. 5*). The source of regional earthquakes for Sabah comes from the active subduction zones marked by the Manila Trench, Negros Trench, Sulu Trench, Cotabato Trench and North Sulawesi Trench (Tongkul, 1992; Tongkul, 1993; Tongkul, 2006).

Three light earthquakes were recorded within 100 Km radius of the Ulu Padas (Upper Padas) area in Sabah where the dam is located. One occurred near Pensiangan, Sabah, with a magnitude of  $m_b=4.1$ , another at Kuala Penyu, Sabah ( $m_b=4.5$ ) and the third at Long Semado, Sarawak ( $m_b=4.5$ ). The Pensiangan and Long Semado earthquakes appear to be associated with a southward extension of the NE-SW trending Ranau-Labuk Bay seismic zone. This reverse active fault was found near to the Upper Padas Hydroelectric Dam site.

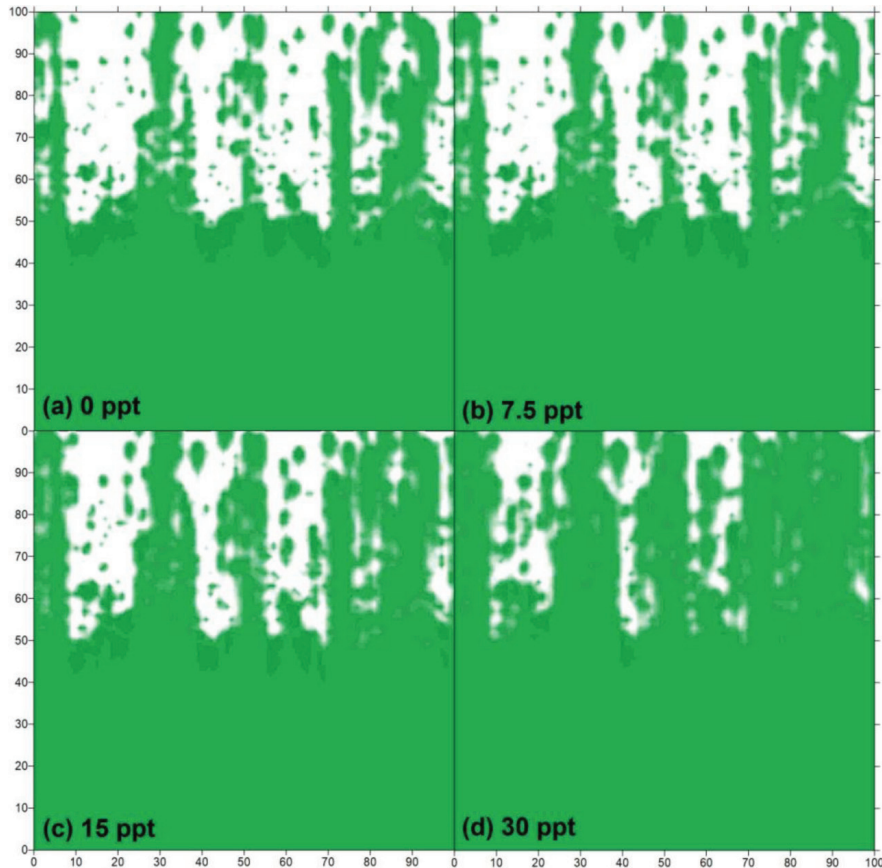


*Fig. 4: Distribution of mangroves (green) and hammocks (white) at the end of a 47-year simulation without a storm surge (0 ppt), and subject to storm surges that saturate the vadose zone homogeneously to the following levels of salinity for one day during year 27: light (7.5 ppt), medium (15 ppt) and heavy (30 ppt) surges*

The seismic hazard analysis of the Upper Padas Dam (*Fig. 6*) was conducted to define the earthquake design parameters needed for the structural analysis. The project site is located at longitude 115.8° East and latitude 4.8° North. The purpose was to develop a probabilistic seismic hazard analysis (PSHA) (McGuire 1995) and define the Operating Basis Earthquake (OBE), Maximum Considered Earthquake (MCE) and design earthquake (ICOLD 1983; ICOLD 1989). For an earthquake with an annual rate of exceedance of 0.00693 (OBE), or earthquake with probability of exceedance of 50% in 100 years, this PSHA study recommends an earthquake with PGA of 0.0263 g (=25.8 cm/s<sup>2</sup>) for the Upper Padas Hydropower Dam design. A previous study by Sweco International has recommended PGA of less than 50 cm/s<sup>2</sup>. Meanwhile, disaggregation of the seismic hazard of OBE (with 144 years return period) has shown that the design earthquake for OBE is an earthquake with a mean magnitude  $m_b$  of 5.4 and mean distance 145.1 km. This study also recommends the adoption of PGA of 0.0397g (=38.9 cm/s<sup>2</sup>) and/or 0.067 g (=65.8 cm/s<sup>2</sup>) for regular structures in the dam site area. Reservoir triggered seismicity is taken into account in defining design earthquake following ICOLD (2004). The seismic risk of the dam is predicted in the class of II (moderate) based on Bureau and Ballantine (2002).

**Earthquake Epicenter in Areas Surrounding Sabah & Sarawak  
(1973 - Present) (Source: USGS/NEIC Database)**

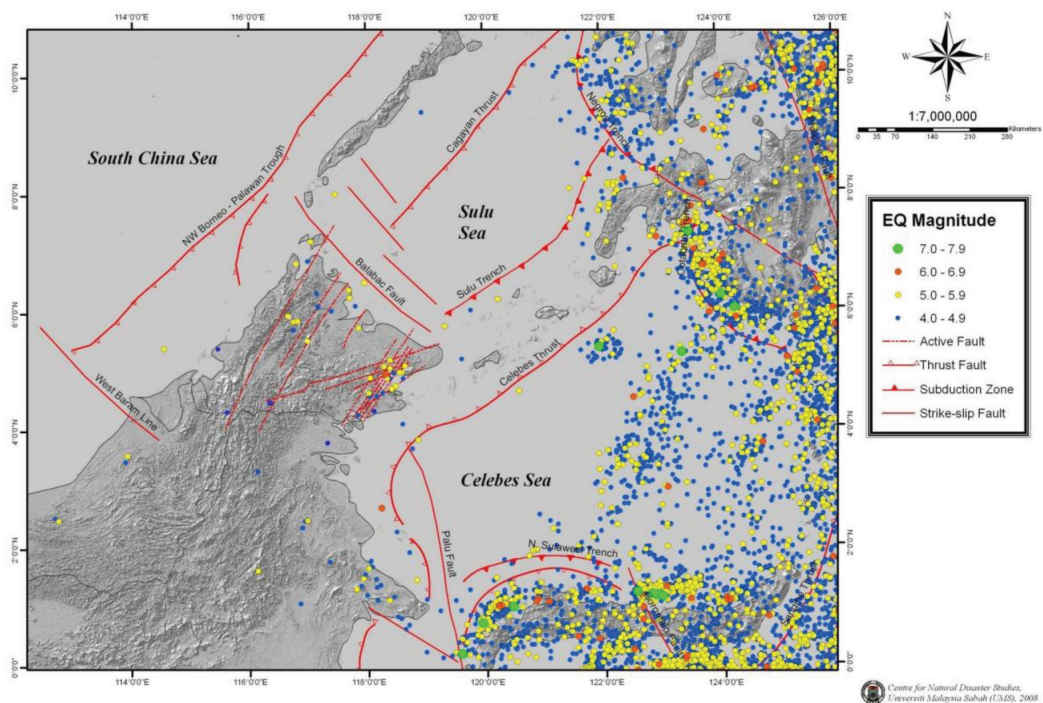


Fig. 5: Seismicity surrounding Sabah based on USGS/NEIC and JMG Databases.  
Earthquakes onshore Sabah are associated with NE-SW trending faults (NEIC, 2007)

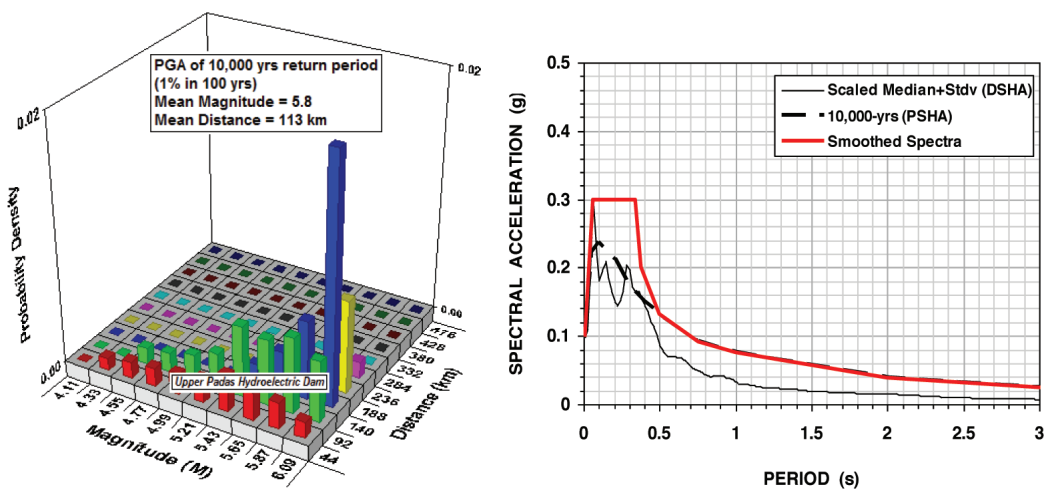
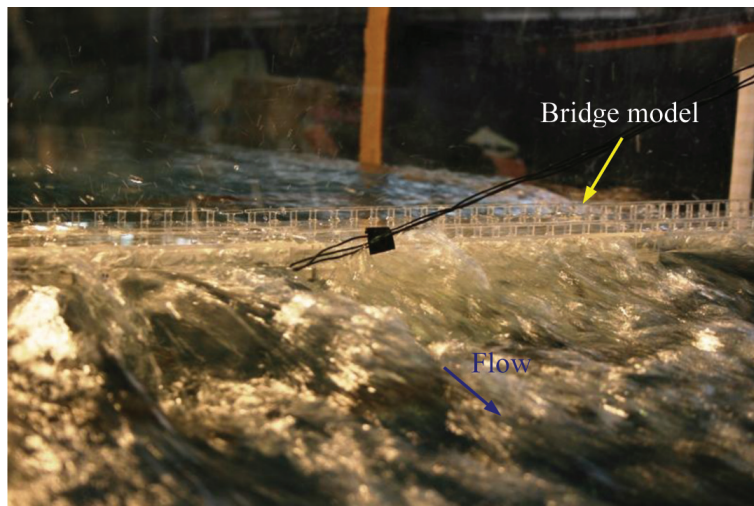


Fig. 6: Disaggregation of seismic hazard and design spectral acceleration for  
Upper Padas Dam

### TSUNAMI FORCE FOR ONSHORE STRUCTURES

To ensure integrity and stability of the coastal structures subject to tsunami attack, the determination of wave forces exerted on these structures is essential. When tsunami propagates to near-shore region, the wave breaks and transforms into turbulent bore. Turbulent bore exhibits complicated wave characteristics because it consists of irregular waves and substantial air entrainment. In the runup zone, tsunami advances as a dry-bed surge. Turbulent bores and dry-bed surges have distinctive characteristics and exert different forces on the structures (Yeh, 2007). Local bathymetry and topography are important factors that influence tsunami force on the structures. It is important to note that physical modelling is one of the practical approaches to study the tsunami-induced forces on the structures. Meanwhile, wave flume experiment was conducted to simulate tsunami with certain predicted characteristics. Local bathymetry and topography were also incorporated and the wave propagation towards the shoreline was analyzed. Wave height and flow velocity time histories were measured at various locations along the shoreline using wave gauges and current meters. The desired wave forces and wave pressures were then measured by attaching force transducers and pressure gauges on the structures. Solitary wave was used as a representative of tsunami in deep sea and the transformed turbulent bore in shallow water. An example of the physical simulation for tsunami attacking a bridge structure is shown in *Fig. 7*. A hydraulic analysis on an inland bridge subjected to tsunami is described in Lau *et al.* (2008).



*Fig. 7: Inland bridge subjected to tsunami*

However, the implementation of the physical modelling is time consuming, costly and is limited by certain feasible scales in the laboratory. Thus, an alternative is to perform numerical wave flume experiment on tsunami-structure interaction. A numerical simulation using computational fluid dynamic principles was successfully adopted to simulate tsunami flow in the numerical wave flume (Lau *et al.*, 2009). The experimental results obtained were then adopted to calibrate and validate the numerical model. In order to simulate tsunami-structure interaction, an I-girder bridge was incorporated in the numerical model, which was subsequently upgraded to the prototype scale. The simulated result for an inland bridge subjected to tsunami at various time frames is shown in *Fig. 8*. Detailed results of wave height, flow velocity, wave forces and pressures were obtained. The findings of the study have enhanced the understanding of tsunami interaction with the structures.

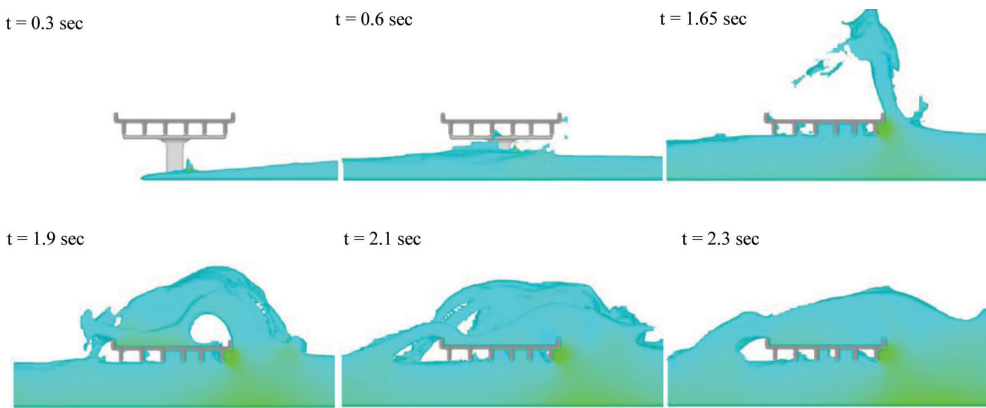


Fig. 8: Wave impingement on the bridge model

## CONCLUSION

This paper has presented a brief overview of the recently established Disaster Research Nexus (DRN) in Universiti Sains Malaysia (USM). Several research projects on earthquake and tsunami simulations within the scope of DRN have been successfully completed. It is hoped that this exposition will lead to active research collaborations among scientists working in similar areas of interest in the near future. The simulated results appear to agree with the runup heights surveyed soon after the 26 December 2004 tsunami. Therefore, TUNA may be used for tsunami simulation to provide propagation heights and runup heights.

## ACKNOWLEDGEMENT

The financial support provided for this study (Grants 1001/PMATHS/817024, 1001/PMATHS/817025, 1001/PMATHS/811093 and 302/PMATHS/611897) is gratefully acknowledged.

## REFERENCES

- Bureau, G., & Ballentine, G. D. (2002). A comprehensive seismic vulnerability and loss assessment of the state of south carolina using HAZUS. Part VI. Dam inventory and vulnerability assessment methodology, 7th National Conference on Earthquake Engineering, July 21–25, Boston, Earthquake Engineering Research Institute, Oakland, CA.
- Harada, K., & Imamura, F. (2000). *Experimental study on the resistance by mangrove under the unsteady flow*. Proceeding of the 1<sup>st</sup> Congress of APACE, p. 975-984.
- Harada, K., & Kawata, Y. (2004). Study on the effect of coastal forest to tsunami reduction. *Annals of Disas. Prev.*, Res. Inst., Kyoto Univ., No. 47 C.
- Hébert, H., Schindelé, F., Altinok, Y., Alpar, B., & Gazioglu, C. (2005). Tsunami hazard in the Marmara Sea (Turkey): a numerical approach to discuss active faulting and impact on the Istanbul coastal areas. *Marine Geology*, 215, 23-43.
- Hiraishi, T., & Harada, K. (2003). Greenbelt tsunami prevention in South-Pacific region. *Report of the Port and Airport Research Institute*, 42(2), 3-25.
- ICOLD (1983). ICOLD 46, Seismicity and dam design, Bulletin vol. 46, International Commission on Large Dams.

- ICOLD (1989). ICOLD 72. Selecting seismic parameters for large dams, *Bulletin*, 72, International Commission on Large Dams.
- ICOLD (2004). ICOLD 137, Reservoir and seismicity: state of knowledge, *Bulletin*, 137, International Commission on Large Dams.
- IOC (1997). Numerical Method of Tsunami Simulation with the Leap Frog Scheme, 1, Shallow Water Theory and Its Difference Scheme. In *Manuals and Guides of the IOC* (p. 12-19). Intergovernmental Oceanographic Commission, UNESCO, Paris.
- Koh, H. L., Teh, S. Y., & Izani, A. M. I. (2007). Tsunami Mitigation Management. Special Feature: Natural Disaster Management Technologies. The United Nations Asian and Pacific Centre for Transfer of Technology (UN-APCTT) Nov-Dec 2007, *Asia Pacific Tech Monitor* 24(6), 47-54.
- Koh, H. L., Teh, S. Y., Liu, P. L.-F., Izani, A. M. I., & Lee, H. L. (2009). Simulation of Andaman 2004 Tsunami for Assessing Impact on Malaysia. *Journal of Asian Earth Sciences*, 36(1), 74-83.
- Koh, H. L., Teh, S. Y., Liu, P. L.-F., & Che Abas, M. R. (2010). Tsunami Simulation Research and Mitigation Programs in Malaysia Post 2004 Andaman Tsunami. In N. Veitch, & G. Jaffray (Eds.), *Tsunamis: Causes, Characteristics and Warnings, and Protection* (Chapter 2, pp. 29-56). New York: Nova Science Publishers, Inc., Hauppauge.
- Koh, H. L., DeAngelis, D. L., & Teh, S. Y. (2011). Mangrove Wetland Ecosystem Modeling in the Everglades. In James N. Metras (Ed.), *Mangroves: Ecology, Biology and Taxonomy*. Nova Science Publishers, Inc., Hauppauge, New York.
- Lau, T. L., Lukkunaprasit, P., Ruanggrassamee, A., & Ohmachi, T. (2008). *Physical Modeling: An Estimation of Wave Forces on an Inland Bridge Subject to Tsunami Bores*. Proceedings of the 5<sup>th</sup> International Conference on Urban Earthquake Engineering, Tokyo, Japan, March 4-5, pp. 441-446.
- Lau, T. L., Ohmachi, T., & Inoue, S. (2009). *Numerical Simulation of Tsunami Flow around I-Girder Bridge Decks*. Proceedings of the 6<sup>th</sup> International Conference on Urban Earthquake Engineering, Tokyo, Japan, March 3-4, 2009, pp. 823-828.
- Levy, J. K., & Gopalakrishnan, C. (2005). Promoting Disaster-resilient Communities: The Great Sumatra-Andaman Earthquake of 26 December 2004 and the Resulting Indian Ocean Tsunami. *International Journal of Water Resources Development*, 21(4), 543-559.
- Massel, S. R., Furukawa, K., & Brinkman, R. M. (1999). Surface wave propagation in mangrove forests. *Fluid Dynamics Research*, 24(4), 219-249.
- Mazda, Y., Wolanski, E., King, B., Sase, A., Ohtsuka, D., & Magi, M. (1997). Drag force due to vegetation in mangrove swamps. *Mangroves and Salt Marshes*, 1, 193-199.
- McGuire, R. K. (1995). Probabilistic Seismic Hazard Analysis and Design Earthquakes: Closing the Loop. *Bulletin of the Seismological Society of America*, 85(5), 1275-1284.
- NEIC (2007). Earthquake database. National Earthquake Information Center. Available at <http://neic.usgs.gov/neic/epic>.
- Quartel, S., Kroon, A., Augustinus, P. G. E. F., Van Santen, P., & Tri, N. H. (2007). Wave attenuation in coastal mangroves in the Red River Delta, Vietnam. *Journal of Asian Earth Sciences* 29(4), 576-584.
- Sternberg, L., Teh, S. Y., Ewe, S., Miralles-Wilhelm, F., & DeAngelis, D. (2007). Competition between Hardwood Hammocks and Mangroves. *Ecosystems*, 10(4), 648-660.
- Teh, S. Y., DeAngelis, D., Sternberg, L., Miralles-Wilhelm, F. R., Smith, T. J., & Koh, H. L. (2008). A Simulation Model for Projecting Changes in Salinity Concentrations and Species Dominance in the Coastal Margin Habitats of the Everglades. *Ecological Modelling*, 213(2), 245-256.

Earthquake and Tsunami Research in USM: The Role of Disaster Research Nexus

- Teh, S. Y., Koh, H. L., Liu, P. L.-F., Izani, A. M. I., & Lee, H. L. (2009). Analytical and Numerical Simulation of Tsunami Mitigation by Mangroves in Penang, Malaysia. *Journal of Asian Earth Sciences*, 36(1), 38-46.
- Tongkul, F. (1992). The Ranau earthquake: possible causes. *Sabah Society Journal*, 9(4), 315-322.
- Tongkul, F. (1993). Tectonic control on the development of the Neogene basins in Sabah, Malaysia. *Bulletin of Geological Society of Malaysia*, 33, 95-103.
- Tongkul, F. (2006). The structural style of Lower Miocene sedimentary rocks, Kudat Peninsula, Sabah. *Bulletin of the Geological Society of Malaysia*, 49, 119-124.
- Yeh, H. (2007). Design tsunami forces for onshore structures. *Journal of Disaster Research*, 2(6), 531-536.



## Synthesis of *Jatropha curcas*-based Methyl Ester and Ethyl Ester as Biodiesel Feedstocks

Azhari Muhammad Syam, Robiah Yunus\*, Tinia Idaty Mohd. Ghazi and Thomas Choong Shean Yaw

Department of Chemical and Environmental Engineering,  
Faculty of Engineering, Universiti Putra Malaysia,  
43400 Serdang, Selangor, Malaysia  
\*E-mail: robiah@eng.upm.edu.my

### ABSTRACT

Research on the use of *Jatropha curcas* triglycerides as biodiesel feedstock has received worldwide attention due to its inherent characteristics. Unlike palm oil, *J. curcas* oil is not edible, and thus, it will not disturb the food supply. However, to the researchers' experiences with the synthesis of *J. curcas*, oil-based biodiesel has shown that the fuel characteristics depend largely on the type of alcohol used as the excess reactants. Transesterification reaction is chosen for this process with sodium methoxide as the catalyst. Comparison studies on the yield of esters using methanol and ethanol, as well as the impacts on the reaction rate are discussed. The effects of reaction time and molar ratio on the reaction conversion are also examined. The determination of reaction yield is based on the conversion of triglycerides into alkyl esters as the main product. The findings are described as follows: the highest percentage yield of product is attained at 96% for methanol as an excess reactant, and this is 90% when ethanol is used. The optimum conditions of parameters are achieved at 6:1 molar ratio of alcohol to triglycerides, 50 min of reaction time and reaction temperature of 65°C for methanol and 75°C for ethanol. The biodiesel properties of both ester fuels were determined according to the existing standards for biodiesel and compared to the characteristics of diesel fuel.

**Keywords:** *Jatropha curcas* triglycerides, methyl ester, ethyl ester, catalyst

### INTRODUCTION

Biodiesel is the product of the transesterification reaction between vegetable triglycerides and alcohol. It possesses many advantages as it is derived from a renewable and domestic resource. Among liquid bio-fuels, biodiesel is gaining acceptance and market share as diesel fuel (Demirbas, 2003). As an alternative fuel, biodiesel can be used in neat form or mixed with petroleum-based diesel. Compared to fossil-based diesel, biodiesel has a more favourable combustion emission profile, such as low emission of carbon monoxide, particulate matter and unburned hydrocarbon (Zhang *et al.*, 2003).

As one of the domestic commodities, vegetable oils have the potential to substitute a small fraction of petroleum distillates and petroleum based petrochemical in the future. According to Srivastava and Prasad (2000), the use of vegetable oil, such as palm, soy bean, sunflower, cotton seed, peanut, rapeseed, corn and castor oils as alternative fuels for diesel engines, dated back to almost nine decades ago. Generally, biodiesel feedstock was treated by using certain process technology to reduce the viscosity of product. The vegetable oil, triacylglycerol or is often called triglycerides, is a mixture of fatty acid triesters of glycerol (Tapanes *et al.*, 2008). The most common method used

---

Received: 18 April 2011

Accepted: 12 September 2011

\*Corresponding Author

to produce biodiesel is by transesterification which refers to a catalyzed chemical reaction involving vegetable triglycerides and alcohol to yield fatty acid alkyl esters and glycerol as by-product (Zhang *et al.*, 2003). Another term for this particular process is alcoholysis. This reaction method is carried out under atmospheric condition and the stepwise of reaction is as shown in equations (1) to (3). Normally, transesterification can be catalyzed by both homogeneous and heterogeneous catalysts.



where TG, DG, MG, GL, R and R' denote triglycerides, diglyceride, monoglyceride, glycerol, alkyl and long hydrocarbon chain, respectively.

Alkali catalysts are the most common, since the process is faster and the reaction conditions are moderate (Freedman *et al.*, 1984). Barnwal and Sharma (2005) reported that the alkali metal alkoxides are found to be effective transesterification catalysts as compared to acidic catalysts. Potassium and sodium hydroxide are the familiar homogeneous alkali catalysts applied in the transesterification of oil with very low free fatty acid content. The fatty acid composition of various types of vegetable triglycerides is given in Table 1. The characteristics of the triglycerides depend largely on the type of fatty acids present in the oil. Table 1 shows that *Jatropha curcas* and other vegetable triglycerides contain high percentages of unsaturated compounds, except for palm triglycerides. This finding indicates that these vegetable triglycerides are suitable to be used as biodiesel feedstock, specifically for low temperature applications. The catalyst type and loading required for the reaction are also dependent on the feedstock.

TABLE 1  
The chemical composition of vegetable triglycerides (Sources: <sup>b</sup>Tapanes *et al.*, 2008;  
<sup>c</sup>Crabbe *et al.*, 2001; <sup>a</sup>Srivastava & Prasad, 2000)

No	Vegetable triglycerides	Fatty acid composition, wt %				
		16:0	18:0	18:1	18:2	18:3
1	<i>Jatropha curcas</i> <sup>b</sup>	16	6-7	42-43.5	33-34.4	>0.80
2	Palm <sup>c</sup>	41-47	3.7-5.6	38.2-43.5	6.6-11.9	0.5
3	Corn <sup>a</sup>	12	2	25	61	0
4	Cottonseed <sup>a</sup>	28	1	13	58	0
5	Peanut <sup>a</sup>	11	2	48	32	1
6	Rapeseed <sup>a</sup>	3	1	64	22	8
7	Sunflower <sup>a</sup>	6	3	17	74	0
8	Soy bean <sup>a</sup>	12	3	23	55	6
9	Mahua <sup>a</sup>	16-28.2	20-25.1	41-51	8.9-13.7	0

Another important parameter in the selection of suitable vegetable oils for biodiesel feedstock is the FFA content of the feedstocks. In particular, feedstock with high content of FFA will trigger the incidence of saponification reaction to produce soap emulsion of which shall reduce the biodiesel yield and affect the recovery of the by-product (Schuchardt *et al.*, 1997). To avoid saponification reaction, the FFA content of feedstock should be less than 1.0% (Tiwari *et al.*, 2007). Berchmans and Hirata (2007) reported that the quality of *J. curcas* oil was degraded due to poor handling and long storage period prior to utilization. Various chemical reactions, such as hydrolysis, polymerization

## Synthesis of Jatropha curcas-based Methyl Ester and Ethyl Ester as Biodiesel Feedstocks

and oxidation, cause deterioration in the quality of oil. The increase of free fatty acid value was due to the hydrolysis of triglycerides in the presence of moisture and oxidation. The triglycerides should be treated via acidic pre-treatment step to lower the percentage of FFA and improve the quality so that it could be used directly as the feedstock for biodiesel production (Azhari *et al.*, 2008).

The main objective of this experimental work was to determine the optimum condition for biodiesel production using two types of alcohol derivatives, namely methanol and ethanol. Finally, the properties of the biodiesel were analyzed according to the standard methods.

## MATERIALS AND METHODS

### Materials

*Jatropha curcas* oil (triglycerides) was produced using a multi-purpose solvent extractor. The isopropanol of 99.7% purity (Systerm), sulphuric acid of 98% (Fisher Scientific), phenolphthalein of 1% (Systerm) and potassium hydroxide of 99% purity (Systerm) were used for the FFA pre-treatment. The acidic pre-treatment process was aimed to decrease the FFA percentage of the biodiesel feedstock. The raw *J. curcas* triglycerides used in this experimental work contained 20.6% of FFA. The esterified *J. curcas* triglycerides have about 0.6% of the FFA content. Meanwhile, sodium methoxide (Systerm) was utilized as the catalyst in transesterification reaction, and methanol of 99.8% purity (R&M Chemicals) was used for both esterification and transesterification. Ethanol of 99.5% purity (Systerm) was only used for transesterification. Ethyl acetate and N,O-Bis(trimethylsilyl) trifluoroacetamide (BSTFA) were from Fluka for sample preparation. In this study, the percentage of the catalyst loading for the entire experiments was fixed at 1.0% w/w, whereas, the alcohol to triglycerides molar ratio was varied from 4:1 until 7:1. Experiments were conducted using the following equipments; batch reactor, separator funnel, burette and other related glass ware.

### The Pre-treatment of *Jatropha curcas* Triglycerides

In this study, the pre-treatment step was carried out to reduce the FFA content of the *Jatropha curcas* oil (triglycerides) to below 1% (w/w). Firstly, the *J. curcas* oil was poured into the reactor and heated. The solution of sulphuric acid in methanol at concentrations 1.0% w/w was heated at 60 °C, and then added to the reactor containing the heated oil. The ratio of methanol to *J. curcas* oil was 60% w/w and the time taken for the pre-treatment was 180 minutes. After the reaction was completed, the mixture was allowed to settle down for 2 h and the methanol water fraction at the top layer was removed. The feedstock with the lowest acid value was then utilized in the subsequent transesterification reaction to produce biodiesel (Azhari *et al.*, 2008).

### Experimental Procedure

The reactor was initially charged with the desired amount of feedstock (50 g) and heated to 65 °C using a water bath under constant temperature (*Fig. 2*). The mixture of alcohol (methanol or ethanol) and catalyst was then added to the reactor at which the reaction was assumed to commence. The unreacted alcohol and catalyst were removed via washing process. The complete biodiesel production process is illustrated in *Fig. 1*.

### Analytical Methods

The FFA percentage of the feedstock was analyzed using acid based titration technique with 0.1 N of alkali as the standard solution. 2.5 g of *J. curcas* oil was weighed for the analysis after which the

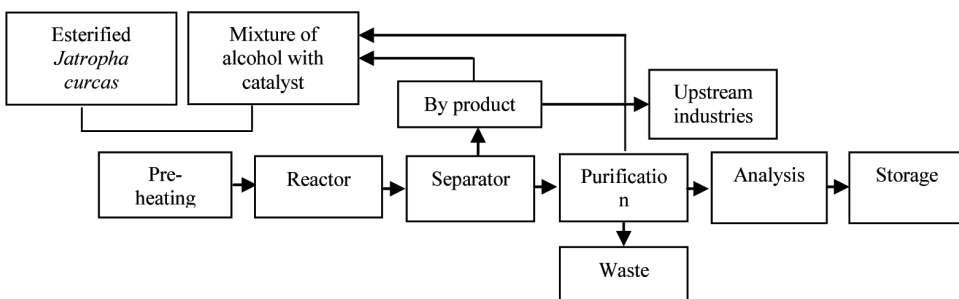


Fig. 1: Schematic of biodiesel production process

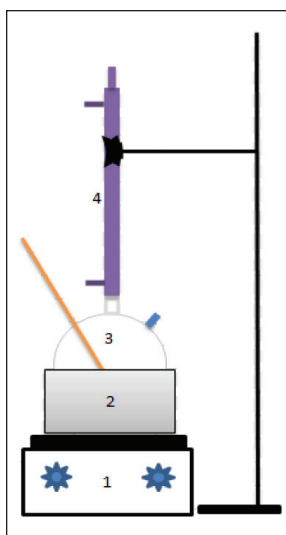


Fig. 2: Schematic of reactor configuration; (1) Heater c/w stirrer, (2) Water bath, (3) Batch reactor, and (4) Graham condenser

neutralized solvent was added into the sample. The sample was then shaken gently while titrating with the standard solution until the first permanent colour appeared (Lin *et al.*, 1995).

The analysis of the products was conducted using gas chromatography (Agilent 6890 Series), with capillary column SGE 12m × 0.53mm, 0.15µm ID column HT5 (SGE, Australia, Pty. Ltd.), with hydrogen at 26.7 ml/min as a carrier gas and a split ratio of 1:1. The oven temperature was set at an initial temperature of 80 °C, held for 3 minutes, increased from 6°C/min to 340 °C and held for 6 more minutes. The injector and detector temperatures were 300 °C and 360 °C, respectively (Yunus *et al.*, 2002).

## RESULTS AND DISCUSSION

### *The Effects of Alcohol Molar Ratio and Temperature*

In this experimental work, the initial content of FFA in *Jatropha curcas* triglycerides was 20.6 %. After the pre-treatment step, it was reduced to an acceptable level (less than 1.0%) prior to

transesterification reaction. This stage was conducted via esterification of *J. curcas* triglycerides with alcohol and mineral acid as the catalyst.

The effect of alcohol molar ratio on *J. curcas* oil (triglycerides) (JCO) plays a significant role on the yield of alkyl esters (biodiesel). In this reaction, the alcohol derivatives chosen for the study were methanol and ethanol. The reaction stoichiometry of *J. curcas* triglycerides requires three moles of alcohol to react with one mole of triglycerides to yield three moles of fatty acid alkyl esters and one mole of glycerine. Based on the thermodynamic equilibrium, a large excess of alcohol is required to force the reaction to the right so that it will be in favour of biodiesel production. Based on the yield of the product, the maximum molar ratio employed in this experimental work was seven folds. The effects of methanol to the JCO molar ratio on the yield of methyl esters formed from alcoholysis were investigated at various amounts of excess methanol and reaction temperatures (see Fig. 3).

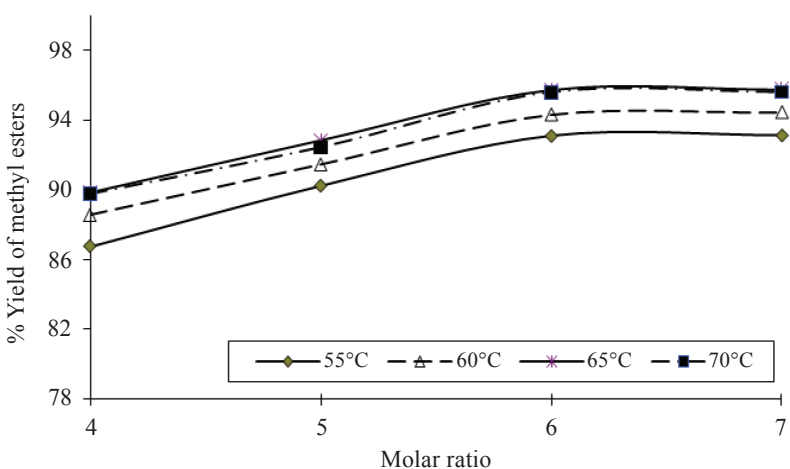
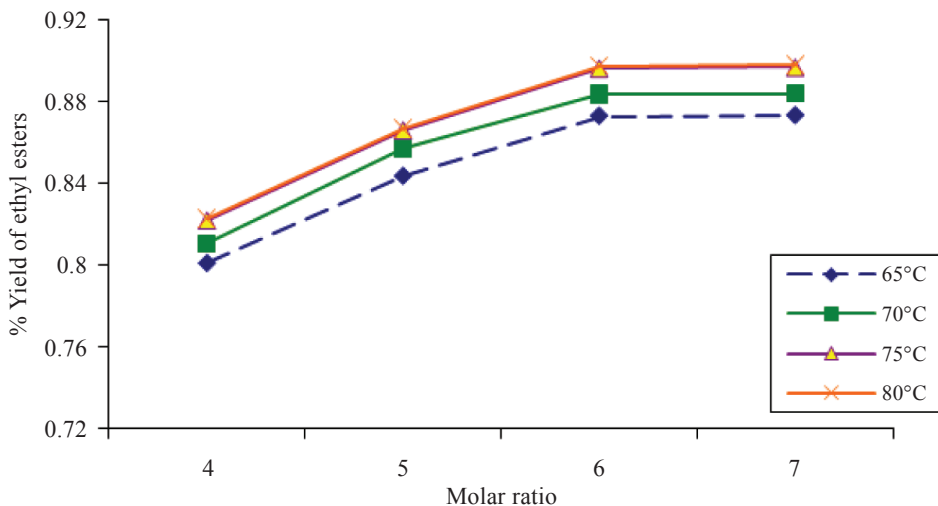


Fig. 3: The effect of methanol to JCO molar ratio at various temperatures (catalyst loading at 1% w/w)

The maximum reaction yield at all the temperatures is achieved at a molar ratio of 6:1, as shown in Fig. 3 and 4. At lower molar ratios, an incomplete conversion is apparent since the percentage yield of *J. curcas* triglycerides is only 86.7% for the reaction using methanol, while the lowest yield was recorded at 80% for the ethanol. This indicates that a higher molar ratio of the excess reactant to *J. curcas* triglycerides has resulted in a better transesterification reaction until it reaches the optimum value at 6:1 molar ratio for both the alcohol derivatives. Since the transesterification process is a reversible reaction, the increase in the amount of alcohol will shift the reaction to the right, and this further promotes a formation of alkyl esters. The use of excess reactant results in a significant improvement on the product yield. The highest product yield was recorded at 96% using methanol and this was 90% using ethanol (see Fig. 4). This could be due to the difference in the molecular structure of methanol and ethanol. In more specific, the two carbon chains in the hydrocarbon structure of ethanol have caused more energy and time to be required to form ethoxide ion as compared to methanol which possesses a single carbon chain. In a similar study by Tapanes *et al.* (2008), a slower reaction rate was reported using ethanol as an excess reactant compared to methanol.

Fig. 3 and 4 also show that the optimum temperatures for the transesterification reactions for methanol and ethanol are 65°C and 75°C, respectively. Above these temperatures, the reactions are no longer effective because of the boiling point constraints of these alcohols.



*Fig. 4: The effect of ethanol to JCO molar ratio at various temperatures (catalyst loading at 1% w/w)*

#### *The Effect of Reaction Time*

Fig. 5 shows the progress of transesterification reaction at various operating temperatures. The reaction was slow during the early part of the reaction due to the time taken for the mixing and dispersion of alcohol into *J. curcas* oil. However, the reaction progressed rapidly after 20 min until the equilibrium was reached at about 40 min of reaction. This phenomenon demonstrates the reaction pathways which take place during the step wise transesterification process to produce biodiesel. There have not been many discussions done on reaction pathways using sodium methoxide catalyst. However, Freedman *et al.* (1984) reported that the reactions of soybean and sunflower triglycerides with the methoxide catalyst were very fast at the initial part of the reaction. Other researchers have also reported that the difference between the reaction rates should be in the pre-step, where the alkoxide is formed. Figure 5 also shows that since ethoxide is stronger than methoxide, the formation of methoxide ion is easier than ethoxide ion (Tapanes *et al.*, 2008), and thus, producing a higher product yield.

The effect of temperature was also examined and is shown in Fig. 5. As discussed earlier, the biodiesel yield is affected by the reaction temperature. Since the reaction is endothermic, high temperature increases the rate of reaction. Although the curves show that the rate of reaction increases with temperature, the properties of the alcohol limit the maximum temperature allowable for the reaction. Above its boiling point, the alcohol will vaporize and thus, a disequilibrium condition takes place and thus results in a lower rate of reaction. In this study, the optimum reaction temperature is 65°C for methanol and this is 75°C for ethanol.

#### *The Properties of Jatropha curcas Biodiesel*

According to Kinast (2003), the potential of methyl and ethyl esters as biodiesel feedstocks is dependent on its quality and must be comparable to the biodiesel standards of certain countries. The properties which define the quality of biodiesel are also used for mineral oil based diesel fuel. Since biodiesel can be produced from vegetable oil of varying origins and quality, it is necessary to have a fuel quality standard to guarantee engine performance and also as a prerequisite for a

## Synthesis of Jatropha curcas-based Methyl Ester and Ethyl Ester as Biodiesel Feedstocks

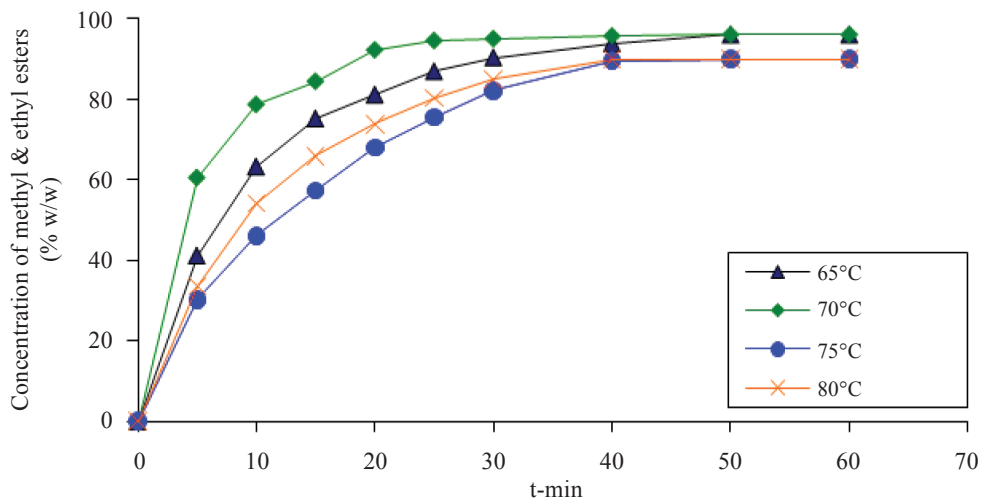


Fig. 5: The effect of reaction time on the concentration of Jatropha curcas methyl and ethyl esters at various temperatures (amount of catalyst loading is 1% w/w)

successful market penetration of biodiesel (Srivastava & Prasad, 2000; Meher *et al.*, 2004). Table 2 presents the properties of the *J. curcas*-based biodiesel and a comparison to the characteristics of fossil-based diesel fuel.

In this study, the physical properties of *J. curcas* alkyl esters, such as kinematics viscosity, density, flash point, pour point, cloud point, moisture content, iodine value, calorific value and acid number, were analyzed. The results show that the calorific value of *J. curcas* ethyl esters is comparable to that of the fossil diesel fuel. In addition, the flash point is higher than the diesel fuel. Although the iodine value of *J. curcas* alkyl esters is nearly comparable to that of the diesel fuel, the pour point and cloud point are slightly higher. In terms of viscosity, which controls the fuel injection, the biodiesel shows fairly higher values compared to the diesel fuel. This is good for engine lubrication. In correlation with ignition method, the flash point indicates the temperature

TABLE 2  
The physical properties of *Jatropha curcas* alkyl esters and their comparison to the characteristics of diesel fuel (Sources: <sup>a</sup>Pramanik, 2003; <sup>b</sup>Puhan *et al.*, 2005; <sup>c</sup>Ali & Hanna, 1994; <sup>d</sup>Ikwuagwu *et al.*, 2000; <sup>e</sup>Altin *et al.*, 2001).

No	Properties	JME*	JEE*	FDF*
1	Density (g/cc), 30°C	0.865	0.889	0.836-0.850 <sup>d</sup>
2	Kinematics viscosity (cSt)	4.33	5.46	2.4 <sup>c</sup>
3	Moisture content (%)	0.16	0.17	<0.05 <sup>f</sup>
4	Pour point, °C	-15	-10	-33 <sup>f</sup>
5	Cloud point, °C	-9	-4	-15 <sup>e</sup>
6	Flash point, °C	176	181	60 <sup>d</sup>
7	Iodine value	99	107	84 <sup>g</sup>
8	Calorific value, MJ/Kg	38.72	40.96	43 <sup>h</sup>
9	Acid number	0.14	0.56	0.02 <sup>g</sup>

\* JME = *Jatropha curcas* methyl esters, JEE = *Jatropha curcas* ethyl esters, FDF = Fossil-based diesel fuel

above which the fuel will ignite when exposed to a spark (Thompson *et al.*, 1998). The flash points for both biodiesels are higher than the diesel; thus, they are generally safer but most likely require special ignition devise for start up.

In a similar study, Knothe *et al.* (1996) reported that the neat vegetable oil and its methyl esters have nearly identical iodine values. As a result, biodiesel from vegetable oil with high content of unsaturated fatty acid compounds will have low pour point and cloud point. This degree unsaturation was selected as an important criterion for fatty acid alkyl esters. Furthermore, Azam *et al.* (2005) reported other significant characteristics which include kinematics viscosity, flash point, moisture content and acid number. Acid number is due to oxidative degradation of the substance. A few reports also highlighted that the oxidative degradation develops from the hydroperoxide toward secondary oxidation products. It is influenced by the nature of the original fatty substance (in terms of the number of double bounds) and its quality with particular reference to the presences of hydroperoxides, natural antioxidants, pro-oxidizing agents, as well as air and high temperature condition.

## CONCLUSION

The alcoholysis of *Jatropha curcas* triglycerides in the presence of sodium methoxide catalyst using ethanol and methanol as the excess reactants was studied. The results have shown that the rate of reaction and product yield are affected by the molar ratio of alcohol to JCO, reaction time and reaction temperature. Meanwhile, the difference in the molecular structure of the alcohols affects the product yield. The optimum operating conditions were molar ratio of alcohol to JCO at 6:1 and the optimum reaction time at 50 min. The highest percentage yield of product for methanol was achieved at 96%, whereas the highest product yield was 90% with ethanol. The properties of the *J. curcas*-based biodiesels were analysed and found to be comparable to that of the fossil-based diesel fuel.

## ACKNOWLEDGEMENTS

We acknowledge the financial support of the Higher Education Ministry of Malaysia through the Fundamental Research Grant Scheme.

## REFERENCES

- Ali, Y., & Hanna, M. A. (1994). Alternative diesel fuels from vegetable oils. *Bioresource Technology*, 50, 153-163.
- Altin, R., Çetinkaya, S., & Yücesu, H. S. (2001). The potential of using vegetable oil fuels as fuel for diesel engines. *Energy Conversion & Management*, 42, 529-538.
- Azam, M. B., Waris, A., & Nahar, N. M. (2005). Prospects and potential of fatty acid methyl esters of some non-traditional seed oils for use as biodiesel in India. *Biomass & Bioenergy*, 29, 293-302.
- Azhari, Faiz, M., Yunus, R., Ghazi, T. I. M., & Choong, T. S. Y. (2008). Reduction of free fatty acids in crude *Jatropha curcas* oil via an esterification process. *International Journal of Engineering and Technology*, 5, 92-98.
- Barnwal, B. K., & Sharma, M. P. (2005). Prospects of biodiesel production from vegetable oils in India. *Renewable & Sustainable Energy Reviews*, 9, 363-378.
- Berchmans, H. J., & Hirata, S. (2007). Biodiesel production from crude *Jatropha curcas* L. seed oil with a high content of free fatty acids. *Bioresource Technology*, 99, 1716-1721.

Synthesis of Jatropha curcas-based Methyl Ester and Ethyl Ester as Biodiesel Feedstocks

- Canakci, M. (2007). The potential of restaurant waste lipids as biodiesel feedstocks. *Bioresource Technology*, 98(1), 183-190.
- Crabbe, E., Nolasco-Hipolito, C., Kobayashi, G., Sonomoto, K., & Ishizaki, A. (2001). Biodiesel production from crude palm oil and evaluation of butanol extraction and fuel properties. *Process Biochemistry*, 37, 65-71.
- Demirbaş, A. (2003). Biodiesel fuels from vegetable oils via catalytic and non-catalytic supercritical alcohol transesterifications and other methods: a survey. *Energy Conversion & Management*, 44, 2093-2109.
- Freedman, B., Pryde, E. H., & Mounts, T. L. (1984). Variables affecting the yields of fatty esters from transesterified vegetable oils. *Journal of the American Oil Chemists' Society*, 61(10), 1638-1643.
- Ikwuagwu, O. E., Ononogbu, I. C., & Njoku, O. U. (2000). Production of biodiesel using rubber [*Hevea brasiliensis* (Kunth. Muell.)] seed oil. *Industrial Crops and Products*, 12(1), 57-62.
- Kinast, J. A. (2003). *Production of biodiesels from multiple feedstocks and properties of biodiesels and biodiesel/diesel blends*. USA: National Renewable Energy Laboratory.
- Knothe, G., Dunn, R. O., & Bagby, M. O. (1996). Technical aspects of biodiesel standards. *INFORM*, 7, 827-829.
- Lin, S., W. Sue, T. T., & Ai, T. Y. (1995). *PORIM test methods* (p. 40-42). Malaysia: PORIM Press.
- Meher, L. C., Vidya, S. D., & Naik, S. N. (2004). Technical aspects of biodiesel production by transesterification – a review. *Renewable and Sustainable Energy Reviews*, 10(3), 248-268.
- Pramanik, K. (2003). Properties and use of Jatropha curcas oil and diesel fuel blends in compression ignition engine. *Renewable Energy*, 28(2), 239-248.
- Puhan, S., Vedaraman, N., Ram, B. P. B., Sankarnarayanan, G., & Jeychandran, K. (2005). Mahua oil (Madhuca India seed oil) methyl ester as biodiesel-preparation and emission characteristics. *Biomass & Bioenergy*, 28, 87-93.
- Schuchardt, U., Sercheli, R., & Vargas, R. M. (1997). Transesterification of vegetable oils: a review. *Journal of Brazilian Chemical Society*, 9(1), 199-210.
- Srivastave, A., & Prasad, R. (2000). Triglycerides-based diesel fuel. *Renewable and Sustainable Energy Reviews*, 4, 111-133.
- Tapanes, N. O., Aranda, D. G., de Mesquita Carneiro, J. W., & Antunes, O. A. C. (2008). Transesterification of Jatropha curcas oil glycerides: theoretical and experimental studies of biodiesel reaction. *Fuel*, 87, 2286-2295.
- Thompson, J. C., Peterson, C. L., Reece, D. L., & Beck, S. M. (1998). Two-year storage study with methyl and ethyl ester of rapeseed. *Transactions of the American Society Agricultural Engineers*, 41, 931-939.
- Tiwari, A. K., Kumar, A., & Raheman, H. (2007). Biodiesel production from Jatropha oil (Jatropha curcas) with high free fatty acids: an optimized process. *Biomass & Bioenergy*, 31, 569-575.
- Yunus, R., Fakhru'l-Razi, A., OOI, T., & Basri, S. (2002). A simple capillary column gas chromatography method for analysis of palm oil-based polyol esters. *Journal of the American Oil Chemists' Society*, 79, 1075-1080.
- Zhang, Y., Dubé, M. A., McLean, D. D., & Kates, M. (2003). Biodiesel production from waste cooking oil: 1. process design and technology assessment. *Bioresource Technology*, 89, 1-16.



## New Vane-Type Wind Turbine of High Efficiency

R. Usubamatov\*, A. Y. Qasim and Z. M. Zain

School of Manufacturing Engineering, University Malaysia Perlis,  
Kampus Tetap, Ulu Pauh, Arau, 02600 Perlis, Malaysia.

\*E-mail: ryspek@unimap.edu.my

### ABSTRACT

Wind energy has often been touted as one of the most reliable sources of renewable energy that should be used for people. Today, wind energy (mainly by propeller type wind turbines) produces less than one percent of the total energy used worldwide. Practically, a standard three-blade propellers efficiency of use of the wind energy is around twenty percents and this is due to its design and shape that use the wind lift force and a rotating turbine. In addition, these turbines are quite expensive due to the complex aerodynamic shape of the propellers which are made of composite materials. The new world boom for wind turbines obliges inventors to create new wind turbine designs that have high efficiency and are better than any known design. This paper proposes the new patented invention of the vane-type wind turbine which uses wind energy more efficiently and is only dependent on the acting area of the vanes. The vane wind turbine was designed to increase the output of a wind turbine that uses kinetic energy of the wind. Due to its high efficiency, simple construction and technology, the vane wind turbine can be used universally, apart from the fact that it is made from cheap materials. The new design of the vane-type wind turbine has quite small sizes than the propeller type one of same output power.

**Keywords:** Wind turbine, vane

### INTRODUCTION

Wind power is the conversion of wind kinetic energy into a useful form, such as mechanical or electrical energy that can be harnessed for practical use using wind turbines. Wind energy is one of the cheapest and cleanest of the renewable energy technologies compared to all other known types. The potential energy created by wind power is plentiful, and helps to reduce greenhouse gas emissions when it displaces fossil fuel derived electricity. The wind turbine technology has steadily improved. Typical capacity for a single unit is now 250-500 KW. The competitiveness and environmental advantages of wind energy are obvious (Cermak, 1975).

Designing a wind turbine system that can generate power with a high efficiency requires a thorough understanding of the principles of aerodynamics and the structural dynamics of the rotor system. Various wind turbine mechanisms have been proposed and built for capturing and converting the kinetic energy of wind. In area of the wind energy, there are three basic types of the wind turbine that are commonly used today. These include the horizontal axial propeller and the vertical axial Darrieus and Savonius turbines, and there are many variants of each design as well, as a number of other similar devices under development (*Fig. 1*). The propeller type turbine is most commonly used in large-scale applications constituting nearly all of the turbines in the global market, while the vertical axis turbines are more commonly implemented in the medium

---

Received: 18 April 2011

Accepted: 12 September 2011

\*Corresponding Author

and small-scale installations. The technical characteristics of wind turbines are found elsewhere (Heier, 1988; Spera, 1994; Manwell *et al.*, 2002; Munson *et al.*, 2002; Betz, 1996). However, a simple analysis of these wind turbine designs shows that these designs are not perfect and the wind force is not using in full-scale due to some engineering reasons.

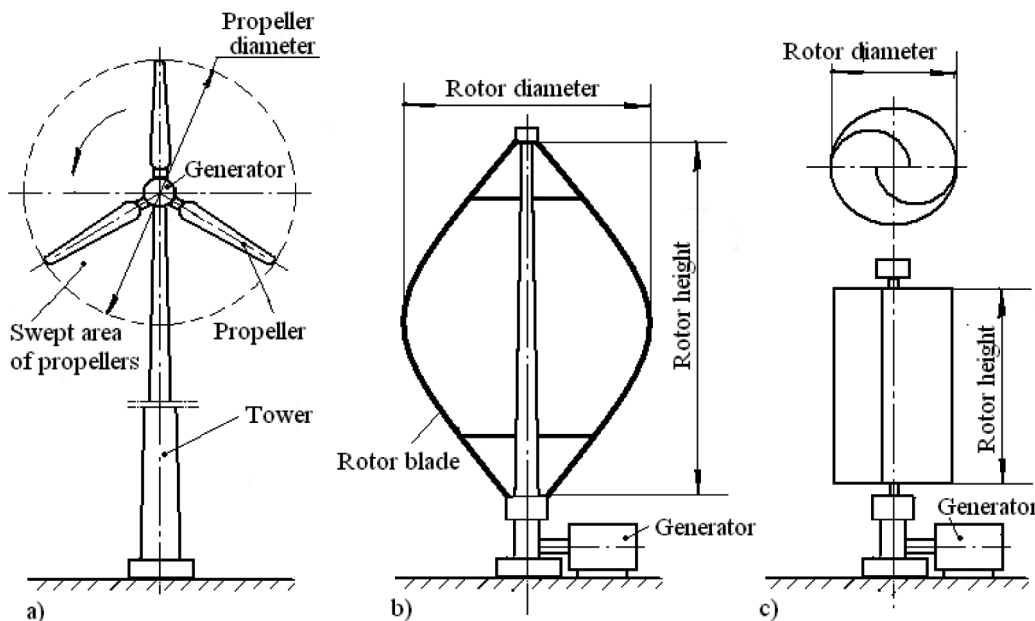


Fig. 1: Wind turbine configurations: (a) – propeller type; (b) – Darrieus; (c) - Savonius

#### *Propeller Type Wind Turbines*

Modern propeller type wind turbines use wind lift force as an aircraft wing due to the shape and geometry of the blades, and are neither built with many rotor blades nor with very wide blades. It is important to note that the number of the blades of a turbine has great impact on its performance. Meanwhile, a large number of rotor blades decrease the stability of the turbine. The experiments show that two wind turbines are with the same diameters; the one which has three blades generated even more power than the other with 12 blades due to the fact that the aerodynamic loss from the many-bladed turbines is huge. The long size of the blade creates technical problem for lifting of the propeller on the top of the pole and assembling process. The spin of the propeller around the vertical axis of the pole results in a gyroscopic effect on the body, and increases the gyroscopic fatigue (Spera, 1994). Turbine propeller blades are designed from composite materials with very complex optimality criteria involving more than aerodynamic efficiency. Computational cost of the propeller blade is too high to estimate many design variables.

Propeller type turbines built on tower and cannot use guy wires for support because the propeller spins both above and below the top of the tower. These turbines require a strong tower that grows dramatically with the size of the propeller. Other disadvantage of the propeller type wind turbine is that most of the wind passing through the space between the blades and its kinetic energy does not use by blades. However, the actual efficiency of the propeller type turbines is less twenty percentages (Heier, 1998).

### *Darrieus Wind Turbine*

This type of vertical axis wind turbine consists of a number of airfoils which are usually vertically mounted on a rotating shaft or framework. Vertical turbine is equally effective no matter which direction the wind is blowing. The Darrieus wind turbines use only the wind lift force as a result of acting the wind speed on the airfoil, and its efficiency is rarely realized due to the physical stresses and limitations imposed by a practical design and wind speed variation. The Darrieus wind turbines can rotate in high-speed with low torque and can be useful for small pumps and small electrical generators. Nonetheless, the efficiency of the Darrieus type turbines is less than ten percent (Iwashita *et al.*, 2004). There are also major difficulties in protecting the Darrieus turbine from extreme wind conditions and in making it self-starting.

The Darrieus turbine blade generates maximum torque at two points on its cycle. This leads to a sinusoidal power cycle that creates resonant modes that can cause the blades to break. Some designs of the blades canted into a helix that spreads the torque evenly over the entire revolution, thus preventing destructive pulsations. Another problem of the mass of the rotating mechanism is at the periphery that leads to very high centrifugal stresses on the blades which must be stronger and heavier than otherwise to withstand them. This design uses much more expensive material in the blades while most of the blade is too near the ground to give any real power (Manwell *et al.*, 2002). Modifications of the Darrieus turbine are the Giromill and Cycloturbines (Munson *et al.*, 2002). The main advantage of these designs are that the torque generated remains almost constant over a fairly wide angle, and have the advantage of being able to self-start by pitching the “downwind moving” blade flat to the wind in order to generate drag and start the turbine spinning at a low speed. On the downside, the blade pitching mechanism is rather complex and is generally heavy, while the wind-direction sensor needs to be added to pitch the blades properly.

### *Savonius Wind Turbines*

These turbines are one of the simplest self-starting vertical-axis turbines. Aerodynamically, they are drag-type devices, consisting of two or three scoops. Turbines use the cavity shape of the blades that allows the pressure wind to rotate turbines with low speed and creates high bending moment on the shaft of the turbine due to big area of the curved elements. The Savonius wind turbines are useful in the medium and small-scale installations. The efficiency of the Savonius type turbines is around fifteen percent (Manwell *et al.*, 2002). The two-scoop rotor that looks like an ‘S’ shape are in the cross section, and because of the curvature, the scoops have less drag when moving against the wind. The differential drag causes the Savonius turbine to spin. Some designs have long helical scoops to give a smooth torque. Much of the swept area of the Savonius rotor is near the ground, making the overall energy extraction not much effective due to the lower wind speed at lower heights. The most ubiquitous application of the Savonius wind turbine is the ventilator which is commonly seen on the roofs of vans and buses and it is also used as a cooling device.

The short review presented for the known wind turbines is the challenge for engineers and scientists. All types of the wind turbines are not perfect design and therefore cannot be used in the full-scale wind energy due to geometrical and technical problems. These technical characteristics of the known designs of the wind turbines show that there is a necessity to design a new type of the wind turbines mentioned above, which lacks the ability to be used in a wide area of application. First, the new design should use wind force and its kinetic energy in full-scale by the active area of blades, vanes or other elements of the wind turbine. This approach gives less geometrical sizes of the wind turbine. In addition, the new wind turbine should have a design that allows changing torque of the output shaft with change of the wind force. The presented problem is solved by the new

design of the vertical axis vane-type wind turbine that has a simple construction, is technologically simple in production, and uses the drug force by active area of the working elements. A sketch of the vane-type wind turbine is illustrated in *Fig. 2*.

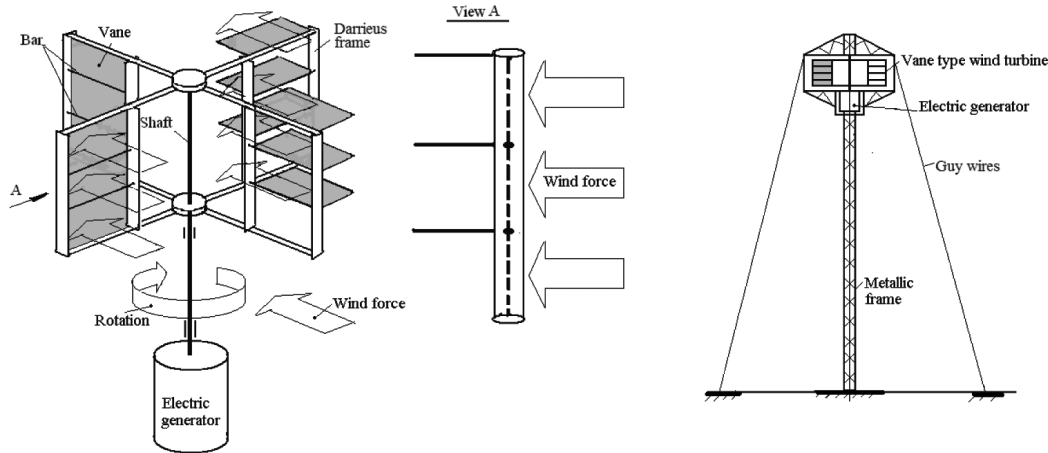


*Fig. 2: A sketch of the vane type wind turbine (a) and general view of the wind station (b)*

### REAL WIND TURBINE POWER EFFICIENCY

The theoretical maximum power efficiency of any wind turbine design is 0.59 ( $C = 0.59$  - the Betz Limit) (Betz, 1996). The real world limit is well below the Betz Limit with the value of 0.35-0.45 and this is common even in the best designed wind turbines, except this one there are other energy losses in a complete wind turbine system (the generator, bearings, power transmission, etc.) and only 10%-30% of the wind power is actually converted into usable electricity.

The wind turbine generators use mainly aerodynamic lift force and drug forces, which act on the surfaces of blades or vanes. At present, researchers state that the horizontal axis propeller type wind turbines theoretically have higher power efficiencies than the vertical axis one (drug force design). However, other research states that at conditions of turbulent with rapid changes in the wind direction, more electricity practically generated by the vertical turbines despite its lower efficiency (Mathew, 2006). Other side practice shows the propeller type hydraulic turbines are not used due to its low efficiency and the design of blades that works by drug force to generate power is used. However, the following is vital information; the power output of a wind generator is proportional to the area swept by the rotor and the power output of a wind generator is proportional to the cube of the wind speed. These peculiarities should be considered as the main factors of the output power to design the new type wind turbines.

To calculate the power of the wind turbines, many complicated equations are used. The fluid dynamic theory gives one formula with minor variation for the calculation of the power for the different wind turbine designs. The fundamental equation that governs the power output of a wind generator is (Mathew, 2006) as follows:

$$P = 0.5 * \rho * V^3 * A * \lambda, \text{ Watt} \quad (1)$$

where:  $P$  - power produced by the wind turbine,  $\rho$  - air density,  $V$  - wind speed approaching the wind turbine,  $\lambda$  - wind turbine efficiency, and  $A$  - projected area of the turbine perpendicular to

the approaching wind,  $m^2$ .  $\lambda$  is wind turbine efficiency that consists the following factors and is calculated using the following formula:

$$\lambda = C_p C * N_g * N_b$$

where  $C_p$  - coefficient of the performance ( $C = 0.35$  for a good design);  $C = C_l$  or  $C_d$  (or resulting of them) - are the lift and drag factors respectively and dependent upon the shape and form of the blades or the vanes and on the orientation of the wind flow with respect to the object;  $N_g$  - generator efficiency (80% or possibly more for a permanent magnet generator or grid-connected induction generator);  $N_b$  - gearbox/bearings efficiency (95% for a good design).

It is well-known that the modern wind turbine is designed with very complex optimality criteria involving more than aerodynamic efficiency. The main objective of a design is to maximize the coefficient  $C$ . For a propeller wind turbine,  $A$  is the swept area of rotating blades, but the actual area of blades 4-5 times less of the swept area. The wind between the propellers passes freely and does not affect on the blades. The real output power of the propeller wind turbine is 4-5 times less than the theoretical power of the turbine. The correction coefficient  $C_p$  reflects this difference.

The manufacturer of the Darrieus-type turbine defines efficiency on the actual area of the blades compared to the swept-area of the entire turbine assembly. The ducted turbines use the projected area of the rotor and disregard the area of the duct. These definitions can result in turbines power with rated efficiencies. Therefore, a great care needs to be taken in evaluating the efficiencies before comparing the performance of different turbines.

A determination of the  $C_d$  drag factor is the most difficult part of this procedure. It is highly variable, and many parameters can affect on the final  $C_d$ . Shape, altitude, inclination to the wind direction, surface roughness, spin, and nose bluntness are just a few factors that can influence  $C_d$ , which can range from 0.18 up to 1.8. From the three methods used in calculating  $C_d$  (experimental; theoretical –simplified and numerical CFD), the most realistic and straightforward method is the wind tunnel. This involves solving Eq. (1) for  $C_d$ , and then placing a model in a wind tunnel, with already known  $\rho$ ,  $A$ , and  $V$ . The test results are used to measure the force acting on the device that holds the model and calculates  $C_d = F / A$ .

## A BRIEF DESCRIPTION OF THE DESIGN AND WORK OF THE VANE-TYPE WIND TURBINE

The new vane-type vertical wind turbine can be designed using two types of construction as shown in Fig. 2 (Usuvamatov *et al.*, 2007; Usubamatov *et al.*, 2009). The first is four frames with the angle of  $90^\circ$  between one and horizontally constructed bars with the vanes that have ability to twist on  $90^\circ$ . The second is the three frames with the angle of  $120^\circ$  between one. The frame's elements should be designed of an aerodynamically form to reduce drug force of frame elements of a turbine. The vanes fastened on the bars are the elements of the frame. The vane bars can be designed vertically, but in such case, the frames will have the vanes flipping effect which can decrease the reliability of a turbine and create noise. The vertical components of a frame can be designed as the Darrieus type to increase the output of the wind turbine. Moreover, the vane-type turbine efficiency can be dramatically increased by the vanes with cavities. The wind force acts on the vanes of the left side frame and creates the torque of the shaft. The vanes on the right side of frame are open and wind force passes through the open frame. The vanes on the left side should be mechanically connected with the right side vanes. In such case, the vanes are double acting, i.e. the wind force closes the vanes on the left side vanes and simultaneously opens the ones on the right side. The torque created by the wind force rotates the frames with the output shaft which transfers the torque via gearing to the electrical generator. The frames should be connected by bars to increase the construction stiffness.

The wind turbine tower (pole) can be made from the metallic frame and used guy wires to support one, i.e. the tower can be tall and the wind turbine can use the high wind velocity. A simple analysis of the vane-type wind turbine shows only the positive technical data and benefits only. The proposed vane type wind turbine possesses all the advantages of the vertical and horizontal type turbines.

### ANALYTICAL APPROACH

The Mathematical modelling of the wind turbine power is a very difficult problem and should be generally solved using the numerical methods of computational fluid dynamics. Finally, the results of the Mathematical modelling should be verified by the practical tests in the aerodynamic wind tunnel. For this contribution range, a simple mathematical description of the wind turbine design and its work can give initial information and ability to evaluate the proposed construction.

For simplicity purposes, two models of the flat-vane wind turbines were analysed. A plan view of the vane-type wind turbine is presented in *Fig. 2*. The first model of the vane-type turbines includes four sections of the vanes assembled on the frames which are perpendicular to each other and joined with the main output shaft. The second one includes three sections of vanes which are  $120^\circ$  to each other and joined with the main output shaft.

Power output is dependent on the wind force and speed and the acting surface area  $A$  of vanes that are located at one side of the output shaft. The relationship between the physical parameters acting on the vane can be considered by known approaches. Acting forces, location of the vanes, wind shadow, and the wind pressure on the vanes are proportional to some power of the wind speed. The first thing is to calculate the force acting on the vanes due to the momentum change of the air impinging upon them. The ultimate simplification is necessary for an analytical approach considering the force acting on stationary vanes. This simplification leads to different results, depending on the assumptions made. The important assumptions made are as follows:

- The wind turbine vanes are smooth.
- The air hitting the vanes has no viscosity. It is further assumed that air, having struck on the vanes, moves off along the surface without causing a tangential frictional force.
- The drag forces acting on the left and right frame components are equal.
- The force component  $F$  acting on stationary vertical vanes of the left side frame is expressed by the following formula (Cermak, 1975; Manwell *et al.*, 2002; Iwashita, 2004).

$$F = (1/2) C_d \rho A V^2 \cos\alpha \quad (2)$$

where all the parameters specified in *Fig. 3*.

In order to determine the starting torque  $T$  on the wind turbine vanes, it is necessary to define the whole vane area and the distance from the centre of the output shaft to the centre of the wind pressure. Then, the formula has the following expression:

$$T = (1/2) A C_d \rho V^2 R \cos\alpha \quad (3)$$

where  $R$  is the distance from the shaft centre line to the centre of pressure of the vane surface, and the other parameters are as specified above.

The output power is calculated using the following equation:

$$P = T\omega = (1/2) A C_d \rho V^2 R \cos\alpha * V/R = (1/2) A C_d \rho V^3 \cos\alpha \text{ (Watt)} \quad (4)$$

where  $\omega$  is angular velocity of rotating, and other parameters are as specified above.

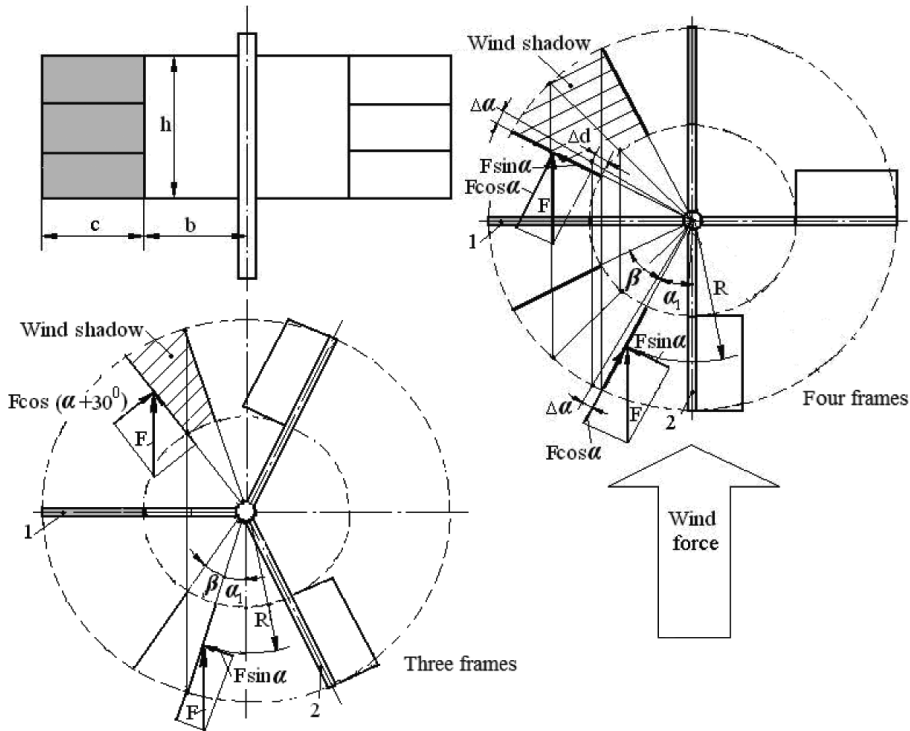


Fig. 3: The vane type wind turbine of four and three frames

The next step is to develop the mathematical model further by considering moving vanes. This entails determining the following:

- The velocity of oncoming air relative to the front surface of the first frame vanes; and,
- The effect of air on the surface of the second frame vanes.

In rotating the frames with vanes, pressure builds up along the surface of an object. A surface that is more perpendicular to the stream line of wind tends to have higher pressure. The resultant force acts in the centre of pressure that is found by calculating the pressure distribution across the variable vanes location and before integrating it. The forces acting on the sides of the frames can be neglected due to the small face-sided areas.

A good vane design will combine the aerodynamics, the mass properties, and the spin of the vane to permit the projectile to be pointy end forward for the entire airstream line. However, the very location of the frames with vanes contributes to the instability of the forces acting on the vanes and the instability of the output shaft rotation.

The flat vane, with its plane normal to the airstream, represents a common situation for wind force loads on the vane. For a flat vane with its plane normal to the wind flow, the only aerodynamic force will be one parallel to the wind flow, i.e. a wind force.

Practice shows the value of the drag factor  $C_{d, \text{is}}$  variable which is dependent on many factors like vane configuration, wind speed, the wind angle of attack of vanes, etc. There is also a tangential component or 'skin friction' force (Spera 1994). Theoretically, calculating the drag factor is an extremely complex problem. In practical, it is necessary to have the value of the drag factors

defined experimentally by testing of turbines in a wind tunnel to calculate the power generated by the wind turbines. The magnitude of the drag factor for the vane-type turbine is variable from the maximum to minimum because the rotation of vanes has azimuthally changed location from 90° to 0°. To simplify the calculation of the torque for the vane-type turbine, it is accepted the mean drag factor  $C_d = 0.8$  conventionally.

#### *Vane-type Wind Turbine with Four Frames*

The vane-type wind turbine of four frames works with two frames that are located at one side from its vertical shaft. The vanes from the other two frames are open and wind force does not act on their surfaces (*Fig. 2a* and *2b*). The frames with vanes are perpendicular to each other. The location of the acting vanes is variable due to the rotary motion of the turbine, so the torque created by the wind force is also variable. It is very important to know the variation of the torque applied on the shaft to calculate the output power. *Fig. 2b* presents the sketch of the calculation of the forces acting on the vanes that enable the calculation of the torque applied to the wind turbine shaft.

The left side of the vane turbine has two acting frames that create the torque due to the action of the wind force. The vanes of the two frames work at different conditions. The first frame's vanes work with wind shadow at some angles of rotation of the second frame vanes. On the contrary, the second frame's vanes work without wind shadow (*Fig. 2b*, four frames).

The torque created by the first vane has some drops due to wind shadow at some angles of the frame rotation. The angle of the shadow begins from the angle  $\alpha_1$  until the angle  $(\alpha_1 + \beta)$ . The presented angles are calculated from the geometry of vane location using the following formula:

$$(c + b) \sin \alpha_1 = b \cos \alpha_1, \beta = 90^\circ - 2 \alpha_1$$

$$\text{where } \alpha_1 = \arctan \frac{b}{c + b}$$

The radius of the wind force applied is  $R = b + c/2$ . In the case of wind shadow, the radius  $R$  is variable,  $R = (b + \Delta d) + (c - \Delta d)/2$ . The incremental magnitude  $\Delta d$  is changeable with the incremental angle  $\Delta\alpha$  of vane turns in the zone of wind shadow. The dependency between  $\Delta d$  and  $\Delta\alpha$  has the expression,  $\Delta d = k \Delta\alpha$ , where  $k = b/(\beta/2)$ .

The torque created by the first and second frames with a group of vanes is calculated by the following equations:

- The torque created by the first vanes at the angle of rotation from 0° to  $\alpha_1$  without wind shadow:

$$T = C_1 F [h(c + c/2)] \cos \alpha \quad (5)$$

where  $C_1$  is the drug factor

- The torque created by the first vanes at the angle of rotation from  $\alpha_1$  to  $\alpha_1 + \beta/2$  when the second vanes are at the beginning of the wind shadow zone:

$$T_2 = C_1 F [h(c - \Delta d)(b + \Delta d) + (c - \Delta d)/2] \cos \alpha + C_2 F [(h\Delta d)(b + \Delta d)/2] \cos \alpha \Big|_{\alpha_1}^{\beta/2},$$

$$\begin{aligned} \text{or} \quad T_2 &= C_1 F [h(c - k\Delta\alpha)(b + k\Delta\alpha) + (c - k\Delta\alpha)/2] \cos \alpha + \\ &C_2 F [(hk\Delta\alpha)(b + k\Delta\alpha)/2] \cos \alpha \Big|_{\alpha_1}^{\beta/2} \end{aligned} \quad (6)$$

where  $C_2$  is the drug factor for the vanes at the zone of wind shadow.

- The torque created by the first vanes at the angle of rotation from  $\alpha_1 + \beta/2$  to  $\alpha_1 + \beta$  when the second vanes at the ending of the wind shadow zone:

$$T_3 = C_2 F [h(c - \Delta d)(b + \Delta d) + (c - \Delta d)/2] \cos \alpha + C_1 F [(h\Delta d)(b + \Delta d)/2] \cos \alpha \Big|_{\beta/2}^{\beta} \quad (7)$$

- The torque created by the first vanes at the angle of rotation from  $\alpha_1 + \beta$  to  $90^\circ$  without wind shadow.

$$T_4 = C_1 F [hc(b + c/2)] \cos \alpha \Big|_{\alpha_1 + \beta}^{90^\circ} \quad (8)$$

- The torque created by the second frame vanes at the angle  $\alpha$  of rotation from  $0^\circ$  to  $90^\circ$  without wind shadow.

$$T_5 = C_1 F [hc(b + c/2)] \sin \alpha \Big|_0^{90^\circ} \quad (9)$$

The total torque created using the two frames with closed vanes is calculated using the following equation.

$$\begin{aligned} T = \sum_{i=1}^5 T_i &= C_1 F [hc(b + c/2)] \cos \alpha \Big|_0^{\alpha_1} + \\ &C_1 F [h(c - \Delta d)(b + \Delta d) + (c - \Delta d)/2] \cos \alpha + C_2 F [(h\Delta d)(b + \Delta d)/2] \cos \alpha \Big|_{\alpha_1}^{\beta/2} + \quad (10) \\ &C_2 F [h(c - \Delta d)(b + \Delta d) + (c - \Delta d)/2] \cos \alpha + C_1 F [(h\Delta d)(b + \Delta d)/2] \cos \alpha \Big|_{\beta/2}^{\alpha_1} + \\ &C_1 F [hc(b + c/2)] \cos \alpha \Big|_{\alpha_1 + \beta}^{90^\circ} + C_1 F [hc(b + c/2)] \sin \alpha \Big|_0^{90^\circ} \end{aligned}$$

### *The Vane Type Wind Turbine with Three Frames*

The vane-type wind turbine of the three frames also works with the two frames that are located on the left side from its vertical shaft. The vane on the right side frames are open and wind force does not act on their surfaces (*Fig. 2a, 2c, three frames*). The formula of the torque created by the first and second frames' vanes is the same as for the wind turbine with four frames. However, there is only one difference, i.e. the second frame's vanes act after the rotation of the first frame's vanes on  $30^\circ$ . The wind shadow zone is also different. The total torque created by two frame vanes of three frames wind turbine is calculated using Eq. (10) with different angular coordinates of vane rotations and wind shadow.

### **A WORKING EXAMPLE**

The vane-type turbine without the Darrieus frames has following dimensions:  $c = 1.0$  m – vane width,  $b = 1.0$  m – length of open frame part,  $h = 2.0$  m – height of frame,  $C_d = 1.0$  – drug factor accepted for the vanes rotated. Meanwhile,  $C_d = 0.5$  – drug factor at wind shadow. The force acting on the vane:  $F = 100\text{N}$  – wind force at condition of the wind speed  $V = 10$  m/s. The air density,  $\rho = 1.25 \text{ kg/m}^3$ .

The maximum torque created by one frame is as follows:

$$T_1 = C_1 F [hc(b + c/2)] = 1.0 * 100 [2 * 1(1 + 1/2)] = 300\text{Nm}$$

The maximum torque created by the two frames is calculated using Eq. (10). The theoretical power generated by the vane-type wind turbine is calculated using Eq. (1).

$$P = 0.5 * \rho * V^3 * A * \lambda, \text{ Watt} = 0.5 * 1.25 \text{ kg/m}^3 * 10^3 \text{ m/s}^3 * 4 * 1.0 = 2500 \text{ W} = 2.5 \text{ kW.}$$

#### *The Four Frames Vane Wind Turbines*

The formula of the angle  $\alpha_1$  at the zone of the wind shadow beginning;

$$\alpha_1 = \arctan \frac{b}{b+c} = \arctan \frac{1}{1+1} = 26.56^\circ,$$

The formula of the angle  $\beta$  at the zone of wind shadow  $\beta = 90^\circ - 2 * 26.56^\circ = 36.88^\circ$

The angle of the end of wind shadow is  $\alpha_1 + \beta = 26.56^\circ + 36.88^\circ = 63.44^\circ$

If the coefficient of the wind shadow  $C_2 = 0.5$ , the torque of the first vane at the zone of wind shadow  $\alpha_1 + \beta/2 = 26.56^\circ + 36.88^\circ/2 = 45^\circ$ .

$$T_1 = C_2 F [hc(b+c/2)] \cos 45^\circ = 0.5 * 100 \cos 45^\circ * [2 * 1(1+1/2)] = 106.1 \text{ Nm}$$

The torque of the second vane at the angle of  $45^\circ$  is:

$$T_2 = C_1 F [hc(b+c/2)] \cos 45^\circ = 1.0 * 100 [2 * 1(1+1/2)] \cos 45^\circ = 212.11 \text{ Nm}$$

The total torque with the wind shadow created by the two vanes calculated using Eq. (10)

$$T = T_1 + T_2 = 106.4 + 212.1 = 318.5 \text{ Nm}$$

The torque created by the first vane at the first half zone of the wind shadow beginning  $\alpha = \alpha_1 + \beta/4 = 25.56^\circ + 36.88^\circ/4 = 34.78^\circ$ ,  $\Delta\alpha = 9.22^\circ$  and  $k = b/(\beta/2) = 1/(36.88^\circ/2) = 0.054$  is:

$$\begin{aligned} T_2 &= C_1 F [h(c - k\Delta\alpha)(b + k\Delta\alpha) + (c - k\Delta\alpha)/2] \cos \alpha \\ &\quad + C_2 F [hk\Delta\alpha(b + k\Delta\alpha/2)] \cos \alpha + C_1 F [hc(b + c/2)] \cos \alpha \\ &= 1 * 100 [2(1 - 0.054 * 9.22)(1 + 0.054 * 9.22) + (1 - 0.054 * 9.22)/2] \cos 34.78^\circ \\ &\quad + 0.5 * 100 [2 * 0.054 * 9.22(1 + 0.054 * 9.22/2)] \cos 34.78^\circ \\ &\quad + 1 * 100 [2 * 1(1+1/2)] \sin 34.78^\circ = 376.4 \text{ Nm} \end{aligned}$$

The torque created by the first vane at the second half zone of the wind shadow ending  $\alpha = \alpha_1 + 3\beta/4 = 25.56^\circ + 3 * 36.88^\circ/4 = 53.22^\circ$ ,  $\Delta\alpha = 9.22^\circ$  and  $k = b/(\beta/2) = 1/(36.88^\circ/2) = 0.054$  is:

$$\begin{aligned} T_3 &= C_2 F [h(c - \Delta d)(b + \Delta d) + (c - \Delta d)/2] \cos \alpha \\ &\quad + C_1 F [(h\Delta d)(b + \Delta d/2)] \cos \alpha + C_1 F [hc(b + c/2)] \cos \alpha \\ &= 0.5 * 100 [(1 - 0.5)(1 + 0.5) + (1 - 0.5)/2] \cos 53.22^\circ \\ &\quad + 1 * 100 [2 * 0.5(1 + 0.5/2)] \cos 53.22^\circ \\ &\quad + 1 * 100 [2 * 1(1+1/2)] \sin 53.22^\circ = 367.4 \text{ Nm} \end{aligned}$$

### The Three-framed Vane Wind Turbine

The formula of the angle  $\alpha = 30^\circ + \alpha_1$  at the zone of the wind shadow beginning

$$\frac{b}{c+b} = \frac{\sin\alpha_1}{\cos(30^\circ + \alpha_1)}$$

$$\alpha_1 = \arctan \frac{0.866}{[(c+b)/b] + 0.5} = \arctan \frac{0.866}{[(1+1)/1] + 0.5} = 19.1^\circ$$

$$\alpha = 30^\circ + \alpha_1 = 49.1^\circ$$

The formula of the angle  $\beta$  at the zone of wind shadow is:

$$\beta = 90^\circ - 30^\circ - 2\alpha_1 = 60^\circ - 2*19.1^\circ = 21.8^\circ$$

The formula of the angle  $\alpha$  at the zone of the ending wind shadow;

$$\alpha = 30^\circ + \alpha_1 + \beta = 30^\circ + 19.1^\circ + 21.8^\circ = 70.9^\circ$$

- a) If the coefficient of the wind shadow  $C_2 = 0.5$ , the torque created by the first frame vane at zone of full wind shadow at the angle  $\alpha = 30^\circ + \alpha_1 + \beta/2 = 30^\circ + 19.1^\circ + 21.8^\circ/2 = 60^\circ$

$$T_1 = C_2 F [hc(b + c/2)] \cos 60^\circ = 0.5 * 100 \cos 60^\circ * [2 * 1(1 + 1/2)] = 75.0 \text{ Nm}$$

The torque of the second frame vane at the angle  $60^\circ$  of the first frame turns.

$$T_2 = C_1 F [hc(b + c/2)] \cos 30^\circ = 1.0 * 100 [2 * 1(1 + 1/2)] \sin 30^\circ = 150.0 \text{ Nm}$$

The total torque created by the two vanes at the zone of the wind shadow is calculated using Eq. (10):

$$T = T_1 + T_2 = 75.0 + 150 = 225 \text{ Nm}$$

- b) The torque created by the first vane at the first half zone of the wind shadow beginning at the angle  $\alpha = 30^\circ + \alpha_1 + \beta/4 = 30^\circ + 19.1^\circ + 21.8^\circ/4 = 54.55^\circ$ ,  $\Delta\alpha = 5.45^\circ$  and  $k = b/(\beta/2) = 1/(21.8^\circ/2) = 0.092$  is:

$$\begin{aligned} T_1 &= C_1 F [h(c - k\Delta\alpha)(b + k\Delta\alpha) + (c - k\Delta\alpha)/2] \cos \alpha \\ &\quad + C_2 F [hk\Delta\alpha(b + k\Delta\alpha/2)] \cos \alpha + C_1 F [hc(b + c/2)] \cos \alpha \\ &= 1 * 100 [2(1 - 0.092 * 5.45)(1 + 0.092 * 5.45) + (1 - 0.092 * 5.45)/2] \cos 54.55^\circ \\ &\quad + 0.5 * 100 [2 * 0.092 * 5.45(1 + 0.092 * 5.45/2)] \cos 54.55^\circ \end{aligned}$$

The torque created by the second frame vane at the angle of  $54.55^\circ$  of the first frame turns

$$T_2 = 1 * 100 [2 * 1(1 + 1/2)] \sin 24.55^\circ$$

- c) The torque created by the first vane at the second half zone of the wind shadow ending at the angle  $\alpha = 30^\circ + \alpha_1 + 3\beta/4 = 30^\circ + 19.1^\circ + 3*21.8^\circ/4 = 65.45^\circ$ ,  $\Delta\alpha = 5.45^\circ$  and  $k = b/(\beta/2) = 1/(21.8^\circ/2) = 0.092$  is:

$$\begin{aligned} T_1 &= C_2 F [h(c - \Delta d)(b + \Delta d) + (c - \Delta d)/2] \cos \alpha \\ &\quad + C_1 F [h\Delta d(b + \Delta d/2)] \cos \alpha + C_1 F [hc(b + c/2)] \cos \alpha \\ &= 0.5 * 100 [2(1 - 0.5)(1 + 0.5) + (1 - 0.5)/2] \cos 65.45^\circ \\ &\quad + 1 * 100 [2 * 0.5(1 + 0.5/2)] \cos 65.45^\circ + 1 * 100 [2 * 1(1 + 1/2)] \sin 65.45^\circ \end{aligned}$$

The torque created by the second frame vane at the angle  $65.45^\circ$  of first frame turns:

$$T_2 = 1 * 100 [2 * 1(1 + 1/2)] \sin 35.45^\circ$$

- d) If coefficient of wind shadow  $C = 0.5$ , the maximum torque created by the first vane at the zone of wind shadow at the angle is  $\alpha + \beta/2 = 30.96^\circ + 14.04^\circ = 45^\circ$

$$T_1 = 0.5 * 141.4 \text{ Nm} = 70.07 \text{ Nm}$$

The total torque is created by the vanes at the zone of the wind shadow.

$$T = T_1 + T_2 = 141.4 + 70.07 = 211.47 \text{ Nm}$$

The power generated by the four- and three-framed vane-type wind turbine is expressed by the following formula:

- Four frame,  $P = TV/R = 360 * 10 / 1.5 = 2400 \text{ W} = 2.4 \text{ kW}$   
where the torque  $T = 360 \text{ Nm}$  is average from the diagram (*Fig. 4*)
- Three frame,  $P = TV/R = 260 * 10 / 1.5 = 1733.3 \text{ W} = 1.7 \text{ kW}$   
where the torque  $T = 260 \text{ Nm}$  is average from the diagram (*Fig. 4*)

The diagram (*Fig. 4*) and Table 1 show that the torque and power respectively for the vane-type wind turbine have fluctuation that is numerically expressed by the following data:

$$\delta = \frac{T_{\max} - T_{\min}}{T_{\max}} 100\%$$

$$\text{The four frames turbine } \delta = \frac{T_{\max} - T_{\min}}{T_{\max}} 100\% = \frac{404.8 - 300}{404.8} 100\% = 26\%$$

$$\text{The three frames turbine } \delta = \frac{300 - 225}{300} 100\% = 25\%$$

The torque fluctuation of both type turbines has a small difference and is dependent on the torque loss due to the wind shadow of the vanes.

## RESULTS AND DISCUSSION

The theoretical calculations of the torque created by the vane-type turbines conducted by Equations (1) and (2) show almost the same result. The difference can be explained by the accepted efficiency factor  $\lambda$ , which can vary. Nevertheless, the results also show that this type wind turbines can be

## New Vane-Type Wind Turbine of High Efficiency

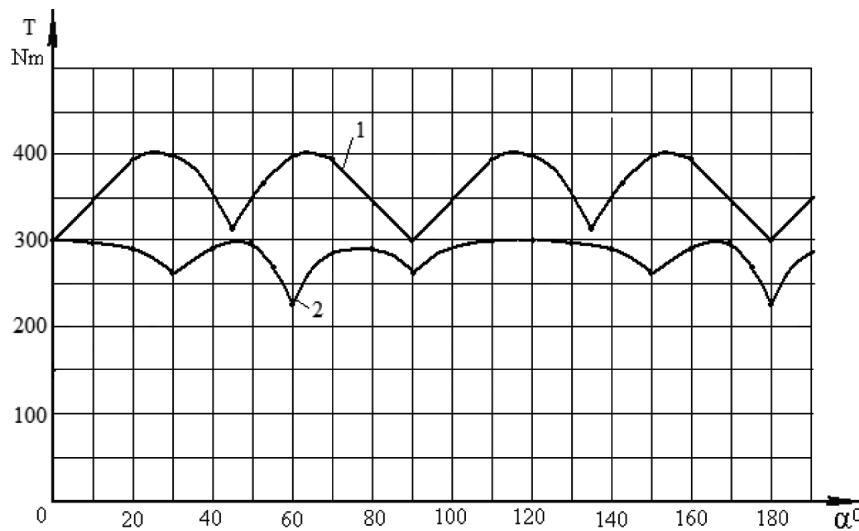


*Fig. 4: Torque versus the angle of output shaft rotation; 1 - four frames wind turbine;  
2 - three frames wind turbine*

**TABLE 1**  
The torque created on the output shaft of the vane type wind turbine

The four frames vane wind turbine											
$\alpha^\circ$	0	10	20	25.6	34.78	45	53.22	63.4	70	80	90
T <sub>1</sub>	300	295.4	281.9	270.5	205.3	106.1	127.2	134.3	102.6	52.1	0
T <sub>2</sub>	0	52.1	102.6	134.3	171.1	212.1	240.3	270.5	281.9	295.4	300
T	300	347.5	394.5	404.8	376.4	318.2	367.5	404.8	394.5	347.5	300
The three frames vane wind turbine											
$\alpha^\circ$	0	10	20	30	40	49.1	54.55	60	65.45	80	90
T <sub>1</sub>	300	295.4	281.9	259.8	229.8	196.4	145	75	98.6	52.1	0
T <sub>2</sub>	0				52.1	98.1	124.6	150	174	229.8	259.8
T	300	295.4	281.9	259.8	281.9	294.5	269.6	225	272.6	281.9	259.8

used to generate power. The efficiency of the vane-type turbines can significantly be increased by changing the shape frames, which can be designed with cavities. Such a design can increase the drag factor. The vertical components of the frames can be designed as the Darriues type wind turbine which can also add around ten percent of power and reduce the fluctuation of the torque. The test of these turbines in the wind tunnel can give correction in the theoretical calculations.

The new vane-type wind turbine can be designed from cheap material that is big positive property. The work of the vane turbine does not have restrictions. In strong wind condition, it is possible to design the vane turbine with less acting number of vanes. At conditions of weak wind, non-active vanes can be activated. In addition, it is also possible to design frames with variable locations of the vanes that change the radius of the frames and increase the torque.

## CONCLUSIONS

The new vane type wind turbine possesses many positives properties of the horizontal and vertical designs of the wind turbines and can be concurrent for the known wind turbine designs, especially for the low speed of the wind. The new turbine presents simple construction, uses a simple technology for manufacturing and be produced from cheap material. Thus, it is possible to design new turbines that can operate in any conditions of the wind force change. For future research, a mathematical modelling of the wind turbine work should be conducted on a theoretical basis of computational fluid dynamics and proved through practical investigations in the wind tunnel. In addition, it is necessary to conduct investigations on the optimal design of the new turbines (power as function of the vanes geometry, weight of turbine, aerodynamic shape, wind speed, etc.). Tests of the vane-type wind turbine in the wind tunnel and correction of the mathematical model can give reliable data to design an effective vane-type wind turbine.

## REFERENCES

- Betz, A. (1996). *Introduction to the Theory of Flow Machines*. (D. G. Randall, Trans.) Oxford: Pergamon Press.
- Cermak, J. E. (1975). Applications of Fluid Mechanics to Wind Engineering, A Freeman Scholar Lecture. *ASME Journal of Fluids Engineering*, 97(1), 9-38.
- Heier, S. (1988). *Grid Integration of Wind Energy Conversion Systems*. New York: John Wiley & Sons, Inc.
- Iwashita, H, Y. D. et al. (2004). *Development of an Elastic Rotor-Blade for the Horizontal Axis Wind Turbine*. Proceedings of Wind energy symposium, pp. 187-190.
- Manwell, J. F., McGowan, J. G., & Rogers, A. L. (2002). *Wind Energy Explained*. England: John Wiley & Son Ltd.
- Mathew, S. (2006). *Wind Energy Fundamentals, Resource Analysis and Economics* (1st ed.) Vol. 1. Springer.
- Munson, B. R., Donald, F. Y., & Theodore H. O. (2002). *Fundamentals of Fluids Mechanics* (4<sup>th</sup> ed). John Wiley & Sons, Inc.
- Spera, D. A. (1994). *Wind Turbine Technology*. New York: ASME Press.
- Usubamatov, R., & Usdubamatov, D. (2007). Vane type wind turbine. Patent # 901, Kyrgyz Republic.
- Usubamatov, R. et al. (2009). Wind power station, *Malaysian patent*, MY-138117, A. 30.04.2009.

## Fabrication of Cellulose Acetate Film From Oil Palm Empty Fruit Bunch (OP-EFB) and Cytotoxicity Evaluation

Dasmawati Mohamad<sup>1\*</sup>, Wan Suzaini Wan Hamzah<sup>1</sup>, Wan Rosli Wan Daud<sup>2</sup>,  
Zainul Ahmad Rajion<sup>1</sup>, Wan Zaripah Wan Bakar<sup>1</sup> and Mazlan Ibrahim<sup>2</sup>

<sup>1</sup>School of Dental Sciences,

<sup>2</sup>School of Industrial Technology,

Universiti Sains Malaysia,

16150 Kubang Kerian, Kelantan, Malaysia

\*E-mail: dasmawati@kck.usm.my

### ABSTRACT

The aims of this study were to fabricate cellulose acetate (CA) film from oil palm empty fruit bunch (OP-EPB), as well as to characterize and evaluate their biocompatibility. Several processes were carried out, and these included prehydrolysis-soda method, chlorine free bleaching method, including oxygen, ozone and peroxide, to produce the cellulose pulp. Then, a liquid phase acetylation method was applied through acetic acid-acetic anhydride-sulphuric acid. Triethyl citrate (TEC) ester was used as additive at different percentages of 10, 20, 30 and 40 wt%. The film produced was characterized by FTIR to identify the functional group of the CA film and their tensile properties were further characterized. Biocompatibility of the film was evaluated using cytotoxicity test. Stem cell derived from human deciduous teeth (SHED) was used with MTS assay. The results showed at 30% of TEC, the tensile strength and elongation of CA (OP-EFB) film was at the optimum and is therefore suitable to be used in dental application. The cytotoxicity evaluated showed that the fabricated CA (OP-EFB) films were non-toxic up to the concentration tested, and are thus compatible with SHED.

**Keywords:** Oil palm empty fruit bunch, cellulose acetate film, cytotoxicity

### INTRODUCTION

In Malaysia, enormous volumes of agricultural wastes, empty fruit bunch (EFB) containing cellulosic fibres are generated annually (Suhaimi & Ong, 2001). Many of these wastes are allowed to rot away unutilized. These agricultural wastes can actually be maximized their utilization, as the focus of this study is, in the production of pulp for papermaking and conversion to cellulose derivatives, specifically cellulose acetate (CA). The application of CA is widely used in photography film, automotive coatings, selective filtration membranes in medicine, and also in dental field. The advantages of CA film, such as being tough, with good dimensional stability and optical properties, made it suitable to be used in dental field. Due to its flexible properties, CA film is usually used to assist dentists while performing tooth restoration. In the fabrication of CA, which is a thermoplastic material (also referred to as bioplastic), must be modified to make it suitable for matrix polymers for commercial composite application. Plastisizers are widely used in the plastic industry to improve their processibility, flexibility and ductility properties. Conventionally, cellulose ester plastics are plasticized with a petroleum-derived phthalate plasticizer, which is not environmental friendly. Mohanty *et al.* carried out a study on cellulose acetate plasticized with varying concentrations

---

Received: 18 April 2011

Accepted: 12 September 2011

\*Corresponding Author

of an eco-friendly triethyl citrate (TEC) plasticizer (2003). The results were very promising and plasticized cellulose acetate was found to be processable at 170-180°C, i.e. approximately 50°C below the melting point of neat cellulose acetate.

The aims of this study were to fabricate cellulose acetate (CA) film from oil palm empty fruit bunches (OP-EPB) and investigate the effects of TEC plasticizer on the tensile properties of the resulting CA (OP-EPB) film. In addition, cytotoxicity was also evaluated. TEC was used as the plasticizer at different compositions. The CA films were characterized by Fourier Transform Infra-Red Spectroscopy (FTIR). Both the tensile strength and percentage elongation were also evaluated. Since the fabricated CA film is intended to be used in dental application and applied for oral purposes, the biocompatibility assessment is needed. One of the criteria for biocompatibility is that the material is not toxic to cells. Therefore, the fabricated CA films underwent a cytotoxicity test using MTS assay and the stem cell from human deciduous teeth (SHED) was also used. Vital staining was carried out as proposed by the National Guidelines for cytotoxicity test ISO 10993.

## MATERIALS AND METHODS

### *Materials*

Oil palm empty fruit bunches (OP-EFB) were collected from SABUTEK (M) Sdn. Bhd. in form of fibrous strands and used as raw material. TEC plasticizer was purchased from Merck Company.

### *Preparation of Cellulose Acetate Film*

#### **Preparation of the raw material**

The raw material (OP-EFB) was cut into pieces and boiled with distilled water for 60 minutes at 170°C, before the pulp underwent soda pulping using sodium hydroxide solution for 100 min at 160°C to remove non-cellulosic materials. Later, it was washed with water and air dried.

#### **Bleaching**

The chlorine-free bleaching process studied here includes three sequential steps of oxygen, ozone and hydrogen peroxide bleaching. Oxygen ( $O_2$ ) bleaching was carried out under alkaline conditions by addition of 1% NaOH (w/w) aqueous solution. Magnesium sulphate (0.1%) was also added as a protection reagent for cellulose. For ozone ( $O_3$ ) bleaching, the ozone was produced from the supplied oxygen gas and was mixed with pulp. Total reaction time was 2.5 min with occasional mixing at 60 rpm. For hydrogen peroxide ( $H_2O_2$ ) bleaching, the pulp was placed in a plastic bag and NaOH MgSO<sub>4</sub> was added according to the weight of the pulp (Tanaka *et al.*, 2002). The reaction was then carried out at 60 °C for 60 min in a water bath.

#### **Acetylation of Cellulose**

The cellulose acetate is usually produced by treating cellulose with acetic acid first as activation phase. To 5 parts of pulp, 90 ml of acetic acid, and 0.5 ml of sulphuric acid were added and stirred vigorously. After one min, 25 ml of acetic anhydride was added and the stirring was continued. Later, an equal volume of water was added into the reaction mixture to precipitate CA. The degree of acetylation of cellulose was determined using a standard method based on ASTM D-871-61T. The degree of acetylation found was 37.41%, and thus, the degree of substitution of CA was 2.2.

### **Preparation of Films**

CA (OP-EFB) film was made using a casting method. First, a mixture solution of CA in acetone at 16 % (w/v) was prepared. Plasticizer material, TEC, was then dissolved in the solvent mixture at different compositions (namely CA1, CA2, CA3, and CA4) as in Table 1 and stirred for 48 h. Next, the mixtures were centrifuged at 3000 rpm for 1 h. The CA solution of 12 ml was slowly and evenly poured into a petry dish of 8 cm in diameter and was dried in a dessicator for 24 h. The thickness of the CA film obtained was approximately 0.1 mm.

TABLE 1  
CA at different compositions of plasticizer

Specimen	CA/Acetone solution (ml) (w/v%)	Plasticizer (ml) Composition of TEC (wt%)
CA1	16	10
CA2	16	20
CA3	16	30
CA4	16	40

### *Characterization*

#### **FTIR Spectroscopy**

The IR spectra of various specimens of the CA films were taken using Nicolet Impact 400 Fourier Transform Infrared spectrophotometer using KBr pellet. For each CA at different compositions of plasticizer, three specimens ( $n=3$ ) were used for the FTIR evaluation. The peaks of C=O, C=C and C-O were taken and compared with a standard CA powder and also experimental CA (OP-EFB) powders.

#### **Tensile Strength and Elongation**

The tests were carried out using a Hounsfield TX0201 Tensile Testing System (H10KS model) according to the ASTM D 882. The thickness of the specimens for the tensile evaluation was maintained at approximately 0.1 mm and the length between the grips was set at 30mm. The measurements of CA films were made at three specimens, ( $n=3$ ) for each CA at different compositions of plasticizer.

#### *Cytotoxicity Evaluation*

The national guidelines for cytotoxicity test ISO /EN 10993-5 are followed for the biocompatibility evaluation. The MTS assay of [3-(4,5-dimethylthiazol-2-yl)-5-(3-carboxymethoxyphenyl)-2-(4-sulfophenyl)-2H-tetrazolium, inner salt] was used for the cytotoxicity evaluation with the CA(OP-EFB) extracts on the stem cell derived from human decidua teeth (SHED). This cytotoxicity test was carried out according to the ISO 10993-5 standard (ASTM Standard D882). The SHED were initially cultured at cell density  $5 \times 10^3$  cells/cm for 24 hours at 37 °C in 96 well plates. The medium was replaced with the sample extract. However, only one representative sample was used for this cytotoxicity evaluation. The plates were incubated in a CO<sub>2</sub> incubator for 72 hours. Next, 5mg MTS powder was measured and mixed thoroughly with 1 ml dulbecco's phosphate buffered saline

(DPBS) in a small sterile universal tube. After being thoroughly mixed, the MTS solution was filtered. 10 $\mu$ l of the MTS solution was added into all the 96 wells after 72 hours of incubation. The plates were further incubated for 2-4 hours in 5% CO<sub>2</sub> incubator. After that, the culture medium and excessive MTS solution were removed by inversion and blotted carefully on tissue paper. Next, 100 $\mu$ l of dimethylsulfoxide (DMSO) was added into each well and gently shaken for 5 minutes to achieve complete dissolution. Finally, an Elisa reader (TECAN) was used to read the absorbance at the reference and test wavelengths of 600nm and 570nm. The cell viability percentages were calculated according to the following equation:

$$\% \text{Cell viability} = \frac{OD_{\text{sample}}}{OD_{\text{control}}} \times 100\%$$

where, OD= Optical density.

## RESULTS AND DISCUSSION

The degree of the substitution of the CA found was 2.2. In general, those cellulose acetates with acetyl substitution numbers of 2.2 or less are biodegradable in soil and marine environment and are therefore suitable for composting compared with higher substitution numbers from 2.2 to 3.0. Hence, the CA (OP-EFB) film produced was confirmed as biodegradable.

The CA (OP-EFB) films of all the different percentages of TEC plastisizers were confirmed using the FTIR evaluations (Table 2). The present of the functional group C=O, C=C, and C-O indicates that the structure of CA was confirmed, as compared to the commercial CA which was done only on the powder form (Table 3). The acetate groups were found in each sample; however, the peak value was different from the control group since they were in the powder form. Nonetheless, there was not much difference between the peaks in the powder form of the commercial CA and (OP-EFB) CA, as shown in Fig. 1.

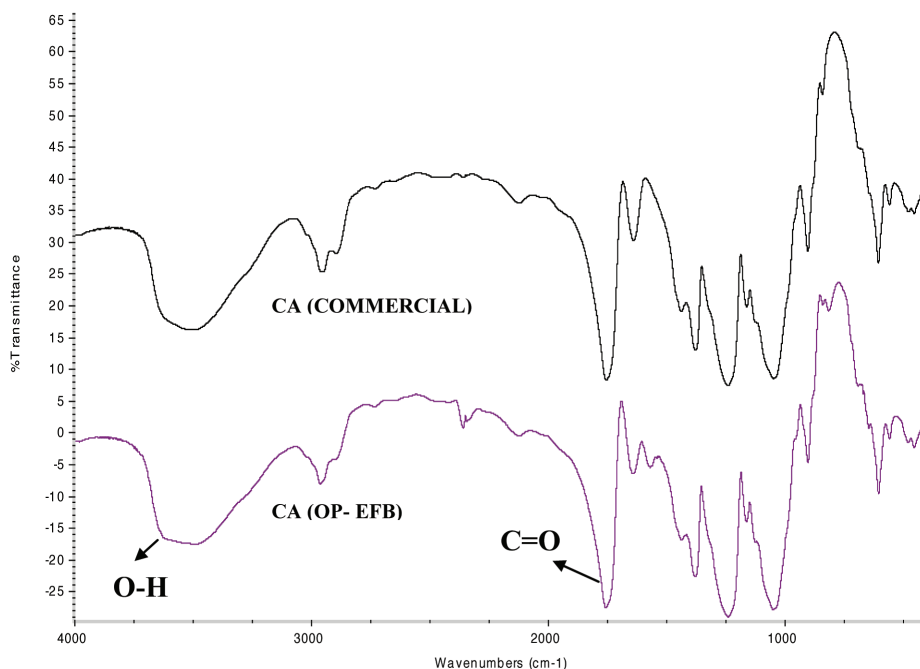


Fig. 1: The FTIR peaks of CA (OP-EFB) films and CA commercial

TABLE 2  
The FTIR peak results of the CA (OP-EFB) films

Specimen	C=O ( $\text{cm}^{-1}$ )	C=C ( $\text{cm}^{-1}$ )	C-O (acetate) ( $\text{cm}^{-1}$ )
CA1	1711.51 (0.85)	1637.41 (0.20)	1071.73 (15.45)
CA2	1736.75 (22.75)	1636.71 (1.26)	1071.69 (2.17)
CA3	1765.42 (1.13)	1636.15 (0.33)	1087.22 (34.00)
CA4	1753.85 (16.10)	1636.27 (0.13)	1152.63 (94.75)

Note: The reported are mean values with their standard deviation in brackets.

The FTIR analysis identified all the important peaks present in the sample CA (OP-EFB), which were nearly similar to the peaks that appeared in the CA commercial. A summary of the peak wave number for all the functional groups C=O, C=C, and C-O present in CA commercial and CA (OP-EFB) is tabulated in Table 3.

TABLE 3  
The FTIR peak results of CA in powder form

Specimen	C=O ( $\text{cm}^{-1}$ )	C=C ( $\text{cm}^{-1}$ )	C-O (acetate) ( $\text{cm}^{-1}$ )
CA (Standard commercial)	1754.56	1638.57	1239.53
CA (OP-EFB)	1754.51	1643.01	1243.31

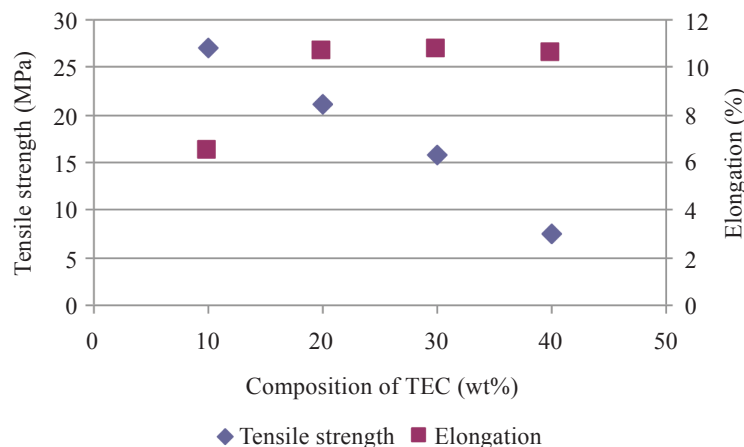
In the tensile properties evaluation, the results presented in Table 4 show an increasing trend of the tensile strength of CA (OP-EFB) films with a decreasing composition of TEC plasticizer. Although 10% of TEC has the highest value of tensile strength, the CA1 film produced was brittle, not very flexible, and it tended to wrinkle. This is shown by having the lowest elongation of 6.51%. At 20% of TEC, CA2 film also has the same features as those of CA1, but with improved elongation properties. On the other hand, CA3 gave a tensile strength of about 15 MPa but the film was very flexible and it showed the highest elongation. An optimum balance between the tensile strength and elongation is depending on the CA application. As the fabricated CA was intended to be used in dental application, which is supposed to bend easily around a tooth, the CA3 composition is therefore suitable. For CA4 film, the tensile strength was the lowest as compared to the other composition of plasticizer. The result found is in agreement with the finding by Mohanty *et al.* (2003).

TABLE 4  
The effect of different compositions of TEC on the tensile strength and elongation of CA (OP-EFB) films

Specimen	CA/Acetone (w/v%)	Composition of TEC (wt%)	Tensile strength (MPa)	Elongation (%)
CA1	16	10	27.04 (1.98)	6.51
CA2	16	20	21.11 (0.22)	10.67
CA3	16	30	15.71 (1.13)	10.76
CA4	16	40	7.48 (0.40)	10.61

Note: Reported are mean values with their standard deviation in brackets.

However, to achieve the tensile strength of CA (OP-EFB) that is similar to the commercial CA films, more extensive research is needed. Their tensile strength is about 100–140 MPa (Zugenmaier & Peter, 2004). Many factors may contribute to their high tensile strength, such as different origins of cellulose, molecular weight, purity, and different methods of film preparation.



*Fig. 2: The effect of TEC plasticizer on the tensile strength and elongation of the CA films*

In this study, CA (OP-EFB) was found to be not fully dissolved in acetone, which resulted in the obtained supernatant after centrifuged had thinner film compared to the commercial CA. Hence, different types of solvent need to be further explored. TEC composition is also important in the final product of CA film. The final application of the CA film is dependent upon the plasticizer composition. Other factors, such as drying method, have also been reported to affect the quality of the film. Meanwhile, the drying process plays an important role in affecting the wrinkles of the fabricated film.

*Fig. 3* presents the cell viability of the CA films in function of extract concentration. IC<sub>50</sub> (50 % Inhibitory Concentration) endpoint was used to evaluate the cytotoxicity effects of the materials at different concentrations applied. From the figure, the percentages of cell viability decrease when the CA extraction concentration is high. However, at the concentrations of 150mg/ml onwards, the curve line becomes a plateau at slightly above 50%. Therefore, the fabricated CA can be considered as non-toxic. However, further test on biocompatibility is still needed, such as genotoxicity and Ames test.

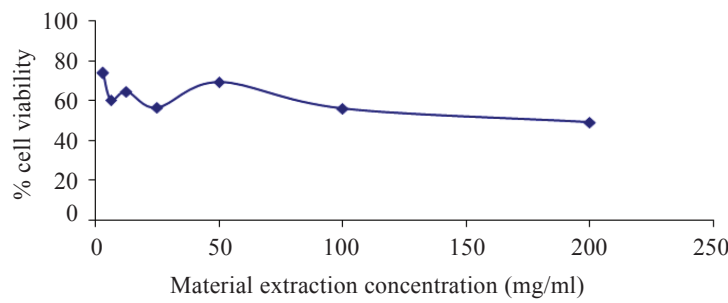


*Fig. 3: The percentage of the cell viability of CA film extraction on SHED*

## CONCLUSIONS

In this study, the CA produced from OP-EFB obtained a DS of 2.2. Therefore, it is possible to use TEC as it is eco-friendly and promoting green technology. However, increasing the amount of TEC plasticizer significantly reduced the tensile strength. The optimum balance of strength and stiffness of the CA film at 30 (wt%) plasticizer is found to be suitable for dental application. The cytotoxicity evaluation provides evidence which indicates that CA (OP-EFB) is non-toxic to the SHED, up to the concentration tested.

## ACKNOWLEDGEMENT

The authors would like to thank all the technicians from Craniofacial Science Laboratory, School of Dental Sciences, Universiti Sains Malaysia who were involved in this project. This study was supported by Yayasan FELDA with the following grant (304/PPSG/6150087/Y104).

## REFERENCES

- ASTM D-871-61T. *Tentative methods of testing cellulose acetate*, ASTM International, West Conshohocken, PA, [www.astm.org](http://www.astm.org)
- ASTM Standard D882. *Standard Test Method for Tensile Properties of Thin Plastic Sheeting*, ASTM International, West Conshohocken, PA, DOI: 10.1520/D0882-10, [www.astm.org](http://www.astm.org)
- ISO /EN 10993-5. *Biological evaluation of medical devices-Part 5 test for cytotoxicity, in vitro method: 8.2 test on extracts*.
- Mohanty, A.K., Wibowo, W.A, Misra, M., & Drzal, L.T. (2003). Development of Renewable Resource-Based Cellulose Acetate Bioplastic: Effect of Process Engineering on the Performance of Cellulosic Plastics. *Polymer Engineering & Sciences*, 43, 1151-1161.
- Tanaka, R., Peng, L. C., & Daud W. R. W. (2002). *Preparation of cellulose pulp from oil palm empty fruit bunches (EFB) by processes including pre-hydrolysis and ozone bleaching*. Paper presented at the USM-JIRCAS Joint International Symposium ~ Lignocellulose - Material of the Millennium: Technology and Application, Penang, Malaysia: Universiti Sains Malaysia.
- Suhaimi, M., & Ong, H.K. (2001). Composting Empty Fruit Bunches of Oil Palm. Food and Fertilizer Technology Center, Technology Bulletin 2001-11-01. Retrieved rom <http://www.agnet.org/library/eb/505a/>
- Zugenmaier, P. (2004). Characteristics of cellulose acetates. *Macromolecular Symposia*, 208, 81–166.



**REFEREES FOR THE PERTANIKA  
JOURNAL OF SCIENCE AND TECHNOLOGY  
(JST)**

August 2011 – January 2012

The Editorial Board of the Journal of Science and Technology wishes to thank the following for acting as referees for manuscripts published in this issue of JST.

Abu Hassan Shaari Md Nor	Mohd Shamsul Bin Anuar
Agus Arsad	Rahmita Wirza OK Rahmat
Ahmad Shukri Muhammad Noor	Razali Yaakob
Aida Isma Mohd Idris	Rohaya Latip
Amru Nasrulhaq Boyce	Rosnita A Talib
Ashutosh Kumar Singh	Rozita Omar
Azmi Abdul Wahab	Salmiaton Ali
Badronnisa Yusof	Shafreeza Sobri
Chantara Theyv Ratnam	Sharipah Soaad Syed Yahaya
Cheong Ai Theng	Sidek Ab Aziz
Desa Ahmad	Siti Khairunniza Bejo
Farah Saleena Taip	Siti Mazlina Mustapa Kamal
Hang Tuah Baharudin, BT	Siti Suri Arshad
Intan Salwani Ahamad	Somayeh Habibi
M Iqbal Saripan	Teng Beng Ti
Mansor Hashim	Wan Ishak Wan Ismail
Mariana Nor Shamsudin	Wan Mahmood Mat Yunus
Mohammad Esmail Arasteh Rad	Zurina Zainal Abidin
Mirnalini Kandiah	

**Special Acknowledgement**

The **JST Editorial Board** gratefully *acknowledges* the assistance of **Doreen Dillah**, who served as the English language editor for this issue.

---

While every effort has been made to include a complete list of referees for the period stated above, however if any name(s) have been omitted unintentionally or spelt incorrectly, please notify the Executive Editor, *Pertanika Journals* at [ndeep@admin.upm.edu.my](mailto:ndeep@admin.upm.edu.my).

Any inclusion or exclusion of name(s) on this page does not commit the Pertanika Editorial Office, nor the UPM Press or the University to provide any liability for whatsoever reason.



# *Pertanika*

*Our goal is to bring high quality research to the widest possible audience*

## **Journal of Science & Technology**

### **INSTRUCTIONS TO AUTHORS**

(Manuscript Preparation & Submission Guidelines)

Revised January 2012

*We aim for excellence, sustained by a responsible and professional approach to journal publishing.  
We value and support our authors in the research community.*

Please read the guidelines and follow these instructions carefully; doing so will ensure that the publication of your manuscript is as rapid and efficient as possible. The Editorial Board reserves the right to return manuscripts that are not prepared in accordance with these guidelines.

### **About the Journal**

*Pertanika* is an international peer-reviewed journal devoted to the publication of original papers, and it serves as a forum for practical approaches to improving quality in issues pertaining to tropical agriculture and its related fields. *Pertanika* began publication in 1978 as Journal of Tropical Agricultural Science. In 1992, a decision was made to streamline *Pertanika* into three journals to meet the need for specialised journals in areas of study aligned with the interdisciplinary strengths of the university. The revamped Journal of Science and Technology (JST) is now focusing on research in science and engineering, and its related fields. Other *Pertanika* series include Journal of Tropical Agricultural Science (JTAS); and Journal of Social Sciences and Humanities (JSSH).

JST is published in **English** and it is open to authors around the world regardless of the nationality. It is currently published two times a year i.e. in **January** and **July**.

#### **Goal of Pertanika**

Our goal is to bring the highest quality research to the widest possible audience.

#### **Quality**

We aim for excellence, sustained by a responsible and professional approach to journal publishing. Submissions are guaranteed to receive a decision within 12 weeks. The elapsed time from submission to publication for the articles averages 5-6 months.

#### **Indexing of Pertanika**

*Pertanika* is now over 33 years old; this accumulated knowledge has resulted in *Pertanika JST* being indexed in SCOPUS (Elsevier), EBSCO and DOAJ.

#### **Future vision**

We are continuously improving access to our journal archives, content, and research services. We have the drive to realise exciting new horizons that will benefit not only the academic community, but society itself.

We also have views on the future of our journals. The emergence of the online medium as the predominant vehicle for the 'consumption' and distribution of much academic research will be the ultimate instrument in the dissemination of the research news to our scientists and readers.

### **Aims and scope**

*Pertanika* Journal of Science and Technology aims to provide a forum for high quality research related to science and engineering research. Areas relevant to the scope of the journal include: *bioinformatics, bioscience, biotechnology and bio-molecular sciences, chemistry, computer science, ecology, engineering, engineering design, environmental control and management, mathematics and statistics, medicine and health sciences, nanotechnology, physics, safety and emergency management*, and related fields of study.

## **Editorial Statement**

*Pertanika* is the official journal of Universiti Putra Malaysia. The abbreviation for *Pertanika* Journal of Science & Technology is *Pertanika J. Sci. Technol.*

## **Guidelines for Authors**

### **Publication policies**

*Pertanika* policy prohibits an author from submitting the same manuscript for concurrent consideration by two or more publications. It prohibits as well publication of any manuscript that has already been published either in whole or substantial part elsewhere. It also does not permit publication of manuscript that has been published in full in Proceedings. Please refer to Pertanika's **Code of Ethics** for full details.

### **Editorial process**

Authors are notified on receipt of a manuscript and upon the editorial decision regarding publication.

**Manuscript review:** Manuscripts deemed suitable for publication are sent to the Editorial Board members and/or other reviewers. We encourage authors to suggest the names of possible reviewers. Notification of the editorial decision is usually provided within to eight to ten weeks from the receipt of manuscript. Publication of solicited manuscripts is not guaranteed. In most cases, manuscripts are accepted conditionally, pending an author's revision of the material.

**Author approval:** Authors are responsible for all statements in articles, including changes made by editors. The liaison author must be available for consultation with an editor of *The Journal* to answer questions during the editorial process and to approve the edited copy. Authors receive edited typescript (not galley proofs) for final approval. Changes **cannot** be made to the copy after the edited version has been approved.

Please direct all inquiries, manuscripts, and related correspondence to:

The Executive Editor  
*Pertanika* Journals, UPM Press  
Office of the Deputy Vice Chancellor (R&I)  
IDEA Tower II, UPM-MTDC Technology Centre  
Universiti Putra Malaysia  
43400 UPM, Serdang, Selangor  
Malaysia  
Phone: + (603) 8947 1622  
[ndeep@admin.upm.edu.my](mailto:ndeep@admin.upm.edu.my)

or visit our website at <http://www.pertanika.upm.edu.my/> for further information.

### **Manuscript preparation**

*Pertanika* accepts submission of mainly four types of manuscripts. Each manuscript is classified as **regular** or **original** articles, **short communications**, **reviews**, and proposals for **special issues**. Articles must be in **English** and they must be competently written and argued in clear and concise grammatical English. Acceptable English usage and syntax are expected. Do not use slang, jargon, or obscure abbreviations or phrasing. Metric measurement is preferred; equivalent English measurement may be included in parentheses. Always provide the complete form of an acronym/abbreviation the first time it is presented in the text. Contributors are strongly recommended to have the manuscript checked by a colleague with ample experience in writing English manuscripts or an English language editor.

Linguistically hopeless manuscripts will be rejected straightaway (e.g., when the language is so poor that one cannot be sure of what the authors really mean). This process, taken by authors before submission, will greatly facilitate reviewing, and thus publication if the content is acceptable.

The instructions for authors must be followed. Manuscripts not adhering to the instructions will be returned for revision without review. Authors should prepare manuscripts according to the guidelines of *Pertanika*.

#### **1. Regular article**

**Definition:** Full-length original empirical investigations, consisting of introduction, materials and methods, results and discussion, conclusions. Original work must provide references and an explanation on research findings that contain new and significant findings.

**Size:** Should not exceed 5000 words or 8-10 printed pages (excluding the abstract, references, tables and/or figures). One printed page is roughly equivalent to 3 type-written pages.

## **2. Short communications**

*Definition:* Significant new information to readers of the Journal in a short but complete form. It is suitable for the publication of technical advance, bioinformatics or insightful findings of plant and animal development and function.

*Size:* Should not exceed 2000 words or 4 printed pages, is intended for rapid publication. They are not intended for publishing preliminary results or to be a reduced version of Regular Papers or Rapid Papers.

## **3. Review article**

*Definition:* Critical evaluation of materials about current research that had already been published by organizing, integrating, and evaluating previously published materials. Re-analyses as meta-analysis and systemic reviews are encouraged. Review articles should aim to provide systemic overviews, evaluations and interpretations of research in a given field.

*Size:* Should not exceed 4000 words or 7-8 printed pages.

## **4. Special issues**

*Definition:* Usually papers from research presented at a conference, seminar, congress or a symposium.

*Size:* Should not exceed 5000 words or 8-10 printed pages.

## **5. Others**

*Definition:* Brief reports, case studies, comments, Letters to the Editor, and replies on previously published articles may be considered.

*Size:* Should not exceed 2000 words or up to 4 printed pages.

With few exceptions, original manuscripts should not exceed the recommended length of 6 printed pages (about 18 typed pages, double-spaced and in 12-point font, tables and figures included). Printing is expensive, and, for the Journal, postage doubles when an issue exceeds 80 pages. You can understand then that there is little room for flexibility.

Long articles reduce the Journal's possibility to accept other high-quality contributions because of its 80-page restriction. We would like to publish as many good studies as possible, not only a few lengthy ones. (And, who reads overly long articles anyway?) Therefore, in our competition, short and concise manuscripts have a definite advantage.

### **Format**

The paper should be formatted in one column format with at least 4cm margins and double spacing throughout. Authors are advised to use Times New Roman 12-point font. Be especially careful when you are inserting special characters, as those inserted in different fonts may be replaced by different characters when converted to PDF files. It is well known that 'ü' will be replaced by other characters when fonts such as 'Symbol' or 'Mincho' are used.

A maximum of eight keywords should be indicated below the abstract to describe the contents of the manuscript. Leave a blank line between each paragraph and between each entry in the list of bibliographic references. Tables should preferably be placed in the same electronic file as the text. Authors should consult a recent issue of the Journal for table layout.

Every page of the manuscript, including the title page, references, tables, etc. should be numbered. However, no reference should be made to page numbers in the text; if necessary, one may refer to sections. Underline words that should be in italics, and do not underline any other words.

We recommend that authors prepare the text as a **Microsoft Word** file.

1. Manuscripts in general should be organised in the following order:

- Page 1: Running title.** (Not to exceed 60 characters, counting letters and spaces). This page should **only** contain the running title of your paper. The running title is an abbreviated title used as the running head on every page of the manuscript.

In addition, the **Subject areas** most relevant to the study **must be indicated on this page**. Select one or two subject areas (refer to the *Scope Form*).

A list of number of black and white / colour figures and tables should also be indicated on this page. Figures submitted in color will be printed in colour. See "5. *Figures & Photographs*" for details.

- Page 2: Author(s) and Corresponding author information.** This page should contain the **full title** of your paper with name(s) of all the authors, institutions and corresponding author's name, institution and full address (Street address, telephone number (including extension), hand phone number, fax number and e-mail address) for editorial correspondence. The names of the authors **must** be abbreviated following the international naming convention. e.g. Salleh, A.B., Tan, S.G., or Sapuan, S.M.

**Authors' addresses.** Multiple authors with different addresses must indicate their respective addresses separately by superscript numbers:

George Swan<sup>1</sup> and Nayan Kanwal<sup>2</sup>

<sup>1</sup>Department of Biology, Faculty of Science, Duke University, Durham, North Carolina, USA.

<sup>2</sup>Research Management Centre, Universiti Putra Malaysia, Serdang, Malaysia.

- **Page 3:** This page should repeat the full title of your paper with only the **Abstract** (the abstract should be less than 250 words for a Regular Paper and up to 100 words for a Short Communication). **Keywords** must also be provided on this page (Not more than eight keywords in alphabetical order).
- **Page 4 and subsequent pages:** This page should begin with the **Introduction** of your article and the rest of your paper should follow from page 5 onwards.

**Abbreviations.** Define alphabetically, other than abbreviations that can be used without definition. Words or phrases that are abbreviated in the introduction and following text should be written out in full the first time that they appear in the text, with each abbreviated form in parenthesis. Include the common name or scientific name, or both, of animal and plant materials.

**Footnotes.** Current addresses of authors if different from heading.

2. **Text.** Regular Papers should be prepared with the headings **Introduction, Materials and Methods, Results and Discussion, Conclusions** in this order. Short Communications should be prepared according to "8. Short Communications." below.
3. **Tables.** All tables should be prepared in a form consistent with recent issues of *Pertanika* and should be numbered consecutively with Arabic numerals. Explanatory material should be given in the table legends and footnotes. Each table should be prepared on a separate page. (Note that when a manuscript is accepted for publication, tables must be submitted as data - .doc, .rtf, Excel or PowerPoint file- because tables submitted as image data cannot be edited for publication.)
4. **Equations and Formulae.** These must be set up clearly and should be typed triple spaced. Numbers identifying equations should be in square brackets and placed on the right margin of the text.
5. **Figures & Photographs.** Submit an original figure or photograph. Line drawings must be clear, with high black and white contrast. Each figure or photograph should be prepared on a separate sheet and numbered consecutively with Arabic numerals. Appropriate sized numbers, letters and symbols should be used, no smaller than 2 mm in size after reduction to single column width (85 mm), 1.5-column width (120 mm) or full 2-column width (175 mm). Failure to comply with these specifications will require new figures and delay in publication. For electronic figures, create your figures using applications that are capable of preparing high resolution TIFF files acceptable for publication. In general, we require **300 dpi or higher resolution for coloured and half-tone artwork** and **1200 dpi or higher for line drawings**. For review, you may attach low-resolution figures, which are still clear enough for reviewing, to keep the file of the manuscript under 5 MB. Illustrations may be produced at extra cost in colour at the discretion of the Publisher; the author could be charged Malaysian Ringgit 50 for each colour page.
6. **References.** Literature citations in the text should be made by name(s) of author(s) and year. For references with more than two authors, the name of the first author followed by 'et al.' should be used.

Swan and Kanwal (2007) reported that ...

The results have been interpreted (Kanwal et al. 2009).

- References should be listed in alphabetical order, by the authors' last names. For the same author, or for the same set of authors, references should be arranged chronologically. If there is more than one publication in the same year for the same author(s), the letters 'a', 'b', etc., should be added to the year.
- When the authors are more than 11, list 5 authors and then et al.
- Do not use indentations in typing References. Use one line of space to separate each reference. The name of the journal should be written in full. For example:
  - Jalaludin, S. (1997a). Metabolizable energy of some local feeding stuff. *Tumbuh*, 1, 21-24.
  - Jalaludin, S. (1997b). The use of different vegetable oil in chicken ration. *Malayan Agriculturist*, 11, 29-31.
  - Tan, S.G., Omar, M.Y., Mahani, K.W., Rahani, M., & Selvaraj, O.S. (1994). Biochemical genetic studies on wild populations of three species of green leafhoppers *Nephrotettix* from Peninsular Malaysia. *Biochemical Genetics*, 32, 415 - 422.

- In case of citing an author(s) who has published more than one paper in the same year, the papers should be distinguished by addition of a small letter as shown above, e.g. Jalaludin (1997a); Jalaludin (1997b).
- Unpublished data and personal communications should not be cited as literature citations, but given in the text in parentheses. 'In press' articles that have been accepted for publication may be cited in References. Include in the citation the journal in which the 'in press' article will appear and the publication date, if a date is available.

**7. Examples of other reference citations:**

**Monographs:** Turner, H.N., & Yong, S.S.Y. (2006). *Quantitative Genetics in Sheep Breeding*. Ithaca: Cornell University Press.

**Chapter in Book:** Kanwal, N.D.S. (1992). Role of plantation crops in Papua New Guinea economy. In Angela R. McLean (Ed.), *Introduction of livestock in the Enga province PNG* (p. 221-250). United Kingdom: Oxford Press.

**Proceedings:** Kanwal, N.D.S. (2001). Assessing the visual impact of degraded land management with landscape design software. In Kanwal, N.D.S., & Lecoustre, P. (Eds.), *International forum for Urban Landscape Technologies* (p. 117-127). Lullier, Geneva, Switzerland: CIRAD Press.

- 8. Short Communications** should include **Introduction, Materials and Methods, Results and Discussion, Conclusions** in this order. Headings should only be inserted for Materials and Methods. The abstract should be up to 100 words, as stated above. Short Communications must be 5 printed pages or less, including all references, figures and tables. References should be less than 30. A 5 page paper is usually approximately 3000 words plus four figures or tables (if each figure or table is less than 1/4 page).

\*Authors should state the total number of words (including the Abstract) in the cover letter. Manuscripts that do not fulfill these criteria will be rejected as Short Communications without review.

**STYLE OF THE MANUSCRIPT**

Manuscripts should follow the style of the latest version of the Publication Manual of the American Psychological Association (APA). The journal uses British spelling and authors should therefore follow the latest edition of the Oxford Advanced Learner's Dictionary.

**SUBMISSION OF MANUSCRIPTS**

All articles should be submitted electronically using the ScholarOne web-based system. ScholarOne, a Thomson Reuters product provides comprehensive workflow management systems for scholarly journals. For more information, go to our web page and click "**Online Submission**".

Alternatively, you may send your electronic files (manuscript, along with the **Form BR 25** comprising *Declaration, Referral A* and *Scope* form) together with a **cover letter** directly to the Executive Editor. If the files are too big to email, mail a CD of your files. The forms and the sample of the cover letter are available from the *Pertanika*'s home page at <http://www.pertanika.upm.edu.my/> or from the Executive Editor's office upon request.

All articles submitted to the journal **must comply** with these instructions. Failure to do so will result in return of the manuscript and possible delay in publication.

Please do **not** submit manuscripts to the editor-in-chief or to UPM Press directly. All manuscripts must be **submitted through the executive editor's office** to be properly acknowledged and rapidly processed:

Dr. Nayan KANWAL  
 The Executive Editor  
*Pertanika* Journals, UPM Press  
 Office of the Deputy Vice Chancellor (R&I)  
 IDEA Tower II, UPM-MTDC Technology Centre  
 Universiti Putra Malaysia  
 43400 UPM, Serdang, Selangor, Malaysia  
 email: [ndeep@admin.upm.edu.my](mailto:ndeep@admin.upm.edu.my); tel: + 603-8947 1622

**Cover letter**

All submissions must be accompanied by a cover letter detailing what you are submitting. Papers are accepted for publication in the journal on the understanding that the article is original and the content has not been published or submitted for publication elsewhere. This must be stated in the cover letter.

The cover letter must also contain an acknowledgement that all authors have contributed significantly, and that all authors are in agreement with the content of the manuscript.

The cover letter of the paper should contain (i) the title; (ii) the full names of the authors; (iii) the addresses of the institutions at which the work was carried out together with (iv) the full postal and email address, plus facsimile and telephone numbers of the author to whom correspondence about the manuscript should be sent. The present address of any author, if different from that where the work was carried out, should be supplied in a footnote.

As articles are double-blind reviewed, material that might identify authorship of the paper should be placed on a cover sheet.

#### **Peer review**

In the peer-review process, three referees independently evaluate the scientific quality of the submitted manuscripts. The Journal uses a double-blind peer-review system. Authors are encouraged to indicate in **referral form A** the names of three potential reviewers, but the editors will make the final choice. The editors are not, however, bound by these suggestions.

Manuscripts should be written so that they are intelligible to the professional reader who is not a specialist in the particular field. They should be written in a clear, concise, direct style. Where contributions are judged as acceptable for publication on the basis of content, the Editor or the Publisher reserves the right to modify the typescripts to eliminate ambiguity and repetition and improve communication between author and reader. If extensive alterations are required, the manuscript will be returned to the author for revision.

#### **The editorial review process**

What happens to a manuscript once it is submitted to *Pertanika*? Typically, there are seven steps to the editorial review process:

1. The executive editor and the editorial board examine the paper to determine whether it is appropriate for the journal and should be reviewed. If not appropriate, the manuscript is rejected outright and the author is informed.
2. The executive editor sends the article-identifying information having been removed, to three reviewers. Typically, one of these is from the Journal's editorial board. Others are specialists in the subject matter represented by the article. The executive editor asks them to complete the review in three weeks and encloses two forms: (a) referral form B and (b) reviewer's comment form along with reviewer's guidelines. Comments to authors are about the appropriateness and adequacy of the theoretical or conceptual framework, literature review, method, results and discussion, and conclusions. Reviewers often include suggestions for strengthening of the manuscript. Comments to the editor are in the nature of the significance of the work and its potential contribution to the literature.
3. The executive editor, in consultation with the editor-in-chief, examines the reviews and decides whether to reject the manuscript, invite the author(s) to revise and resubmit the manuscript, or seek additional reviews. Final acceptance or rejection rests with the Editorial Board, who reserves the right to refuse any material for publication. In rare instances, the manuscript is accepted with almost no revision. Almost without exception, reviewers' comments (to the author) are forwarded to the author. If a revision is indicated, the editor provides guidelines for attending to the reviewers' suggestions and perhaps additional advice about revising the manuscript.
4. The authors decide whether and how to address the reviewers' comments and criticisms and the editor's concerns. The authors submit a revised version of the paper to the executive editor along with specific information describing how they have answered the concerns of the reviewers and the editor.
5. The executive editor sends the revised paper out for review. Typically, at least one of the original reviewers will be asked to examine the article.
6. When the reviewers have completed their work, the executive editor in consultation with the editorial board and the editor-in-chief examine their comments and decide whether the paper is ready to be published, needs another round of revisions, or should be rejected.
7. If the decision is to accept, the paper is sent to that Press and the article should appear in print in approximately two to three months. The Publisher ensures that the paper adheres to the correct style (in-text citations, the reference list, and tables are typical areas of concern, clarity, and grammar). The authors are asked to respond to any queries by the Publisher. Following these corrections, page proofs are mailed to the corresponding authors for their final approval. At this point, only essential changes are accepted. Finally, the article appears in the pages of the Journal and is posted on-line.

#### **English language editing**

Authors are responsible for the linguistic accuracy of their manuscripts. Authors not fully conversant with the English language should seek advice from subject specialists with a sound knowledge of English. The cost will be borne by the author, and a copy of the certificate issued by the service should be attached to the cover letter.

**Note** When your manuscript is received at *Pertanika*, it is considered to be in its final form. Therefore, you need to check your manuscript carefully before submitting it to the executive editor.

**Author material archive policy**

Authors who require the return of any submitted material that is rejected for publication in the journal should indicate on the cover letter. If no indication is given, that author's material should be returned, the Editorial Office will dispose of all hardcopy and electronic material.

**Copyright**

Authors publishing the Journal will be asked to sign a declaration form. In signing the form, it is assumed that authors have obtained permission to use any copyrighted or previously published material. All authors must read and agree to the conditions outlined in the form, and must sign the form or agree that the corresponding author can sign on their behalf. Articles cannot be published until a signed form has been received.

**Lag time**

The elapsed time from submission to publication for the articles averages 5-6 months. A decision of acceptance of a manuscript is reached in 2 to 3 months (average 9 weeks).

**Back issues**

Single issues from current and recent volumes are available at the current single issue price from UPM Press. Earlier issues may also be obtained from UPM Press at a special discounted price. Please contact UPM Press at [penerbit@putra.upm.edu.my](mailto:penerbit@putra.upm.edu.my) or you may write for further details at the following address:

UPM Press  
Universiti Putra Malaysia  
43400 UPM, Serdang  
Selangor Darul Ehsan  
Malaysia



# Pertanika

Our goal is to bring  
high quality research to  
the widest possible  
audience

Pertanika is an international peer-reviewed leading journal in Malaysia which began publication in 1978. The journal publishes in three different areas — Journal of Tropical Agricultural Science (JTAS); Journal of Science and Technology (JST); and Journal of Social Sciences and Humanities (JSSH).

**JTAS** is devoted to the publication of original papers that serves as a forum for practical approaches to improving quality in issues pertaining to tropical agricultural research or related fields of study. It is published four times a year in **February, May, August and November**.

**JST** caters for science and engineering research or related fields of study. It is published twice a year in **January and July**.

**JSSH** deals in research or theories in social sciences and humanities research with a focus on emerging issues pertaining to the social and behavioural sciences as well as the humanities, particularly in the Asia Pacific region. It is published four times a year in **March, June, September and December**.



## Why should you publish in Pertanika Journals?

### Benefits to Authors

**PROFILE:** Our journals are circulated in large numbers all over Malaysia, and beyond in Southeast Asia. Recently, we have widened our circulation to other overseas countries as well. We will ensure that your work reaches the widest possible audience in print and online, through our wide publicity campaigns held frequently, and through our constantly developing electronic initiatives via Pertanika online submission system backed by Thomson Reuters.

**QUALITY:** Our journals' reputation for quality is unsurpassed ensuring that the originality, authority and accuracy of your work will be fully recognised. Each manuscript submitted to Pertanika undergoes a rigid **originality check**. Our double-blind peer refereeing procedures are fair and open, and we aim to help authors develop and improve their work. Pertanika JTAS is now over 31 years old; this accumulated knowledge has resulted in Pertanika being indexed in SCOPUS (Elsevier), EBSCO, DOAJ, CABI and AGRICOLA.

**AUTHOR SERVICES:** We provide a rapid response service to all our authors, with dedicated support staff for each journal, and a point of contact throughout the refereeing and production processes. Our aim is to ensure that the production process is as smooth as possible, is borne out by the high number of authors who publish with us again and again.

**LAG TIME:** Submissions are guaranteed to receive a decision within **14 weeks**. The elapsed time from submission to publication for the articles averages 5-6 months. A decision of acceptance of a manuscript is reached in 3 to 4 months (average 14 weeks).



## Call for Papers

Pertanika invites you to explore frontiers from all fields of science and technology to social sciences and humanities. You may contribute your scientific work for publishing in UPM's hallmark journals either as a regular article, short communication, or a review article in our forthcoming issues. Papers submitted to this journal must contain original results and must not be submitted elsewhere while being evaluated for the *Pertanika* Journals.

Submissions in English should be accompanied by an abstract not exceeding 300 words. Your manuscript should be no more than 6,000 words or 10-12 printed pages, including notes and abstract. Submissions should conform to the *Pertanika* style, which is available at [www.pertanika.upm.edu.my](http://www.pertanika.upm.edu.my) or by mail or email upon request.

Papers should be double-spaced 12 point type (Times New Roman fonts preferred). The first page should include the title of the article but no author information. Page 2 should repeat the title of the article together with the names and contact information of the corresponding author as well as all the other authors. Page 3 should contain the title of the paper and abstract only. Page 4 and subsequent pages to have the text - Acknowledgments - References - Tables - Legends to figures - Figures, etc.

Questions regarding submissions should only be directed to the Executive Editor, *Pertanika* Journals.

Remember, *Pertanika* is the resource to support you in strengthening research and research management capacity.

### An Award Winning International- Malaysian Journal

FEB. 2008

**Mail your submissions to:**

The Executive Editor  
Pertanika Journals, UPM Press  
Office of the DVC (R&)  
IDEA Tower II, UPM-MTDC Technology Centre  
Universiti Putra Malaysia  
43400 UPM, Serdang, Selangor  
Malaysia

Tel: +6 03 8947 1622  
[ndeep@admin.upm.edu.my](mailto:ndeep@admin.upm.edu.my)  
[www.pertanika.upm.edu.my](http://www.pertanika.upm.edu.my)



## Pertanika is Indexed in SCOPUS, EBSCO & DOAJ

